ANALYSIS OF THE METABOLIC CONTROL OF CELL GROWTH USING STABLE ISOTOPE RESOLVED METABOLOMICS

Inaugural-Dissertation

to obtain the academic degree

Doctor rerum naturalium (Dr. rer. nat.)

submitted to the Department of Biology, Chemistry and Pharmacy

of Freie Universität Berlin

by

Matthias Pietzke

born in Nauen, Germany

April 2014

The experiments of this work were conducted from April 2010 to March 2014 in the group of Dr. Stefan Kempa at the MDC Berlin Buch.

1st reviewer: Dr. Stefan Kempa

Berlin Institute of Medical Systems Biology (BIMSB) at the Max-Delbrück-Centrum, Berlin, Germany

2nd reviewer: Prof. Dr. Udo Heinemann

Freie Universität Berlin, Germany
and Max-Delbrück-Centrum Berlin, Germany

Date of Defence: 12.09.2014

A - ACKNOWLEDGMENTS

First of all I want to thank Dr. Stefan Kempa for the opportunity to work in this lab. He gave me the flexibility to develop my own ideas, by giving the right input, impulses and pressure.

Special thank you goes out to all the lab-members for a nice working atmosphere, for help during experiments (e.g. boring cell counting), but also for fruitful discussions about ideas, concepts, methods, strategies, visualizations but also music, photography, movies and other private stuff. It was essential to withstand all the years. In more detail, special thanks goes out to Christin for setting up the cell culture and performing the first experiments together and the cooperative work on the recovery, and to Henning, Chris and Tobias for proofreading. Also the support by my girlfriend Lea was very important, especially in the last months and weeks. You know I will do the same for you!

I also want to thank Prof. Dr. Udo Heinemann for agreeing to read and evaluate this thesis and the Freie Universität Berlin for accepting me as PhD student.

The Max-Delbrück-Center and the Helmholtz association financed this work, which was also very welcome. I hope I fulfilled the expectations; in fact two patents are in preparation.

Additionally I want to thank all the cooperation partners performing experiments with or for me: Sebastian Memczak and Ulrike Ziebold (Rajewski-lab, MDC), Timm Zörgiebel and Florian Blaschke (MDC), Maria Doleptchieva (Poy-lab, MDC), Antje Kettelharke (Cramer-lab, Charité). Even if not everything will be ultimately published I learned a lot, at least.

Schließlich möchte ich noch meinen Eltern danken. Auch wenn ihr die Arbeit nicht lesen könnt, so gäbe es sie nicht ohne euch. Ihr habt mich zu dem gemacht der ich bin, mich während der Schulzeit und des Studiums unterstützt und gefördert. Ihr habt nie aufgehört an mich zu glauben auch wenn der Weg manchmal steinig war, ihr gabt mir eure Geduld und die Freiheiten die ich brauchte. Ich hoffe ihr seid stolz auf mich.

Finally I want to thank Apocalyptica, Beatsteaks, Daturah, Foo Fighters, Hundreds, Laura, Maybeshewill, Mogwai, Muff Potter, Muse, pg.lost and Sleepmakeswaves for making music that kept me motivated, energized and awake during the last weeks of writing this thesis.

B - SUMMARY

Cancer cells typically collected a number of mutations resulting in modified metabolism optimized to fulfill their needs to a maximize growth. In the recent years -with development of reliable high-throughput techniques- there was a shift from measuring single actors to an integrated view of the complex regulatory network in a biological system. This thesis aimed at elucidation and understanding of the metabolic difference between cancer and healthy cells in order to target these differences therapeutically.

Firstly, cancer and healthy cells **differ metabolically** in many aspects. It is generally accepted that most cancer cells have a higher rate of glycolysis that results in elevated level of lactate production, even in the presence of oxygen (known as Warburg effect). Further the function and activity of the TCA cycle and the glutaminolysis in cancer cells is heavily debated. Current, static metabolomics protocols deliver only a limited amount of information and need careful interpretation. With the help of heavy-labeled isotopes the metabolism can be monitored in a more dynamic way. In frame of this thesis a method was established that allows for monitoring changes in the carbon routing of the highly connected central carbon metabolism in human tumor model cell lines. The usage of substrates such as glucose can be compared under different conditions. With this method the high activity of glycolysis and a tight connection to lactate production as well as a truncated TCA cycle could be shown.

Secondly, cancer cells can be characterized by their **permanent and unlimited replication**. During different phases of the cell cycle, cells are expected to have different needs, with respect to precursors for synthesis or energy production. The difference in metabolism during various phases of the cell cycle was monitored with the established approach in synchronized cells. Further the protein-turnover was measured in a pulsed-SILAC approach.

Third, both permanent growth and elevated glycolytic activity are **potential targets for therapy**, aiming at cancer cells but leaving healthy cells unharmed. The established method is perfectly suitable to detect rearrangements of metabolism on the minute time scale, therefore differentiating between direct inhibition of enzymes targeted by inhibitors and long-termed rearrangements of metabolism. The strategy was tested with three different, putative inhibitors of glycolysis: 3-bromopyruvate, glyceraldehyde and 2-deoxyglucose. The monitored effects partially resembled effects previously described in the literature and further evidenced criticism of 2-deoxyglucose as selective inhibitor of glycolysis.

Finally, the methods and strategies developed in cancer-model cell lines were and will be further translated to ***in vivo*** **mouse models**. Pulsed labeling with stable isotope enriched substrates such as glucose or glutamine showed differences in the substrate utilization between female and male HCC tumor model mice.

C - ZUSAMMENFASSUNG

Krebszellen sammeln in ihrer Entwicklung zahlreiche verschiedene Mutationen, die sich häufig in einem veränderten Stoffwechsel manifestieren, einem Stoffwechsel optimiert auf maximales Wachstum. Die Entwicklung von zuverlässigen Hochdurchsatz-Methoden ermöglichte einen Wechsel von der Betrachtung einzelner Aspekte zu einer integrierten Betrachtung des gesamten, komplexen Systems. Diese Arbeit zielt auf ein tieferes Verständnis der Unterschiede zwischen Krebs und gesunden Zellen mit dem Ziel diese Unterschiede therapeutisch auszunutzen.

Krebs- und gesunde Zellen unterscheiden sich in ihrem **Metabolismus.** Die meisten Krebszellen zeigen eine höhere Glykolyse, die sich in einer starken Laktatausscheidung auch in Gegenwart von Sauerstoff zeigt, der wohlbekannte „Warburg-Effekt“. Darüber hinaus werden die Rolle des Citratzyklus und die Rolle des Glutaminstoffwechsels intensiv diskutiert. Klassische Metabolitmessungen liefern nur eingeschränkte Ergebnisse, die vorsichtig interpretiert werden müssen. Das ändert sich durch die Verwendung stabiler, schwerer Isotope. In dieser Arbeit wurde eine Methode etabliert um Veränderungen im Kohlenstoff-Stoffwechsel in menschlichen Tumormodell-Zelllinien mit Hilfe von stabilen Isotopen zu messen. Die Verwendung verschiedener Susbtrate, wie Glukose oder Glutamin, kann somit unter verschiedenen Konditionen verglichen werden. Mit dieser Methode konnte eine starke glykolytische Aktivität, eine enge Kopplung von Pyruvat und Laktat und ein unvollständiger Citratzyklus gezeigt werden.

Krebszellen sind weiterhin charakterisiert durch ein **unbegrenztes Wachstum.** Während verschiedener Phasen des Zell-Zyklus können unterschiedliche metabolische Profile erwartet werden. Das wurde überprüft durch Anwendung der etablierten Methode in verschiedenen Phasen des Zellzyklus von synchronisierten Zellen. Zusätzlich wurde die Protein-Neusynthese mit Hilfe eines „pulsed SILAC“ Ansatzes bestimmt.

Beide Faktoren, erhöhte Glykolyse und permanentes Wachstum sind **potentielle Ziele für Krebstherapien.** Die etablierte Methode ist perfekt geeignet um kurzfristige Veränderungen des Stoffwechsels zu beobachten. Damit können direkte Wirkungen auf die Enzyme von langfristigen metabolischen Umstrukturierungen unterschieden werden. Mit diesem Ansatz wurden drei verschiedene mögliche Inhibitoren der Glykolyse getestet und verglichen, 3-Brompyruvate, Glyceraldehyd und 2-Deoxyglukose. Die beobachteten Effekte spiegeln zum Teil bekannte Effekte wider, liefern aber auch neue Hinweise und stärken die Kritik an 2-Deoxyglukose als selektiven Inhibitor der Glykolyse.

Die gleichen Methoden und Strategien die in Zellkulturproben entwickelt wurden können schließlich auch in ***in vivo*** **Mäuse Modellen** benutzt werden. Der kurzzeitige Einbau von stabilen Isotopen in Intermediate des Stoffwechsels lieferte Hinweise über die notwendigen Zeiträume und über die verschiedenartige Nutzung von Glukose und Glutamin in Mäusen die als Modelle für menschlichen HCC-Tumor dienen.

D – TABLE OF CONTENT

E - ABBREVIATIONS USED

µM	micromolar
2DG	2-deoxglucose
2DG-P	2-deoxyglucose-6-phosphate
3PGA	3-phosphoglyceric acid
aKG	alpha-Ketoglutarate
ATP	adenosinetriphosphate
BrPyr	3-Bromopyruvate
CCM	central carbon metabolism
CI	confidence interval
Cit	citrate
COV	coefficient of variation
Da	Dalton
D-GA	D- isomer of glyceraldehyde
DHAP	dihydroxycetonephosphate
DMEM	Dulbecco's Modified Eagle Medium
DMSO	dimethylsulfoxid
DNA	deoxyribonucleic acid
DTT	dithiothreithol
EC_{50}	effective concentration leading to 50% inhibition
F16BP	fructose-1,6-bisphosphate
F1P	fructose-1-phosphate
F6P	fructose-6-phosphate
FBS	fetal bovine serum
FDG	2-fluorodeoxy-glucose
FSC	forward scatter
G6P	glucose-6-phosphate
GA	glyceraldehyde
GAP	glyceraldehyde-3-phosphate
GAPDH	glyceraldehyde-3-phosphate dehydrogenase
GC-MS	gas chromatography coupled to mass spectrometry
Glc	glucose
Glc-P	glucose-phosphate
Gln	glutamine
Glyc3P	glycerol-3-phosphate
GMD	Golm Metabolome Database
H/L-ratio	heavy-to-light ratio

HCC	hepatocellular carcinoma
HEK293	human embryonic kidney cells
HEPES	4-(2-hydroxyethyl)-1-piperazineethanesulfonic acid
HK	hexokinase
IAA	iodoacetamide
KCl	potassium chloride
Lac	lactate
LC-MS	liquid chromatography coupled to mass spectrometry
L-GA	L- isomer of glyceraldehyde
m/z	mass-to-charge ratio
MCW	methanol:chloroform:water
MeOH	methanol
MeOX	methoxamine (-group)
MIF	mass isotopomer fraction
mM	millimolar
MS	mass spectrometry
MSTFA	N-methyl-N-[trimethylsilyl]trifluoroacetamide
NaCl	sodium chloride
NaOH	sodium hydroxide
NMR	nuclear magnetic resonance
NOI	natural occuring isotopes
PBS	phosphate buffered saline
PGI	phosphoglucoisomerase
PI	propidium iodide
pSIRM	pulsed stable isotope resolved metabolomics
Pyr	pyruvate
R5P	ribose-5-phosphate
RI	retention index
RT	room temperature
Ru-5P	ribulose-5-phosphate
SILAC	stable isotope labeling with amino acids in cell culture
SIRM	stable isotope resolved metabolomics
SSC	sideward scatter
T98G	brain glioblastoma cells
TCA-cycle	tricarboxylic acid cycle
TMS	trimethylsilyl (-group)
u-^{13}C	compound substituted with ^{13}C in all carbon atoms

1. INTRODUCTION

1.1. Metabolomics and the central carbon metabolism

Metabolites are the intermediates of catabolic and anabolic processes and build the connection between utilization of nutrients and the production of cellular material, energy and waste products. Metabolites are differentiated from polymeric compounds like proteins, nucleic acids or polysaccharides, which act as structural or functional components, genetic material or energy storage. Most often an upper limit of 1000 Dalton is used to define metabolites (van der Werf et al., 2007). The study of metabolite composition is called metabolite research or metabolomics, a terminology similar to genomics or transcriptomics on one side and to point out a widespread approach, aiming at the identification and quantification of as many compounds as possible (Dunn, 2008; Fiehn, 2002; Kell, 2004)

The number of possible metabolites varies between sources; the human metabolome database (HMDB) currently lists 2414 endogenous compounds, defined as "a metabolite that is synthesized by the enzymes encoded by our genome or our microfloral genomes" (Wishart et al., 2009). Additionally the Recon2 network, a large comprehensive model of all possible metabolic products, contains 2626 compounds. (Thiele et al., 2013). These values seemed to be a realistic estimation about the possible, detectable space of compounds, other authors report up to 20.000 compounds, including all the secondary metabolites in plants. If all possible combinations in lipids (e.g. triacylglycerols) were taken into account more than 100.000 different compounds are possible (Dunn et al., 2011; Han and Gross, 2005).

Due to the diverse chemical structures, from small, charged molecules like fumarate to large, polar compounds like trehalose, or large unipolar compounds like cholesterol, also the physical and chemical properties of the compounds differ. The same is true for the concentration of compounds, which range from highly abundant storage compounds or important building blocks to hormones which are only produced in some cells, in some situations.

Measuring all metabolites with a single method is very challenging and hard to achieve. Most untargeted methods are well suited for a certain subset of compounds, depending on their properties and concentration ranges. Among the different techniques, mass-spectrometry (MS) is widely used, and most often in combination with chromatographic separation, like gas-chromatography (GC), liquid chromatography (LC) or capillary electrophoresis (CE) (Weckwerth, 2003). The combination of chromatography and mass spectrometry offers reliable separation and identification of multiple compounds in complex mixtures like biological samples (Dunn et al.,

2011). However, even within one method, different extraction and derivatization methods can optimize the detection of different classes of compounds (Gullberg et al., 2004).

In contrast to secondary metabolism that is only active in certain cells, tissues or at distinct time points the primary metabolism is essential to maintain basic cell functions. It covers the most important pathways of nutrient conversion like glycolysis, pentose-phosphate pathway, TCA cycle, and amino acid uptake and conversion. The importance of these pathways can be seen by the fact that these pathways are found nearly identically in bacteria, plants and higher organisms. To account for the function as central hub in the cell between catabolic and anabolic processes the primary metabolism it is also called central metabolism and to further point towards the utilization of carbon atoms by these reactions, as monitored by ^{13}C measurements, the term central carbon metabolism (CCM) is used (Chassagnole et al., 2002; Maier et al., 2010)

1.2. The use of stable isotopes for flux measurements

Within the last decades, the improvement of bioanalytical techniques enabled the use of stable isotope labeled metabolites to track the individual metabolic routes *in vitro* and *in vivo*. The isotope incorporation is measured as a mass-shift by the mass spectrometer or by the spin induced by the odd carbon numbers by NMR (Fan et al., 2012). The introduction of heavy isotopes can add three main information layers that are not detectable by "static metabolomics" (Fig. 1).

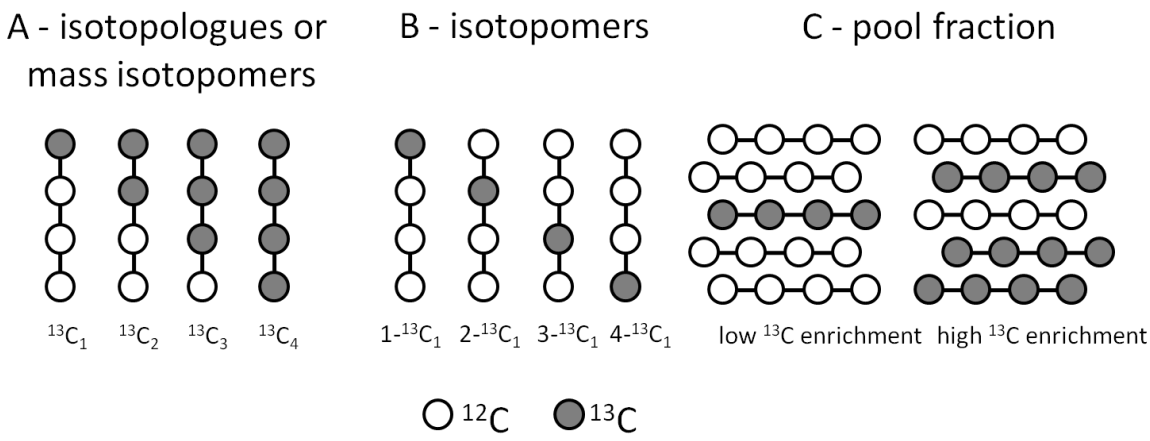

Fig. 1 - The different layers of information that can be deduced from ^{13}C incorporation studies. A – isotopologues differ in their amount of incorporated carbon atoms. B – isotopomers contain the same amount of carbon atoms on different positions. C – ^{13}C pool fraction indicates the fraction of ^{13}C compounds in the total pool size.

The term isotopologue refers to compounds with different numbers of incorporated ^{13}C carbon atoms, whereas the term isotopomers (Fig. 1B) refers to different entities of one compound with the same amount of ^{13}C, but on different positions (Fan et al., 2012; Hellerstein and Neese, 1999; MacNaught and Wilkinson, 1997) Sometimes the term mass isotopomers is used instead of isotopologues to describe a family of isotopes with the same mass, regardless of their composition (Hellerstein and Neese, 1999). The formation of isotopomers and isotopologues is dependent on the used substrates and the pathway usage: For example u-^{13}C glucose typically introduces three carbon atoms into pyruvate that will introduce two carbon atoms into the TCA-cycle via acetyl-CoA (pyruvate dehydrogenase) or three carbon atoms by the action of pyruvate carboxylase, to replenish the TCA-cycle at the level of oxaloacetate. Furthermore, in many cases the information about the fraction of ^{13}C labeled compounds within the total pool of a measured metabolite is important (Fig. 1C) as this represents the enzymatic activity within the network, in other words the turnover of this metabolite.

Isotopologues can be differentiated with GC-MS by the intensity of mass shifts introduced by the heavy atoms. In addition, mass fragments originating from different parts of the molecules contain positional information and can be used to identify isotopomers. Finally, the amount of labeled compound in the pool (fig. 1C) is encoded in the ratio of the heavy to the light m/z, for example 323 to 319 for glucose (Fig. 2). Tools other than GC-MS could also be used to determine the heavy carbon incorporation. The mass shift found with LC-MS measurement identifies the isotopologues and the intensity of the labeled pool size. If fragmentation is possible the MS/MS-fragments contain isotopomeric (positional) information as well. Carbon positions can also be elucidated from spin-couplings within NMR measurements. (Lane et al., 2009; Zwingmann et al., 2001). When heavy isotopes are introduced into a molecule, the measured mass spectrum contains a mass-shift in one or multiple positions, depending on the mass difference of the incorporated isotopes, their number and position (Fig. 2).

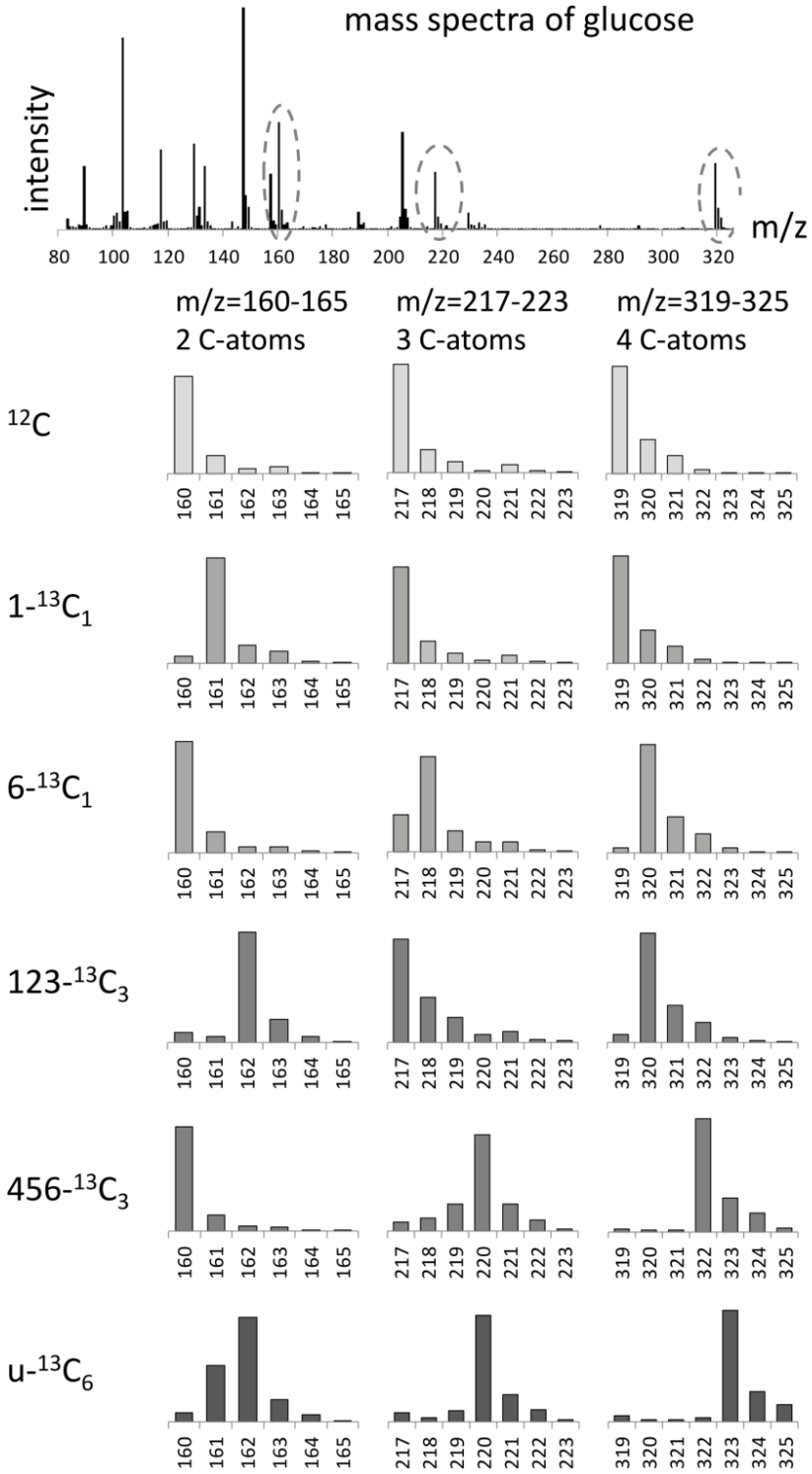

Fig. 2 - Mass-shift in the mass spectra of three fragments of glucose induced by different commercial available ^{13}C-states of the compound and measured by mass spectrometry. Top: Mass spectra of glucose (measured as the 5TMS 1MeOX derivative) with indicated positions of the shown fragments. Each fragment contains a different number of carbon atoms and represents a different part of the molecule. The effect of different ^{13}C-states (on the left side) to each of the fragment masses is shown on the right. ^{12}C indicates unlabeled glucose that contains only naturally occurring isotopes.

Fan and co-workers introduced the use of stable isotope resolved metabolomics (SIRM) of cancer cell metabolism; ^{13}C labeled glucose was used to decode the metabolic properties of lung cancer cells *in vivo* (Fan et al., 2009). We have further developed this concept to dynamically analyze cellular metabolism by pulsed stable isototope resolved metabolomics (pSIRM). The use of pulse labeling and the analysis of stable isotope incorporation in a non-stationary phase allow using fully labeled substrates, as they would give no information in stationary experiments (Noh and Wiechert, 2011). This simplifies the analysis of isotope incorporation specifically for glycolysis. For metabolic pathways like the TCA cycle, distinct positions of the heavy isotopes may encode the individual routes within the network (DeBerardinis et al., 2007; Des Rosiers et al., 1994).

Flux analysis with stable isotopes matured in the field of biotechnology to understand the effect of genetic engineering in bacteria and other microbes. This resulted in adaptations to the special characteristics of microbial metabolism: (I) many microbes have the capability to grow in minimal media with glucose as the sole carbon source, (II) due to their small size they offer a high surface to volume ratio which enables a rapid transport across their membranes, (III) they also possess short generation times. After some hours of ^{13}C incorporation and multiple cell doublings a stable, "stationary" equilibrium of isotope enrichment is achieved. The method of choice for microbial flux measurements is to feed cells with a mixture of ^{13}C isotopes (e.g. 1-$^{13}C_1$-glucose, u-^{13}C-glucose, and ^{12}C glucose) and to elucidate the labeling pattern within protein-bound amino acids. With the knowledge of the network structure, the label within the core metabolism (e.g. glycolysis, TCA cycle) is deduced from the resulting labeling pattern (Zamboni et al., 2009). This approach is robust, the biomass delivers enough amino acids to measure label pattern with reliable intensity and most descriptive fragment masses are identified (Antoniewicz et al., 2007). Further on, software tools were developed to readily calculate fluxes from these data (Zamboni et al., 2005). In contrast, to monitor soluble metabolites in their transient, incomplete labeled state, the quenching of cellular metabolism has to be performed within seconds after introducing ^{13}C into the bacterial culture system (Noh et al., 2007).

The concept of instationarity is illustrated in Fig. 3. After switching to ^{13}C labeled substrates it takes some time until a stable state is reached, which is defined as no (detectable) further increase in label incorporation. Additionally with increasing time the completeness of label incorporation might increase, defined by the number of heavy carbons within the metabolites. Completeness and stationarity are independent from each other, substituting only one of many potential carbon sources, or labeling with incomplete labeled substrates (as 1-^{13}C-glucose) can lead to an incomplete but stationary labeling. With only a single injection of a labeled substrate,

stationarity will never be reached as the compound is consumed and is therefore not able to introduce further labeled carbon atoms into the system. (Fig. 3 - right).

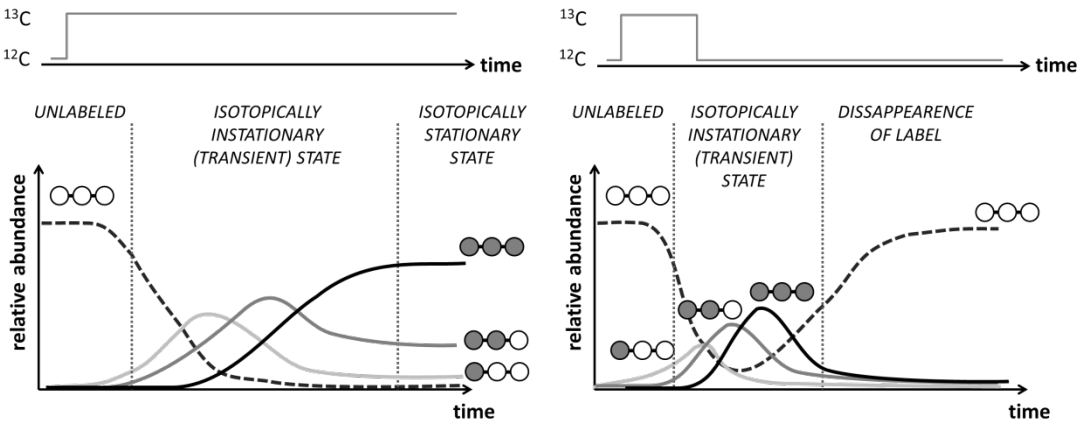

Fig. 3 – Difference between stationary and instationary labeling. A permanent support with ^{13}C-sources (left) lead to a stationary labeling state, characterized by no further increase of label incorporation. Until this state is reached, a transient state of instationarity can be measured. Furthermore with increasing time the amount of incorporated heavy carbon atoms (dark) within the molecules might increase. In contrast to that, a short replacement of ^{12}C- by ^{13}C-sources cannot deliver stationarity, as the introduced heavy carbon atoms further dilute in the system. Inspired by (Wiechert, 2001).

Mammalian cell cultures possess different preconditions for flux analysis than microorganisms. The growth medium is more complex and contains multiple substrates. The generation time is significantly longer (around 24 hours) and further cellular processes can be energy demanding or require precursors of biomass production. Additionally, the compartmentation increases the complexity for mathematical modeling (Zamboni, 2011). A stationary labeling fixed in the biomass may be obtained after much longer incubation times and will be more difficult to interpret. In this case the instationary or pulsed approach is the method of choice. Therefore, the incorporation of ^{13}C into metabolites is measured within a short time scale (minutes) after introduction of ^{13}C substrates. This decreases the costs and the time necessary for the analysis and effectively shrinks the number of variables in the system. The number of compounds that are labeled within a short time frame is smaller than the total numbers of measured metabolites, as only those metabolites will be found labeled that are closely connected to the substrate in the highway of CCM.

1.3. The role of the cell cycle

The cell cycle describes the processes that cells undergo in order to carry out cell division. Shortly after previous cell division the daughter cells are in the G1 (gap 1) phase; they grow to their final size and synthesize material to rebuild their proteins, cell membranes and storage. This period can be the longest period of the cell cycle. During S-phase (synthesis) they duplicate their DNA content, whereas in the G2 phase (gap-2) the cells check if DNA doubling was successful and further prepare to divide. The M-phase (mitosis) is the moment of final division. This is the shortest period and can be further separated into sub-phases, starting from condensing the DNA to separating the daughter cells. Finally, differentiated cells can leave the cell cycle at the G1-stage into a separate phase which is called the G0 arrest; the name indicates that this phase can last months or years in contrast to the similar G1 phase. Cancer cells continuously pass through the cell cycle, even under non-optimal conditions like the absence of growth signals and mistakes during DNA synthesis (Hanahan and Weinberg, 2011).

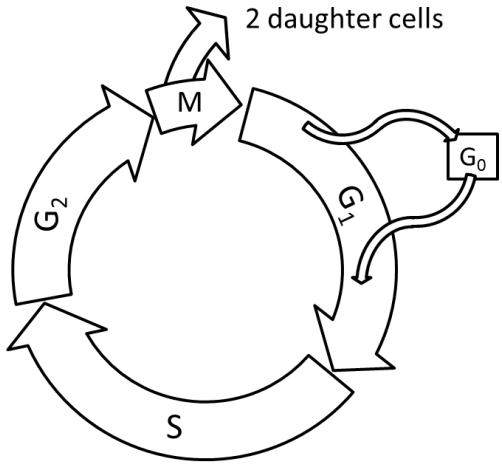

Fig. 4 - The cell cycle.

A widely used technology to measure cell cycle distributions is flow cytometry, in which the DNA content of individual cells is quantified by staining the DNA with fluorophores like propidium iodide (PI) (Darzynkiewicz et al., 2004). The amount of DNA in cells in G1 phase will give a certain signal, which increases during S-phase and has a doubled intensity after the completion of S phase. The fraction of cells with doubled DNA content is attributed to the G2/M phase, including both the G2 and the much shorter M-phase. Other methods measure cell cycle activity by the fraction of cells in S-phase by the incorporation of a thymidine analogue (Dolbeare et al., 1983) or the characteristic expression of cell cycle dependent proteins (Gong et al., 1995; Juan et al., 1996).

Several methods exist to arrest and enrich cells in various stages of the cell cycle, including the use of different drugs or the withdrawal of serum or essential amino acids (Jackman and O'Connor, 2001).

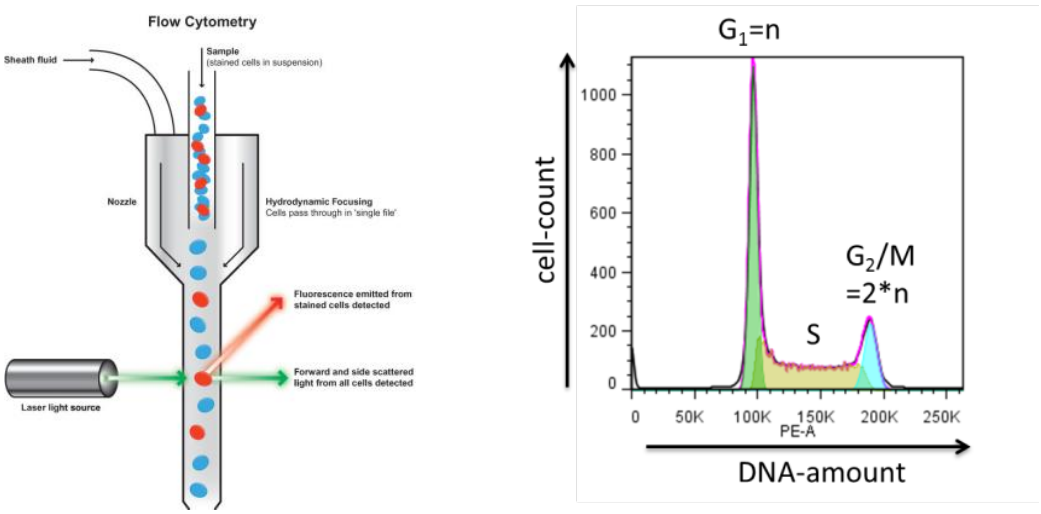

Fig. 5 - Detection of cell cycle phases by flow cytometry. Left: principle of measurement. Cells are transported by a stream of fluid and isolated to individually flow through the detection cell. There cells pass one or more laser-beams, the signals as light scattering and fluorescence intensity are recorded. Right: representation of cell-cycle distribution measured by flow cytometry. The DNA is stained with a fluorophore. The amount of fluorescence is proportional to the amount of DNA (x-axis). Cells in G1 phase of the cell cycle give a defined amount of signal intensity; the number of cells is recorded and plotted on the y-axis. After duplication of DNA and before dividing into 2 cells (G2/M phase) the signal intensity doubled. The intermediate intensities represent cells in the S-phase with a DNA amount between the normal and the doubled state.

1.4. The metabolic difference of cancer cells

Driven by the motivation to heal cancer, researchers started to investigate the metabolic differences between healthy and cancer cells, aiming to employ them as therapeutic targets (Linehan and Rouault, 2013; Pelicano et al., 2006). Especially glucose uptake is elevated in most cancer cells. This property is used for *in vivo* diagnosis via FDG-PET screening (Gambhir, 2002; Groheux et al., 2013). Most cancers do not use their excess amounts of glucose effectively and secret the majority of their glucose as lactate, even in the presence of sufficient oxygen, an effect known as the “Warburg effect” (Garber, 2004; Hsu and Sabatini, 2008; Pedersen, 2007; Warburg, 1956).

Stable isotope resolved metabolomics (SIRM) of cancer cells already revealed interesting differences in their pathway usage compared to other cells, for example the diversion of high amounts of carbon to glycine and serine by genetic amplification of phosphoglycerate dehydrogenase (Locasale et al., 2011). Recently the presence of reductive carboxylation of ketoglutarate described earlier as reaction of the reverse TCA-cycle was identified to be important in hypoxic cancer cells (Metallo et al., 2012). A systematic evaluation of cancer metabolism is still

lacking. Epecially the *in vivo* usage of different substrates must be explored in much greater detail by SIRM approaches. A higher uptake and turnover of substrates could be readily monitored by a higher incorporation of carbon-13 into metabolite pools compared to the non-cancer conditions. (DeBerardinis et al., 2007).

1.5. Glycolytic inhibition as a potential therapeutic target against cancer cells

One of the first strategies for treating cancer was targeting their continuous growth by inhibiting synthesis of precursors for DNA synthesis, e.g. by 5-fluorouracil or methotrexate (Ewald et al., 2008; Tennant et al., 2010). With the discovery of an elevated glycolysis another strategy was promoted targeting the metabolic alterations between cancer and healthy cells. Specifically, the higher dependency of cancer metabolism on glucose or glutamine and the lower flexibility by being unable to use other substrates appeared to be a worthwhile target (Chen et al., 2007; Granchi and Minutolo, 2012; Pelicano et al., 2006; Xu et al., 2005b).

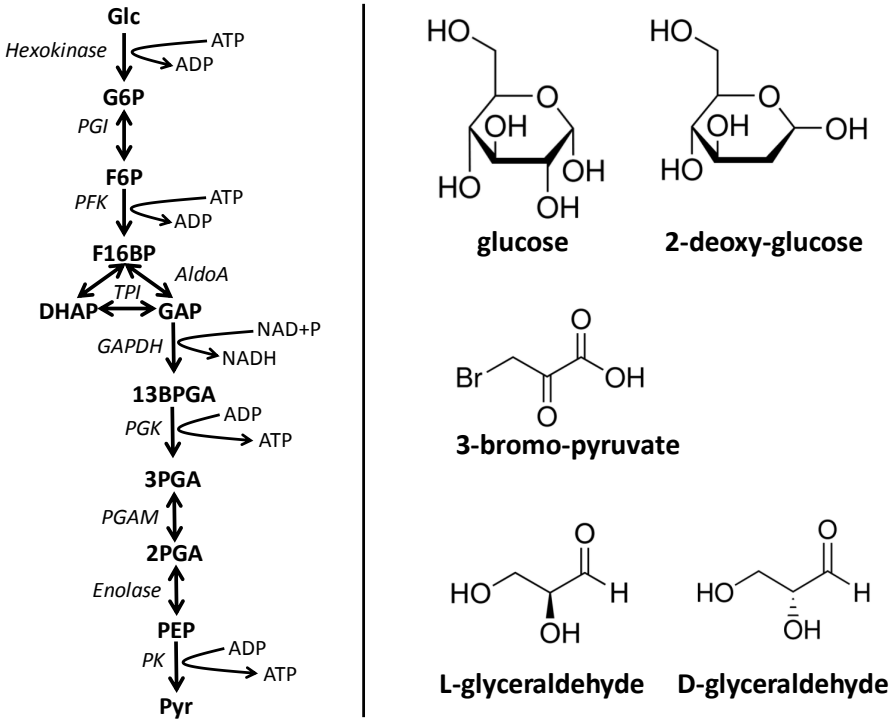

Fig. 6 - Scheme of glycolysis (left) and structure of glucose and potential inhibitors of glycolysis (right).

1.5.1. Inhibition by 2-deoxyglucose

2-deoxyglucose (2DG) is a modified form of glucose, where the carbon at position 2 does not contain a hydroxyl-group, which limits the potential of this compound for some reactions compared to normal glucose. First studies of potential function of 2DG as an inhibitor of glycolysis started in the fifties of the last century, when researchers elucidated the structure and function of glycolysis. It was found that 2DG is phosphorylated by hexokinase with approximately the same speed as glucose (Sols and Crane, 1954), if both are present at the same time the phosphorylation is in favor of glucose (Woodward and Hudson, 1955). Its product 2-deoxyglucose-6-phosphate (2DG-P) is not a substrate for the following reactions and therefore accumulates inside cells. It additionally does not inhibit the hexokinase-reaction allosterically so 2DG was claimed to be the best substrate to measure the activity of hexokinase (Sols and Crane, 1954). Wick and Drury showed that ^{14}C-labeled 2DG was not oxidized in mice, influenced the glucose-disappearance in blood but not the oxidation of acetate (Wick et al., 1957). Uptake of 2DG into cells is insulin-dependent and decreased glucose disappearance from blood (Wick et al., 1955). It was shown that 2DG-P inhibits at least the activity of phosphoglucoisomerase (PGI) (Wick et al., 1957), but function also as an competitive inhibitor of hexokinase (Bachelard et al., 1971). Also glucose-uptake was reported to be affected, with the latter one expressing a K_M-value twice as high as the one for glucose (10m M vs. 5 mM) (Bachelard, 1971). Despite being promising *in vitro* or in cell-culture, *in vivo* applications only with 2DG failed (Tannock et al., 1983), but it was shown that 2DG increased sensitivity of tumors to other drugs, so it remains a valuable tool in combination treatment (Cheong et al., 2011; Goldberg et al., 2012).

A further modification of 2DG, 2-deoxy-fluoro-glucose (FDG) is used in cancer diagnostics to monitor an elevated glucose uptake by trapping this compound inside cells and measure fluoride by positron emission tomography (PET-CT) (Gambhir, 2002; Groheux et al., 2013).

1.5.2. Inhibition by glyceraldehyde

Glyceraldehyde (GA) is the most interesting compound among the potential inhibitors of glycolysis. It is a natural product of fructose breakdown and also linked to glycerol metabolism (Hagopian et al., 2008; Sillero et al., 1969), and in its phosphorylated state as glyceraldehyde-3-phosphate (GAP) it is part of glycolysis.

It was found already in 1929 that glyceraldehyde inhibits anaerobic fermentation in Jensen sarcoma, without affecting respiration in tumor or normal rat tissue (Mendel, 1929). Bruno Mendel concluded in this report that “it is not unlikely that glyceraldehyde which inhibits, in low

concentrations, the anaerobic fermentation of cells without affecting their respiration prevents the formation of carcinomas in normal organism". Some years later it was postulated that this effect is stereospecific, with different activity for the D- and the L-isomer (Needham and Lehmann, 1937). In fact after synthesis of pure L-isomer (Baer and Fischer, 1938) it could be shown that the L-isomer is more effective in inhibition of anaerobic fermentation (Mendel et al., 1938). The enzyme aldolase which typically splits fructose-1,6-bisphosphate (F16BP) to dihydroxyacetonephosphate (DHAP) and glyceraldehyde-3-phosphate (GAP), is also able to fuse DHAP to a variety of compounds: With D-GA fructose-1-phosphate is formed, with L-GA the uncommon sugar sorbose-1-phosphate (Meyerhof et al., 1936). Lardy *et al* showed that sorbose-1-P formed by the L-isomer indeed inhibited anaerobic formation by inhibiting the hexokinase reaction. The sugar was assumed to bind to the allosteric pocket in a similar way as glucose-6-P (Lardy et al., 1950). After some successful *in vivo* applications (Bennett and Connon, 1966; Warburg et al., 1963) and some applications without effect (Brock and Niekamp, 1965; Schramm, 1965) this compound passed into oblivion before it received a second chance as it stimulates insulin secretion in pancreatic beta cells (Hellman et al., 1974; Jain et al., 1975; Schauder et al., 1977).

1.5.3. Inhibition by 3-bromopyruvate

3-bromopyruvate (BrPyr) is the most recently discovered glycolytic inhibitor. It is taken up by the cells with the monocarboxylic acid transporter (MCT-1) and sensitivity to this compound correlates with high MCT1 expression (Birsoy et al., 2013). BrPyr was shown to reacts with sulfhydryl-groups in enzymes; glyceraldehyde-3-phosphate dehydrogenase (GAPDH) was identified as one important and very specific target of pyruvylation by BrPyr (Ganapathy-Kanniappan et al., 2009). Another enzyme that is alkylated by BrPyr is isocitrate lyase (ICL) in *E.coli* (Ko and McFadden, 1990). There were some promising *in vivo* experiments reported, showing that this compound is able to decrease or inhibit tumor growth in mice and rabbits (Geschwind et al., 2002; Kim et al., 2007; Vali et al., 2008) and recently a study in a single human patient was performed (Ko et al., 2012).

1.6. Aim of this study

In this dissertation, a method was established that allows the quantification of changes in the carbon routing of mammalian cancer cell models. The carbon routing and the use of available substrates were compared under different conditions to gain a deeper understanding of the underlying mechanisms. The data analysis was based on previously established tools and strategies like GC-MS based metabolomics, data analysis with ChromaTOF (LECO) and data alignment with MetMax (Kempa et al., 2009). The strategy included sample generation and data processing like the extraction of isotope masses, correction for the natural occurring heavy isotopes, and combining labeling data with metabolite quantities.

The strategy was then employed and tested to describe changes in the metabolic program at different stages of the cell-cycle. Furthermore it was tested if short-termed effects, on a time scale of minutes, induced by small-size inhibitors of glycolysis can be monitored following this approach. The metabolic changes on the whole cell-level might give valuable new insights into the mode of action of glycolytic inhibitors proposed in the literature and obtained usually *in-vitro* or on longer time-scales.

2. CHEMICALS AND MATERIAL

2.1. Lab Equipment

	Instrument	Type	Company
general lab equipment	centrifuge	5417R / 5430	Eppendorf - Hamburg, Germany
	centrifuge	Multifuge 3SR+	Thermo Scientific
	pipettes	Eppendorf Research	Eppendorf - Hamburg, Germany
	thermomixer	Thermomixer comfort	Eppendorf - Hamburg, Germany
	vortex	Vortex-Genie2	Scientific Industries - Bohemia, USA
	speedVac	CHRIST ALPHA 2-4LOplus	CHRIST Osterode am Harz, Germany
	rotator	Rotator SB3	Stuart
	Balance	XS205	Mettler Toledo
	table centrifuge	Micro centrifuge IR	Roth
	Tissuelyzer	Precellys 24	Bertin technologies
cell culture	Clean Bench	HeraSafe KS 18	Thermo Scientific
	Centrifuge	Multifuge 1SR	Thermo Scientific
	Incubator	CB210	Binder - Tuttlingen, Germany
	Cell counter	TC10 Automated Cell counter	BIO-RAD - Hercules, USA
	Centrifuge	Multifuge 3SR+	Thermo Scientific
	Microscope	Axiovert 40C	ZEISS - Oberkochen, Germany
	Microscope	Observer.X1	ZEISS - Oberkochen, Germany
	Water Bath		

2.2. Materials

2.2.1. Cell lines:

HEK293 a human kidney cell line immortalized with adenovirus 5 DNA (ATCC Cat. No CRL-1573) was supplied by Dr. Markus Landthaler at the MDC-Berlin.

T98G a human brain glioblastoma cell line (ATCC Cat.No. CRL-1690) was supplied by Dr. Ulrike Ziebold at the MDC-Berlin.

2.2.2. Chemicals for cell culture

Full name	Short name	Supplier	Prod.No
Glucose-free Dulbecco's modified Eagle Medium	DMEM (no Glucose)	Life – Technologies	11966-025
Dulbecco's Modified Eagle Medium (DMEM) High glucose	DMEM (high glucose)	Life – Technologies	41965039
DMEM no glutamine, no glucose, no sodium pyruvate, no arginine	SILAC-DMEM	Genaxxon	C4230.0500
Foetal Bovine Serum	FBS	Life – Technologies	10270106
Dialyzed FBS for SILAC 550 ML	dial. FBS	Fisher Scientific	11968241
Penicillin-Streptomycin, Liquid	Pen/Strep	Life Technologies	15140-122
D-(+)-Glucose	Glucose	Sigma	G8270-100G
L-Glutamine 200 mM (100X), liquid	Glutamine	Life – Technologies	25030024
$^{13}C_6$-L-Arginine-HCl	medium Arginine	Eurisotop	CNLM-539-H-1
$^{13}C_6$ -$^{15}N_4$-L- Arginine-HCl	heavy Arginine	Eurisotop	CLM-2265-H-1
4.4.5.5-D4-L-Lysine, 2HCl	medium lysine	Eurisotop	DLM-2640-1
u-^{13}C, u-^{15}N L- Lysine, 2HCl	heavy lysine	Eurisotop	CNLM-291-H-1
0,05% Trypsin- EDTA	Trypsin	Gibco	25300-054
Trypan Blue Stain	Trypan Blue	Life Technologies	15250061

2.2.3. Chemicals for metabolite harvest and measurement

Name	abbr.	Supplier	prod.No
Methanol Hypergrade	MeOH	Merck	1.06035.2500
Chloroform	$CHCl_3$		
Methoxyamine hydrochloride	MeOX	Sigma-Aldrich	SAFA226904
Pyridin , waterfree	Pyridine	Sigma-Aldrich	270970-100ml
MSTFA, 20x1 mL	MSTFA	Machery Nagel	701270201
Decane	C10	Sigma-Aldrich	A1457116
Dodecane	C12	Fluka	44020
Pentadecane	C15	Aldrich	P340-6
Heptadecane	C17	Fluka	51578
Octadecane	C18	Fluka	74705
Nonadecane	C19	Fluka	74160
Docosane	C22	Aldrich	134457
Octacosane	C28	Aldrich	O504
Dotriacontane	C32	Fluka	44255
Hexatriacontane	C36	Aldrich	H12552

3. METHODS

3.1. Growth media composition for cell culture

- DMEM: DMEM (no glucose), supplemented with 10% FBS, 1% Penicillin-Streptomycin (Pen/Strep) and 2.5g/l steril filtered glucose
- Q-Medium (high glutamine): DMEM, supplemented with 10% FBS, 1% Pen/Strep, 2.5g/l steril filtered glucose with additional 2mM glutamine
- SILAC-Medium: SILAC-DMEM, supplemented with 10% dialyzed FBS, 1% Pen/Strep, 2.5g/l sterile filtered glucose, the amount of glutamine corresponding to the defined concentration in the medium (normal DMEM=4 mM, Q-Medium =6mM), and completed by addition of $^{13}C_6$-$^{15}N_2$ L-lysine and $^{13}C_6$-$^{15}N_4$ L-arginine.

3.2. Standard cell culture

Cell handling for cultivation purpose was done under aseptical conditions by working under a laminar air-flow. To freeze cells for long-term storage the old media was removed, cells were trypsinized and transferred to DMEM without glucose and antibiotics and with 10% FBS. After centrifugation for 2min at 1300 rpm the pellet was resuspended in 2ml of DMSO diliuted 1:10 with PBS. The suspension was transferred to cryotubes and in a bath of propylalcohol ("Mr Frosty") stored in a -80°C deep freezer overnight. The alcohol helps to maintain a slow temperature decrease of ~1°C per minute. The next day cells were transferred in nitrogen tanks and stored at -180°C.

Cells were thawed by putting the cryotubes into a water bath (37°C) to rapidly increase the temperature of the cells and transfer the content of the tube to a 10 cm cell-culture plate (Greiner bio-one) that already contains 10ml of prewarmed growth media. After 1 day cells were split or media was exchanged to remove remaining DMSO.

Cell were further cultivated in 10 or 20 cm cell-culture plates (Greiner bio-one) in glucose-free DMEM supplemented with 2.5g/l glucose, 10% FBS, 1% Pen/Strep and cultivated in an incubator (Binder) at 37°C with a humidified 5% CO_2-atmosphere. Every 2-3 days cells were trypsinized and passaged with appropriate split ratios (1:3 or 1:4 for HEK293 cells and 1:4 - 1:6 for T98G cells).

3.3. Sample preparation for metabolomics

3.3.1. Standard metabolomic harvest for adherent cells

Experiments and harvests were performed typically after 1 or 2 days of seeding, when cells reached a confluency of around 70%. The seeding densities were adapted in advance for each cell line. To maintain a highly active metabolism the growth media was replaced 24 and 4 hours prior harvesting, with 10 and 5 ml, respectively. With this strategy starvation by decreased nutrient availability and the accumulation of metabolic end-products is reduced.

Media was sucked or poured off and replaced by 5ml of a prewarmed (37°C) wash buffer. The buffer was composed of 137mM NaCl, 3mM KCl and 5mM HEPES and was adjusted with NaOH to pH of 7.1-7.4. This buffer mimics the composition of PBS but replaces phosphate, which gives a peak in GC-MS measurements, by HEPES. Additionally this buffer contained the main nutrients glucose and glutamine, in the same concentration as in the growth media, typically 2.5 g/l glucose and 4mM glutamine. The presence of these nutrients was expected to avoid any signs of nutrient starvation even with short wash steps but removed all other components.

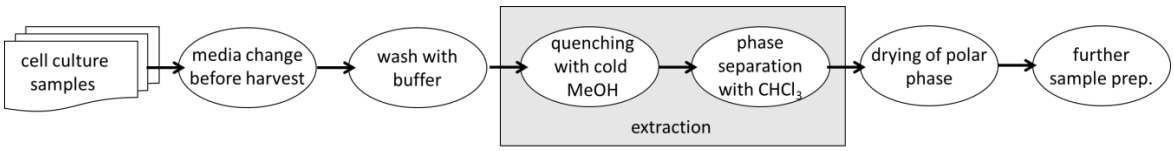

Fig. 7 – Workflow of cell harvest procedure.

Then the buffer was removed, followed by an immediate addition of 5ml prechilled (-20 to -40°C) 50% methanol. Cells were scratched with a cell-scraper, resuspended and transferred to a falcon filled with 1ml of chloroform. If necessary, cells were frozen at this point in liquid nitrogen, stored at -80°C and extracted at a later time. Extraction can be expected to start with the addition of methanol, by leakage of the cells and continues at scratching which damages cells. To further extract the intracellular metabolites the cell suspension was shaken for 30 minutes at 4°C and 750 rpm (Eppendorf thermomixer) with interspersed vortexing and centrifuged to establish a phase separation. 4.5 ml of the polar (upper) phase were transferred into a new falcon and dryed under vacuum. In order to perform an effective derviatisation the samples needed to be transferred to an Eppendorf tube; for that purpose a second extraction was performed. 530 µl of ice-cold 20% MeOH were added to each sample, and shaken at 4°C and 750 rpm with interspersed vortexing, until the pellet was completely dissolved. 2x 300µl were transferred into two different Eppendorf tubes and dryed under vaccum.

3.3.2. Standard metabolomic harvest for weakly adherent cells

Some cell lines like HEK293 cells do not attach strongly to the cell culture plate and do not sustain multiple washing steps. For these cells a different harvesting strategy was developed. First, cells were resuspended in their original growth media, followed by a first gentle centrifugation (200 x g, 3 minutes at room temperature). Then the supernatant was sucked off and cells were resuspended in 3.5 ml wash buffer (as described above), 1.5 ml was transferred into Eppendorf-tubes, followed by a short centrifugation (20 seconds) in a table centrifuge. Buffer was poured off and the pellet frozen in liquid nitrogen. Frozen cell pellets were extracted with 500µl ice-cold methanol:chloroform:water (MCW) (5:2:1) with breaking the cell pellet by a pipette tip, followed by 30 min of intensive shaking and vortexing. Half the volume of water was then added, samples were shaken again for 15 minutes, centrifuged and the polar phase was collected in full or split into 2 replicates. The sample was subsequently dried under vaccum.

3.3.3. Performing labeling experiments

To perform labeling experiments the standard workflow (section 3.3.1) was slightly modified. In the wash buffer either the glucose or glutamine was replaced by its u-^{13}C counterpart, to produce label buffer. The contact with the buffer was prolonged to allow an incorporation of the heavy carbon atoms. For this the sample was incubated up to 3 minutes at 37°C in presence of the label buffer. For time periods longer than 5 minutes a full label media was used. Basically this was DMEM with all other components but with u-^{13}C-glucose. This media was incubated for the given time at 37°C, followed by a short wash (20-30 seconds) with a label buffer as described above.

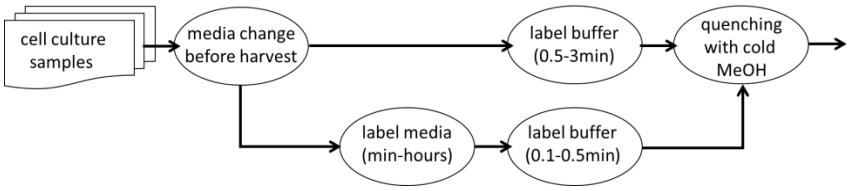

Fig. 8 – Modification of harvest procedure (Fig. 7) to introduce a ^{13}C-labeling. The short termed labeling is performed only in label buffer (above), whereas for longer time periods an incubation with full label media, followed by a short wash with label buffer is performed (below). Further sample preparation is the same for all, including unlabeled conditions (Fig. 7).

3.3.4. Preparation of the Ident-mix

Individual compounds were obtained in highest available purity from Sigma-Aldrich, VWR or Merck. Stock solutions of all compounds were prepared in 20% MeOH with 1mg/ml. Stock solutions of instable compounds (phosphorylated compounds) were prepeared fresh, other stocks could be prepared in advance and stored at -20°C. 4 falcon tubes were labeled and per copy of ident-mix 5µl of every compound were aliquoted into every 2 of these tubes to a defined scheme (Suppl. table 3). Usually up to 40 mixes were prepared, resulting in pipetting of 40 * 5µl = 200 µl of every compound into the falcons. Some compounds with small signal intensity were added in double the amount. During preparation, the mixtures were kept on ice. 50µl of the mixtures were aliquoted into labeled Eppendorf-tubes and dryed under vaccum.

3.3.5. Preparation of the Quant-mix

The preparation of the Quant-mix was similar to that of the Ident-mix. The Quant-mix was also prepared in multiple stocks, lasting some months. Stock solutions of all compounds were prepared in 20% MeOH with 1 mg/ml, except for fructose-1,6-bisphosphate and glutamic acid which were prepared in 2 mg/ml and glucose, lactic acid and erythritol which were prepared with 10 mg/ml. Predefined amounts of samples were mixed together into a single falcon at 4°C. As the samples were dried after preparation, the quantitiy of the compounds in the different Quant-mixes was defined by the volume of the aliquoted stocks. The summed up volume of all individual stocks was aliquoted and defines the undiluted 1:1 state. Aliquoting and drying exactly half of this amount produced the 1:2 dilution, drying one fifth the 1:5 dilutionand so on. Stocks with 1:1, 1:2, 1:5, 1:10, 1:20, 1:50, 1:100 and 1:200 were prepared, the 1:20 sample and below were prepared from an 1:20 dilution.

3.3.6. Derivatization

Chemical derivatization is necessary to increase volatility of polar compounds and enable their measurement on GC-MS (Halket et al., 2005) and was carried out by a protocol slightly modified from the one reported elsewehere (Roessner-Tunali et al., 2003). Dried extracts were dissolved in 20 µl of a 40 mg/ml methoxyamine hydrochloride-solution (MeOX) in pyridine and derivatized for 90 min at 30°C at constant shaking, followed by a 45 min. treatment with 80 µl of N-methyl-N-[trimethylsilyl]trifluoroacetamide (MSTFA) at 37°C. Per Milliliter of MSTFA, 20 microliters of a retention index standard mixture (n-decane, n-dodecane, n-pentadecane, n-octadecane, n-nonadecane, n-docosane, n-octacosane, n-dotriacontane, and n-hexatriacontane dissolved in hexane – concentration in mixture approx. 2 mg/ml) was added before trimethylsilylation. Samples were centrifuged (10 min., 14000 g) and supernatant was transferred into glass vials.

3.3.7. GC-MS measurement

0.8 microliter of sample was injected in splitless mode or with a split ratio of 1:5 into a Gerstel CAS4-injector, equipped with a baffled glass-liner (Gerstel). The Initial temperature of the temperature-controlled injection was 80°C, hold for 30 sec, followed by a ramp with 12°C/min to 120°C and then followed by a second ramp with 7°C/min to 300°C and a final hold time of 2 min. Gas chromatographic separation was performed on an Agilent 6890N (Agilent), equipped with a Varian VF-5ms-column of 30m length, 250 µm inner diameter and 0.25 µm film thickness (Agilent). The temperature of the oven starts at 70°C with a hold for 2 minutes, followed by a first temperature gradient with 5°C/min up to 120°C with a hold for 30 sec, followed by a second ramp with 7°C/min up to 350°C with a final hold time of 2 min. Separation was driven with helium as carrier gas, with a flow of 1.2 ml. Mass Spectrometric detection was performed on a LECO-Pegasus III- TOF-MS-System (LECO) with electron impact ionization at 70 volts with an ion-source and transfer-line temperature of 250°C. Spectra were recorded in a mass range of 60 to 600 Da with 20 spectra acquired per second and a detector voltage of 1750 V.

3.3.8. GC-MS data analysis

The vendor software ChromaTOF Version 4.42 (LECO Corp. St. Joseph – USA) was used for metabolite evaluation with the following parameters: baseline offset of 1, peak width of 4 s, signal to noise ratio of 20, peak smoothing of 11 data-points. Retention indices were calculated based on alkanes as retention index standards. The Golm Metabolome Database (GMD) modified with updated retention index information and expanded with new compounds was used for identification of metabolites (Kopka et al., 2005). For labeling experiments, a resampling was performed before data processing, to avoid deconvolution of isotope peaks. Data in this case were exported as peg-files with a resampling factor of 4, resulting in five recorded spectra per second, and reimported into ChromaTOF, and processed as described above. Quantification using external calibration curves was also performed with the quantification routine of ChromaTOF.

After manual verification of correct identification of compounds by the library search, peak information of identified compounds was exported as tab-separated txt-files, including: Name, quant mass, retention index, 1st dimension retention time, 2nd dimension retention time, area, concentration, match, reverse, quant signal/noise, type, concentration units and the peak true spectrum in absolute values.

For further data analysis the tool MetMax developed in cooperation with the MPIMP in Potsdam-Golm was used (Kempa et al., 2009). It combines the peak information (areas or quantities) of

different measurements of a data set and creates a data matrix (retention analysis mode). Additionally it is used to extract isotope intensities in predefined mass-ranges (isotope concentrator mode). The tool can be downloaded free of charge at http://gmd.mpimp-golm.mpg.de/apps/metmax

3.4. Flow cytometry for detecting cell cycle phases

Cells were grown in 10cm dishes and treated as described in the experimental sections. The media, which also contains all the swimming cells, was collected into a 13ml falcon. Two milliliter of prewarmed (37°C) trypsin was added to plate and cells were resuspended thoroughly. Cell suspension was transferred to the same falcon and mixed with the sampled media by inverting the falcon. Cells were centrifuged at 4°C and 1200 rpm for 5 minutes. The supernatant was sucked off and cells were resuspended in 10ml of ice cold PBS. Cells were centrifuged a second time at 4°C and 1200 rpm for 5 minutes. The supernatant was removed and cells were resuspended by dropwise addition of 1 ml icecold 80% ethanol. Doing the last step slowly is important for a good separation of individual cells. Pellets were left standing overnight at 4°C. If the measurement was not performed on the next day cells were stored at -20°C, otherwise the preparation was continued on the following day.

Cells were centrifuged for 10min at 1000 rpm and 4°C. The supernatant was discarded and cells were washed with 5ml icecold PBS. The suspension was centrifuged a second time for 5min at 1200 rpm and 4°C and the supernatant discarded a final time. RNAse A was dissolved in water to a concentration of 10 mg per milliliter and mixed 1:20 with PBS. The pellet was resuspended in 525µl of PBS with RNAse and incubated for 30 minutes at 37°C to digest double stranded RNA which might interfere with DNA staining. 10-15µl of propidium-iodide solution (1mg/ml) was added to every sample and the solution was transferred into a FACS tube. If necessary, the sample was diluted with PBS to an appropiate density for the flow cytometer.

Flow cytometry measurements were performed on a Becton Dickinson LSR II flow cytometer (Becton Dickinson – USA, controlled by vendors FACSDiva Software v. 6.1.3). Forward and sideward scatter as well as propidium iodide fluorescence were recorded. Similar gates as described below were set during data acquisition, all events were recorded to analyze the whole data later with acquisition finished after 10.000 or 20.000 gated events (cells). As the intensity of fluorescence signal is strongly dependent on the cell to propidium iodide ratio and the cell number was variable, the amplification value for the PE-channel was adjusted to measure the G0 peak at an amplitude of around 75.000.

Data analysis was performed using FlowJo version 7.6.5 (Tree Star, Inc. - USA). First cell fragments and aggregates were excluded by plotting sideward scatter (SSC) against forward scatter (FSC) and gating out too small and too large particles. (Fig. 9 – A). In the next step the amplitude of the propidium-iodide fluorescence (PE-channel = PE-A) was plotted against the width of the PE channel (PE-W) to further exclude aggregates. Finally the histogram of the PE-amplitude was plotted and the cell-cycle plugin of the FlowJo software fitted the curves under the histogram and calculated the percentage of each cell cycle phase. The first big peak is the G_0/G_1 phase with the lowest chromosome complement. The peak with the doubled amplitude is the G_2/M peak after doubling the DNA, everything in between is assigned to the S-phase, where the DNA duplication is still in progress.

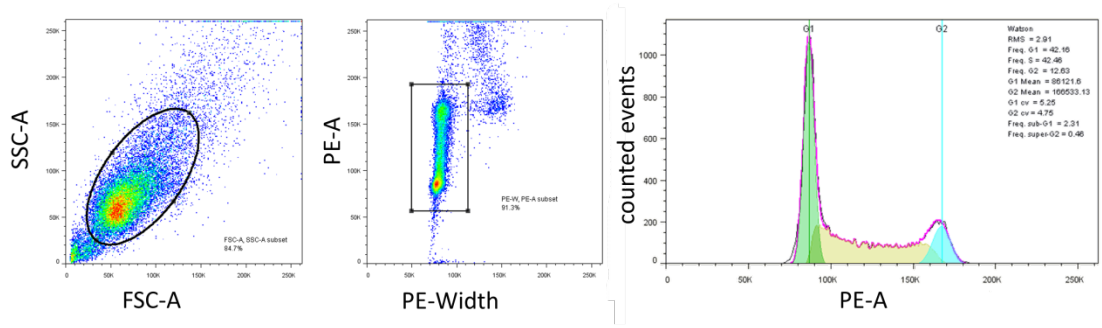

Fig. 9 – Gating of recorded events in flow cytometer to calculate cell-cycle distributions.

3.5. Proteomics Preparation

3.5.1. Solutions:

Urea buffer: 8M Urea (Roth) in 100 mM TRIS-Buffer, pH 8.2

Dithiothreithol (DTT) 200 mM stock solution (100x)

Iodoacetamide (IAA) stock solution 1.1 M (100x) in water or urea buffer

AmBic solution: 50 mM Ammonium Bicarbonate in water

3.5.2. Harvest and extraction

Proteomic sample preparation was performed as described earlier (Mastrobuoni et al., 2012). Frozen cell pellets were resuspended in 500 µl of Urea buffer and vortexted. DNA was sheared with a syringe. The disulfide bridges of each protein sample were reduced with 2mM (final concentration) of dithiothreitol (DTT) (Sigma) for 30 minutes at room temperature followed by a two rounds of sonification for 45 seconds with 60% power (Bandelin - Sonoplus HD2070). Samples were spun down for 4 min at maximum speed to remove cell debris; the clear supernatant was

transferred to a new Eppendorf-tube. Protein concentration was determined by Bradford assay (Pierce) with BSA calibration curve. Proteins were further alkylated in iodoacetamide 11 mM (Sigma) for 20 minutes at room temperature in the dark.

100 µg of protein lysates were then diluted with 1.5 volumes of 100 mM ammonium bicarbonate and incubated with LysC endoproteinase (WAKO) overnight at 37 °C. After LysC digestion the samples have been further diluted with 1.5 volumes of ammonium bicarbonate 50mM and incubated with 10 µl of immobilized trypsin (Applied Biosystems) under rotation for 4 hours at 30°C. After digestion 18 µg of each sample were desalted on Stage Tips prior to LC-MS analysis (Ishihama et al., 2006).

Each fraction was analyzed in duplicate on a LC-MS/MS system (Eksigent nanoLC and Thermo - LTQ-Orbitrap Velos). A mixture of two solvents was used for separation of peptides, with buffer A composed of 5 % acetonitrile and 0.1 % formic acid and buffer B of 80% acetonitrile and 0.1 % formic acid. During a 255 minutes gradient the ratio of both buffers increased from 5% Buffer B at the beginning to 60% buffer B at the end of the run.

Resulting raw data were analyzed using the MaxQuant proteomics pipeline v1.4.0.5 (Cox and Mann, 2008) and an in-house database containing swissprot protein data was used, with carbamido-methylation of cysteins and oxidation of methionins as static and variable modifications, respectively.

3.6. Additional Data analysis

Further data analysis and visualization was done with Microsoft Excel, GraphPad Prism 6 or VANTED 2.01 (Junker et al., 2006). If not noted otherwise the mean with standard deviation is plotted into figures. For clustering of protein data Multiple Experiment Viewer 4.3 (MeV) was used (Saeed et al., 2003).

3.7. Experimental description

3.7.1. Experimental verification of correcting strategies by mixing ^{13}C with ^{12}C-glucose

Individual stock solutions of ^{12}C-glucose and an equimolar amount of $^{13}C_1$-glucose were prepared and tested by drying and measuring identical volumes. The ^{12}C and ^{13}C solutions were mixed in different ratios in triplicates, dried, derivatised, measured on the GC-MS and analysed as described above. The mass-range 319-324 was extracted from the glucose-byproduct and analysed.

3.7.2. Reproducibility of harvest procedure and label incorporation

$6.5x10^5$ living cells were seeded into 10 cm cell culture plates with 10ml DMEM (2.5 g/L glucose, 4 mM glutamine, 10 % FBS, 1 % PenStrep). Media changes were performed 24 and 4 hours before the harvest to avoid nutrient deprivation. 72 hours after seeding the cells were harvested. Two additional plates were grown independently to count the cell number at harvest. Three plates were harvested as described including the application of ^{13}C-glucose for 3 min. After derivatization extracts were pooled and measured 6 times to calculate technical reproducibility. Five plates were treated completely independently and measured in four technical replicates. Additionally, two plates were harvested in the same way but with unlabeled substrates to use the reference spectra for normalization.

3.7.3. Cell Cycle experiment

This experiment was conducted together with Sebastian Memczak from the MDC Berlin. He performed the pre-cultivation, and the synchronization as well as determination of cell cycle progression by western blots and cell cycle analysis. Experiments were harvested together and I did the sample preparation and data analysis for metabolomics and proteomics.

T98G cells were seeded in 15 cm cell culture plates with high glutamine medium supplemented with 2.5 g/l glucose. Cells were synchronized by incubation with 0.4 mM mimosine (final concentration) for 24 hours. This leads to the cell cycle arrest between G1 and S-phase. Cells were allowed to grow synchronously by replacing mimosine containing media with fresh media. The new media contained heavy labeled amino acids ($^{13}C_6$ -$^{15}N_4$-Arginine and u-^{13}C, u-^{15}N L- Lysine, to measure the rate of protein synthesis in a pulsed SILAC approach (Schwanhausser et al., 2009). Every two hours for a total time period of 24 hours cells were harvested by the method described

for facultative adherent cells (section 3.3.2), but with additional cell scraping. In more detail, cells were gently scraped from the plates using a cell lifter in their initial growth media and transferred to a falcon, gently centrifuged, resuspended with label buffer prewarmed to 37°C and incubated for 2.5 minutes. The cell suspension was split into 3 samples, centrifuged and cell pellets were frozen in liquid nitrogen. One pellet was used for metabolomics and one for proteomics. Two individually grown plates were harvested per time-point, resulting in two biological replicates. The late and early time points were released from block 12 hours prior to the early time points, so total harvest time was around 12 hours. Metabolomics and proteomics measurements and analysis was performed as described above.

3.7.4. Growth inhibition under influence of glycolytic inhibitors

Cells were pooled and seeded with appropriate split-ratios or cell-number into 6-well plates and supplied with 2ml media. 24 hours after seeding cells, the cell number of the control plate was estimated to determine the starting value and treatment cells received the drugs in different concentrations and were further incubated under standard conditions. After another 24 hours, if not noted otherwise, cell viability and cell numbers were estimated. For microscopy the media volume was reduced prior to or after adding the drug to 1ml, to decrease the height of the light path.

To include swimming cells into the cell count the whole growth media, including potential swimming cells, was transferred to a falcon. Then 500µl of prewarmed trypsin was added to every well and cells were resuspended and transferred to the same falcon, followed by centrifugation (4 minutes, 1350 rpm, RT). The supernatant was sucked off and cells were resuspended with 1ml of media. Then the cell suspension is mixed 1:1 with Trypanblue-solution and counted in TC10 cell counter (BioRad).

Data were plotted with GraphPad Prism 6 (GraphPad Software – USA). After log-transformation of concentrations (x-axis) a non-linear curve-fitting was performed (dose-response curve (inhibitor) with variable slope = 4 parameters).

3.7.5. Incorporation of ^{13}C-Glyceraldehyde

T98G and HEK293 cells were pooled and seeded in appropriate density and cultivated under standard conditions in 10cm dishes and in triplicates as described above. One day after seeding the media was exchanged to maintain high glycolytic activity. ^{13}C-Glyceraldehyde in aqueous

solution (Campro Scientific) was added to a final concentration of 2mM as either the D-isomer or a mixture of D/L-isomer, as the pure L-isomer was not available. Cells were incubated at 37°C with these compounds for 15 min, 45 min or 2h. After this time cells were shortly washed (~20 seconds) with a wash buffer containing glucose and glutamine, but no glyceraldehyde to measure intracellular amounts of this compound. Directly after washing cells were quenched by cold methanol treatment and extracted as above. Control cells were treated in the same way but without any addition.

3.7.6. Effect of glycolytic inhibition to metabolism

Trypsinized T98G cells were pooled and seeded in an appropriate cell DMEM at 2.5 g/l glucose. After cells grew for 24 hours 3-bromopyruvate (BrPyr) or 2-deoxyglucose (2DG) were added from sterile stock solutions to final concentration of 2mM for BrPyr and 2, 4, 10 mM for 2DG. Control plates for BrPyr experiments received 2 mM of mannitol as osmotic control. The 2DG and BrPyr experiment were performed independently. 12 minutes after adding the inhibitors the media was sucked off and replaced with 5 ml of pre-warmed label buffer with 2.5 g/l U-^{13}C-glucose, 2 mM of glutamine and the same inhibitor concentration for 3 minutes and harvested as described above.

3.7.7. *In vivo* study in mice to monitor gluconeogenesis from pyruvate

Mouse handling was perfomed by Maria Dolaptchieva at the MDC Berlin (M. Poy lab). Briefly summarized, wild type mice (C57-Bl6, 6 weeks old) were used, 4 mice served as control and 6 mice received an injection of 2µg u-^{13}C-Pyruvate per gram of bodyweight. After 7, 14 or 20 minutes the blood of 2 mice was collected and pooled, centrifuged and 50µl of blood plasma was frozen. The mice were killed, the liver removed and snap-frozen. Liver samples were ground in a mortar under liquid nitrogen and 50mg of liver sample was extracted with 1 ml of methanol:chloroform:water (5:2:1, v/v/v) under continuous shaking for 45 min. at 4°C. Then 0.5 ml of deionized water was added and samples were further shaken for 15 minutes at 4°C. Phases were separated by centrifugation, and the polar phase was sampled and dried under vacuum. Samples were derivatized and measured as described above.

3.7.8. *In vivo* study to elucidate differential use of substrates in HCC tumor models

Experiments were performed at the Charité Berlin by Antje Kettelhake and colleagues (T. Cramer lab). Briefly summarized, HCC tumor model mice, between 16 and 19 weeks old, received i.p. injections of sterile filtered solutions of u-^{13}C-glucose (0.5 mg/g body weight) or u-^{13}C-glutamine (0.25 mg/g body weight) dissolved in PBS. Five and ten minutes later mice were killed, the liver was harvested and immediately frozen in liquid nitrogen.

1ml of methanol:chloroform:water (5:2:1, v/v/v) was added per 50mg of liver and tissue was ground with a spatula tip of circonia beads in a tissuelyzer. After further shaking for 30 minutes at 4°C and further addition of half the volume of water, followed by phase separation, the polar phase was sampled and dried under vacuum. Samples were derivatized and measured as described above.

4. RESULTS

4.1. Section 1 - Method development of pulsed stable isotope resolved metabolomics (pSIRM) of cell culture samples

Central metabolism is highly flexible and continuously adjusted to the physiological program and the needs of the cells. To gain deeper insights into the dynamics of metabolism techniques enabling a quantitative and time resolved analysis of the metabolome are needed to allow a detailed view of carbon routing through central carbon metabolism (CCM). A strategy was developed that enabled the direct measurement of dynamic metabolic activity over the central carbon pathways using mass spectrometry. Additionally, stable isotope-labeled substrates are applied to cells and time resolved isotope enrichment and quantification of metabolites are performed within a single measurement.

After thoroughly reading the available literature no clear “standard method” was reported, but every lab using its own approach, reporting some advantages over other methods. We therefore decided to set up an own, standardized protocol for all performed experiments. An essential modification to other reported protocols is the presence of the main nutrients glucose and glutamine, until the activity of metabolism is stopped by quenching or freezing.

4.1.1. A high percentage of the central carbon metabolism can be measured by GC-MS.

To get a first overview about the dimensions of detected compounds in cell-culture samples, HEK293 cells were harvested as described in chapter 3.3.2 and measured in two dimensional mode on a GC-GC MS, followed by an in-depth analysis against the Golm Metabolome Database (GMD) to identify as many compounds as possible (Suppl. table 1). Most of the compounds detected mapped to the highly connected central carbon metabolism (CCM) (Table 1). Further modifications were made to improve the separation and unequivocally identification of the most important pathways of the CCM. Lactate and pyruvate are measured baseline separated if a split-injection (1:5) is performed (Fig. 10). Citrate and isocitrate are separated by modifying the temperature-gradient, 3-phosphoglyceric acid (3PGA) could be better measured when the alkan-mix for retention index calculation contained C17 instead of C18 (not shown). In general the chromatography is less complex if the polar and unpolar phase were separated during sample preparation and measured individually. This provides an improved peak identification, due to fewer overlapping peaks.

Table 1 – Coverage within different compound classes in the central carbon metabolism by GC-MS based analysis of human cell culture samples. The total number of compounds within different subpathways is presented in the first column and compared against the compounds detectable by GC-MS as pure standards and these that are found in extracts of tumor model cell lines.

class	total	detectable by GC-MS	found in biological samples
glycolysis	11 G1P, G6P, F6P, F1,6BP, DHAP, GAP, 3PGA, 1,3BPG, 2PGA, PEP, Pyr	8* (G1P), G6P, F6P, F1,6BP, DHAP, 3PGA, 2PGA, PEP, Pyr	8* (G1P), G6P, F6P, F1,6BP, DHAP, 3PGA, 2PGA, PEP, Pyr
TCA-Cycle	10 Acet-CoA, Cit, Acon, IsoCit, 2KG, Succ, Succ-CoA, Fum, Mal, OAA	8 Cit, Acon, IsoCit, 2KG, Succ, Fum, Mal, OAA	6 Cit, 2KG, Succ, Fum, Mal, OAA
PPP	7 6PGlcLactone, 6PGlcA, Ribu5P, R5P, S7P, Ery4P, Xyl5P	3 6PGlcA, Ribu5P, R5P	2 6PGlcA, R5P
proteinogenic amino acids	20 Ala, Arg, Asn, Asp, Cys, Gln, Glu, Gly, His, Ile, Leu, Lys, Met, Phe, Pro, Ser, Thr, Trp, Tyr, Val	17 Ala, Arg, Asn, Asp, Gln, Glu, Gly, Ile, Leu, Lys, Phe, Pro, Ser, Thr, Trp, Tyr, Val	16 Ala, Arg, Asn, Asp, Gln, Glu, Gly, Ile, Leu, Lys, Phe, Pro, Ser, Thr, Tyr, Val
C3 bodies	6 Lac, Glyceric acid, Glycerol, Glcerol3P, beta-Ala, Dihydroxyacetone	6 Lac, Glyceric acid, Glycerol, Glcerol3P, beta-Ala, Dihydroxyacetone	5 Lac, Glyceric acid, Glycerol, Glcerol3P, beta-Ala
total	53	41	37

*G1P and G6P usually coelute, but they can be differentiated in the less abundant byproduct

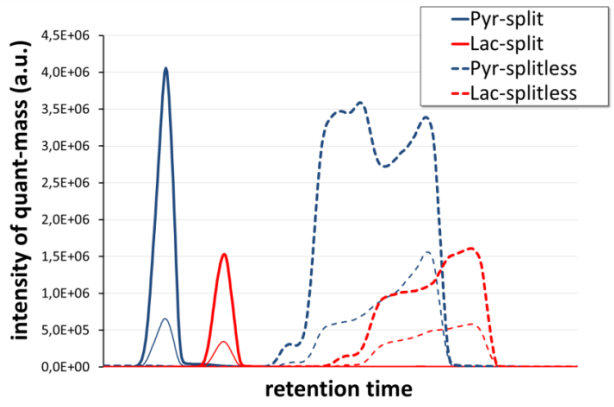

Fig. 10 – Separation of pyruvate and lactate needs split injection. Different amounts of pyruvate and lactate were measured by GC-MS with 1:5 split injection and in splitless mode. The lower amount in splitless mode (thin line) resulted in the same amount on GC-column as the high amount sample in split mode (thick line).

4.1.2. The Ident-mixture enables a more reliable and semiautomated identification in complex biological samples.

In contrast to most liquid chromatography based methods, gas-chromatography is capable to separate most of the structural isomers as cis-trans isomers (maleic acid vs. fumarate), positional isomers (citrate vs isocitrate) or mesomers (glucose and galactose). Due to their chemical similarity the mass-spectra are also very similar (Fig. 11), making it impossible to identify the compounds solely on their spectra-information. To effectively identify these compounds it is necessary to include the retention behavior as a second, independent factor.

The retention index (RI) is a more robust criteria for the retention behavior than the retention time (Halket et al., 2005), but changing parameters on the GC-MS system can even influence the measured retention indices of the compounds. The RI differed by up to ten RI units from the RI information collected in the GMD. To deliver reliable identification of compounds even under changing conditions during further method-improving, a set of identification mixtures was developed.

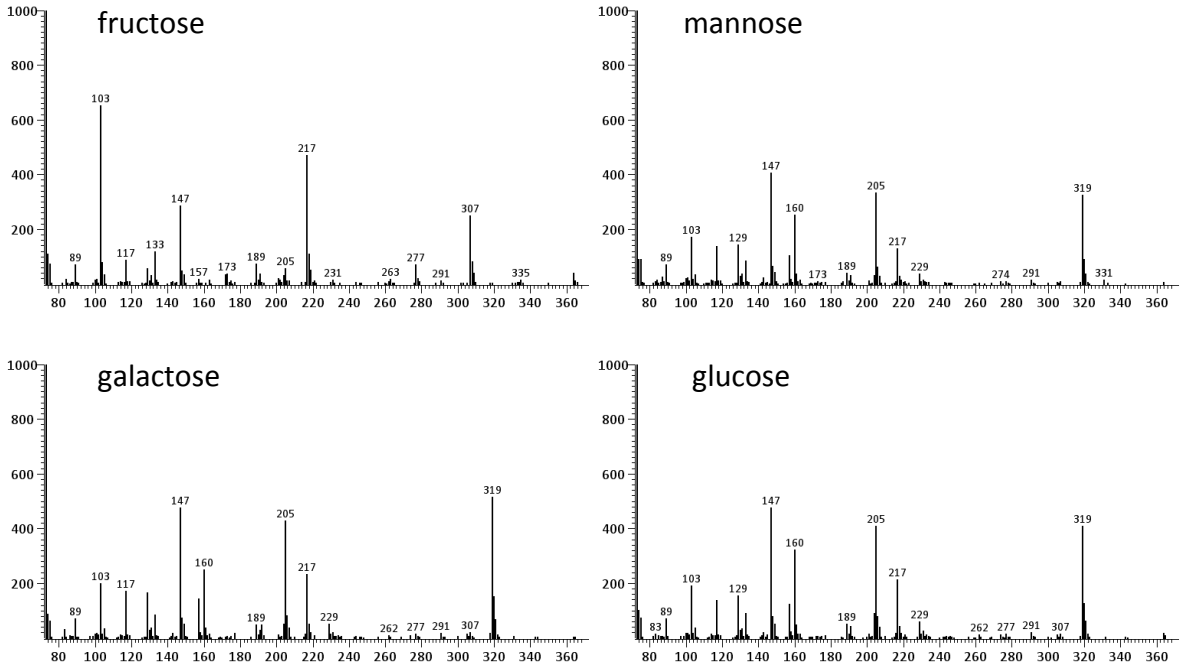

Fig. 11 – Similarity of mass spectra of hexoses. Mass spectra of four common hexoses, in their MeOX+MSTFA derivatization products reveal strong similarities. With exception of fructose, which is a ketose, the mass-spectra of the three aldoses are nearly identical, due to their chemical similarity.

101 important compounds of the central carbon metabolism were selected to prepare four different Ident-mixes (Ident A-D). The compound information is binarily encoded in these mixes; every compound is present in only two of the four mixes, so every mixture contains between 50 and 52 compounds. Similar compounds, with regards of similar mass spectra and/or retention information, are distinguishable by their appearance in the different mixtures. For example, citrate is present in mix B and mix D and isocitrate in mix A and C. Also the sugars and sugar phosphates exhibit similar mass spectra and elute within five RI units, resulting in a difficult identification that improved significantly when Ident-mixtures were used. The strategy is illustrated in Fig. 12; the four different Ident-mixes were measured and analysed in parallel to the samples within the same batch. If there is any uncertainty the Ident-mixes can be overlaid and the compound can be identified by the occurrence in the Ident-mixes. The complete list can be found in Suppl. table 3

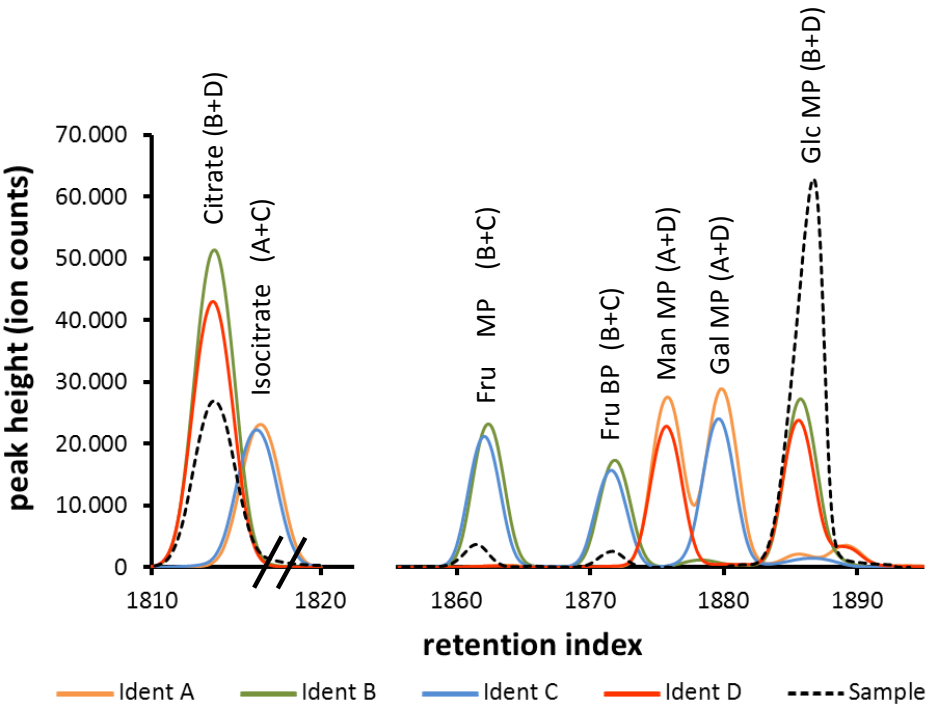

Fig. 12 – Guided identification using Ident-mixtures. Every compound is present in two different Ident mixtures (colored lines), with different distributions for compounds with similar retention indices. Every sugar can easily be verified by the presence of a signal in the associated Ident-mix even without the right retention indices. In this example the sample (black, dotted line) contained citrate, fructose and glucose but no or very low amounts of isocitrate, mannose and galactose. The letters in brackets indicate the associated distribution in the different Ident-mixes. BP/MP=byproduct/mainproduct of derivatization.

The spectral information in combination with the ident-combinations were stored in a spectra-library and build the background for an automated computer-aided identification. Finally, the SILVIA-tool for high-throughput data analysis, programmed by Henning Kuich in our group made use of this identification strategy and includes a semi-automated identification (Kuich, 2014). With this program the identification by Ident-mixtures is supported and is now a standard procedure in the lab and will be further expanded in the future.

4.1.3. Multiple metabolites can be simultaneously quantified with external calibration curves

A strategy for an absolute quantification of metabolites should be established that still allows a high sample throughput. Isotopic dilution is often applied for LC-MS based quantification; it enables correcting for strong matrix effects and ion suppression (Mashego et al., 2004). As the introduced isotopes during labeling studies interfere with isotopes used for quantification it is necessary to run different measurements for quantification and isotopomer extraction which doubles measuring time (Munger et al., 2008).

In frame of this thesis, an external calibration was established by which calibration curves for multiple metabolites could be used to quantify a large number of samples (Roessner-Tunali et al., 2003). A mixture of metabolites in known amounts was created, mimicking the composition of the cellular metabolome, qualitatively and quantitatively. The mixture ("Quant-Mix") was stepwise adapted and improved to better match quantities in the calibrations and samples.

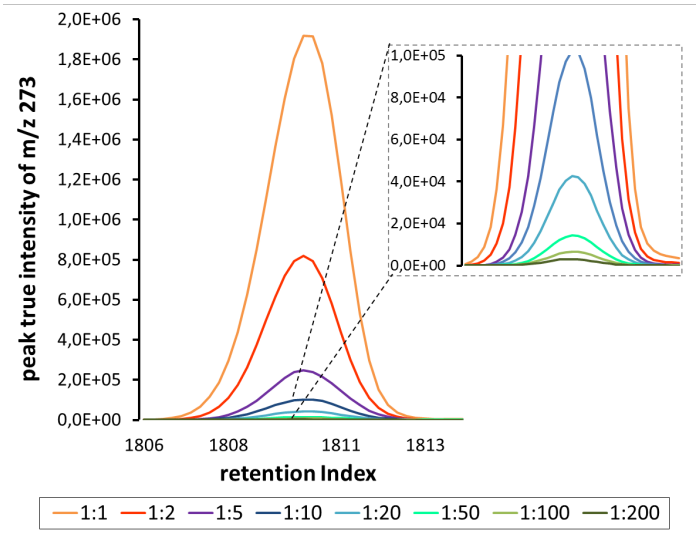

Fig. 13 – Illustration of quantification standard to quantify metabolites. Here the peak of citrate is shown for different dilutions of the Quant-mixture, from 1:1 (highest quantity) to 1:200 (lowest quantity). The concentration range starts slightly above the detection limit and reaches a very large peak size that is close to saturation. This increases the probability of the measured samples to be within the quantifiable range.

This Quant-mix is currently composed of 63 compounds (Suppl. table 2) and is measured in eight different dilutions spanning a 200-fold concentration range for each compound (Fig. 13). This delivers enough flexibility to quantify different kinds of biological samples, from extracted cell-culture samples, to media or tissue samples. These mixtures result in 73 calibration curves (including by-products for some compounds) with 54 curves with $R^2 > 0.95$ (74%). The calibration improved when a quadratic calibration was used instead of a linear calibration. Applying this strategy to cell culture samples typically quantified around 40 different compounds (Fig. 16, Suppl. table 4).

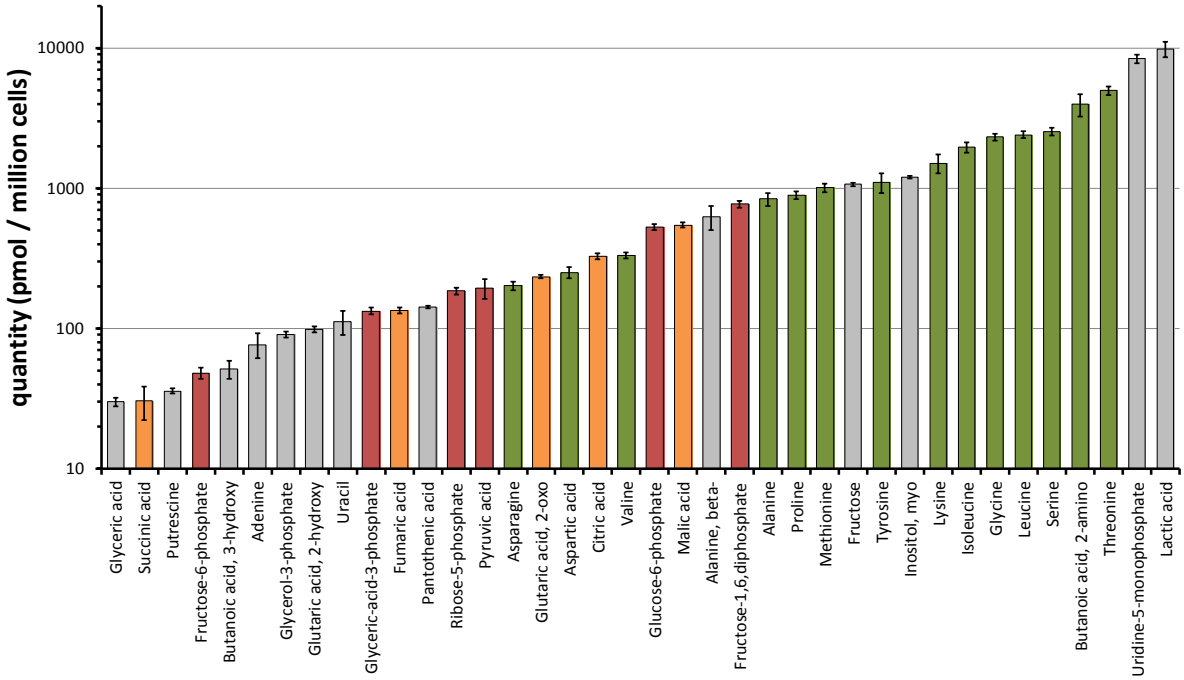

Fig. 14 – Concentration of metabolites within cells differs by many orders of magnitude but measurement is very reproducible. Shown are quantities of detected metabolites in T98G cells, as average of averages from 5 biological replicates measured in quadruplicates with their standard deviation. Different colors indicate compound classes: orange = TCA-cycle, red = glycolysis, green = amino acids, grey = other.

To further test the external calibration for quantification of metabolites in presence of a complex matrix, a "spike-in" experiment using the quantification mixture and cell extracts was performed (Fig. 15). The quant-mix and an extracted sample were measured separately as well as the extracted sample spiked to the quant-mixture. The shift between the measured quantity of the quant (black symbols and line) and the quant with spiked sample (red symbols and line) should represent the quantity of the sample (green line). Moreover without any discrimination or matrix effect an addition of the obtained quantities after measurement would give the same result as a simultaneous measurement in the spiked sample (blue symbols and line). In fact most compounds showed similar curves for calculated quant + sample and measured quant + sample.

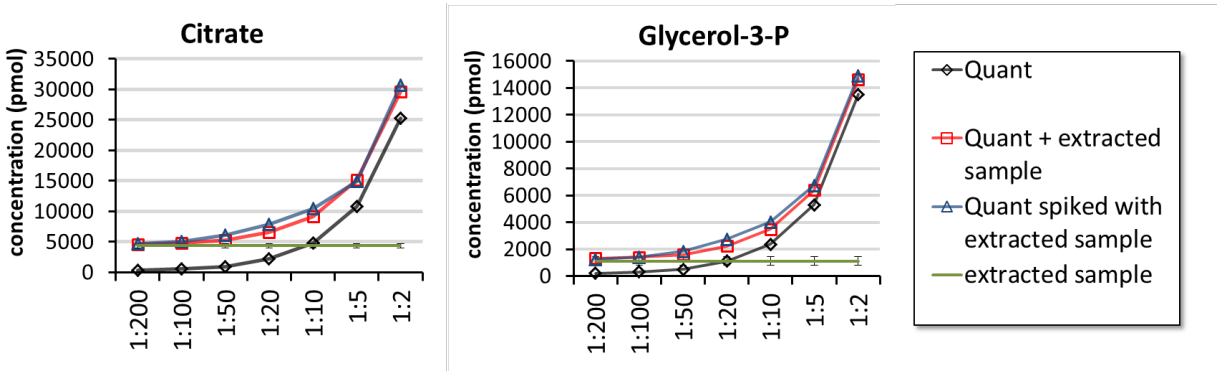

Fig. 15- Concept of quant-addition experiment. An extract of cell culture sample was measured alone in repetitions (green line), as well as the quant-mix up to dilution 1:2 (black symbols and line). Furthermore the extracted sample was spiked to the quant-mix and measured together (blue symbols and line), whereas the red symbols and lines represents the summed up quantity of the pure extracted sample and the quant-mix measured independently. Error bars were omitted for simplicity, except for the extracted sample.

For all quantified compounds a comparison between the addition of the individual measured values for sample and quant and the simultaneous measurement in the quant spiked with sample were made (Fig. 16). Overall there is a perfect linear trend, for the majority of compounds, with most compounds located between the -20 and +50 percent border. From this data the recovery for every metabolite was calculated for every condition of the quant mix individually by:

equation 1: $$recovery = \frac{quantity\ in\ quant\ with\ spiked\ sample}{quantity\ in\ quant + quantity\ in\ sample}$$

As the calculation of recovery appeared to be most useful in conditions where the amount and sample is approximately in a 1:1 ratio, the calculated recoveries were filtered, to match these criteria (Suppl. table 5). In the example above (Fig. 15) the recovery for citrate was calculated with the 1:10 quant mix and for glycerol-3-phosphate with the 1:20 mix. Interestingly, in the presence of matrix interactions the recovery of the compounds was found to be in average 111% with 60% (23 out of 38 compounds) between 90 and 120 percent. These data indicate that compounds were better measured with more of the compound present, which fits to the finding that calibration curves can be better fitted if a quadratic fit is employed.

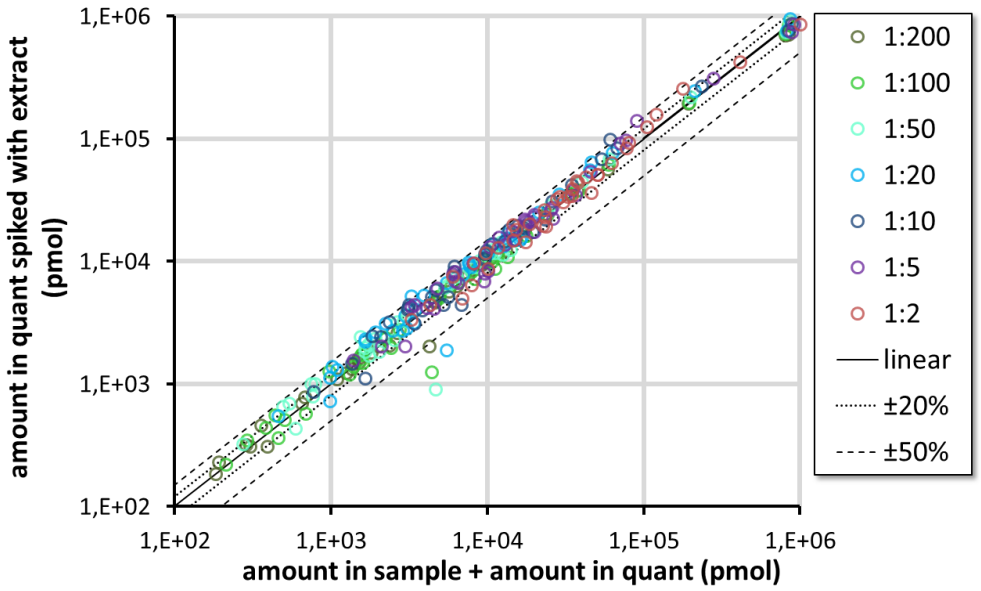

Fig. 16 – Comparison of all quantified compounds, for determination of potential matrix effects. On the x-axis the sum of the metabolites quantified in extracted sample and quant mixes measured separately was plotted and on the y-axis the amount of quant-mix spiked with sample, measured together. Without any matrix effect both values should be the same and should be located on the linear trend line (black). The averages of all replicates were shown for the individual metabolites as well as additional lines for the +/-20% (dotted line) and the +/-50% interval (broken line).

Additionally a recovery of standards in presence of a biological matrix (*E.coli* extracts) with more than 100% was also reported by Koek *et al*; they concluded that the adsorption of a single compound to the analytical system or breakdown was decreased with other compounds masking the surfaces (Koek et al., 2006).

4.1.4. The sample preparation and the quantification of compounds in cell culture samples is reproducible

Technical and biological reproducibility has been determined to validate the reliability of this approach for the measured intensities and label incorporation (section 4.1.9). For determination of technical reproducibility a pooled, derivatized extract was injected repeatedly into the system and for determination of the biological reproducibility measurements were performed from independently generated samples.

The coefficient of variation (COV) was calculated for all unambiguously identified metabolites by dividing the calculated average by the standard deviation. The vast majority (80%) of all compounds could be measured with a COV smaller than 15%, with technical replicates performing slightly better than biological replicates (Fig. 17).

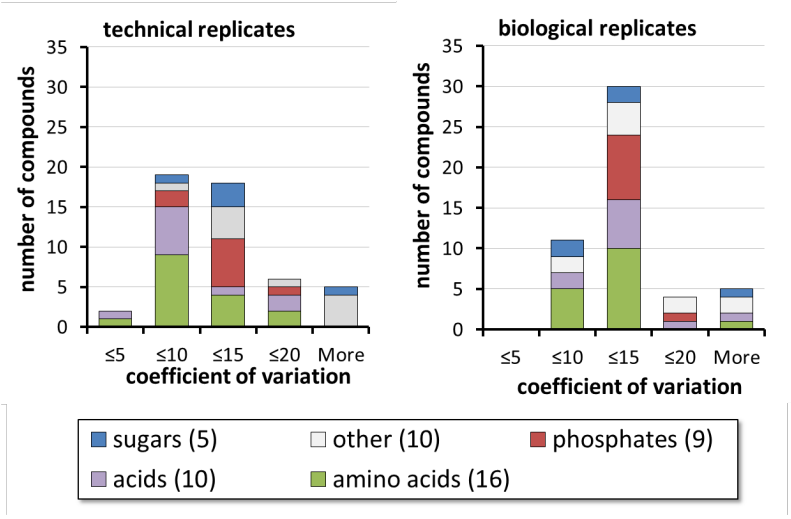

Fig. 17 - Coefficient of variation (COV) for different classes of metabolites measured as technical or biological replicates.

4.1.5. The natural ^{13}C abundance must be subtracted

Mass spectrometers are able to differentiate between different isotopic species of a molecule. For example pyruvate has the molecular formula $C_3H_4O_3$ and an average mass of 88.06 Dalton. Measuring this compound with a mass spectrometer without derivatization, e.g. in an LC-MS approach would yield up to 3 detectable mass-peaks, with 96.15% intensity in m0 (88 Da), 3.27% in m+1 (89 Da) and 0.58% in m+2 (90 Da), mainly produced by the 1.1% natural occurrence of carbon-13 (Fig. 18 -left). Derivatizing pyruvate, a prerequisite for GC-MS measurement increases the number of atoms in the molecule and its mass. After trimethylsilylation and methoximation the molecular mass rises to 189 Da. This further increases the probability of heavy isotopes to be present (Fig. 18 -right). The relative abundance of the lightest isotope (189 Da) decreases to 84.5% and the intensity of the m+1, m+2, m+3 masses increase to 11.3, 3.9 and 0.25%, respectively. The reason for this is the high number of carbon atoms introduced by the derivatization-reaction as well as the addition of silicon, which has 4.7 and 3.1 of natural occurrence on the m+1 and m+2 position, respectively (Berglund and Wieser, 2011). Therefore GC-MS based ^{13}C-incorporation experiments need to be more thoroughly normalized for natural occurring isotopes (NOIs) than LC-MS or NMR based studies where the number of carbon atoms in the molecule is the most important aspect to consider. The mass isotopomer with the lowest mass (m0) is attributed as “unlabeled” or “light”, whereas the higher masses are denoted as “heavy”. The true incorporated label by carbon-13 might therefore interfere with the abundances of natural occurring isotopes.

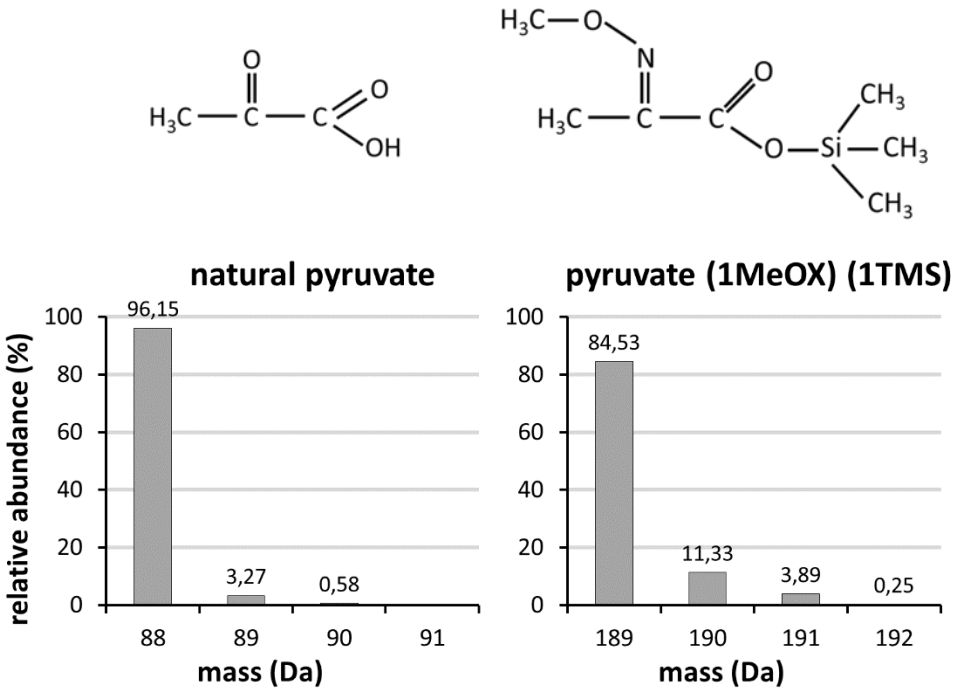

Fig. 18 - Impact of derivatization on the abundance of natural occurring isotopes in pyruvate. Left: unmodified pyruvate. Right: pyruvate after trimethylsilylation and methoximation. The relative abundances of each mass, summed up to 100 percent, are shown. Isotope abundances were calculated with Scientific Instrument Services - Isotope Distribution Calculator and Mass Spec Plotter (http://www.sisweb.com/mstools/isotope.htm) with sum formulas of both molecule species. The numbers above bars indicate the calculated percentages.

In order to detect and quantify the heavy carbon incorporation during ^{13}C-labeling studies the influence of the naturally occurring heavy isotopes (NOIs) has to be known and how their effect can be eliminated. For this the measured isotope pattern of trimethylsilylated and oximated pyruvate (m/z=174) was extracted and used for further *in silico* calculations. The relative isotope abundances were then mixed in defined ratios on various positions, mimicking mass-shifts produced by different amounts of incorporated ^{13}C-atoms (Table 2).

Table 2 – *In silico* mixing of light and heavy masses. Shown here for the isotope pattern of one fragment of pyruvate (1MeOX) (1TMS) and with an assumed label on the m+2 position but with different $^{13}C/^{12}C$ ratios. Note that all isotopic positions of a certain condition sum up to 100%

		defined $^{13}C/^{12}C$ ratio										
		0%	5%	10%	20%	33%	50%	66%	80%	90%	95%	100%
position	m0	85.3	81.0	76.8	68.2	57.1	42.6	29.0	17.1	8.5	4.3	0.0
	m+1	10.5	10.0	9.4	8.4	7.0	5.2	3.6	2.1	1.0	0.5	0.0
	m+2	**3.9**	**8.0**	**12.0**	**20.2**	**30.7**	**44.6**	**57.6**	**69.0**	**77.1**	**81.2**	**85.3**
	m+3	0.3	0.8	1.3	2.3	3.7	5.4	7.0	8.4	9.5	10.0	10.5
	m+4	0.0	0.2	0.4	0.8	1.3	2.0	2.6	3.1	3.5	3.7	3.9
	m+5	0.0	0.0	0.0	0.1	0.1	0.2	0.2	0.3	0.3	0.3	0.3
	m+6	0.0	0.0	0.0	0.0	0.0	0.0	0.0	0.0	0.0	0.0	0.0

With these data the precision of different calculation strategies under the influence of several factors was estimated. First the incorporated label was calculated by dividing the relative intensity of the proposed heavy position, through the sum of both the light and the heavy intensity (equation 2). In the example in Table 2, intensity of the m+2 was divided by the sum of the intensities at the m+2 and the m0 position.

equation 2: $$\boldsymbol{Label}\,(\%) = \frac{\boldsymbol{intensity_{heavy}}}{\boldsymbol{intensity_{heavy}+intensity_{light}}} * \mathbf{100}\%$$

The calculated label using this equation was plotted in Fig. 19 against the expected label which is defined by the mixing ratio of the heavy and light component. It was obvious that the position where the label was introduced had a strong impact. With the label present on the m+1 or m+2 position, the incorporated label interfered with the remaining natural heavy abundance, resulting in a clear overestimation of labeling. This could be seen for the samples with a mass shift between light and heavy of 1 Dalton (blue line) or 2 Dalton (red line). In contrast to that, the natural abundance on the m+3 and m+4 position was essentially absent and did not influence the calculation noticeable (green and violet line). Furthermore, if the incorporated label was strong enough (high ratio between heavy and light) the effect of natural occurring isotopes approximated to zero and the precision increased. With a label incorporation of 75% or higher the label was calculated with less than 1% error, even on the m+1 position. This exemplary calculation was based on the mass-spectra of pyruvate, bigger compounds may have a more significant amount of natural abundance also in the m+3 and m+4 position, however the trend was found to be obvious: With a low label incorporation and a small mass-shift these calculation resulted in an over estimation and needed to be corrected for natural occurrence rates.

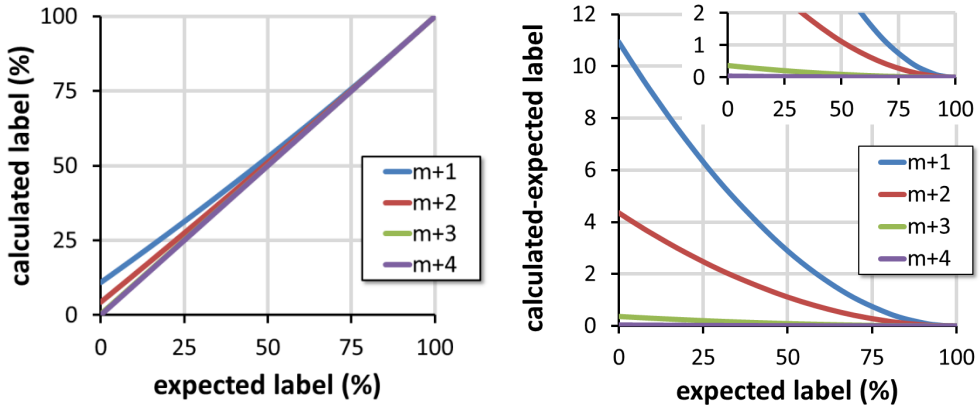

Fig. 19 – Impact of mass shift between heavy and light mass to the precision of label calculation. Measured mass fractions of pyruvate were mixed *in silico* with different mass-shifts between light and heavy mass and in known ratios (expected label on x-axis). The label was calculated based on the relative abundances of the masses with equation 2 and plotted on the y-axis, to illustrate the precision of the calculation. On the right figure the expected label was subtracted from the calculated label to indicate the difference. The insert shows the small intensity range.

In the next steps a calculation strategy for subtracting the naturally occurring isotopes (NOIs) from measured labeled samples was established. If the sum formula of the monitored fragment is known, the isotope distribution can be calculated by the use of the sum formula. This is not possible for unknown compounds or known compounds with unclear fragmentations. In order to include also these compounds into further analysis, a strategy to separate naturally occurring isotopes and the isotopes introduced by heavy carbon labeling was developed. Basically, the isotope pattern of an unlabeled reference sample built the basis for the calculation of NOIs.

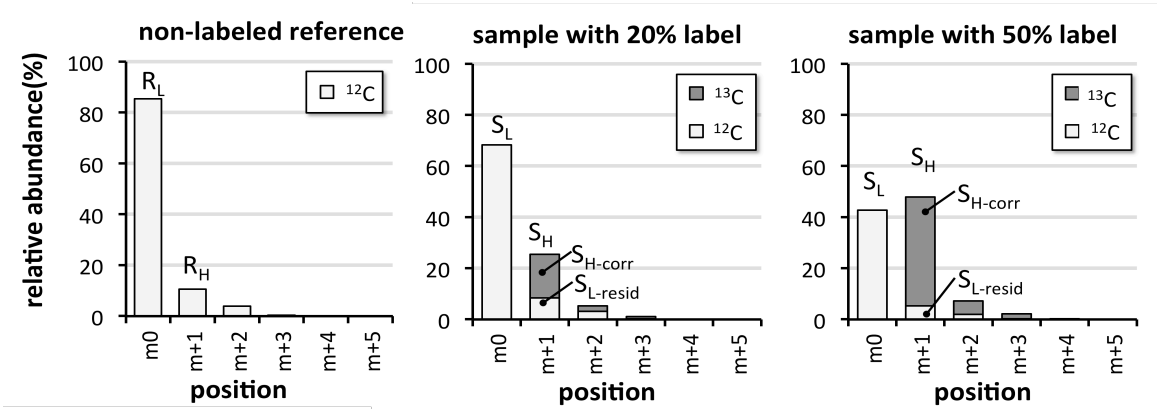

Fig. 20 – The impact of introduced heavy carbon atoms to the intensity of natural occurring isotopes. The non-labeled reference sample exhibited a well detectable amount of natural occurring isotopes (R_H) originating from the light mass (R_L) on the m+1 and m+2 position (light bars in the left figure). With an introduced label in the sample (dark bars in the middle and the right figure) here on the m+1 position, the relative abundance of the light mass in the sample (S_L) decreased and with this the amount of NOIs from the m0 fragment ($S_{L\text{-}resid}$).

With increasing amount of label incorporation the relative abundance of the unlabeled fragment (m0) decreases and with this the naturally occurring isotopes originating from the m0 fragment (Fig. 20 and Table 2). The leftover NOIs of the unlabeled fragment needed to be correlated to the amount of remaining light intensity in the sample. The measured isotopomer abundance at the heavy position (in the example above m+1) of the sample (S_H) contained both the information of the true incorporated label and the NOI from the light, unlabeled position and needed to be corrected for the latter, resulting in the corrected heavy abundance in the sample (S_{H_corr}) with:

equation 3: $$\boldsymbol{S_{H-corr} = S_H - S_{L-resid}}$$

The remaining NOI from the unlabeled position ($S_{L\text{-}resid}$) in the sample could be calculated by the use of naturally occurring isotope abundances on the labeled position in the unlabeled reference sample by:

equation 4: $$\boldsymbol{S_{L-resid} = \frac{R_H}{R_L} * S_L}$$

$S_{L\text{-}resid}$ = the residual natural isotopes from the unlabeled position on the heavy position in the sample

R_H / R_L = the ratio of the heavy to light mass isotopomer abundances in the reference, which is a function of the chemical composition of the molecule and could therefore assumed to be constant

S_L = the remaining abundance of the light mass isotopomer abundance in the sample

After the correction, the final label incorporation is be calculated similar to (equation 2) with the corrected values.

equation 5: $$\boldsymbol{Label(\%) = \frac{S_{H-corr}}{S_{H-corr}+S_L} * 100\%}$$

4.1.6. Correction of natural abundance and calculation of label incorporation can be done in a single step in an untargeted way.

When a compound is labeled at multiple positions, the naturally occurring isotopes from both the unlabeled mass and from the different isotopologues interfere with the following masses. The effect is illustrated in Fig. 21 where a hypothetic mass spectrum of a compound is shown that is composed of 40% unlabeled, and 20% labeled masses on each position m+2, m+3 and m+4 as measured by the mass spectrometer with the proportions of each isotopologue.

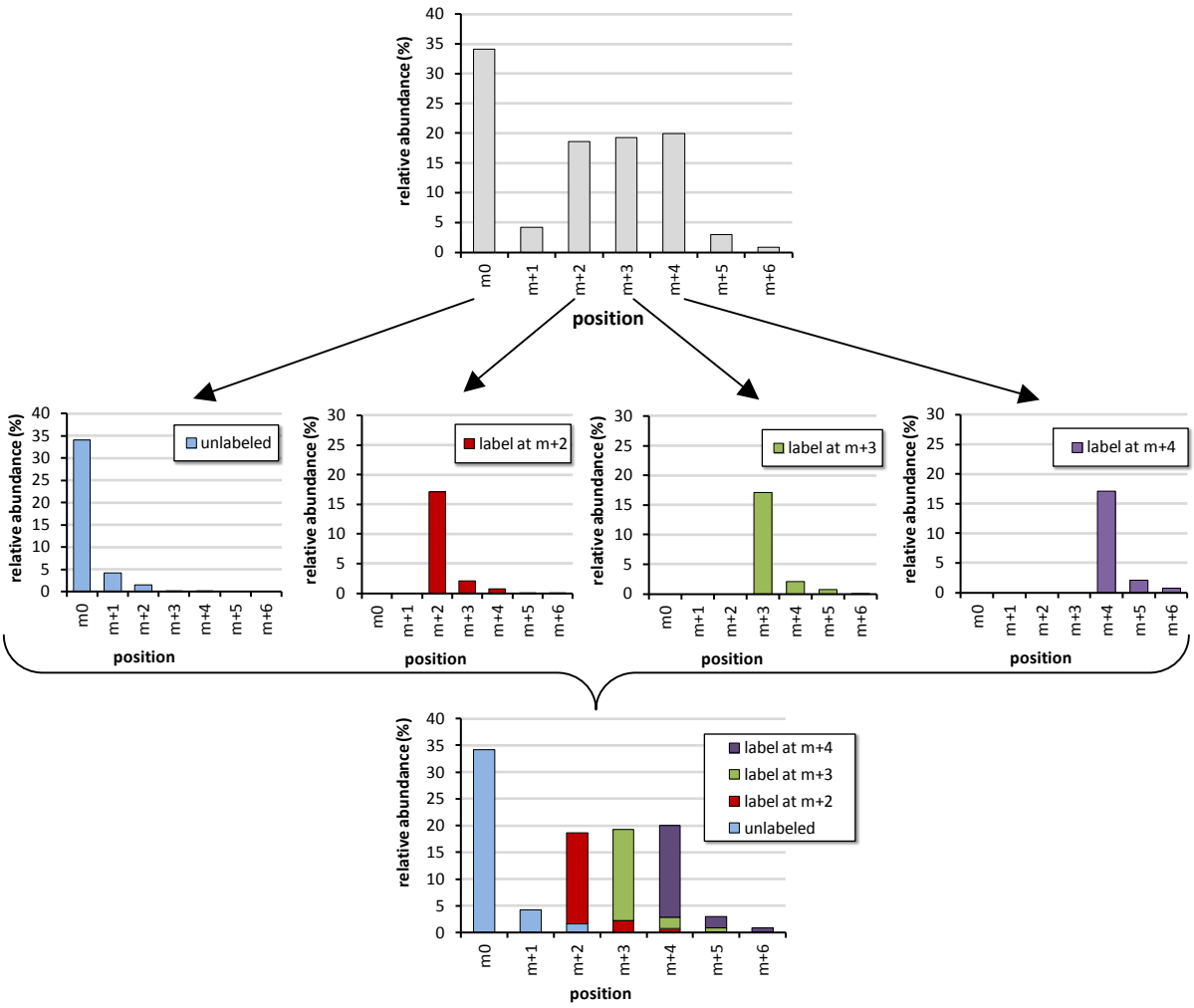

Fig. 21 – Mixing of isotope intensities with NOIs of the precedent isotopologue. Shown is an *in silico* mixture of a compound to 40% unlabeled and with 20% label each on positions m+2, m+3 and m+4 as measured by the mass-spectrometer (top, grey bars). The individual labeled species are indicated by different colors (middle), to illustrate the overlap in their isotope pattern (bottom).

The calculation of NOIs at every position is similar to the calculation of the NOIs from the unlabeled compound presented in equation 3 – 5 and needs to be performed stepwise for each position (Suppl. table 7). This strategy delivered the anticipated results with a single mass per isotopologue or if all NOIs of an isotopologue were added together, as the additional NOIs are a function of the intensity of the main mass.

If the labeled fractions on the individual positions are summed - as in the example given above to 40% unlabeled and 60% labeled - this complex calculation is not necessary. The formulas can be simplified to a single calculation by comparing the remaining intensity of the light m0 isotope in the sample (S_L) to that of the unlabeled reference (R_L).

equation 6: $$\boldsymbol{Label}\ (\%) = \left(\mathbf{1} - \frac{\boldsymbol{S_L}}{\boldsymbol{R_L}}\right) * \mathbf{100}\%$$

To further verify the calculation strategies, the *in silico* mixing approach was repeated with measured chemical standards. For this ^{13}C-glucose was mixed with ^{12}C-glucose in mixtures of known ratios, derivatized, measured and analyzed. 6-$^{13}C_1$-glucose was used as correction is most important for compounds that contained only a small mass shift between heavy and light mass (Fig. 19). The mass range from m/z of 319 to 324 was extracted and applied for further calculations. In order to use the equations introduced above, that need the isotopic abundances expressed as percent the measured intensities of isotope masses were transferred to mass isotopomer fraction (MIF). The whole extracted mass range summed up to 100% and the MIF was calculated for every mass within this mass-range by dividing the intensity of each mass by the sum of the intensities over the whole mass range, multiplied by 100% (equation 7 and illustrated in Table 3).

equation 7: $$MIF_x = \frac{intensity_x}{\sum_{i=0}^{n} intensity_i} * 100\%$$

This calculation is similar to the calculation of fractional abundance reported by Hellerstein (Hellerstein and Neese, 1999) and eliminates differences in intensities between multiple measurements (Table 3).

Table 3 - Example calculation of isotope incorporation using the targeted correction strategies for chemically defined samples. $^{13}C_1$-Glucose mixed in known ratios with natural glucose was measured by GC-MS and the intensities of the masses were extracted in the monitored mass range. The mass isotopomer fraction (MIF) at every position was calculated as shown above.

		measured intensities in a.u.			MIF in (%)		
m/z	**position**	**^{12}C**	**10 % $^{13}C_1$**	**50 % $^{13}C_1$**	**^{12}C**	**10 % $^{13}C_1$**	**50 % $^{13}C_1$**
319	m0	156460	153425	84507	66.6	60.2	33.2
320	**m+1**	**48250**	**63669**	**112421**	**20.6**	**25.0**	**44.2**
321	m+2	23579	28289	38071	10.0	11.1	15.0
322	m+3	5038	7389	15467	2.1	2.9	6.1
323	m+4	1199	1716	3268	0.5	0.7	1.3
324	m+5	228	262	751	0.1	0.1	0.3
	Sum	234754	254750	254485	100	100	100

After transforming the measured intensities into percentage distributions of mass isotopomers, the incorporated label was calculated without correction and after application of both correction strategies, the untargeted and targeted strategy aiming at the m+1 position (Fig. 22 and Table 4).

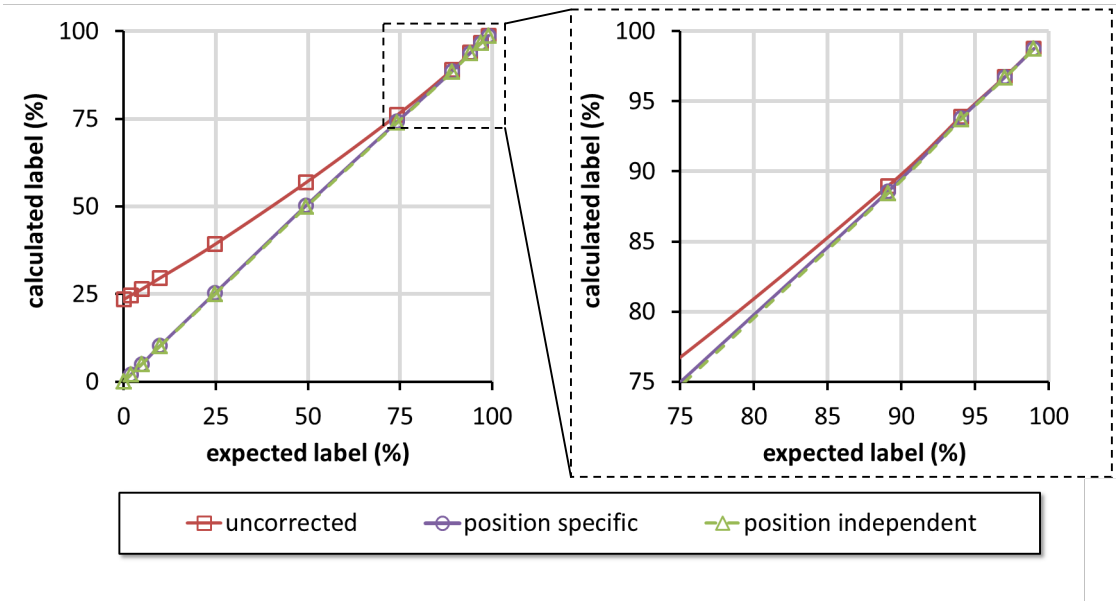

Fig. 22 – Verification of strategies to correct for natural occurring isotopes. 6-$^{13}C_1$-glucose was mixed with unlabeled glucose in known ratios (expected label) and the measured mass fragment intensities (m/z 319-324) were used to calculate the label without correction (equation 2), with targeted correction strategy aiming to the m+1 position (equation 5) or with untargeted method (equation 6).

Very similar to the *in silico* approach (Fig. 19), ignoring the need for correction resulted in a dramatic overestimation of the label incorporation in situations where only low label incorporation is present. In contrast both correction strategies effectively correct for the natural occurring isotopes and deliver the same and accurate results (Table 4).

Table 4 - Verification of strategies to correct for natural occurring isotopes. 6-$^{13}C_1$-glucose (purity 99%) was mixed with unlabeled glucose in known ratios (expected label) and the measured mass fragment intensities (m/z 319-324) were used to calculate the label without correction (uncorrected), with untargeted correction (position independent) or with targeted correction strategy aiming at the m+1 position (position dependent).

	calculated label		
expected label	uncorrected	position independent	position dependent
0%	23.4 ± 0.09	0.0 ± 0.12	0.0 ± 0.16
1.98%	24.7 ± 0.25	2.0 ± 0.32	2.1 ± 0.42
4.95%	26.4 ± 0.21	5.0 ± 0.27	5.0 ± 0.36
9.9%	29.6 ± 0.20	10.1 ± 0.29	10.3 ± 0.33
24.75%	39.2 ± 0.79	25.0 ± 1.26	25.3 ± 1.19
49.5%	56.8 ± 0.89	49.8 ± 1.28	50.3 ± 1.18
74.25%	76.1 ± 0.78	74.0 ± 0.94	74.2 ± 0.91
89.1%	89.0 ± 0.04	88.4 ± 0.03	88.6 ± 0.04
94.05%	93.9 ± 0.14	93.7 ± 0.15	93.8 ± 0.15
97.02%	96.8 ± 0.19	96.7 ± 0.20	96.7 ± 0.19
99%	98.7 ± 0.04	98.7 ± 0.05	98.7 ± 0.04

4.1.7. Mass isotopomer distributions are concentration dependent.

Calculating mass isotopomer fractions (MIF) from the same compound was not constant and revealed unexpected differences between several experiments. For example the calculated distribution of isotopes within a pyruvate molecule (Fig. 18) did not completely match the measured values (Table 2). Only a few reports discuss the influence of compound concentration on the measurement of isotopomer fractions or ratios of isotopomers (Antoniewicz et al., 2007; Patterson and Wolfe, 1993). To further test if concentration dependency might be the reason for the findings, the effect of different concentrations to the isotopomer distribution was evaluated. Spectra were collected from a number of experiments, including both biological samples and pure standards. To further increase the range of analyzed intensities (concentrations), different sugars and sugar phosphates were analyzed. In detail the spectra for glucose, glucose-6-phosphate, fructose, fructose-1,6-bisphosphate, and 3-phosphoglycerate were extracted. As all compounds are sugars and therefore share the same backbone structure, they all expose similar fragments. Here the m/z of 217 was found very prominent in all compounds and was used for subsequent calculations. The relative intensity of the fragment 217 (light) within the range of its naturally occurring isotopes (217-222) was plotted against the intensity (summed peak heights) of this range (Fig. 23).

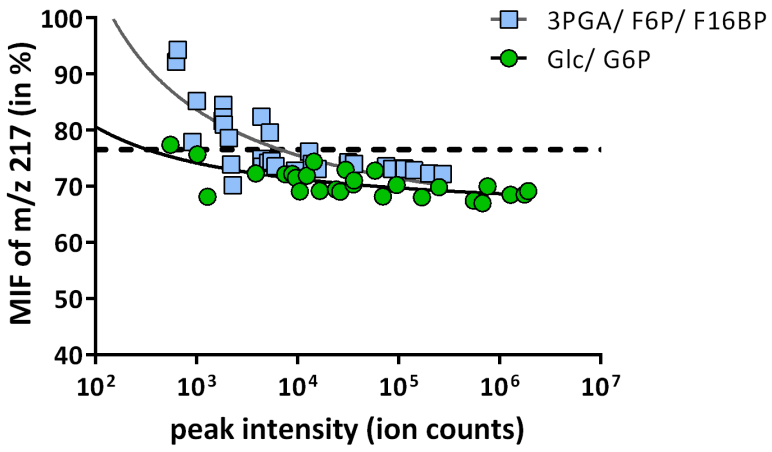

Fig. 23 – Concentration dependency of mass isotopomer distribution. The mass isotopomer fraction (MIF) of m/z=217 within the mass-range of its possible natural occurring isotopes is plotted against the peak intensity for different sugars and sugar phosphates. The theoretically expected value of 76.6%, calculated from the sum formula of the fragment, is shown by the dotted line.

It is evident that there is a concentration-dependent effect. The fraction of the fragment 217 within the whole mass-range decreased with increasing intensity of the measured compounds, meaning that the proportion of the heavy fragments increased. And with higher intensity also the precision of the measurement increased, in the lower intensity range the variability was much

higher. Only in the low to middle-high intensity range the measured values matched the calculated ones. Additionally, both glucose-species were around 5% lower than all the other compounds, indicating that the fragmentation in glucose derived compounds was different to other sugars. Therefore any theoretical calculated value has to be used with great care

4.1.8. Many metabolites of the CCM in mammalian cell lines can be found labeled and have a turnover on the minute time scale

The extraction of the information from heavy isotope incorporation was performed with a workflow established earlier. Chromatograms were processed using GC-MS vendors software ChromaTOF (LECO) and spectral information was extracted from exported text files by the tool MetMax (Kempa et al., 2009). This strategy makes use of a predefined list of potential labeled metabolites and isotopic mass range to be extracted. Potentially labeled compounds were detected under within multiple experiments and under various labeling conditions with different substrates and for different periods of time and masses suitable for extraction of isotope information were selected.

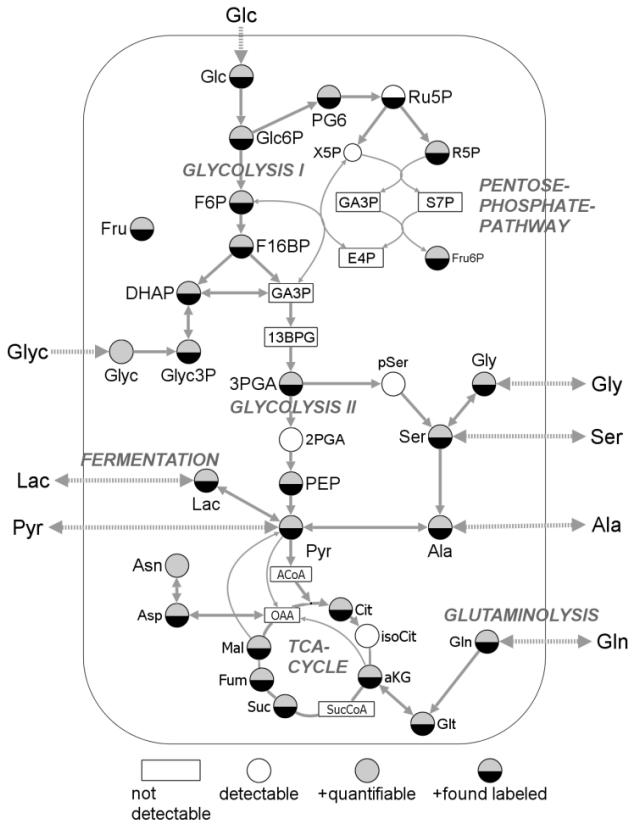

Fig. 24 - Map of the central carbon metabolism highlighting detected, quantified and metabolites found labeled, after application of u-^{13}C -glucose or u-^{13}C-glutamine in cell culture experiments. "Not detectable" refers to metabolites that cannot be measured by GC-MS, whereas "detectable" defines compounds that could be measured but were not found in cell culture samples, "quantifiable" refers to compounds present in the Quant-Mix.

A high number (up to 30) of compounds in the central carbon metabolism could be found labeled by either ^{13}C-glucose or ^{13}C-glutamine labeling (Fig. 24). For the labeled compounds, fragment masses were selected that efficiently represents label incorporation into these compounds. These masses (Table 5) delivered a good intensity and were not present in coeluting compounds, ensuring specificity for the whole mass-range from the unlabeled to completely labeled state. The mass lists covering the labeled fragments, with one or two additional masses above the highest labeled state, were imported into MetMax, enabling the automatic extraction of isotopic abundances for multiple compounds simultaneously.

Table 5 – Mass ranges used for extraction of label information in ^{13}C-labeling experiments. Some metabolites like TCA-cycle intermediates can be labeled on multiple positions; the most intensively labeled position is reported here.

		mass fragment m/z			
Metabolite	**derivatization**	**unlabeled**	**No. of carbon atoms**	**labeled by ^{13}C-glucose**	**labeled by ^{13}C-glutamine**
3-Phoshphoglyceric acid	4TMS	357	2	359	/
Alanine	3TMS	188	2	190	/
Aspartic acid	3TMS	232	3	235	/
Citric acid	4TMS	273	5	275	277
Dihydroxyacetonephosphate	1MeOX 3TMS	400	3	403	/
Fructose	1MeOX 5TMS	217	3	220	/
Fructose-1,6-bisphosphate	1MeOX 7TMS	217	3	220	/
Fructose-6-phosphate	1MeOX 6TMS	217	3	220	/
Fumaric acid	2TMS	245	4	247	249
Glucose	1MeCX 5TMS	319	4	323	/
Glucose-6-phosphate	1MeOX 6TMS	217	3	220	/
Gluconic acid-6-phosphate	7TMS	217	3	220	/
Glutamic acid	3TMS	246	4	/	250
Glutamine	3TMS	156	4	/	160
Glutaric acid	2TMS	261	5	/	266
Glutaric acid, 2-hydroxy	3TMS	247	4	/	251
Glutaric acid, 2-oxo	1MeOX 2TMS	198	5	200	203
Glycerol	3TMS	218	3	221	/
Glycerol-3-phosphate	4TMS	357	2	359	/
Glycine	3TMS	276	1	277	/
Lactic acid	2TMS	219	3	222	/
Malic acid	3TMS	233	3	235	236
Phosphoenolpyruvic acid	3TMS	369	3	372	/
Pyruvic acid	1MeOX 1TMS	174	3	177	/
Ribose-5-P	1MeOX 5TMS	217	3	220	/
Serine	3TMS	204	2	206	/
Succinic acid	2TMS	247	4	249	251

In order to investigate the time that is needed to introduce heavy carbons into metabolite pools, cells were treated for different periods of time with u-^{13}C-glucose label buffer for time points shorter than 15 minutes and label media strategy for longer time points (see section 3.3.3). Intermediates of the upper glycolysis (the hexosephosphates) were nearly completely labeled already within 2 minutes of label incorporation. Metabolites branching off from glycolysis were

sufficiently labeled to extract their label information reliably; however, to be completely labeled they need longer incorporation time. Intermediates of the TCA cycle were only slowly labeled by ^{13}C-glucose and even some hours of incubation, the labeling was not complete as many other sources, like amino acids, permanently fed into the TCA cycle (not shown). For the determination of activity of glycolysis, a time between 2 and 3 minutes was used for further experiments, as this time gave sufficient label on the one hand and decreased the treatment time on the other.

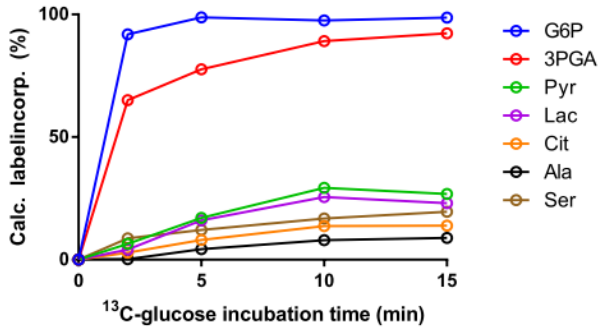

Fig. 25 - Time course of ^{13}C-label incorporation. HEK293 cells were labeled for up to 15 minutes with label buffer containing u-^{13}C glucose and label in metabolites was measured at different time-points.

4.1.9. Label incorporation and quantification of metabolites can be obtained from a single sample with high precision

Parallel to the measurement of metabolite quantities (Section 4.1.3), the reproducibility of the label incorporation within technical and biological replicates was determined. T98G cells were harvested repeatedly and the incorporation of u-^{13}C-glucose into metabolites of the central carbon metabolism was measured. (Fig. 26 and Suppl. table 6)

As expected (and illustrated above) with glucose as ^{13}C-substrate the glycolytic intermediates were strongly labeled; the intermediates of the upper glycolysis were labeled to 80 percent. At the branch points of glycolysis the label decreased, fructose and glycerol-3-phosphate were labeled with approximately eight percent, lactate and pyruvate with nearly 20 percent. The TCA cycle intermediates were only poorly labeled (1-2 %) except citrate which was labeled by around eight percent. This indicates a special position of citrate within the TCA-cycle and supports findings that the TCA-cycle is truncated with citrate being transported to the cytosol and split there to support cytosol with reducing equivalents and acetyl-CoA for lipid synthesis (Filipp et al., 2012b).

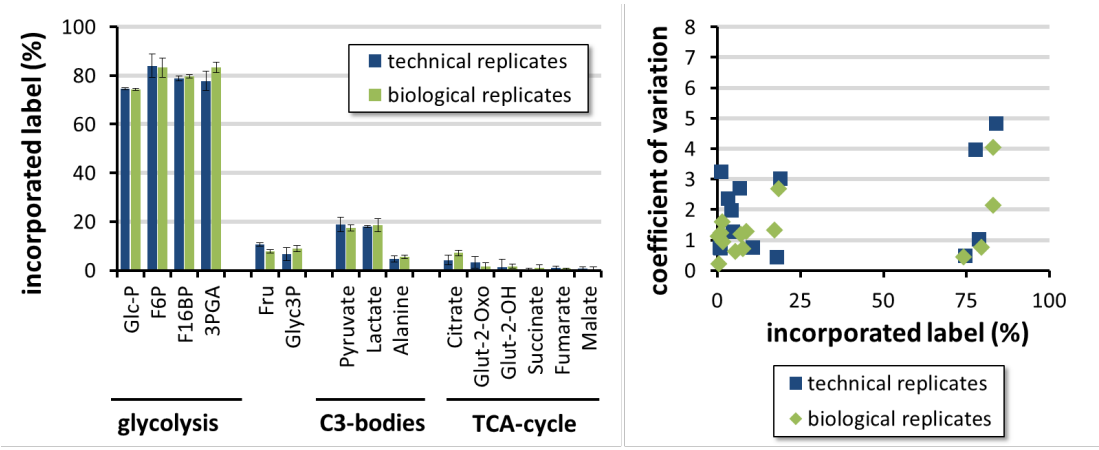

Fig. 26 - Intensity and reproducibility of label incorporation into central carbon metabolites. Left: Averages and standard deviations of technical replicates (six repeated injections of a pooled sample) and biological replicates (five different samples harvested and prepared independently under identical conditions). Right: relationship of the coefficient of variation and incorporated label intensity for technical and biological replicates.

The calculated error (coefficient of variation) was found to be between one and four percent for nearly all compounds, independent from the total amount of label (Fig. 26-right) or peak intensity (not shown). The reproducibility for technical and biological replicates was very similar.

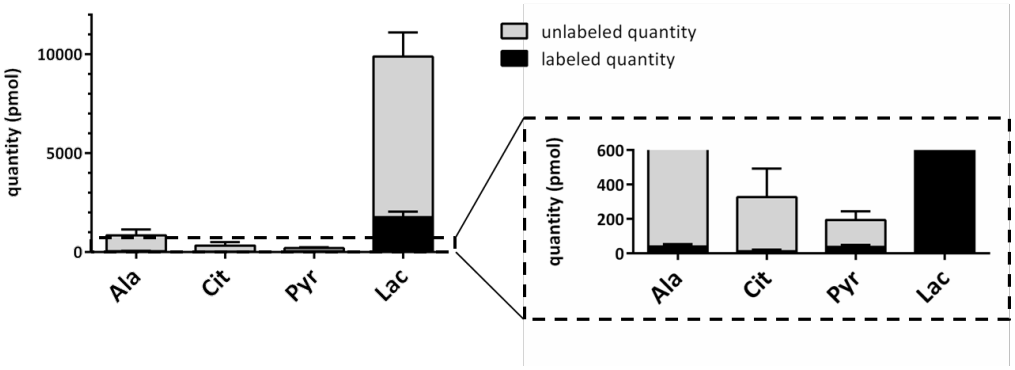

Fig. 27 – Combining labeling information with measured quantities. Here the pyruvate-branching point is illustrated with possible products of pyruvate. Quantity is expressed in pmol / million cells.

Combining the labeling data with the quantification of metabolites revealed further interesting aspects of carbon routing inside of cells. The percentage of label was very similar in pyruvate and lactate. Interestingly the amount of lactate in cells was approximately 50 times higher, with 10.000 pmol per million cells for lactate and 200 pmol per million cells for pyruvate (Fig. 27). For that reason also the labeled fraction of lactate by far exceeded the labeled fraction of pyruvate.

These data indicate an extremely tight coupling of pyruvate and lactate turnover that leads to a rapid exchange of labeled pyruvate molecules with the existing lactate pool. This could be explained either by a very imbalanced NADH/NAD^+ ratio, metabolic compartmentation, or channeling (Zwingmann et al., 2001) and should be further investigated.

4.2. Section 2 – Cell cycle Experiment

Proliferating cells have a higher demand for energy and intermediates for biosynthetic products than resting cells, which is reflected by a more active metabolism and altered metabolic routes. A deeper understanding of the regulation that drives cells into proliferation can offer new opportunities for cancer therapy (Vermeulen et al., 2003). Proliferating thymocytes for example showed a higher activity of important enzymes of the CCM, resulting in a higher glucose utilization, higher rates of lactate secretion, and a higher glutamine utilization (Brand, 1985). The differential regulation of glycolysis and glutaminolysis was attributed to degradation of regulators of metabolism like 6-phosphofructo-2-kinase/fructose-2,6-bisphosphatase, isoform 3 (PFKFB3) and glutaminase 1 (GLS1) by the anaphase-promoting complex/cyclosome (APC/C), a large multimeric ubiquitin ligase that targets key mitotic regulators for destruction by the proteasome (Colombo et al., 2011; Moncada et al., 2012).

The differences in the carbon routing through the CCM during the cell cycle were monitored with the pSIRM method. Additionally, we measured protein intensities and turnover by a pulsed SILAC-approach, to identify similarities and differences of metabolic regulation at the level of proteomics and metabolomics simultaneously. For this cells were synchronized by two different strategies, released from block and simultaneously supplied with heavy labeled amino acids to measure time-dependent protein turnover. Additionally at every time point the incorporation of u-^{13}C-glucose was performed for 2.5 minutes to measure activity in glycolysis in addition to the measurements of all other metabolites.

4.2.1. After release from mimosine block cells immediately start entering S-phase

T98G cells were synchronized with two different strategies: 48 hours of serum starvation or 24 hours of inhibition with 0.4 mM mimosine. Serum starvation accumulates cells outside of the cell cycle in a G_0 arrest and mimosine a small, uncommon non-proteinogenic amino acid, inhibits transition from G1 to S-phase (Krude, 1999; Lalande, 1990; Watson et al., 1991). After removing the cell cycle block, cells reenter the cell cycle and start to divide. By the sudden release into the

cell cycle, cells of the population start from the same point, and continue to divide synchronized for a certain period of time until individual differences slowly lead to a desynchronization.

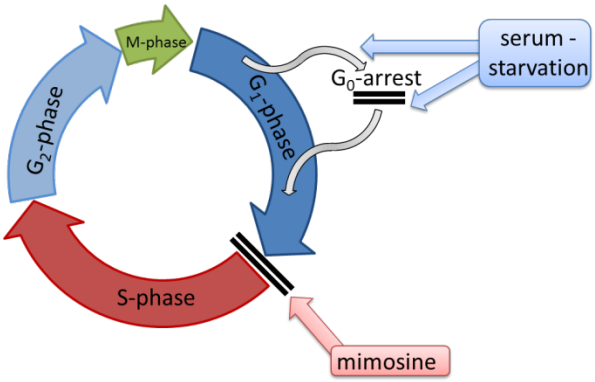

Fig. 28 - Strategy of cell synchronization. Cell division of T98G cells was stopped by two different strategies in different stages of the cell cycle. After release into fresh media cells continued in the cell cycle resulting in synchronized growth.

Synchronization of growth after withdrawal of the cell-cycle block was determined by my cooperation partner Sebastian Memczak (Rajewski-lab, MDC Berlin) by measurement of the cell cycle distribution using flow cytometry (not shown) and western blot analysis for known cell cycle markers (Fig. 29). Combining the information obtained from these experiments in combination with the reported action of mimosine led to the conclusion that cells rapidly went into S-phase after removal of mimosine.

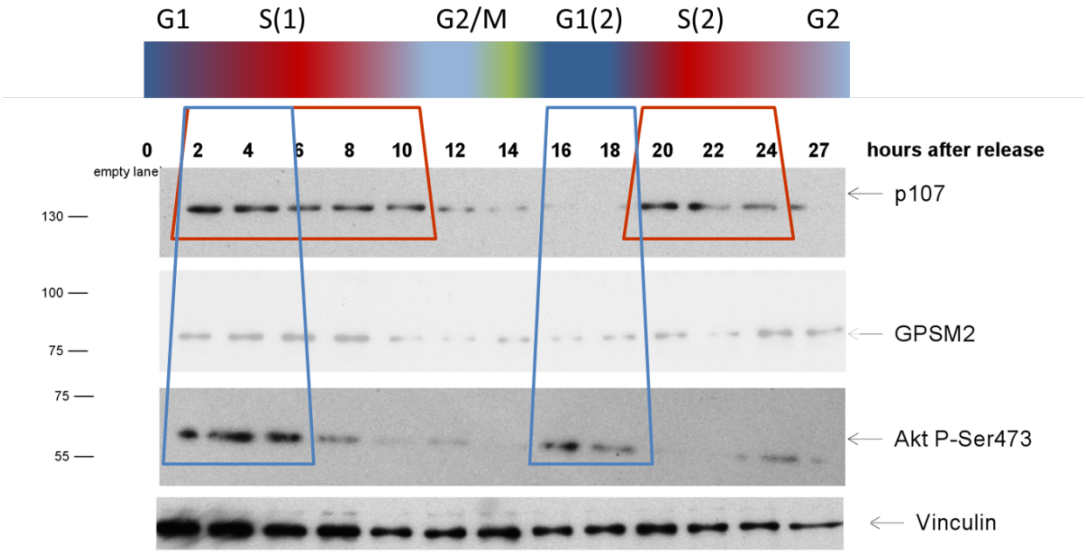

Fig. 29 – Validation of cell cycle synchronization by western blot analysis. P107 peaks in S phases, GPSM2 is a protein of the spindle pole assembly and should be important during M-phase, whereas P-Akt is elevated in early G1-phase. Vinculin was used as loading control. Above the blot the proposed cell cycle phases are shown. Blot was done by S. Memczak.

After approximately 12 hours, cells finished S-phase and went into G2/M phase, followed by a very short G1 phase. It further seemed that cells went into a second S- phase at around 20 hours. Ultimately this indicated that cells were effectively synchronized by mimosine treatment, and that this synchronization lasted throughout a full cell-cycle.
Serum starvation on the other hand appeared less suitable for our study; reentering the cell cycle into the S-phase took around 8 hours after release from this treatment followed by long S-phase duration (not shown). All further data analysis was primarily focused on the mimosine treated cells.

4.2.2. Proteins showed a continuous increase in their heavy to light ratios.

Cells released from cell cycle arrest received fresh media containing the heavy labeled amino acids arginine and lysine. These essential amino acids were taken up by the cells and incorporated into newly synthesized proteins (Ong et al., 2002). The heavy to light ratio (H/L) is an indicator for the rate of synthesis of proteins, with respect to their degradation and therefore an indicator of protein turnover. Proteins were measured with an untargeted mass spectrometry approach, the measured heavy to light ratios were filtered for outliers and averaged over the 2 measured biological replicates.

Proteins were clustered with k-means clustering, resulting in 6 different clusters (Fig. 30). In summary most proteins show similar behavior over the time: a gap of around 2-4 hours, followed by a continuous increase in the H/L ratios until 12 hours after release from block. Between 12 and 16 hours H/L ratios remained constant, followed by a second increase. Remarkably, this pattern strongly resembled the identified synchronization scheme, monitored by western blots. During S-phases (4-10 and 20-24 hours) we observed a high protein synthesis, detected by increasing H/L ratios, and during G2-M-G1 transition (12-16 hours) protein synthesis remained static.

The strongest differences between several proteins were found in the absolute intensity of H/L incorporation instead of temporal changes. More than half of all measured proteins barely reached a H/L ratio of 1 after 24 hours (Cluster 4 and 6), 90 proteins reach a H/L ratio between 1 and 3 (cluster 3), 32 proteins a H/L ratio around 4 (cluster 2) finally 11 proteins showed an extremely high turnover found with a very high H/L ratio already in early time points (cluster 1).

Table 6 - Proteins in cluster 1, with an extreme and immediate turnover.

protein name	gene-ID	H/L ratio (averaged over all timepoints)
Coiled-coil-helix-coiled-coil-helix domain-containing protein 2	CHCHD2; CHCHD2P9	5.91
Protein-lysine 6-oxidase	LOX	4.96
SPARC	SPARC	4.67
Transforming growth factor-beta-induced protein ig-h3	TGFBI	4.37
Serine protease 23	PRSS23	4.36
Collagen alpha-3(VI) chain	COL6A3	4.28
Sequestosome-1	SQSTM1	3.59
Lysyl oxidase homolog 2	LOXL2	3.50
Metalloproteinase inhibitor 3	TIMP3	3.38
Insulin-like growth factor-binding protein 5	IGFBP5	3.32
Fatty acid desaturase 2	FADS2	3.17

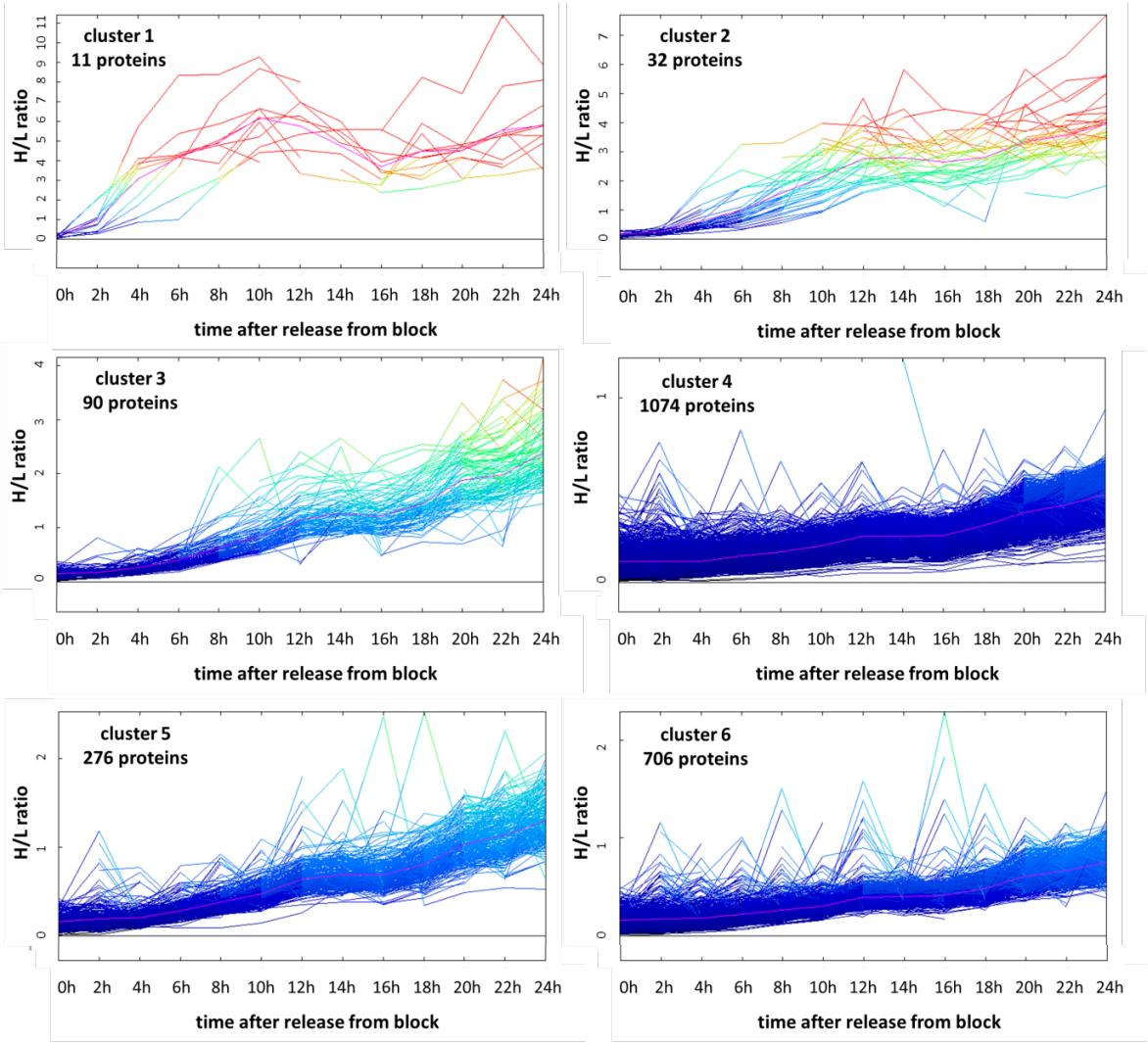

Fig. 30 – k-means clustering of all proteins from T98G cells synchronized by mimosine-treatment. The H/L ratios were plotted against the time after release from the cell-cycle block. The different clusters mainly differ in their total intensity of H/L ratios. The resulting mean of every cluster is displayed by the purple lines. The color of the lines indicate the intensities of the heavy to light ratios.

Table 7 - proteins in cluster 2, with surpassing high turnover rate.

protein name	gene-ID	H/L ratio (averaged over all timepoints)
Ubiquitin-conjugating enzyme E2 C	UBE2C	3.11
G2/mitotic-specific cyclin-B1	CCNB1	3.03
Kinesin-like protein KIF20A	KIF20A	2.85
Cell division cycle protein 20 homolog	CDC20	2.83
Collagen alpha-1(VI) chain	COL6A1	2.73
Collagen alpha-2(I) chain	COL1A2	2.67
Protein AF1q	MLLT11	2.66
Laminin subunit beta-1	LAMB1	2.63
Ubiquitin-conjugating enzyme E2 S	UBE2S	2.55
Sodium-coupled neutral amino acid transporter 2	SLC38A2	2.54
Laminin subunit gamma-1	LAMC1	2.43
Acyl-CoA desaturase	SCD	2.42
Casein kinase I isoform alpha	CSNK1A1	2.28
Histone H1x	H1FX	2.20
Fibronectin;Anastellin;Ugl-Y1;Ugl-Y2;Ugl-Y3	FN1	2.15
Targeting protein for Xklp2	TPX2	2.06
Collagen alpha-2(VI) chain	COL6A2	2.06
DNA-directed RNA polymerase II subunit RPB1	POLR2A	1.93
BCL2/adenovirus E1B 19 kDa protein-interacting protein 3	BNIP3	1.87
Protein transport protein Sec61 subunit gamma	SEC61G	1.85
Galectin-3-binding protein	LGALS3BP	1.82
Aurora kinase A	AURKA	1.81
Syntenin-1	SDCBP	1.80
Squalene synthase	FDFT1	1.74
Catenin alpha-1	CTNNA1	1.72
Nucleobindin-1	NUCB1	1.72
Importin subunit alpha-2	KPNA2	1.69
E3 ubiquitin-protein ligase UHRF1	UHRF1	1.67
Uridine-cytidine kinase 2	UCK2	1.67
Protein regulator of cytokinesis 1	PRC1	1.67
Microtubule-associated proteins 1A/1B light chain 3B	MAP1LC3B; MAP1LC3B2	1.61
Heat shock factor-binding protein 1	HSBP1	1.61

In the next step 90 enzymes of central carbon metabolism were selected and plotted in the same way as before to compare their behavior relative to all other proteins (Fig. 31, Suppl. table 8). With a single exception (fatty acid desaturase 2 (FADS2) - Table 6) the majority of the enzymes showed a very low synthesis and ended with a H/L-ratio of less than one after 24 hours, therefore presenting a similar turnover pattern as the majority of all other measured proteins. It is known

that fatty acid synthesis is essential for cancer growth, but usually this based on a high activity of fatty acid synthase, but not fatty acid desaturase. (Zecchin et al., 2011)

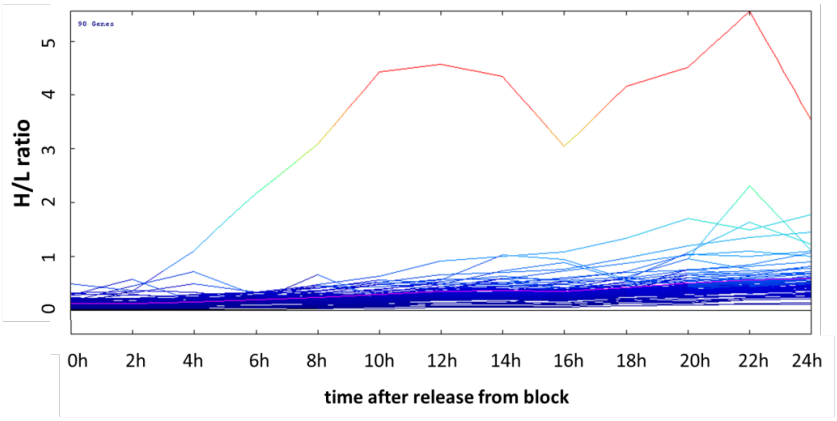

Fig. 31 – H/L ratios of 90 metabolic enzymes from T98G cells synchronized by mimosine-treatment.

The proteins clustering within the same group were tested for further similarities by performing a gene ontology ontology (GO) enrichment analysis. For this the protein-IDs of each cluster were uploaded individually to WebGestalt (**WEB**-based **GE**ne **S**e**T** **A**na**L**ysis **T**oolkit) (Wang et al., 2013; Zhang et al., 2005) and compared against the list of all measured proteins. A GO enrichment analysis was performed with default settings (hypergeometric statistics, BH adjustment of multiple tests, Top10 significance level and 2 minimum number of genes for a category)

In **cluster 1** (with only 11 proteins), in total eight proteins were assigned to the biological process "developmental process" and six proteins were assigned to the function "metal ion binding". Moreover a strong enrichment for the extracellular compartment (8 proteins, p-value $8.93*10^{-8}$) was found.

In **cluster 2** (with 34 proteins), an enrichment was found in the processes "cell division" (9 proteins), "cellular component organization" (21 proteins), "cell morphogenesis" (9 proteins), "M-phase" (10 proteins). Of the molecular functions the class "enzyme binding" was prominently enriched (11 proteins) and in cellular components again the extracellular matrix was found to be prominent with 8 proteins, but also "spindle pole" with 5 proteins.

In **cluster 3** (with 90 proteins) the enrichment was less clear, but there was a slight an enrichment in extracellular matrix proteins and spindle pole assembly. Additionally "transcription from DNA polymerase II promoter" was enriched with 19 proteins, and localization in the endoplasmic reticulum.

As positive control the 90 selected enzymes were also tested and were found to be indeed enriched in the molecular function “catalytic activity” and biological process “small molecule metabolic processes” with p-value of $2*10^{-25}$ and $8*10^{-39}$, respectively.

To normalize for different turnover rates and identify differences in their temporal behavior, H/L ratios of measured proteins were normalized to range between zero and one and clustering was repeated (Fig. 32). This strategy delivered even more similarities in the temporal behavior of the proteins: A nearly linear increase in the H/L ratios from 2 to 12 hours, followed by a gap from 12-16 hours, ultimately followed by a more (cluster 3+5) or less (cluster 4) linear increase in the H/L ratio until the end, was observed.

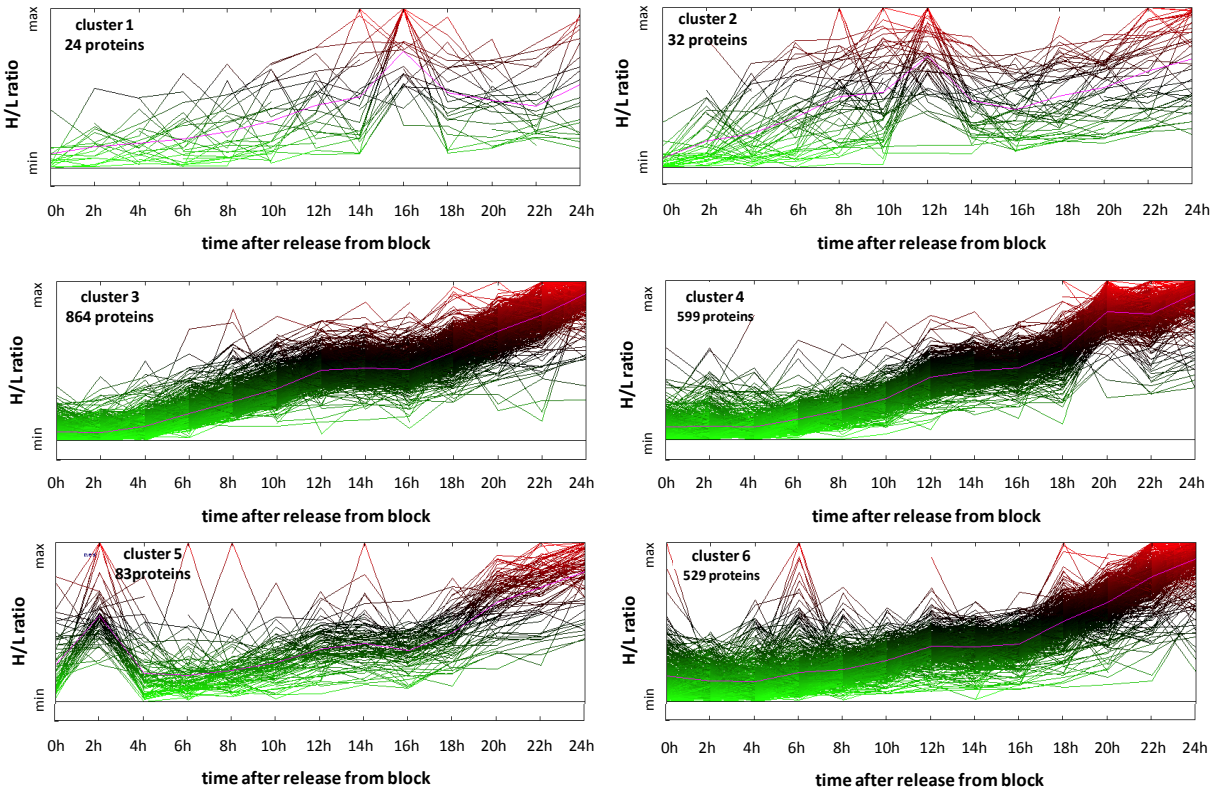

Fig. 32 - k-means clustering for normalized H/L ratios of all proteins from T98G cells synchronized by mimosine-treatment. The H/L ratios were normalized to range between zero and 1 for the lowest or highest measured values and plotted against the time after release from the cell-cycle block. The color scales for green at zero, black at 0.5 and red at 1.

4.2.3. Glycolysis and glutaminolysis are differentially active

For the first time intracellular metabolites were measured in an untargeted way in cells synchronously passing through the cell cycle, sampled every two hours after release from the block. Additionally, at every time point we also included short termed ^{13}C-glucose incorporation to measure the rate of glycolysis.

Essentially all glycolytic intermediates showed similar behavior and peaked at six hours and again but with smaller intensity at 22 hours after release from the mimosine block. (Fig. 33). We identified both time periods as S-phases. Additionally, TCA cycle intermediates showed a similar behavior within their group which is different to the group of glycolytic intermediates; they peaked around 14 hours, in the middle of the M-phase and continuously rose from there till the end of measurements. The measured amount of citrate is in all time points lower than the starting point, it probably accumulated during the arrested cell cycle. 2-hydroxyglutarate showed a similar pattern, demonstrating its close connection to TCA cycle intermediates. Also alanine decreased compared to the starting value, and is poorly measured afterwards. Remarkably, the amount of aspartate decreased at the 14 hours time point, indicating a possibly increased supplementation to the TCA cycle.

With most compounds being well balanced over the time, some compounds (beta-alanine, alpha-ketoglutarate and hypotaurine) showed a high increase over time (up to 4-fold).

Overall this data indicates that glycolysis played an important role during S-phase but TCA cycle activity was important during the M-phase, where no substrates for biosynthesis were needed, but energy for division and subsequently the restructuring to two daughter cells.

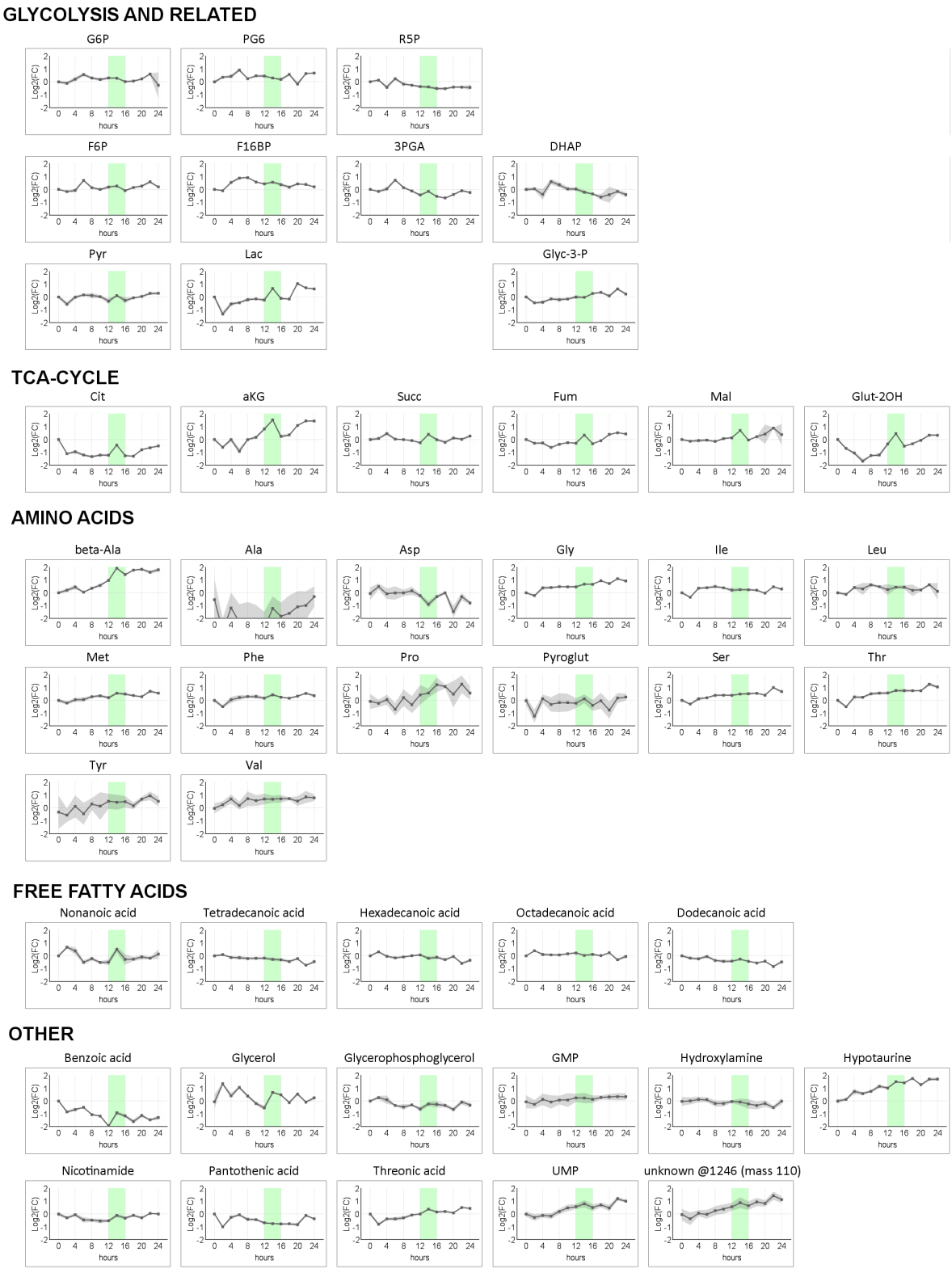

Fig. 33 - Metabolite profiles after release from mimosine-block. Log2-fold changes relative to the zero hour time point, right before release from block, were plotted. The green area indicates the time-period from 12 to 16 hours, the time with lowest protein synthesis around the M-phase.

The consideration of the ^{13}C label incorporation revealed further aspects of similarity within the regulation of glycolysis. The normalized labeled intensities that included both changes in intensity and in label incorporation were plotted in Fig. 34. Dihydroxyacetonephosphate showed high variability but all other compounds were measured well. Essentially all compounds showed similar behavior. Around 2 hours after release from block they increased, resulting in a peak around 6 hours, reflecting the early S-phase (Fig. 29). In the late S and G2 phase glycolysis appeared to be less important and labeled intensity decreased to the lowest level around 16 to 18 hours, followed by a second increase in the presumed second S-phase around 20-22 hours. Lactate furthermore increased over time, which might reflect an accumulation of lactate in the media over time.

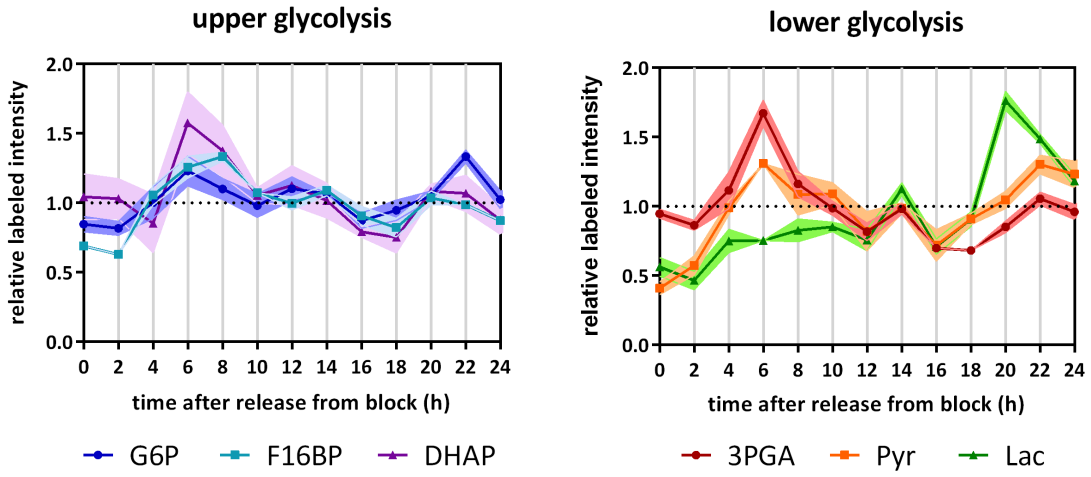

Fig. 34 - Relative labeled intensities in glycolytic intermediates after incorporation of ^{13}C-glucose for 3 minutes at different time points after release from mimosine block. The calculated label was multiplied with the measured, normalized intensities. In contrast to Fig. 33 results were displayed not relative to the zero hour time point but to the average over all time points, so data points center around 1 (dotted line). Average is shown by dots and line and standard deviation by shaded areas.

4.3. Section 3 – Measuring the effect of glycolytic inhibitors on the central carbon metabolism and growth

The results of the first labeling experiments revealed a strong activation of the glycolytic pathway in the analyzed cell lines. Furthermore, the results of the cell cycle experiments indicate that glycolysis was even more pronounced and important during the S-phase of the cell cycle.

It was further tested if disturbing the glycolysis reversely affected cell growth and cell cycle distributions. The status of the cells under glucose-starvation and the influence of three different glycolytic inhibitors (2-deoxyglucose, 3-bromopyruvate and glyceraldehyde) was monitored. The three inhibitors were considered to inhibit different enzymes within the glycolytic cascade: hexokinase (HK), phosphoglucoisomerase (PGI) and glyceraldehyde 3-phosphate dehydrogenase (GAPDH) (Fig. 35).

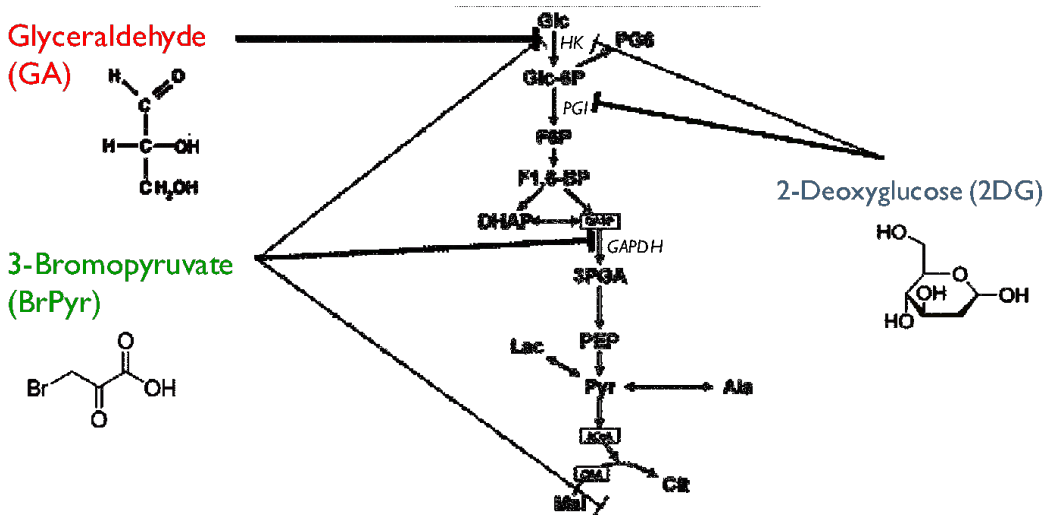

Fig. 35 - Scheme of CCM with expected targets. Glycolysis is shown up to the entry into the TCA-cycle, with the enzymes indicated that were reported to be inhibited by the three different inhibitors.

Reading the literature indicated strong discrepancies in the described action of these compounds that were not always supported by current experimental data. It appeared necessary to test these compounds with the newly developed pSIRM approach and to monitor the impact of these compounds on metabolism on a short time scale. The inhibition was expected to manifest by differences in the ^{13}C-incorporation into various intermediates of the glycolysis.

I developed a specific experimental strategy to address this question and to monitor short-termed and direct effects of these compounds on enzymes of the glycolytic cascade (Fig. 36). The analyzed cells exhibited a certain glycolytic flux, dependent on their activity, age, nutrient state and other factors. When an inhibitor is added to cells it needs some time to develop its full

inhibitory potential: The concentration within the cells rises with its uptake and the inhibitor needs to be transformed to its active state and has to inactivate the enzymes. This was taken into consideration by pre-incubation of the cells for at least 12 minutes with the compounds to be tested, followed by incorporation of ^{13}C-glucose for 3 minutes to assess glycolytic activity. ^{13}C-glucose incorporation was performed still in presence of the inhibitor to maintain a persistent inhibition for a total time of 15 minutes. In parallel, control samples were analyzed that were not incubated with inhibitor or were treated with an osmotic control (e.g. NaCl, Mannitol). In some experiments a longer incubation time of 30 or 60 minutes was tested in addition. The measurement of the untreated control cells reported the current measured state of glycolytic activity, as a reference against drug inhibited cells in which glycolysis was expected to found decreased.

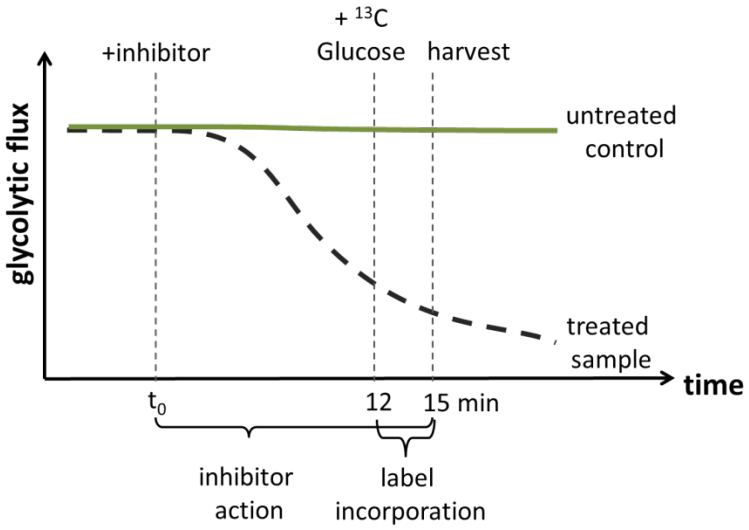

Fig. 36 – Experimental setup to determine short term inhibition of glycolytic flux. Samples were incubated with potential inhibitors of glycolysis for a total time of at least 15 minutes to generate inhibitory potential of the compound and decreased glycolytic flux (black line). In the last 3 minutes ^{13}C-glucose-labeling was applied to measure glycolytic activity, which was compared against an untreated control sample (green line)

4.3.1. All compounds inhibit cell growth and induced a stress phenotype in a dose dependent manner

For **glyceraldehyde,** experiments performed in the forties to sixties of the last century proposed an activity in the low millimolar range (Needham et al., 1951; Stickland, 1941). Insuline secretion by glyceraldehyde was found and studied with concentrations between 5 and 20 mM (Alcazar et al., 1995; Hellman et al., 1974; MacDonald et al., 1989; Malaisse et al., 1975) .

2-deoxyglucose was reported to be effective in the high millimolar range. An ATP depletion by 2DG after 5 hours was shown with concentrations between 4 and 10 mM (Xi et al., 2011). Zhang et al. tested 5 mM on 12 different cancer cell lines and found a decreased growth rate, with some cell lines undergoing apoptosis and other cell lines developing resistance (Zhang et al., 2006). In HCT116 cells an ATP decrease was shown for 2DG between 20 and 40mM (Ihrlund et al., 2008).

3-Bromopyruvate caused decrease of ATP-levels in HCT116 cells at a concentration of around 50-100 µM (Ihrlund et al., 2008). Ko *et al* reported that in VX2 tumor slices the K_M for lactate production (as measurement of glycolytic activity) was 15.5 mM for 2DG and 2.4 mM for BrPyr, but effects on respiration of isolated mitochondria was shown at 1.2 mM BrPyr (Ko et al., 2001). In another report decreased cell viability of human hepatocellular carcinoma (HCC) by 50% after 3h at concentrations around 200 µM and after 24h at 130 µM, with VX-2 cells being twice as sensitive (Ganapathy-Kanniappan et al., 2009).

No references could be found where these inhibitors were used on HEK293 or T98G cells. Additionally, the experiments in this dissertation were performed typically with a glucose-concentration of 2.5 g/l (14 mM), nearly half the concentration used in most other experiments using standard-DMEM composition of 4.5 g/l (25 mM). At least for a competitive inhibition as expected for 2DG a dependency on the glucose concentration can be anticipated. Both factors, the cell line used and the glucose concentration in the media should influence the effectivity of the compounds, making it necessary to initially test which concentration affect our chosen cell models. The compounds were added to the cells with different concentrations 24 hours after seeding. Growth and appearance were monitored under a microscope 24 or 48 hours after drug addition (Fig. 37- Fig. 40). All tested compounds showed a concentration dependent effect that could be monitored under the microscope: Cell-density decreased, meaning cell division is inhibited or cells die. Ultimately cells lost their shape and started to detach. This effect is very prominent in HEK293 cells that even under normal conditions do not attach so strongly to cell culture plates, so that every counting method that requires washing of cells would therefore overestimate the effect of the drugs and should be interpreted very carefully. If these swimming cells are still alive they should be included in further analysis.

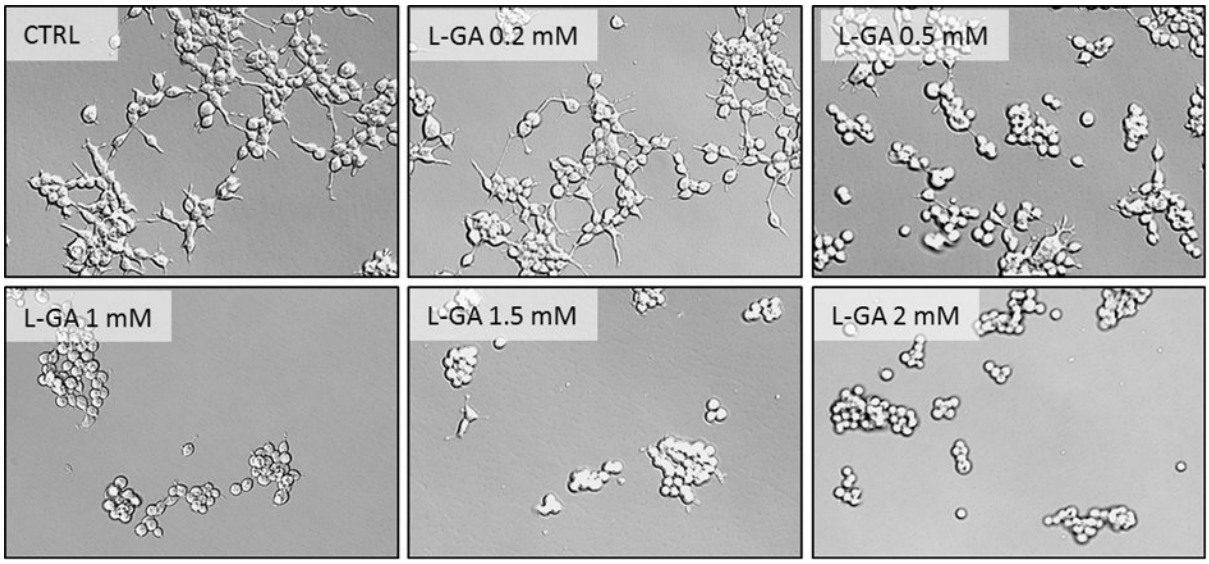

Fig. 37 - The effect of different concentrations of L-Glyceraldehyde on the appearance of HEK293 cells. The drug was added 24h after seeding and pictures were taken 24 hours after drug addition with 20 fold magnification.

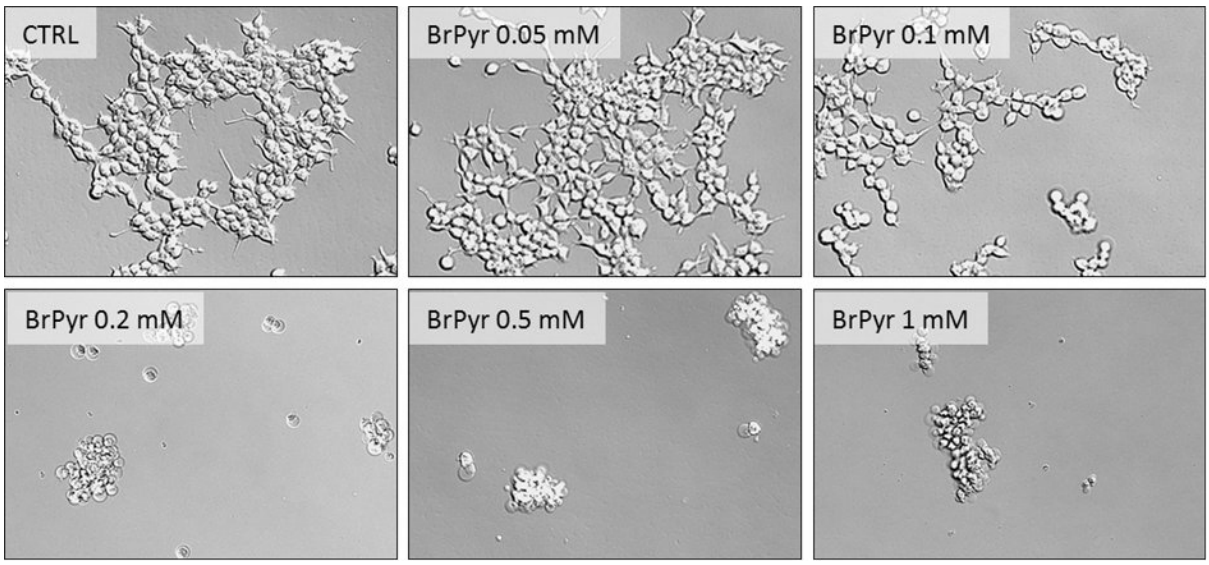

Fig. 38 - The effect of different concentrations of 3-Bromopyruvate on the appearance of HEK293 cells. The drug was added 24h after seeding and pictures were taken 24 hours after drug addition with 20 fold magnification.

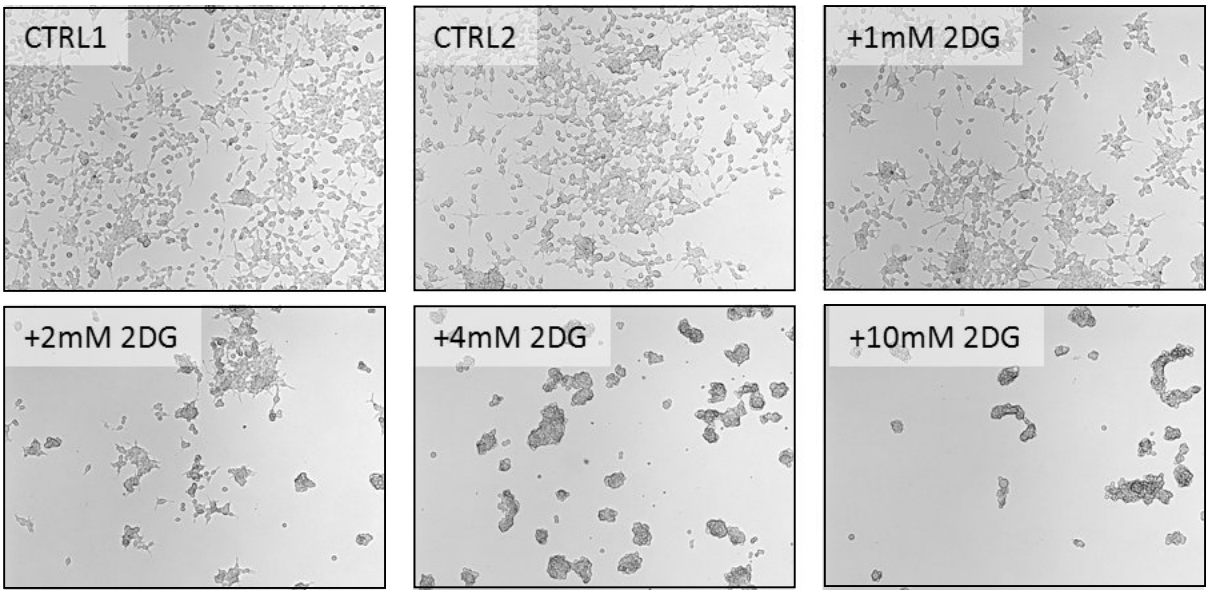

Fig. 39 – The effect of different concentrations of 2-Deoxyglucose on the appearance of HEK293 cells. The drug was added 24h after seeding and pictures were taken 48 hours after drug addition with 10 fold magnification.

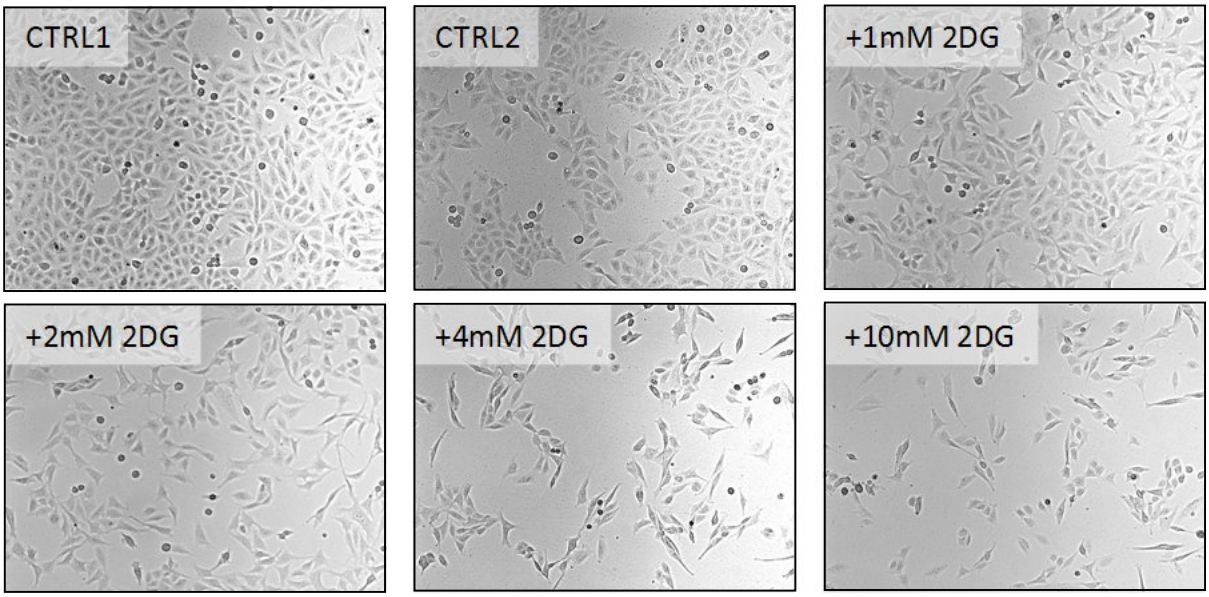

Fig. 40 - The effect of different concentrations of 2-Deoxyglucose on the appearance of T98G cells. The drug was added 24h after seeding and pictures were taken 48 hours after drug addition with 10 fold magnification.

4.3.2. Further estimation of effective concentrations

The results from the previous section showed that these compounds have an effect on the tested cell lines, with BrPyr being effective in lower concentrations than the other compounds. To further quantify the effect and clarify if the swimming cells were dead, cell counts and viability were measured, including swimming cells, under the influence of different concentrations of the tested drugs. Glyceraldehyde and 3-bromopyruvate were tested in 7 different concentrations from 1-10.000 µM; 2DG was tested in 4 different concentrations from 1.000-10.000 µM (Fig. 41 - Fig. 44 and Table 8).

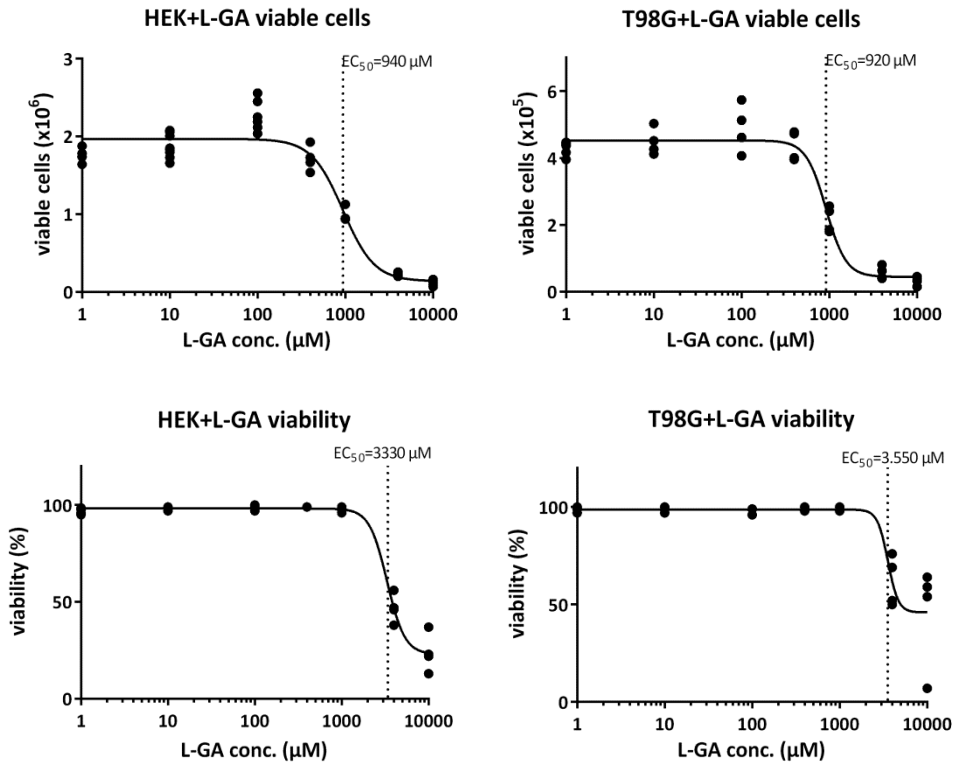

Fig. 41 – Effect of L-GA to viable cell number or viability of HEK293 and T98G cells. Cells were seeded into 6-well plates in DMEM supplemented with 2.5 g/l glucose. After 24 hours of growth drugs were added in different final concentrations. After an additional 24 hours, viable cells (per well) and viability were examined using the trypan-blue exclusion method, including all the swimming cells. 2 replicate wells were counted twice and plotted independently. EC_{50} -values were calculated with GraphPad Prism 6.0.

The EC_{50} for L-glyceraldehyde, the concentration in which 50% of the possible decrease of the analyzed factor is measured (Neubig et al., 2003), was the same between the two cell lines but was distinct between the readouts, viable cell number or viability (Fig. 41). Within the 24 hours after addition cells could further divide and increase their number, but under the influence of the drug the division had stopped. At a concentration of around 0.9 mM the cell number decreased to 50%. This effect was primarily based on a decreased growth as the viability decreased to 50% at around 3.3 mM. At around 1mM of L-GA cells started to swim, however this concentration was

not effective to decrease viability. This also demonstrates that swimming cells were not dead at the time of analysis; decreases of viability started around 2mM. Interestingly, both cell lines showed a slight increase in cell number at 100 µM.

Further experiments were performed at a concentration of 2mM, which was the midpoint between the EC_{50} for growth inhibition and viability. This concentration also differentiated induction of swimming cells between the different isomers, with the L-isomer being more effective.

In terms of growth inhibition BrPyr was the more effective compound (Fig. 42). Inhibition of viable cell number to 50% started at 90 µM in HEK293 cells and 230 µM in T98G cells, which is $1/10^{th}$ or $1/4^{th}$ of the concentration needed for L-GA, and is in line with the concentrations reported in the literature. The effect on viability again needed a 3 fold higher concentration of this compound, similar to the difference found in L-GA treatment. The sensitivity for BrPyr was different between these two cell lines, with HEK293 cells being more sensitive, an effect not seen for L-GA (Fig. 41).

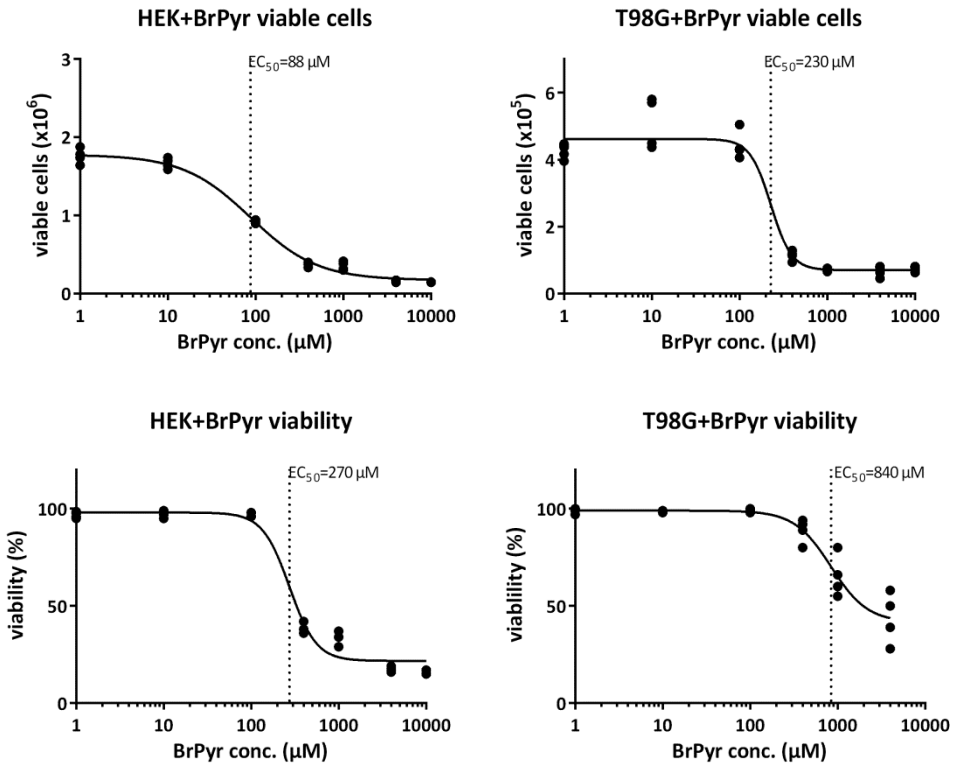

Fig. 42 - Effect of BrPyr on viable cell number or viability of HEK293 and T98G cells. Cells were seeded into 6-well plates in DMEM supplemented with 2.5 g/l glucose. After 24 hours of growth drugs were added in different final concentrations. After additional 24 hours viable cells (per well) and viability were examined using the trypan-blue exclusion method, including all the swimming cells. 2 replicate wells were counted two times and plotted independently. EC_{50} -values were calculated with GraphPad Prism 6.0.

Furthermore the application of both compounds decreased the glucose-consumption of the tested cells as reported in Fig. 43. Untreated cells and cells treated with very low concentrations of either inhibitor consumed glucose, therefore decreasing the residual amount of glucose in the media. Under high drug concentrations the remaining glucose level stayed higher, probably at the value present at the time point of drug addition (not tested). The effect in HEK293 cells was more pronounced as they consumed more glucose in total.

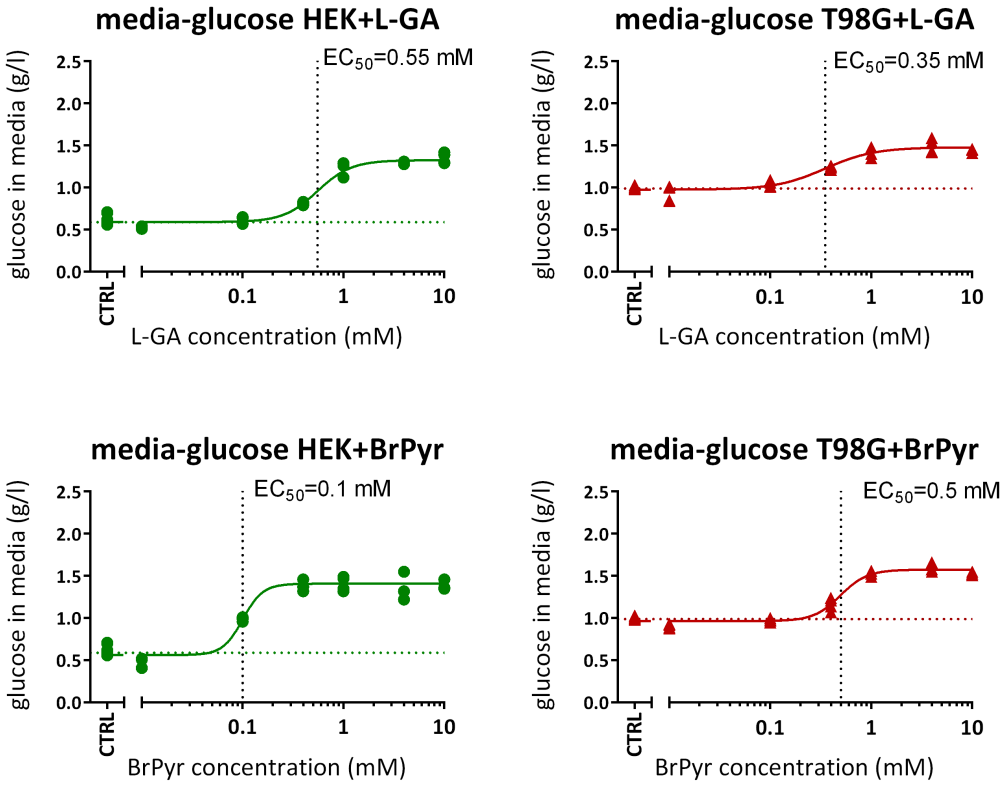

Fig. 43 - Effect of BrPyr and L-GA to glucose consumption of HEK293 and T98G cells. Cells were seeded into 6-well plates in DMEM supplemented with 2.5 g/l glucose. After 24 hours of growth drugs were added in different final concentrations. After additional 24 hours viable cells media was sampled and measured by GC-MS. Glucose concentration was calculated with an external calibration curve. EC_{50} -values were calculated with GraphPad Prism 6.0.

The results are summarized and compared in Table 8. In some cases, decreasing the viability needed higher concentrations than decreasing the cell growth that in most cases happened at higher concentrations than decreases of glucose consumption. Remarkably, under the impact of bromopyruvate the inhibition of glucose consumption and growth was at similar concentrations for HEK293 cells, but in T98G cells glucose consumption was decreased at lower concentrations.

Table 8 – Calculated effective doses for inhibiting glucose consumption, cell growth or viability of tested drugs in two different cell lines. The correlation coefficient (R^2), the concentration in which 50% of inhibition occoured (EC_{50}) and the 95% confidence interval (CI) were calculated with non-linear curve-fitting using GraphPad Prism.

Drug		HEK293			T98G		
		glucose-consumption	viable cells	viability	glucose-consumption	viable cells	viability
L-GA	R^2	0.9704	0.9316	0.9812	0.9389	0.9559	0.8259
	EC_{50} (µM)	553.6	941.0	3336	350.6	919.4	~ 3560
	95% CI	556.5 - 625.0	760.9 - 1164	2553 - 4360	258.8 - 475.0	801.8 - 1054	(Very wide)
BrPyr	R^2	0.9508	0.9920	0.9833	0.9701	0.9631	0.9180
	EC_{50} (µM)	100.5	87.90	274.3	497.0	227.6	840.7
	95% CI	88.41 - 114.3	73.90 - 104.6	229.7 - 327.7	430.4 - 574.0	159.0 - 325.8	619.4 - 1141

The growth inhibitory effect of 2DG was not studied in such detail but the difference between treated and untreated cells was found to be less intense. This could be mainly explained by the lack of this compound to significantly decrease viability of cells in the analyzed concentration range (Fig. 44). However the inhibition of growth induced by 2DG has an EC_{50} of 1.1 or 1.4 mM in HEK293 and T98G cells, respectively.

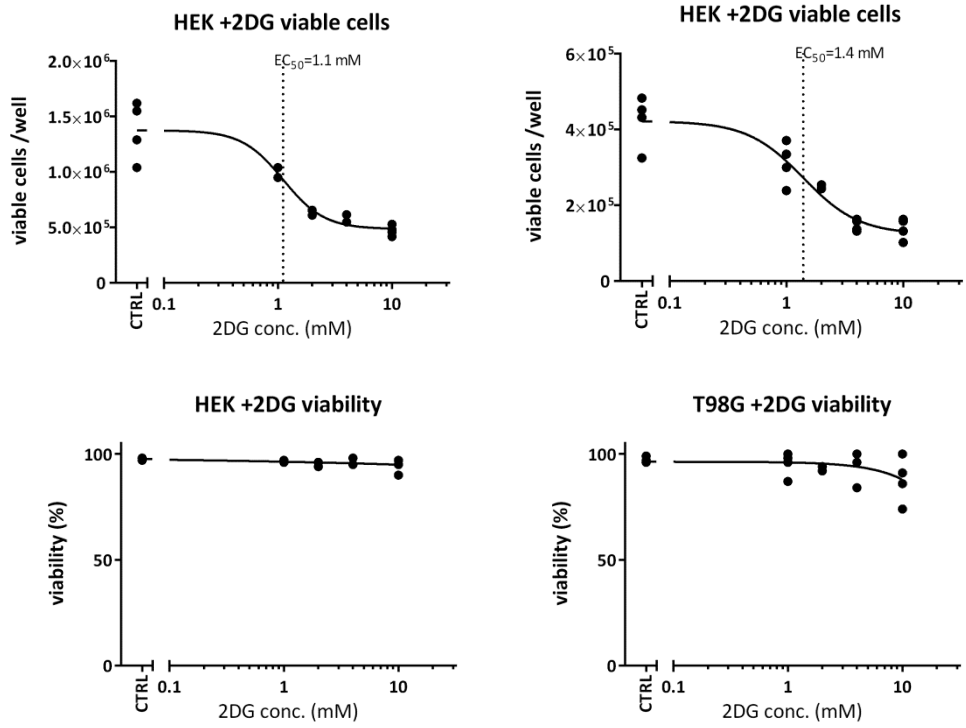

Fig. 44 - The effect of different concentrations of 2-Deoxyglucose on growth of HEK293 (left) or T98G cells (right). The drug was added 24h after seeding and cells were counted 48 hours after drug addition.

4.3.3. L-Glyceraldehyde inhibits glycolysis downstream of the hexokinase reaction

The potential inhibition of glycolysis was further studied with the pSIRM approach, as illustrated in Fig. 36. Cells were treated for 15, 30 and 60 minutes with D- or L-glyceraldehyde, glycolytic activity was measured with 3 minutes of ^{13}C-glucose labeling and compared to an untreated control. The effect of both isomers on intensity (peak area) for metabolites of the CCM, relative to the intensities measured in untreated control, is displayed in Fig. 45, by the left three bars. Similarly, the effect on label incorporation is plotted in the middle three bars and the effect on labeled intensity, the product of label and intensity, is plotted on the right.

The different isomers of glyceraldehyde showed remarkable differences in their action, whereas the duration of treatment had only a minor effect. The time-effect was not linear, indicating that already after 15 minutes an effect close to the maximum inhibition occurred. Both isomers decreased the amount of glucose-phosphate by around 25%, a further decrease in intermediates of the glycolysis was not found for the D-isomer and was found to be between 50% (F6P) and 10-20% (3PGA). Notably, the label incorporation into the upper glycolysis was not affected by either compound.

Significantly, the label incorporation into the metabolites of the lower glycolysis (3PGA, Pyr, Lac) and even alanine and citrate decreased drastically under L-GA treatment, the biggest difference between D-GA and L-GA treatment was found in lactate with labeled intensity decreasing to 1/4th to 1/8th of the intensity in the control under L-GA treatment, or 75 to 87.5% decrease. In contrast the labeled intensity in lactate was nearly unaffected under D-GA treatment. These results indicate that in contrast to expectations, the inhibition of glycolysis occurs after the formation of fructose-6-phosphate and before the formation of 3-phosphoglycerate. The intensity of glycerol increased under the influence of both compounds, indicating a possible transformation of GA to glycerol.

Fig. 45 - Effect of D- or L-glyceraldehyde on glycolysis of T98G cells (next page). T98G cells were treated for 15, 30 or 60 minutes with 2mM of D- or L-GA and labeled for 3 minutes with u-^{13}C-glucose. Fold change of intensity (first 3 bars), label (middle 3 bars) and the product of both, the labeled intensity (right 3 bars) are plotted for the individual time points, indicated with reactions and catalyzing enzymes. The y-axis are log2-scaled and differentially scaled for the upper part of glycolysis (Glucose-P, Fructose, F6P, 3PGA) and the lower part of glycolysis (glycerol, glycerol-3-P, pyruvate, lactate, alanine). Arrows between metabolites show enzymatic reactions indicated with the enzyme names, whereas dotted lines show multistep reactions without indicating every intermediate. Additional abbreviations: AAT=alanine aminotransferase, GK=glycerolkinase, AKR1 = aldo-keto reductase family 1

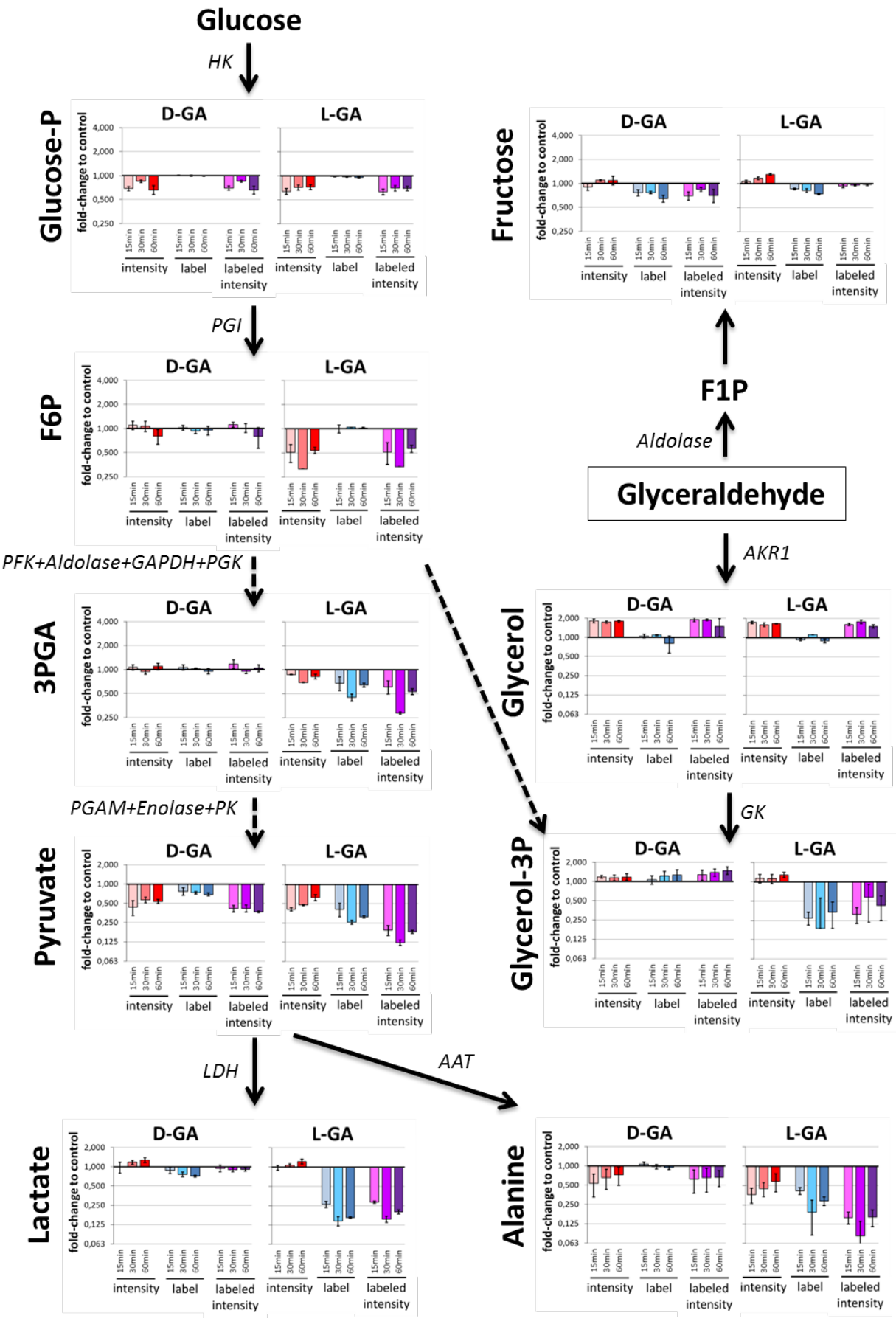
Glucose
HK
Glucose-P
D-GA
L-GA
fold-change to control
4,000
2,000
1,000
0,500
0,250
15min 30min 60min
intensity
label
labeled intensity
PGI
F6P
PFK+Aldolase+GAPDH+PGK
3PGA
PGAM+Enolase+PK
Pyruvate
0,125
0,063
LDH
Lactate
AAT
Alanine
Fructose
F1P
Aldolase
Glyceraldehyde
AKR1
Glycerol
GK
Glycerol-3P

To better characterize and compare the response of the CCM intermediates to different treatment conditions a new visualization strategy was developed: The two independent readouts of "change in intensity" and "change in label incorporation" were plotted on the orthogonal axes into an x-y-diagram (Fig. 46). This enables the identification of effects mainly influencing label incorporation or pool sizes, which would be plotted close to one of the axes, and additionally reflects the combination of both factors by the occurrence in one of the four quadrants. The diagonal line of equivalence represents combination of factors with same values but different directions, balancing each other to a net change of zero, e.g. two-fold up and two-fold down. With higher distance from this line the overall effect measured in a metabolite is higher.

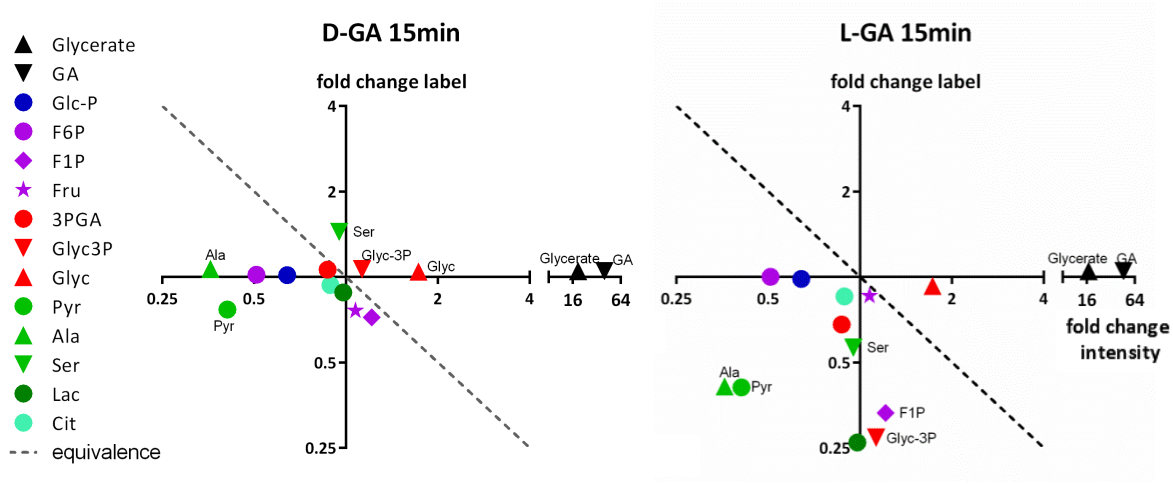

Fig. 46 – Influence of glyceraldehyde on metabolites of the central carbon metabolism. T98G cells were treated for 15 minutes with 2mM of D- or L-GA and labeled for 3 minutes with u-^{13}C-glucose. Fold changes of intensity (x-axis) and label incorporation (y-axis) were calculated against untreated control sample. Glycerate and glyceraldehyde were unlabeled and arbitrarily set to fold change of label value of 1.05.

A similar inhibitory effect as in T98G cells could be monitored in HEK293 and MCF7 cells (Fig. 47). D-GA had only a small effect within the glycolytic cascade whereas L-GA decreased the label incorporation after phosphorylation of glucose and before formation of 3PGA. The effect in MCF7 cells appeared to be stronger, than the effect monitored in HEK293 cells.

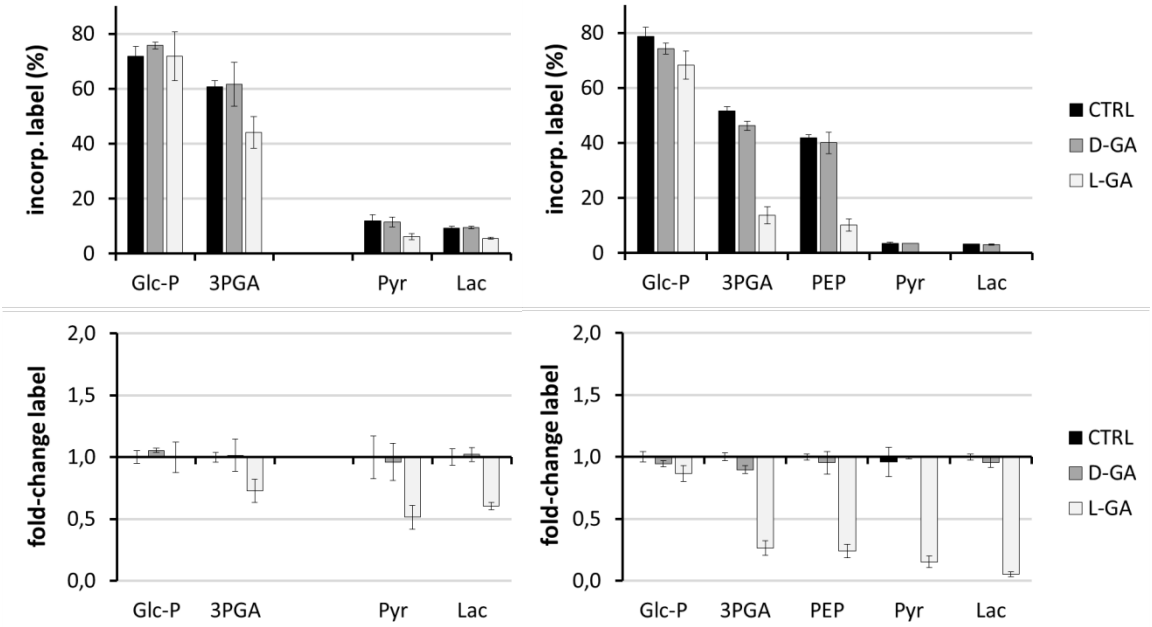

Fig. 47 – Inhibition of label incorporation into glycolytic intermediates of HEK293 cells (left) and MCF7 cells (right). Cells were treated for 15 minutes with 2mM of each isomer and label incorporation was measured after incorporation of u-^{13}C glucose for 3 minutes.

4.3.4. Bromopyruvate inhibits glycolysis primarily at GAPDH-reaction

The possible inhibitory effect of 3-Bromopyruvate (BrPyr) to glycolysis was tested by measuring the incorporation of u-^{13}C-glucose in its presence and the comparison of these treated cells to an untreated control sample. An initial concentration of 2mM was chosen to directly compare the intensity of the inhibition with the effect induced by glyceraldehyde (4.3.3) and 2-deoxyglucose (4.3.5), tested in the same concentration, even though the concentration of BrPyr was above its EC_{50} (4.3.2). The impact of BrPyr on metabolism was very strong in the tested concentration (Fig. 48). The label in the intermediates of the upper glycolysis decreased, to one third in G6P and F16-BP and to 1/8th in F6P. Interestingly, F6P and F16-BP dramatically increased their pool sizes (3-4 fold) resulting in a nearly net-change of zero on the labeled intensity of F6P and a slight increase in F16-BP. Also the pool size of 6-Phosphogluconic acid (6PG) increased. The elevated pool size of these compounds indicates that they could no longer be used and accumulated. This might also be a reason for their decreased label incorporation, as F6P is a feedback inhibitor of hexokinases. 3PGA abundance decreased to a level around the detection limit. Basically, no ^{13}C reaches the compounds of lower glycolysis, the decrease in label in pyruvate and lactate is nearly 100%. The accumulation of hexose-phosphates, the disappearance of 3PGA and the dramatic decrease of carbon from glucose ending up in metabolites downstream of 3PGA, perfectly fit to the proposed

inhibition of GAPDH by BrPyr (Ganapathy-Kanniappan et al., 2009). Remarkably, the label decreased dramatically in most compounds while their pool size remained nearly constant (Fig. 48), indicating a distinct block in the carbon flow without changing pool sizes. This would not be detectable by methods monitoring only pool sizes and exemplifies the importance of the pSIRM method.

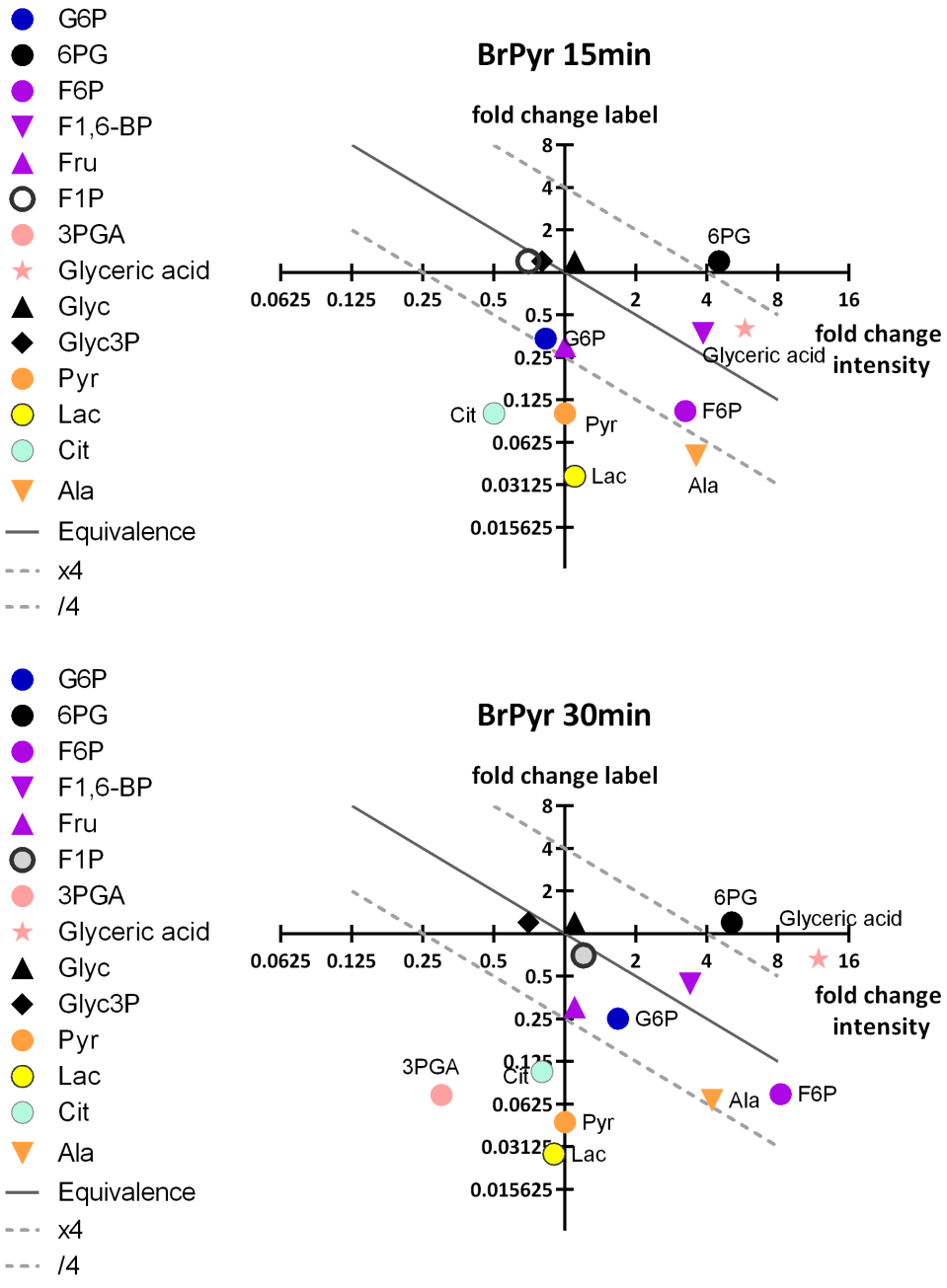

Fig. 48 – Influence of 3-bromopyruvate on metabolites of the central carbon metabolism. T98G cells were treated for 15 or 30 minutes with 2mM of 3-bromopyruvate and labeled for three minutes with u-^{13}C-glucose. Fold changes of intensity (x-axis) and label incorporation (y-axis) were calculated against untreated control sample. For some compounds (black symbols) no label could be calculated for one condition and arbitrarily set to 1.2. In addition to the line of equivalence also the level of four-fold change up or down is displayed.

Additionally a dramatic increase in the pool size of glycerate was found, this compound was also partially labeled and therefore a derivative of glucose metabolism, indicating an unexpected alteration of carbon flow. Under the assumption that GAPDH is inhibited no 3PGA is formed, and indeed I did nearly not detect 3PGA anymore, glycerate may be somehow formed from glyceraldeheyde-3-phosphate, sharing some similarities to the metabolism of glyceraldehyde.

4.3.5.2-Deoxyglucose is rapidly phosphorylated but only acts indirectly on glycolysis

2-Deoxyglucose was reported to be phosphorylated by hexokinase to 2-deoxyglucose-6-phosphate (2DG-P). In fact in cells incubated with 2-deoxyglucose in the millimolar range a phosphorylated compound could be detected, with a mass spectrum similar to other sugar-phosphates and a retention between pentose-phosphates and hexose-phosphates. This compound could be later identified as the predicted 2-deoxyglucose-6-phosphate (2DG-P) by the use of an authentic chemical standard. The accumulation of this compound was quantified relative to glucose-6-phosphate by its calibration curve, assuming a similar ionization and fragmentation efficacy of this compound compared to G6P (Fig. 49).

With 2mM treatment and after 15 minutes of incubation 2DG-P already exceeded Glc-P by a factor of 7 and F6P by more than a factor of 55. This increased by longer incubation times or higher concentrations of 2DG in a nearly linear manner, to a level 38 times higher than that of Glc-P and 1200 times that of F6P. As these concentrations were far out of the calibration range the absolute quantification further relied on linear extension of the calibration curve, but the dimension of the 2DG-P production was found to be dramatic. The quantity of 2DG-6P moreover decreased the concentration of Glc-P by only 20-30% and that of F6P, which is already of low abundance, by 50-70%.

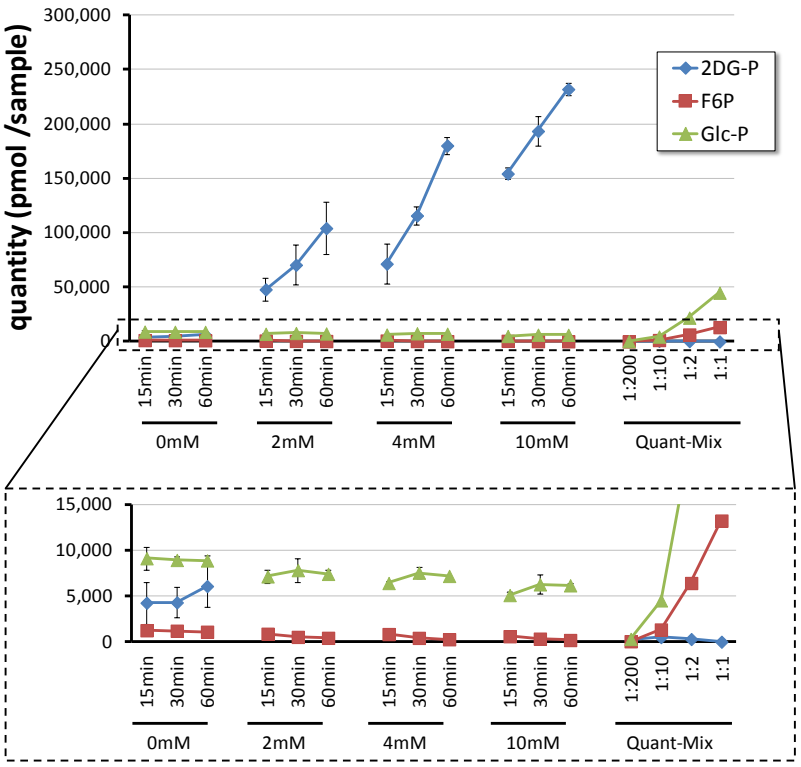

Fig. 49- Accumulation of 2-deoxyglucose-phosphate inside of cells. T98G cells were incubated with different concentrations of 2DG and for the indicated time-points. The 2DG-6P concentration was determined by using the same fragment masses and the same calibration curve as for Glc-P. Some points of the calibration curve are shown and indicated with "Quant-Mix". The insert shows the range of low intensities on the y-axis. Two independent biological samples measured in technical duplicates are shown with average and standard deviation.

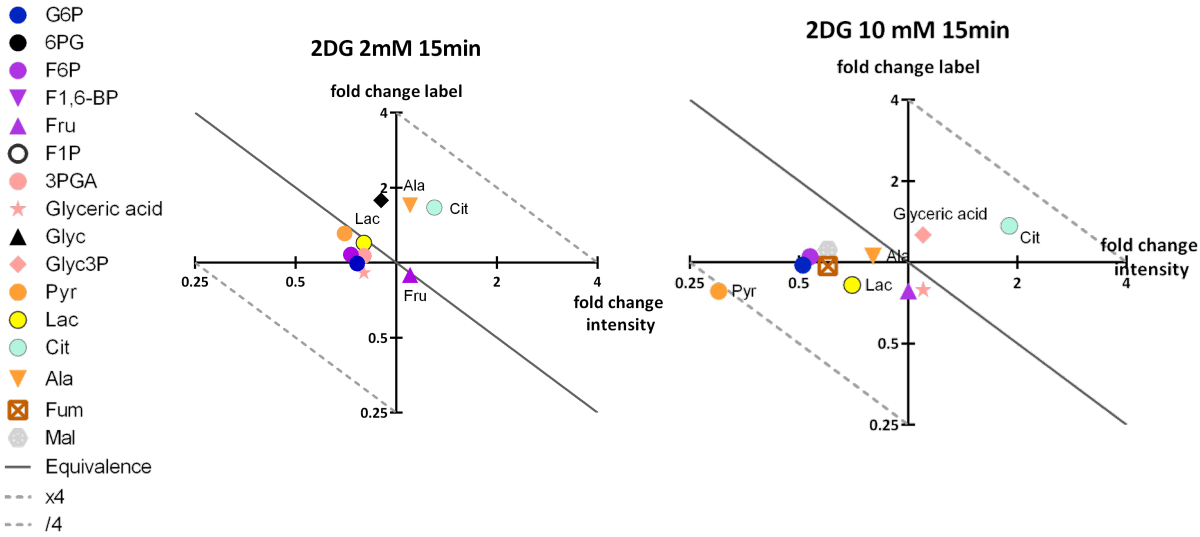

Fig. 50 – Influence of different concentrations of 2DG on metabolites of the central carbon metabolism. T98G cells were treated for 15 minutes with 2 mM or 10 mM 2-deoxyglucose and labeled for 3 minutes with u-^{13}C-glucose. Fold changes of intensity (x-axis) and label incorporation (y-axis) were calculated against untreated control sample.

Despite this dramatic accumulation the application of 2mM 2-deoxyglucose induced only small changes to metabolites of the central carbon metabolism (Fig. 50). Increasing the concentration to 10mM had a stronger impact, but in comparison to glyceraldehyde or BrPyr inhibition, the effect was primarily on the intensity (pool sizes) and not the labeling. The decrease of label incorporation was only around 20 percent. Additionally, nearly all compounds decreased in pool size by 20-50 percent, indicating a limited overall metabolic performance under the influence of 2DG. Interestingly, the intensity and label incorporation of citrate was elevated, and pyruvate reduced by approximately the same amount, indicating that the flow of pyruvate into citrate increased.

4.3.6. The fate of glyceraldehyde can be monitored

Based on the previous results, the effect of glyceraldehyde should be further characterized. According to Lardy *et. al.* the action of glyceraldehyde is mediated by a reaction of glyceraldehyde with DHAP catalyzed by the enzyme aldolase. With the D-isomer of GA the resulting product is fructose-1-phosphate, with the L-isomer the product is sorbose-1-phosphate, which shares structural similarity with glucose-6-phosphate. Sorbose-1-P was shown to inhibit the hexokinase reaction in vitro without affecting utilization of sugar phosphates, so it was concluded that it might bind to the allosteric site of hexokinase (Needham et al., 1951). The further utilization of the uncommon sugar-phosphate sorbose-1-P is hindered compared to fructose-1-P, making this compound more stable and the L-isomer of glyceraldehyde more effective. Additionally, the trapping of glyceraldehyde inside the cell and hijacking the metabolic machinery to produce inhibitory end-products should therefore be dependent on DHAP concentration and the activity of aldolase. Both factors should discriminate against highly glycolytic cancer cells. A higher expression of aldolase (and other enzymes of glycolytic pathway) was found by proteomic analysis of human lung squamous carcinoma (hLSC) (Li et al., 2006). Additionally, glyceraldehyde can also be incorporated into other pathways or in glycolytic intermediates, which could reduce the effective concentration of GA within the cells (Fig. 51).

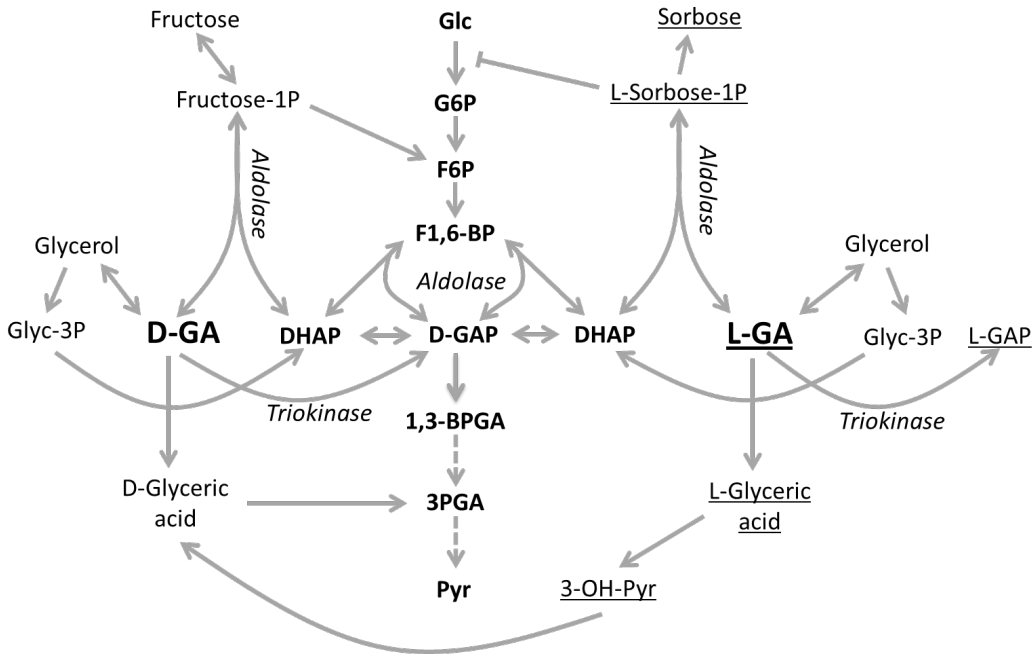

Fig. 51 – Potential products of glyceraldehyde-metabolism. Glycolysis is shown in the middle with DHAP mirrored for better illustration. Underlined compounds are specific products of L-GA metabolism.

In addition to the formation of fructose- or sorbose-1-phosphate by aldolase, glyceraldehyde could be directly phosphorylated under ATP-consumption by triokinase to glyceraldehyde-3-phosphate, another stereospecific compound, with D-glyceraldehyde-3-phosphate being part of the glycyolysis and the L-isomer without known function (Landau and Merlevede, 1963). D-or L-glyceraldehyde could also be oxidized to D- or L-glyceric acid (by aldehyde-reductase). The D-isomer could be phosphorylated to 3-phosphoglyceric acid and feed into glycolysis, whereas the L-isomer could be converted via 3-hydroxypyruvate (3-OH-Pyr) to D-glycerate (Antony et al., 1969). Furthermore, both compounds could be reduced by alcohol dehydrogenase to glycerol, which can be phosphorylated to glycerol-3-phosphate to be used either for synthesis of fats or enter the glycolysis as DHAP.

The possible reactions are dependent on the presence and activity of the enzymes catalyzing these reactions. They are not necessarily present in all tissues and the expression in different tissues was focus of different studies (Antony et al., 1969; Hagopian et al., 2008; MacDonald, 1989).

The hypothesis of production of sorbose-1-phosphate and the potential degradation products of glyceraldehyde into useful substrates of central carbon metabolism or dead end metabolites was tested in our cell models. The cells were supplied with ^{13}C-D-GA or ^{13}C-DL-GA for up to 2 hours and the incorporation of ^{13}C into metabolites of the CCM was monitored (Fig. 52 and Fig. 53).

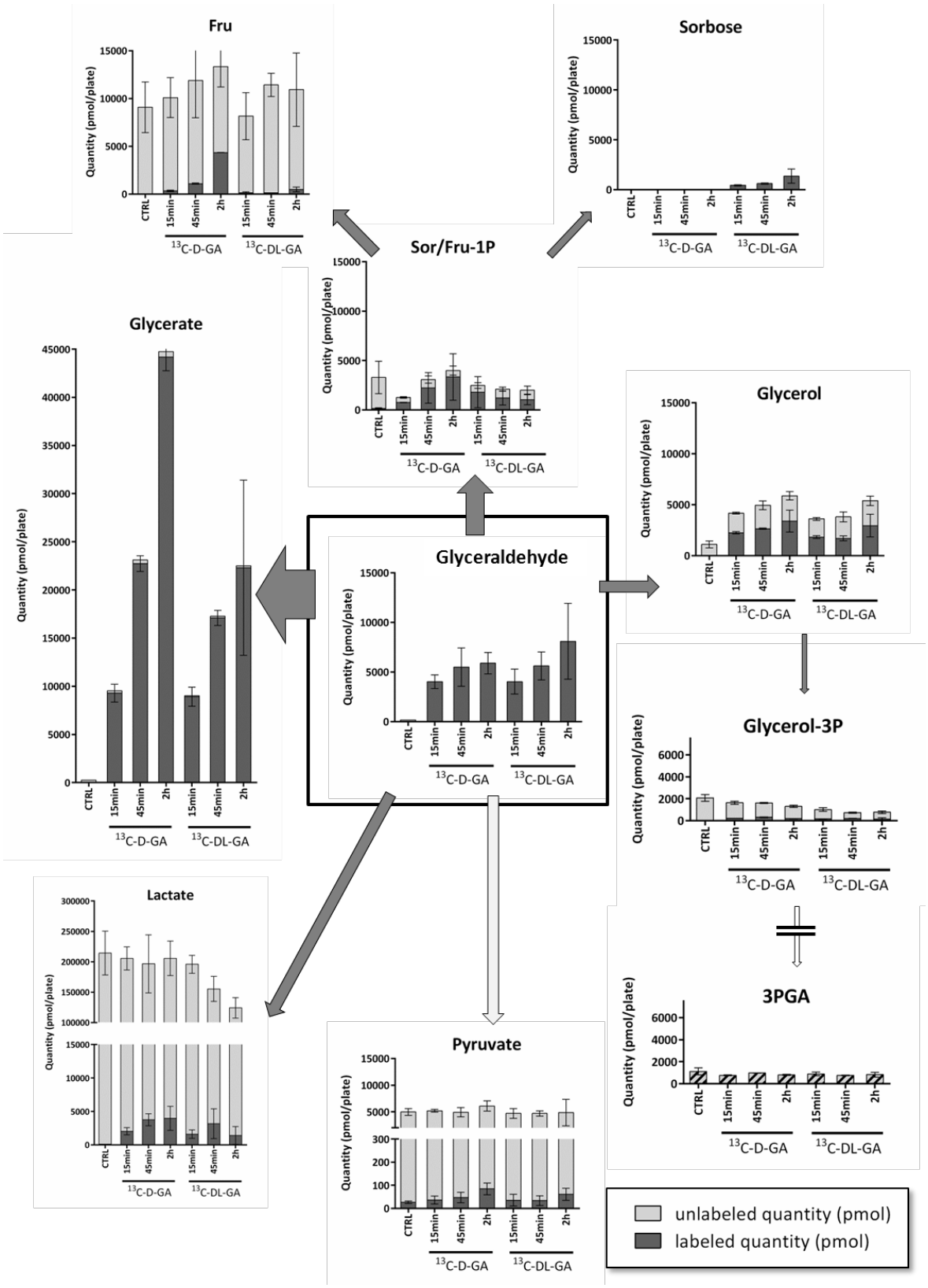

Fig. 52 – Direct products of glyceraldehyde metabolism in HEK293. Cells were treated for 15min, 45min, or 2h with 2mM of ^{13}C-D-glyceraldehyde or ^{13}C-DL-glyceraldehyde, and ^{13}C incorporation into possible targets of GA metabolism was monitored by GC-MS.

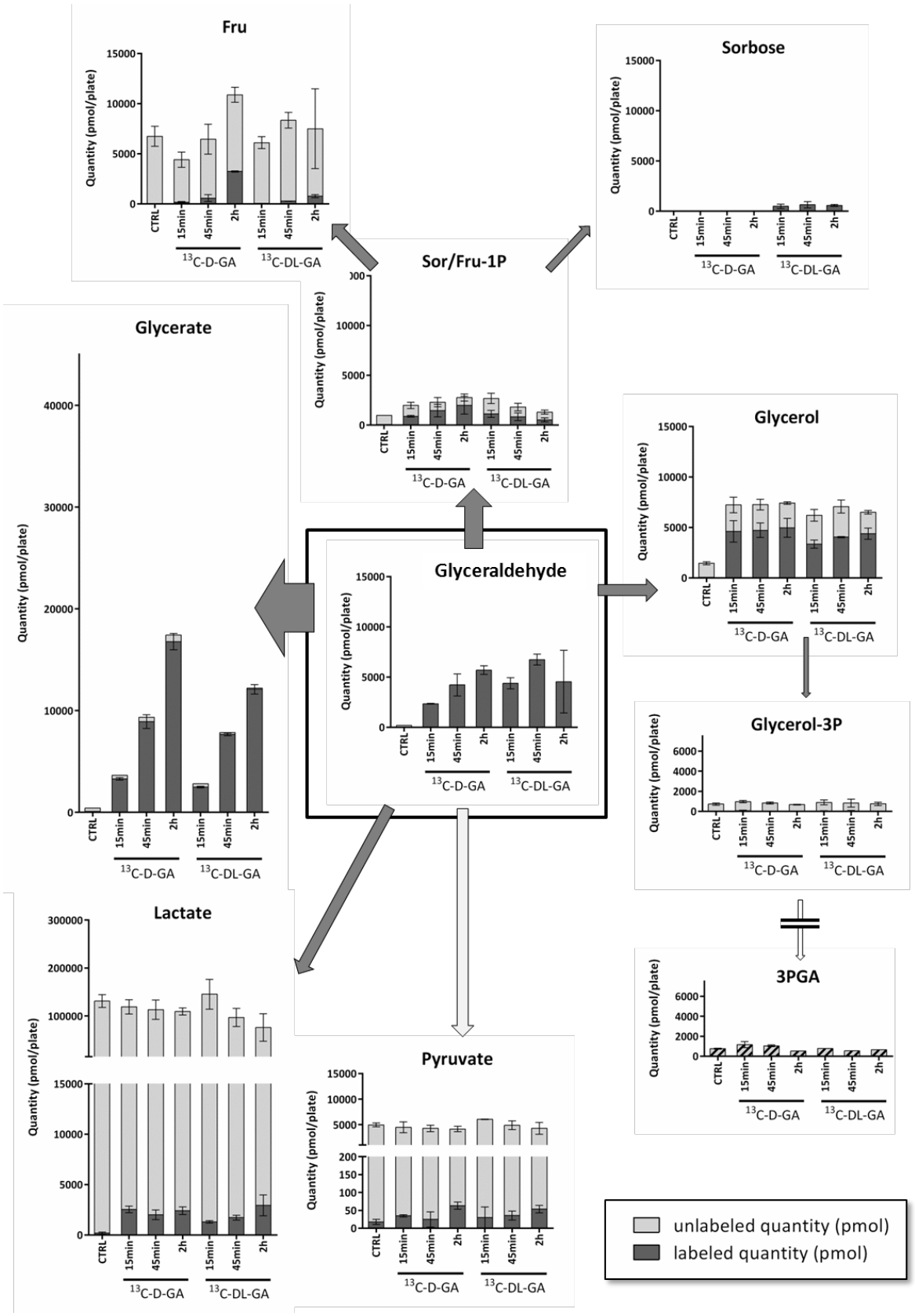

Fig. 53 – Direct products of glyceraldehyde metabolism in T98G Cells. Cells were treated for 15min, 45min, or 2h with 2mM of ^{13}C-D-glyceraldehyde or ^{13}C-DL-glyceraldehyde, and ^{13}C incorporation into possible targets of GA metabolism was monitored by GC-MS.

Glyceraldehyde and some of its products was found inside of the cells. As expected, a high amount of a compound similar to fructose-1-P was found, likely representing sorbose-1-P. However, this presumed sorbose-1-P peak could not be verified as no commercial standard compound existed at time of this study. The production of this compound is much higher from the D-isomer than from the L-isomer. From this sugar-phosphate, the production of fructose or sorbose could be confirmed, with fructose being produced from the D-Isomer and sorbose produced only from the DL-isomer. From both compounds glycerol was produced, too, but apparently most of the glyceraldehyde of both isomers was converted to glycerate, dramatically exceeding the endogenous amount of glycerate. No substantial label and no increase in quantity of 3-phosphoglycerate or any similar compound (e.g. 1-phosphoglycerate) could be detected, and no production of hydroxypyruvate or dihydroxyacetone was observed. In pyruvate and lactate, around 1-2 percent of label was detected, which is around the false discovery limit for pyruvate but appeared to be valid for lactate. The ratio lactate to pyruvate was similar to the ones detected earlier (Fig. 27). Due to the high quantity of lactate found in the cells, the total amount of ^{13}C ending up in lactate appeared similar to that being delivered into glycerol; however, this should be substantiated by pSIRM-studies conducted on longer time scales.

4.3.7. Sorbose itself has no effect to growth or viability

One of the most prominent differences in the metabolism of the metabolic fate of the different glyceraldehyde isomers is the production of sorbose. This compound is only made by ^{13}C-DL-GA, most probably by spontaneous dephosphorylation of the produced sorbose-1-phosphate.

To further test if sorbose itself is sufficient to induce a growth inhibition similar to the one induced by glyceraldehyde, the two cell lines were incubated with different amounts of sorbose for 24 hours, followed by cell counting and an estimation of cell viability (Fig. 54).

Incubating either HEK293 or T98G cells with concentrations of up to 10mM sorbose for 24 hours had no influence on shape and appearance of cells (not shown) or on viability and cell number. A functional effect of externally applied sorbose can thereby be excluded.

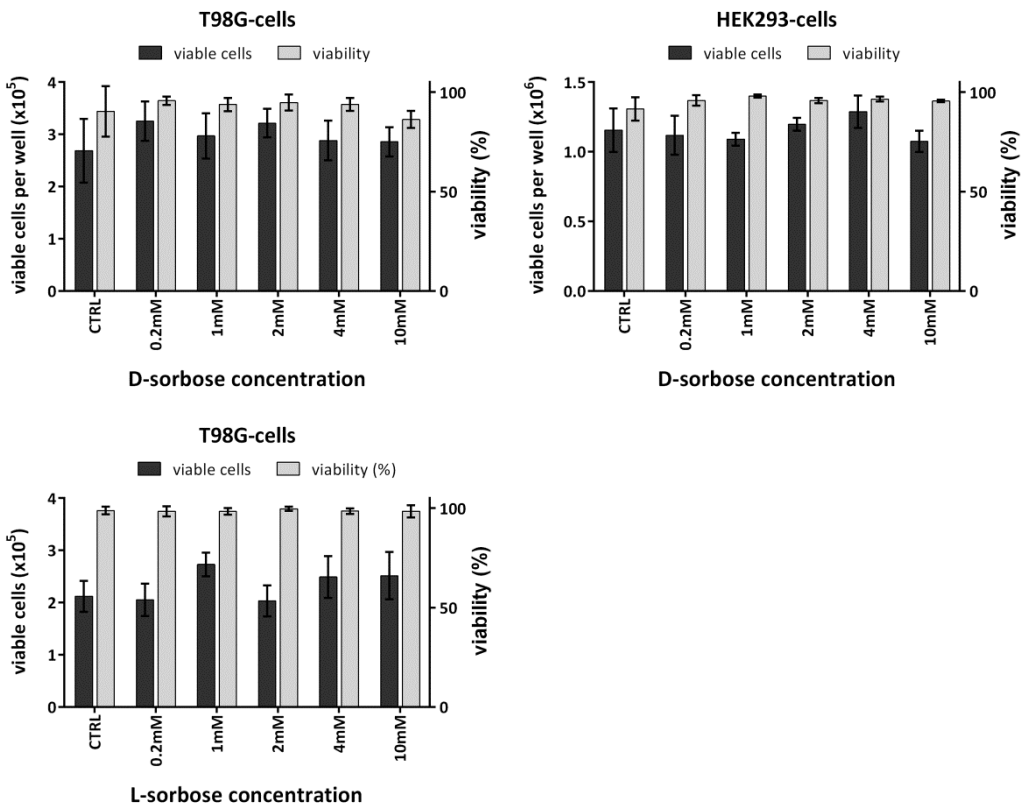

Fig. 54 – Growth and viability of T98G (left) or HEK293 cells (right) under the influence of different concentrations of D-sorbose (top) or L-sorbose (bottom) in the growth media. Cells were seeded into 6 well plates. After 24 hours, different amounts of a 200mM stock-solution of D-sorbose (in PBS) were added to each well. Further 24 hours later cells were trypsinized and counted. Viability was determined using the trypan-blue exclusion method. L-Sorbose was only applied to with T98G cells.

4.3.8. Glyceraldehyde further induces a growth crises which depends on the availability of glucose

The phenomenon of swimming cells under glyceraldehyde treatment was further investigated. The detachment occurred at concentrations of D- or L-glyceraldehyde of around 1-2 mM, a concentration resulting in little influence on cell viability (Fig. 41, Table 8). The cells are therefore not dead within the analyzed time frame. HEK293 cells were treated with different concentrations of glyceraldehyde 24 hours after seeding and incubated for additional 18 or 24 hours. All cells, including the swimming ones, were harvested and processed for cell cycle analysis by flow cytometry with propidium iodide staining of DNA content.

Both isomers of glyceraldehyde induced a concentration dependent, replicative stress, indicated by an incomplete cell cycle with an accumulation of cells in the S-phase (Fig. 55). This effect was more pronounced and occurred at lower concentrations of the L-isomer compared to the D-isomer.

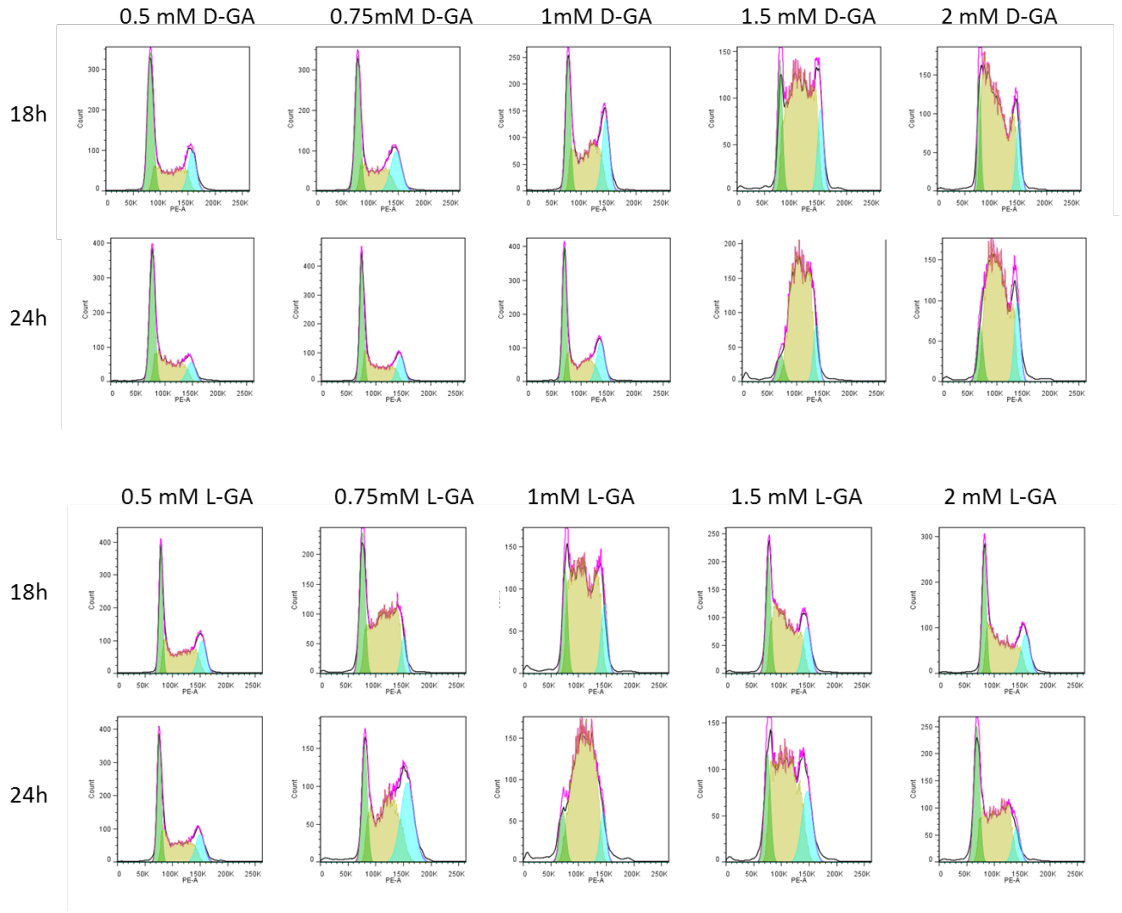

Fig. 55 – Concentration dependent disturbance in cell cycle phases. HEK293 cells were incubated 18 or 24h with different concentrations of D-glyceraldehyde (top) or L-glyceraldehyde (bottom). The cell cycle distribution was monitored by flow cytometry after staining of DNA content. Deriving percentage values for cell-cycle phases is sensitive to tiny changes in curve-fitting under these extreme conditions and was judged to be pointless.

Next I investigated if the incomplete cell-cycle might be caused by glycolytic inhibition, resulting in a contradictory signaling between availability of glucose without the ability of utilizing it to generate energy. I performed a similar experiment in the presence of different amounts of glucose (Fig. 56). The absence of glucose typically induced an increase in G1-phase (Fig. 57). Without glucose the replicative stress-phenotype induced by glyceraldehyde was less pronounced. Glucose in concentrations as low as 0.3 g/l completely restored the effect, seen best for the L-isomer.

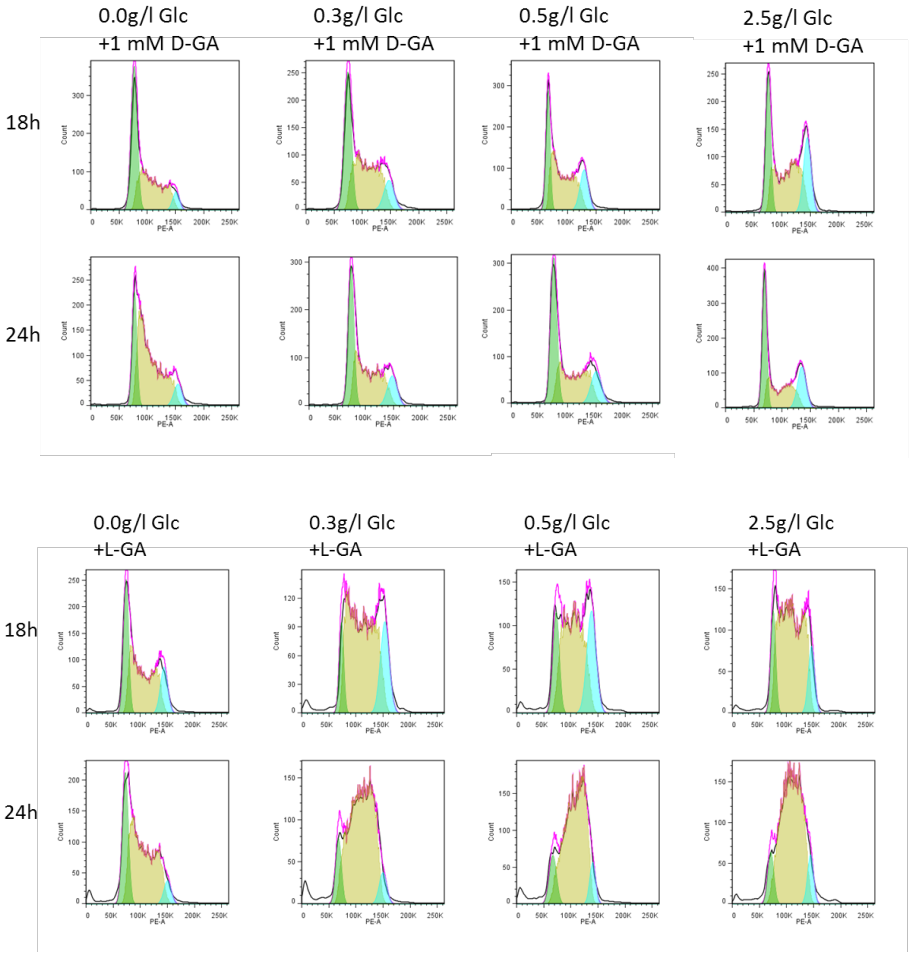

Fig. 56 - Disturbance in cell cycle phases after GA treatment with different concentrations of glucose. HEK293 cells were incubated 18 or 24h with 1mM of D-glyceraldehyde (top) or L-glyceralgehyde (bottom). The cell cycle distribution was monitored by flow cytometry after staining of DNA content.

Finally, it was tested if this is a general effect of glycolytic inhibition or if this is a special effect of glyceraldehyde. For this the experiment was repeated with a comparison between glyceraldehyde and 3-bromopyruvate (Fig. 57). The effect found with glyceraldehyde was not detectable after incubation with 3-bromopyruvate. Concentrations with an inhibitory effect on cell growth or viability had only minor effects on cell cycle distributions, with a minor increase in G2/M-phase, indicating that the inhibitory effect of BrPyr did not affect the cell cycle.

2-Deoxyglucose was not tested, but reported in the literature to act similar to glucose-starvation and leads to an increase of G1 phase (Giammarioli et al., 2012).

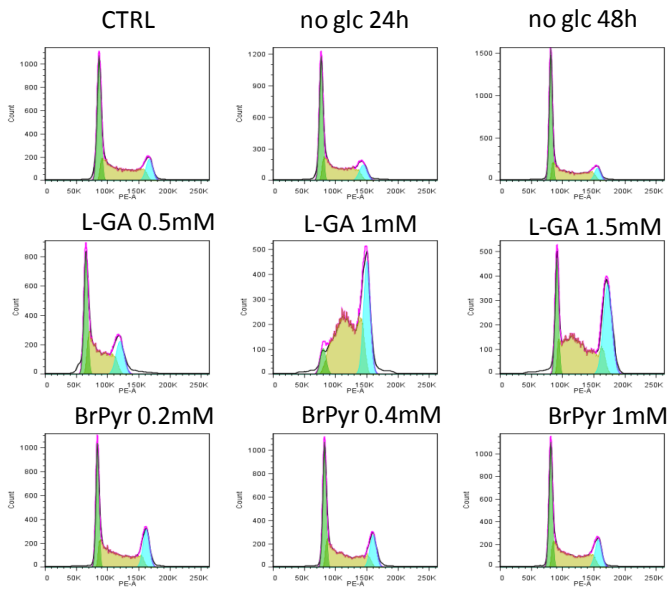

Fig. 57 - Comparison of the cell cycle distributions in HEK293 cells after treatment with glyceraldehyde, 3-bromopyruvate and glucose starvation. The cell cycle distribution was monitored by flow cytometry after staining of DNA content.

4.4. Section 4 - *in vivo* applications of pSIRM

The ultimate goal of the pSIRM approach is to monitor and understand processes inside living organisms for which cell culture is often only a poor replacement. The strategies developed in cell-culture build the foundations for performing experiments *in vivo*. However, these *in vivo* experiments impose restrictions with regard to sampling time points and sample sizes and become even more pronounced when translating the approach into human studies. In order to elucidate the *in vivo* potential of pSIRM, two pilot experiments were performed that aimed at the identification of informative time frames and substrates.

4.4.1. *In vivo* monitoring of gluconeogenesis from ^{13}C-pyruvate

In an initial experiment to study gluconeogenesis in mice, ^{13}C-pyruvate was injected into wild type mice (C57-Bl6) and the quantity and label-incorporation in blood plasma and liver samples was monitored at different time points after injection.

The single injection of pyruvate resulted in a sudden increase of pyruvate levels in plasma and even more in liver after 7 minutes of ^{13}C-pyruvate incorporation (Fig. 58). This completely exchanged the existing pyruvate pools, which was also reflected by strong label incorporation in liver and plasma pyruvate. Further direct products of pyruvate metabolism like lactate and alanine drastically increased in pool size and label incorporation indicating a strong flux into these compounds. Also the TCA-cycle intermediates were strongly labeled 7 minutes after injection of pyruvate. Notably, also TCA-cycle intermediates were found labeled in the blood plasma, indicating a rapid exchange between tissues and blood.

As indicated in Fig. 3 a bolus injection of ^{13}C-labeled substrate leads to pulsed labeling state, the incorporation of the label decreased when the amount of injected compound is used up. In this experiment the decline was detectable already at the 14 minutes time point, the quantity of compounds and the label incorporation decreased. After 20 minutes the label further diminished lasting longest in hepatic pyruvate and TCA-cycle intermediates in liver and plasma. Some amount of gluconeogenesis occurred, with label in plasma-glucose found higher and longer persisting than that in liver-glucose.

Apparently, these results indicate that a large fraction of pyruvate was directly oxidized in the TCA cycle of the liver or other tissues as muscles. It further turned out that the variability of pool sizes between different mice (seen in difference between height and width in Fig. 58) was much higher than label incorporation, making it necessary to include more replicates (more than 5 mice).

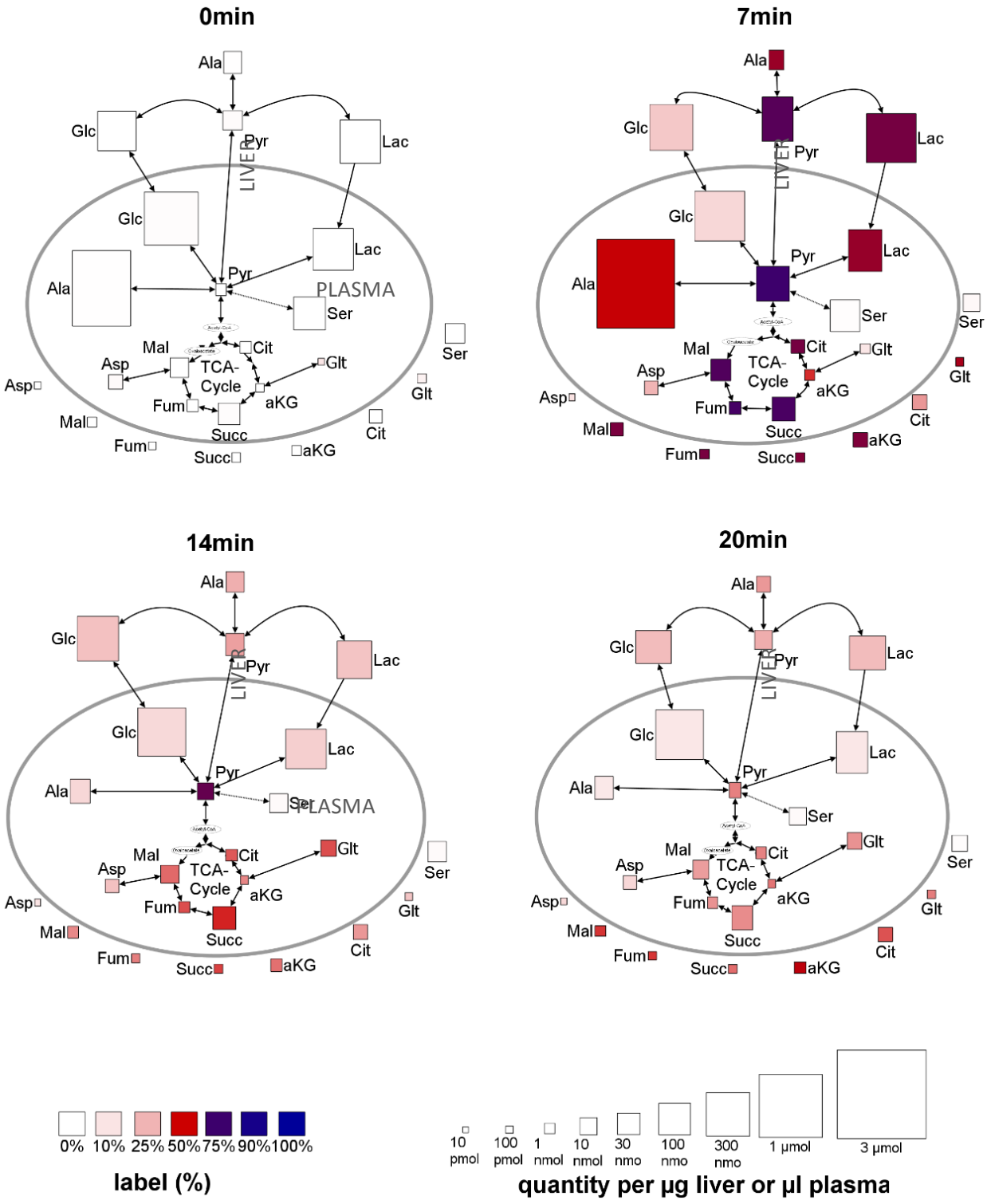

Fig. 58 – *In vivo* labeling of blood serum and liver metabolites in mice with ^{13}C-pyruvate. Shown are different time-points (7-20 minutes) after injection of 2µg/g body weight of ^{13}C-pyruvate and an untreated control. The size of the symbols indicate quantity of the compounds per µg liver or µl plasma, with height showing average + confidence interval and width the average minus confidence interval (95%). The color indicates the label incorporated into each compound. Four mice were used for control and two mice per treatment and time point, with samples measured in duplicates.

4.4.2. *In vivo* usage of glucose and glutamine in HCC model-mouse

The impact of high glycolytic activity in cancer in relation to the function and activity of mitochondrial metabolism is intensively discussed. Otto Warburg believed that elevated glycolysis is a result of impaired mitochondrial metabolism, but nowadays it is known and accepted that glutamine utilization and TCA cycle activity is remarkably important for cancer cells (DeBerardinis et al., 2007). The TCA cycle is used less than a pathway to oxidize carbons to CO_2 but to produce precursors for different synthesis as fatty acids or amino acids, in close coordination with carbons entering and leaving at different stages of the cycle (Filipp et al., 2012a). Even with elevated glycolytic activity and high lactate secretion in tumor cells, glucose is substantially fueled into the TCA cycle (Guppy et al., 2002).

The utilization of the two important substrates, glucose and glutamine was monitored in liver samples of ASV-B-mice after five and ten minutes of injection of ^{13}C-labeled substrates. These mice were transformed with the ATLII-SV4 transgene, leading to an effective, spontaneous development of hepatocellular carcinoma (HCC) in male but not in female mice. (Dubois et al., 1991).

The intensity of and the label incorporation into intrahepatic glucose reflected the uptake of the ^{13}C glucose from the blood (Fig. 59). The uptake appeared to be quite similar between the different sexes. The glucose levels in female mice were a bit elevated in female mice; the same was true for label incorporation as an indicator for glucose turnover. In contrast to the ^{13}C-pyruvate experiment (section 4.4.1) the injected concentration of glucose or glutamine was better balanced to the endogenous pool size, which did not induced such a sudden increase in the pool size of these compounds (Fig. 59 + Fig. 60). The results obtained in this experiment may therefore be more physiological and did not report the response of metabolism to dramatic changes. As anticipated, labeled glucose could only be found in mouse samples treated with ^{13}C glucose. With doubled time the label in glucose further increased, indicating that the utilization of glucose is still in an intermediate, instationary phase.

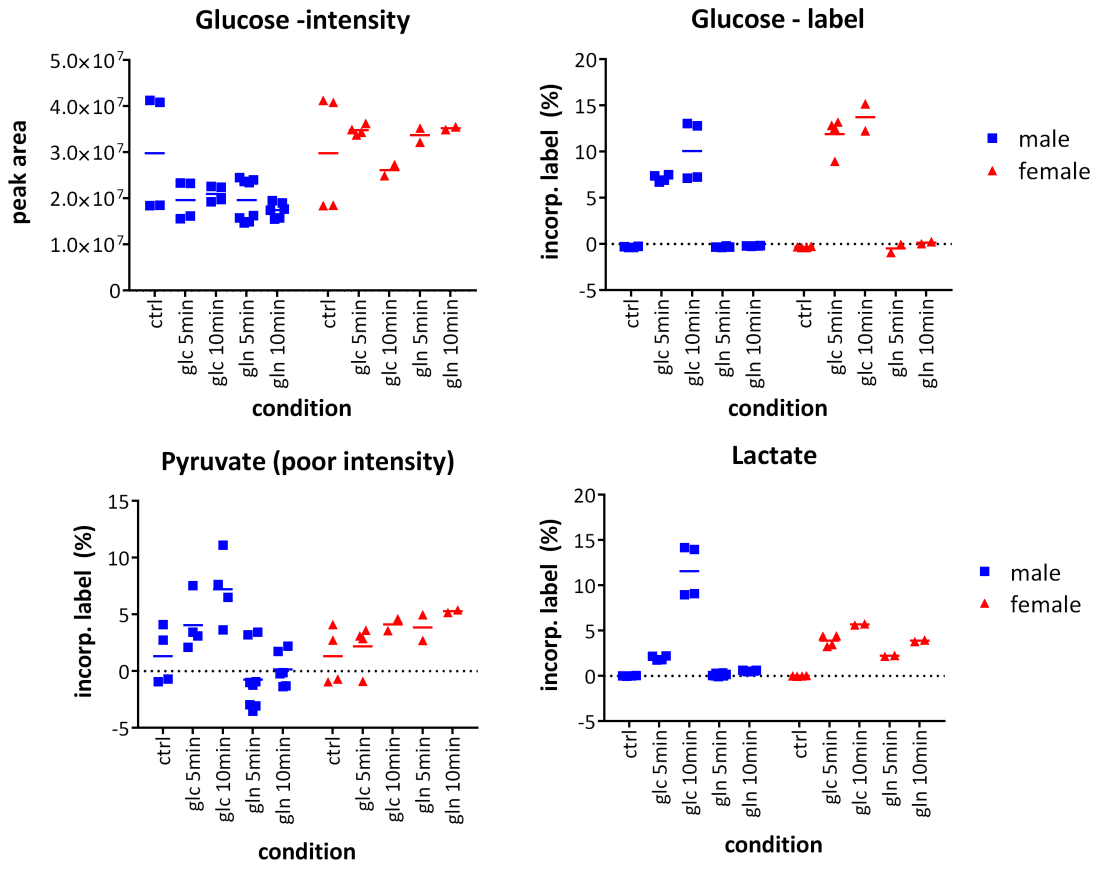

Fig. 59 - Glycolytic intermediates in liver samples of HCC tumor model mice. Mice received either u-^{13}C-labeled glucose or u-^{13}C-labeled glutamine and were killed after five and ten minutes. Label incorporation into different metabolites of liver samples were calculated. The two individual replicates from same sample are shown individually.

The further utilization of glucose was reflected in the amount of label incorporation into poorly measured pyruvate and well measured lactate (Fig. 59) and further into citrate, with the latter one additionally representing the glutamine utilization via glutaminolysis by the TCA cycle (Fig. 60). The label incorporation into lactate was higher in the male mice indicating a switch to the less effective fermentation pathway. Interestingly, some label appeared in lactate under ^{13}C glutamine conditions, suggesting a transfer of carbons from mitochondria to cytosol, originating from malate (malic enzyme) or exported citrate (citrate-lyase)

Label incorporation from ^{13}C glucose into citrate was comparable between the sexes, with glucose introducing two carbon atoms through its processing to acetyl-CoA (Fig. 60). Noteworthy, the label incorporation from glutamine into citrate was greatly elevated in female mice, which was also in accordance with the differences found in glutamate, the first product in the glutaminolysis-pathway, and similar to the results of the other TCA-cycle intermediates (Fig. 61). More remarkably is a high level of label on the m+5 position in citrate.

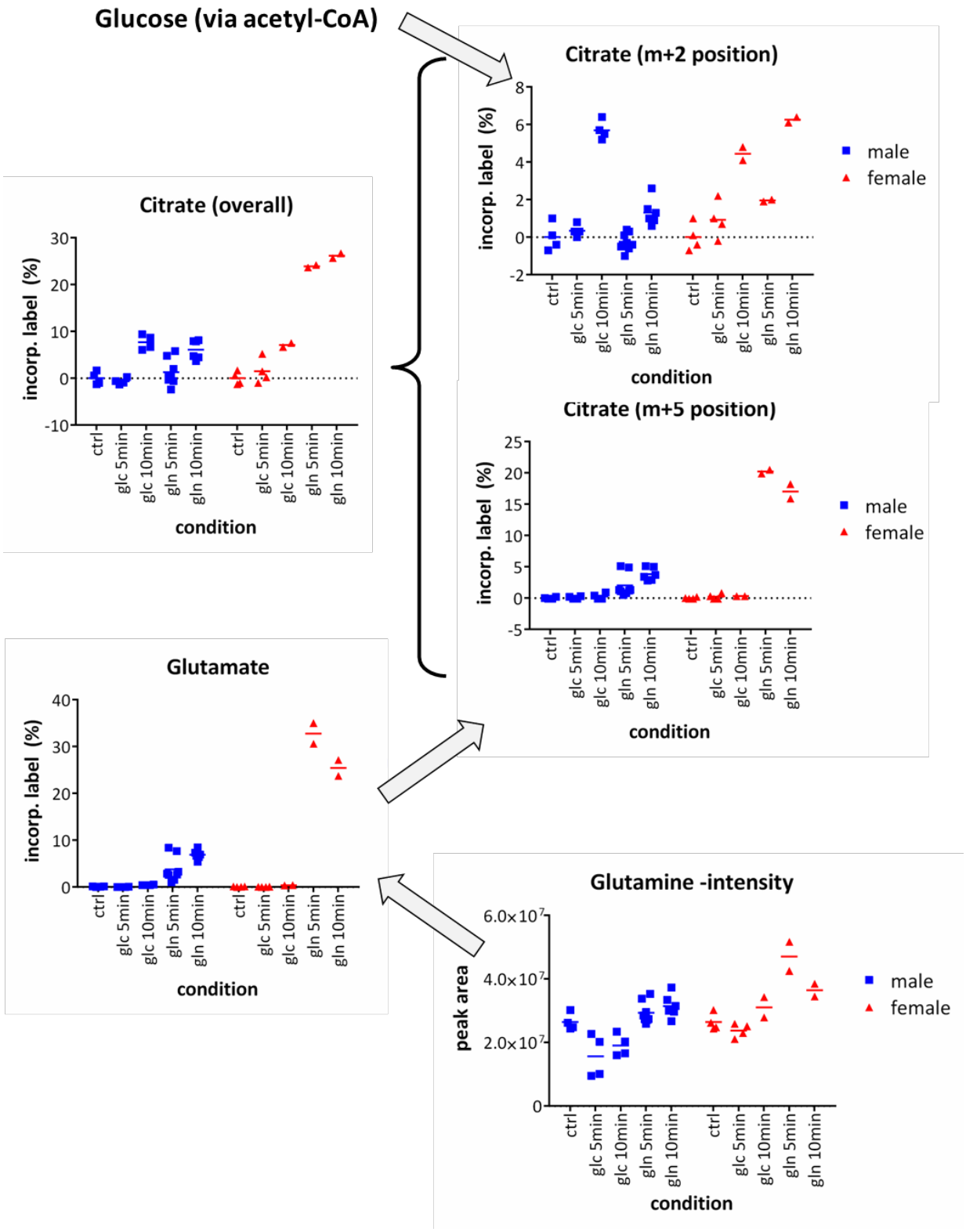

Fig. 60 - Label incorporation into citrate in liver samples of HCC tumor model mice. Mice received either u-^{13}C-labeled glucose or u-^{13}C-labeled glutamine and were killed after five and ten minutes. Label incorporation into different metabolites of liver samples was calculated. The two individual replicates from same sample are shown individually.

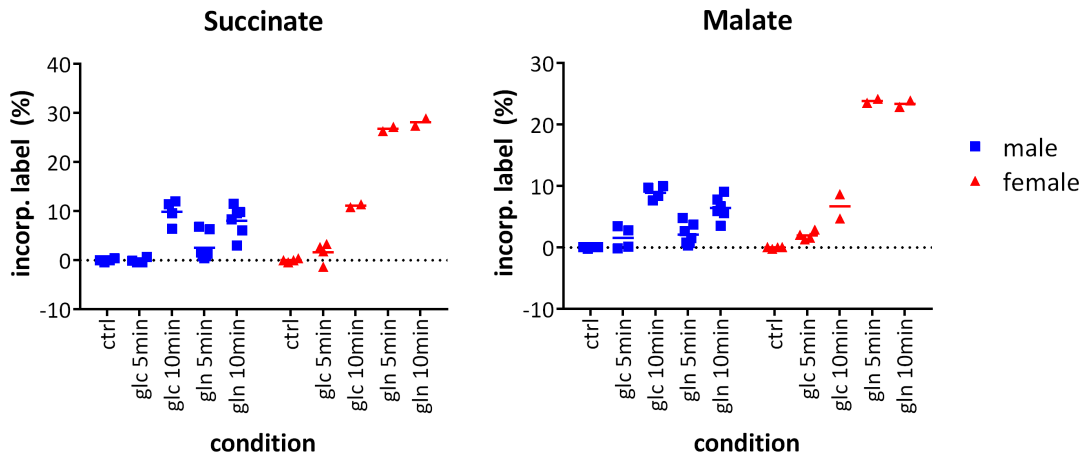

Fig. 61 - Label incorporation into intermediates of TCA cycle in HCC tumor model mice. Mice received either u-^{13}C-labeled glucose or u-^{13}C-labeled glutamine and were killed after five and ten minutes. Label incorporation into different metabolites of liver samples were calculated. The two individual replicates from same sample are shown individually.

As illustrated already in Fig. 60, the number of incorporated carbon atoms into citrate (and other TCA-cycle intermediates) delivered information about the direction of the carbon flow in the TCA-cycle. For a deeper understanding the incorporated label was calculated on all possible positions, after subtracting overlapping isotopomer patterns in the highly abundant citrate fragment with m/z of 273 representing 5 of the 6 carbon atoms. Despite the fact that female mice exhibited a stronger utilization of glutamine, measured by a higher total incorporation rate, the isotopomer patterns are very similar (Fig. 62). In both sexes most of the label originating from ^{13}C-glutamine was found on the m+5 position.

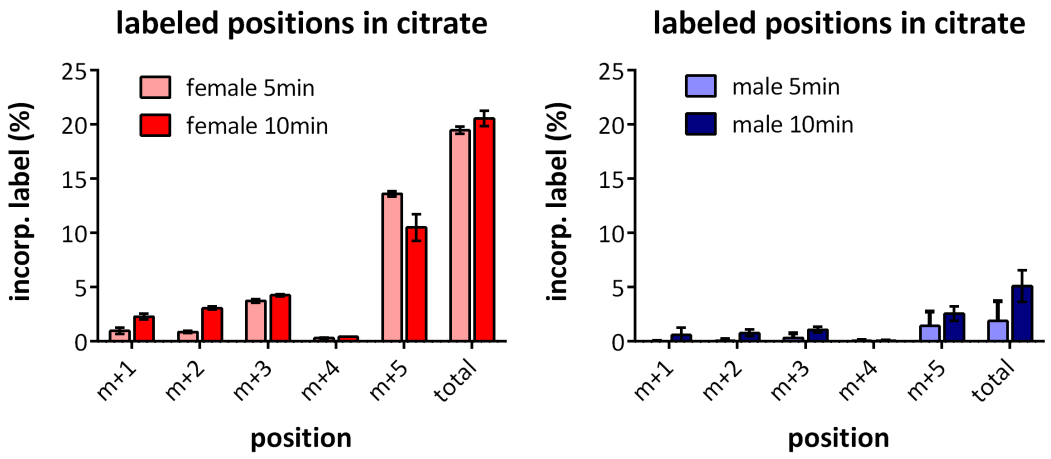

Fig. 62 - Incorporated label at all measured positions within the citrate molecule, after injection of u-^{13}C-glutamine into male or female HCC mice model. Label incorporation at different positions of citrate measured in liver samples was calculated. Technical and biological replicates were averaged, and plotted with standard deviation.

Producing citrate in the normal, oxidative direction of the TCA-cycle requires the fusing of acetyl-CoA and oxaloacetate (Fig. 63 - left) to build citrate. The necessary import incorporation of acetyl-CoA from unlabeled glucose constantly dilutes the label from glutamine after multiple rounds of TCA-cycle. Under this situation a label in m+5 can only be achieved when labeled acetyl-CoA (derived from ^{13}C labeled glucose) fuses with ^{13}C labeled oxaloacetate from ^{13}C glutamine. Without the addition of labeled glucose, the only possibility to obtain label on the m+5 position would be by the action of malic enzyme (ME) converting malate to pyruvate that could reenter TCA-cycle (Filipp et al., 2012a). However this would require intensively labeled malate and should also be reflected in intensively labeled pyruvate, which was found labeled to five percent similar to lactate, rendering it nearly impossible to introduce such a strong label on the m+5 position in citrate.

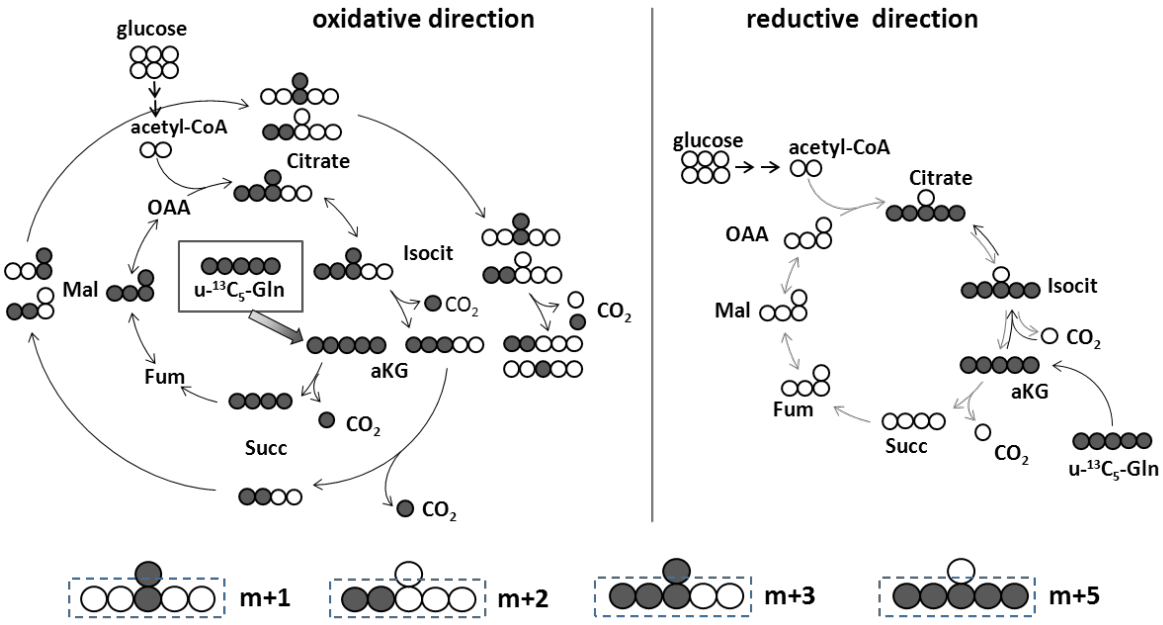

Fig. 63 - The action of oxidative and reductive TCA-cycle activity produce label on different positions within TCA cycle intermediates. Here labeling with u-^{13}C glutamine is illustrated (dark circles), fusing with unlabeled glucose (white circles). The detected citrate fragment (m/z 273) contains 5 of 6 carbon atoms of citrate and the impact of heavy carbon atoms to the measured mass shifts is illustrated at the bottom. Glutamine is deaminated to glutamate and further to alpha-ketoglutarate (aKG) where it enters the TCA cycle. In the oxidative pathway (left) the decarboxylation of aKG leads to labeling on m+3 position in citrate in the first round (center) and to labeling on the m+2 or m+1 position in the second round after another addition of unlabeled acetyl-CoA. By the activity of reversed TCA-cycle (right) all carbon atoms from glutamine end up citrate resulting in a label in m+5 position. Figure was modified from a template generously supplied by Fabian Bindel.

Another possibility to incorporate a label in citrate on the m+5 position is the activity of a reversed or reductive TCA-cycle, which is also often reported as a cancer characteristic (Metallo et al., 2012; Wise et al., 2011). In this direction glutamine feeds into alpha-ketoglutarate that is ultimately carboxylated to yield citrate. Therefore all 5 carbon atoms from glutamine end in citrate leading to full label on the measured m+5 position without completely labeling the remaining TCA cycle intermediates (Fig. 63 - right).

The results of the *in vivo* experiments support the assumption of a reversed TCA-cycle, a carboxylation of alpha-ketoglutarate (made from glutamine) to build citrate even in the tumor-free female mice, probably as a function to support gluconeogenesis or fatty acid production.

5. DISCUSSION

5.1. Labeling – a shorter timescale reveals new insights

Isotope pulse labeling was an important tool to unravel the most important metabolic pathways in plants and animal cells (Calvin and Benson, 1949; Krebs and Johnson, 1937). The further development of analytical techniques like mass spectrometry and nuclear magnetic resonance allowed quantitative and structurally resolved analyses of stable isotope incorporation, thereby enabling a time resolved analysis of known metabolic pathways, and potentially, the discovery of new connections within the metabolic network (Locasale et al., 2011). The pSIRM workflow reported in this thesis integrates information about stable isotope incorporation and metabolite pool sizes, simultaneously extracted from a single measurement.

The pSIRM approach follows the concept of Nöh *et al.* who proposed a distinct advantage of dynamic labeling in comparison to steady-state label incorporation (Noh and Wiechert, 2011). Differentiation of metabolic network activity is not determined by position dependent mapping to carbon transitions but by the intensity the label propagates within the metabolic network and the amount of label within the network. Uniformly labeled ^{13}C-substrates that would yield no information in stationary labeling can be used for dynamic labeling (Noh and Wiechert, 2011). The use of less complex labeled material and a shorter incubation time, makes analysis both cheaper and more generally applicable (Wiechert and Noh, 2013). The consideration of fragments not containing the complete carbon backbone but measured with high intensity further increased the coverage and reliability of measurements.

Here u-^{13}C glucose was used with incorporation times between 2.5 and 3 minutes. During this time the upper glycolysis is nearly completely labeled with some degree of ^{13}C-incorporation in the branching points (Fig. 25, Fig. 26), a finding similar reported elsewhere (Munger et al., 2008). To fulfill the needs for complete mathematical modeling proposed by Nöh and Wiechert multiple sampling time points are necessary to describe to complete dynamic behavior from the unlabeled to labeled state to infer turnover constants (Noh and Wiechert, 2011), which requires elaborative calculations. However, full mathematical modeling and quantitative description of all fluxes was not our major aim. In contrast I could show, that the measurement of label incorporation obtained at a single or a few time points are enough to differentiate between various metabolic states, defined naturally between different kind of cells or under different culture conditions.

5.2. Calculation of label incorporation – sometimes the wheel needs to be reinvented.

The untargeted character of GC-TOF-MS in principal allowed for the measurement of ^{13}C incorporation in an unbiased manner even in unknown compounds (Hiller et al., 2010). In this thesis a subset of metabolites that are typically found to be labeled under the chosen conditions was reported (Fig. 24, Table 5). These compounds cover the most active parts of the central carbon metabolism: the glycolysis, its branching points including lactate, serine and alanine as well as the TCA cycle. Under longer labeling periods, however, more compounds are labeled)not shown).

Furthermore, I established a workflow to extract and analyze labeling data with software and tools currently employed in the lab (Fig. 64). An essential part of this strategy is the calculation of mass isotopomer distributions corrected for natural occurring isotope overlap and the summary of isotopic enrichment into single values (total label in percent). For this two different calculations were established. The first strategy aims at the correction of naturally occurring isotopes on a single, or a few labeled positions, in a targeted way, calculating the label on the analyzed position(s). The second strategy summarizes all potential labeled positions into a single value by measuring the disappearance of the unlabeled fragment intensity.

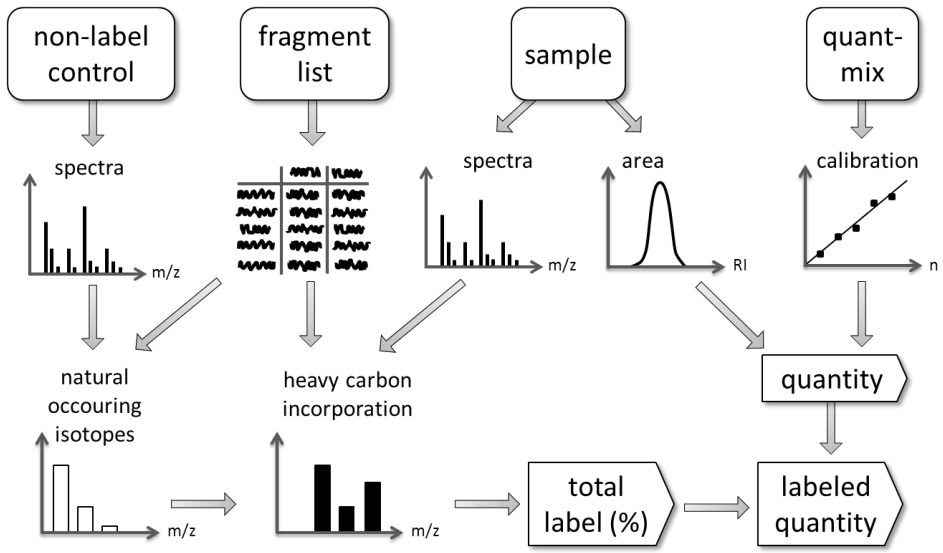

Fig. 64 – Data analysis pipeline. From the same sample the mass spectra and areas are extracted. An unlabeled control sample serves as template to correct for natural occurring isotope abundances and to calculate the total label incorporation, which is combined with the relative intensity or absolute quantity obtained using calibration curves.

A huge variety of correction strategies is reported in the literature, from simple to very complex matrix calculations (Jennings and Matthews, 2005; Lee et al., 1991; Moseley, 2010; van Winden et

al., 2002). Some approaches were already included in specialized software packages (Hiller et al., 2013; Millard et al., 2012; Nanchen et al., 2007).

Typically the natural isotopic distribution is calculated from the known chemical composition of the measured fragments (Huege et al., 2014). Choosing the right literature values for natural isotope abundance was reported to have bigger effects than differences between some tested calculation methods (van Winden et al., 2002), the same is true if correction is only applied for ^{13}C or also for ^{2}H, ^{17}O or ^{18}O (Wittmann and Heinzle, 1999).

In order to include labeled but not yet identified compounds or identified compounds with unclear fragmentation, the developed calculation strategy based on measured mass spectra of unlabeled reference samples. During writing of this thesis it turned out that this strategy was reported already 50 years ago (Biemann, 1962), and since then cited a lot but never summarized. Additionally it was unclear if this approach also works with complex molecules, e.g. metabolites after trimethylsilylation and methoximation. It could be shown that this old approach effectively corrected measured derivatized chemical standards (Fig. 22 and Table 4). The putative error in calculation is smaller than the measured variation between samples (Suppl. table 6). The calculation is convenient to perform and can be included into data analysis pipelines in R or Microsoft's Excel. The proposed propagation of errors is minimized when only targeted masses expected to be labeled were corrected.

Additionally, the concentration dependency of mass isotopomer pattern remained a still overseen fact (Antoniewicz et al., 2007; Patterson and Wolfe, 1993) but was shown to be significant in our measurements. This effect has an influence on the results of calculations, especially for the untargeted approach. It seems to be unrealistic that a compound differs by the factor of ten between different measurements, resulting in concentration effect in mass isotopomer distribution. But on the other hand, structurally similar compounds as sugars, producing the same fragments, in fact differed by some orders of magnitude (Fig. 14) and therefore showed different mass isotopomer distributions (Fig. 23). For this approach presented here, it is essential to extract a reference distribution from a reference measured with approximately the same intensity as the sample.

With improvements of the data analysis pipeline in the future, the sensitivity of the system will be increased, e.g. by extraction of isotopes distributions by their areas instead of peak heights. The ultimate goal is a more automatized data analysis, which eventually could include more advanced calculation methods as the one described by Jennings and Matthews which is also based on measured standards (Jennings and Matthews, 2005).

5.3. Label incorporation can be summarized into a single number

After correction for natural occurring isotopes the normalized mass isotope distributions are either directly plotted or included into mathematical models, however including multiple masses makes an interpretation and understanding of the obtained data difficult. Here a strategy was adopted from NMR approaches, to report the label incorporation into a single number to more easily interpret and visualize results between different conditions (section 4.1.5 and 4.1.6).

This calculation differed from the calculation of molecular carbon labeling (MCL) reported in Bak *et al.* or ^{13}C enrichment reported by Szecowka *et al.*, in which the number of incorporated carbon atoms is also taken into consideration, by multiplying the calculated label on every position with the number of carbon atoms at this position and dividing the sum by the total number of carbon atoms (Bak et al., 2006; Szecowka et al., 2013).

equation 8: $$enrichment = \sum_{n=1}^{i} \frac{i \, x \, m_n}{i}$$

with: i = number of carbon atoms

and m_n = calculated label (in %) at the individual positions

With this approach a compound can only be labeled by 100 percent if it is completely labeled at all carbon atoms. Contrary to that, in the calculations presented in this thesis the complete labeled state is defined by the absence of unlabeled compounds. Therefore a compound could be 100 % labeled even with all heavy carbon atoms in the m+2 mass isotopomer.

For us it seemed to be more comprehensible to use a calculation strategy that is independent from the number of carbon atoms in the molecule, otherwise the label from one pyruvate ending in citrate would be only one third (2 of 6 atoms) of that ending up in lactate (3 of 3 atoms) whereas in both cases one pyruvate is consumed. Additionally when fragments were measured not that do not contain the whole carbon backbone the formula need to be adapted to the number of observed carbon atoms and lose some detail.

In most situations the amount of incorporated label (expressed as percentage) is the most important description, even more when compared to concentration changes. In other cases the position of the label incorporation is also necessary to consider e.g. to differentiate between forward or reverse TCA cycle (Fig. 62) or single inputs into the TCA cycle versus permanent cycling and mixing of heavy carbons. The position differentiates between different pathways usages and should be reported under these circumstances.

5.4. Interpretation of labeling data under changing conditions improves with inclusion of quantities

Understanding, interpreting and finally modeling of heavy isotope incorporation under isotopic non-steady states ultimately requires quantitative data (Wiechert and Noh, 2013). As shown for the different directions of pyruvate usage (Fig. 27), the bioconversion routes of glyceraldehyde (Fig. 52, Fig. 53) and the accumulation of 2-DG-P (Fig. 49) quantitative data delivered another level of information essential for an understanding of the results.

The use of external calibration could be applied for the quantification of up to 63 compounds simultaneously without dramatic increase in measuring time, therefore enabling a high sample throughput. It could be shown that the quantification of compounds suffers less from matrix effects due to the strong electron impact ionization (EI) employed in GC-TOF-MS measurements resulting in a reproducible quantification for a high number of compounds (Fig. 14, Fig. 17), that was valid even in complex samples (Fig. 16).

The external calibration applied here offers advantages over other methods of quantification. Quantification by isotope dilution, a strategy typically employed for LC-MS data, would interfere with isotope masses introduced by the heavy carbon labeling and could not be used in these cases. This would make it necessary to run independent measurements for samples incubated with ^{13}C-substrates to determine label incorporation and samples incubated with ^{12}C substrates for quantification (Hofmann et al., 2008). This doubles measurement time and the transfer of quantification data from one sample to another induces another error, thereby decreasing reliability of the approach. Additionally, isotope dilution is based on ^{13}C labeled standards for every compound to be quantified, which can be limit its application by limited availability and high costs of commercial standards (Lei et al., 2011). To overcome this problem it was also reported to grow cells for multiple cell doublings with ^{13}C labeled substrates to generate completely labeled samples and quantify them with spiked unlabeled standards (Munger et al., 2008).

5.5. Analysis of metabolites and proteins during cell cycle progression

Untargeted proteomics and metabolomics were used simultaneously to decode the impact of cell cycle phases to protein or metabolite level. The rate of protein synthesis was monitored, after release from a cell cycle block, by a pulsed SILAC approach through the measurement of the incorporation of heavy amino acids arginine and lysine into newly synthesized proteins. We found that cell cycle dependent regulated protein synthesis manifested in different H/L-pattern with most proteins mainly differed in their total synthesis rate, resulting in different H/L ratios reached at the end of experiment. Furthermore, most proteins hardly doubled in the measured time frame (Fig. 30), even though cells passed the M-phase of the cell cycle (Fig. 29).

In one reported study about protein turnover 100 proteins in a human cancer cell line (H1299) were tagged with fluorophores and the dynamic fluorescence signaling was measured (Eden et al., 2011). The measured protein half-lives ranged between 45 minutes and 22.5 hours, the time of cell cycle, with an average of protein half live around 8 hours.

In contrast Schwanhäusser *et al.* reported a protein half live between 30 minutes and 200 hours, with a median of 46 hours with an untargeted proteomics approach in NIH3T3 mouse fibroblasts (Schwanhausser et al., 2011). This indicates that most proteins were primarily synthesized during the process of cell division, as they measured a doubling time of cells of around 27.5 hours.

I further translated the measured H/L ratios of the cell cycle experiment to protein turnover rates, to compare the outcome with previously published studies. For this the H/L ratios of the proteins were plotted against the time after addition of SILAC media (Fig. 65 -A). More than 1800 proteins (87 %), exhibited a linear correlation with a R^2 higher than 0.8 (Fig. 65 -B) and were used for further calculations. The slopes of the linear correlations were inter- or extrapolated to a H/L ratio of one. At this value the same amount of newly synthesized, heavy proteins match the amount of old, light proteins. This simpler calculation than the one presented by Schwanhäusser *et al.* should however be sufficient enough to compare at least the scales of protein turnover.

This analysis delivered similar results to the data delivered by Schwanhäusser *et al.* indicating that the untargeted proteomic approaches deliver same results, while the fluorescence labeling strategy (Eden et al., 2011) delivered shorter turnover rates. Either their approach was biased towards shorter lived proteins, as fluorescence was monitored in 24 hour windows or the proteomic approaches are biased to longer lived proteins. The strategy with linear extrapolation will miss a few short lived proteins (Cluster 1 in Fig. 30), as a rapid increase with elevated high level delivered poor linear trend over the whole time period.

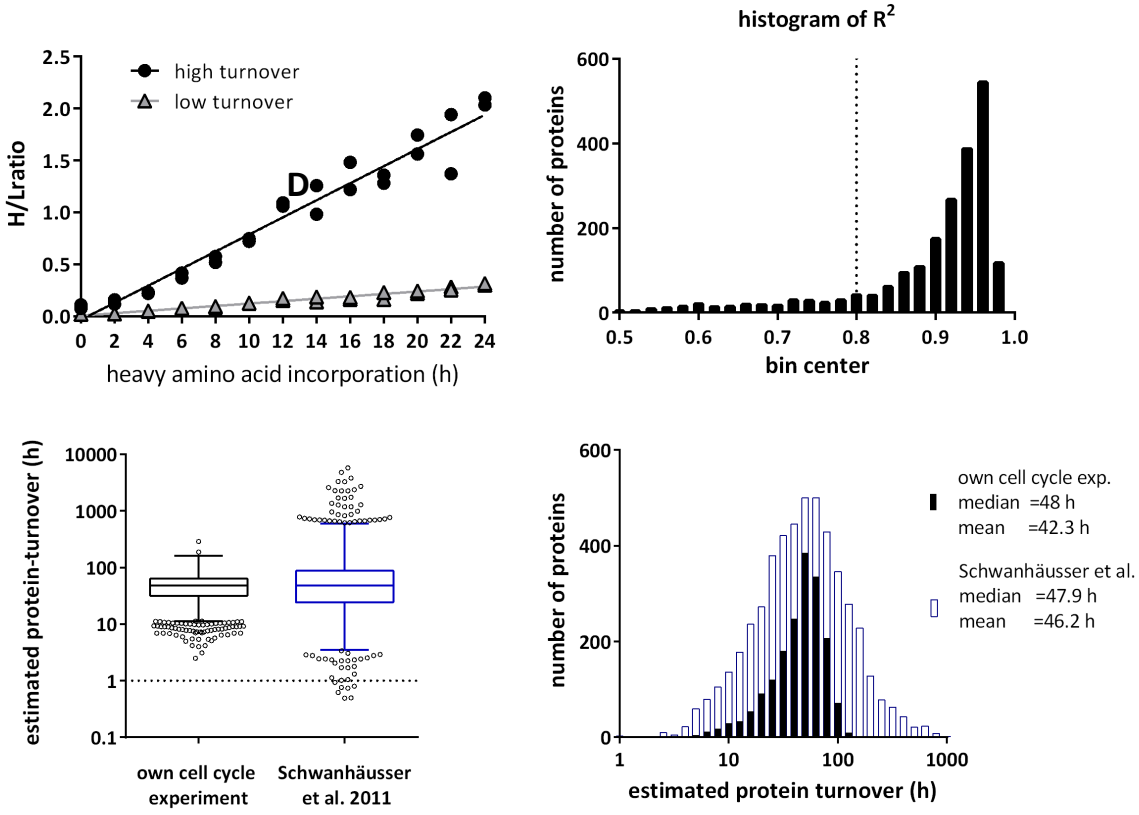

Fig. 65 - Transformation of H/L ratios to protein turnover rates. A - Time-dependent increase of H/L ratios of two exemplary proteins, with high turnover (black symbols and low turnover (triangles). B - The vast majority of proteins fitted well within the linear correlation. For further analysis proteins with an R^2 higher than 0.8 were used. C and D - Transformation of slopes of linear calibration to protein half live and comparison to the half-lives reported by Schwanhäusser *et al.* delivered similar distribution and median values.

More remarkably many proteins that were reported in other studies with a high turnover were also found in this study with a rapid and strong increase in H/L ratio (SPARC, Collagen II, Laminin) (Schwanhausser et al., 2011).

The data also showed that most proteins and nearly all of the selected metabolic enzymes showed very similar profiles of protein synthesis rates as measured by the H/L ratios (Fig. 32). Combined with estimated cell cycle phases the protein synthesis was elevated during S-phases and stopped around the M-phase of the cell cycle.

Factors other than protein synthesis might also account for differential regulation during the cell-cycle: Colombo *et al.* reported selective degradation of enzymes during different cell cycle phases (Colombo et al., 2011). Olsen and Vermeulen measured the phosphoproteome of synchronized cells and showed that many proteins were phosphorylated differentially in different phases of the cell cycle (Olsen et al., 2010). And ultimately in another experiment with 500 fluorescenctly

tagged proteins, Farkash-Amar *et al.* showed that also translocation of proteins between the cytosol and nucleus is cell cycle dependent. Of their 500 analyzed proteins they reported 11% to cycle in intensity and 35% in distribution (Farkash-Amar et al., 2012).

These data indicate that in addition to the here reported H/L ratios, also the protein levels should be considered in further analysis. Unfortunately the measured protein levels showed higher variability between time points and replicates and need more thoroughly normalized and filtered before they reveal their secrets.

The metabolite data were very similar and well balanced between the different states. Nevertheless we found indications for an elevated activity of glycolysis in the middle of the S-phase, which is in contrast to a recent review where glycolysis was described to be essential for G1 to S phase transition, with all other phases solely relying on glutaminolysis (Estevez-Garcia et al., 2014).

To further test the relationship between glycolysis and growth I performed further experiments in which the glycolysis was inhibited and the impact to growth and behavior of the cell cycle was monitored.

5.6. pSIRM as an strategy to understand short termed processes like the inhibition of glycolysis

Instationary labeling with heavy carbon atoms allowed the measurement of short-termed changes within metabolism that cannot be monitored by long-term label incorporation experiments. As example stationarity in label incorporation of protein-bound amino acids was reported to need six cell doublings and instationarity was measured between six and 72 hours (Murphy et al., 2013), a time frame far beyond any acute response time. Here the pSIRM approach was applied in combination with metabolic inhibitors to identify the primary and direct effect of these compounds to enzymes of the glycolytic cascade and to eventually identify the position of the drug target within the metabolic network. With this strategy presented here the inhibition can be as short as the period of labeling, but the putative inhibitors were allowed pre-incubated before starting the labeling to develop their full inhibitory potential. I initially started to monitor a single time point for label incorporation to use the experimental capacity to test and compare different inhibitor concentrations or time points simultaneously.

Changes in both pool sizes and label incorporation determine the total flux; this is also attributed by the newly developed plot, where both independent values were plotted on different axis (Fig.

46, Fig. 48, Fig. 50). With constant flux, meaning a quantitatively identical introduction of new molecules into a given metabolite pool, the increase in concentration of a compound resulted in a decrease in the incorporated label and vice versa. By the action of some of the inhibitors a decrease in pool size of hexose-phosphate was monitored that was not counteracted by an increase in the label of these compounds. In more detail the level of F6P decreased under nearly every treatment indicating that this compound is very sensitive to disturbances. This decrease could be interpreted as an inhibition of the early steps of glycolysis. Considering the fact that glycolytic intermediates were nearly completely labeled within the time frame of the experiment (Fig. 25) these compounds cannot further increase the incorporated label to compensate for the decrease in intensity. Similarly the already small label in citrate and other TCA cycle intermediates further decreased under the inhibitory effect of L-GA and BrPyr, rendering it more complicated to reliably calculate the incorporated label.

The data presented here show that it is possible to compare and describe the effect of different compounds with one single label condition. However to deeper understand their action more time-points increase the readout and the reliability of data interpretation. A shorter time point as 30 seconds might be better suited to detect differences in the upper glycolysis, whereas a longer labeling time as 10 minutes or another substrate (pyruvate or glutamine) increase the quality of interpretation of changes in TCA cycle activity.

5.7. The L-isomer of glyceraldehyde is an more effective inhibitor of glycolysis than the D-isomer

Glyceraldehyde is part of the metabolism and can be formed naturally by different substrates like fructose or glycerol (Hagopian et al., 2008; Sillero et al., 1969). It can further be converted into compounds of the CCM like glyceraldehyde-3-phosphate (Landau and Merlevede, 1963) and glycerol (Antony et al., 1969), compounds inhibiting glycolysis (Needham et al., 1951), or compounds with no further usage that accumulate and potentially acidify the cells (MacDonald et al., 2006).

The possibility of these reactions is dependent on the expression of catalyzing enzymes and the presence of essential co-factors. Therefore the transformation of glyceraldehyde into potential products was monitored by use of ^{13}C labeled glyceraldehyde in two different cell lines, in a time-scale similar to that tested also for the inhibition (Fig. 52 and Fig. 53). The ^{13}C labeled D-isomer was compared against a mixture of ^{13}C D- and L isomer as pure ^{13}C L-GA was not available. According to the proposed mode of action both isomers produced a peak at the retention index of fructose-1-phosphate (Lardy et al., 1950). This peak could indeed also include sorbose-1-phosphate, as ^{13}C-sorbose was detected in cells that were treated with DL-isomer of

glyceraldehyde and ^{13}C-fructose in cells treated with the D-isomer. The amount of produced sugar-phosphate is similar to that of produced glycerol. However, most of the glyceraldehyde ends up in glycerate, which dramatically exceeds the amount of natural glycerate in the cells. Transformation of most of the glyceraldehyde mainly into glycerol and glycerate with some amount of lactate was also reported in lenses of cow, rat and rabbits (Van Heyningen, 1969).

With the exception for the production of sorbose, only small differences between the D- and the DL- isomer were found in the incorporation of glyceraldehyde in the monitored time frame, and gave no hint for a different inhibitory effect of both isomers on glycolysis (see below). Moreover both tested cell lines (T98G and HEK293) delivered similar results of glyceraldehyde conversion. This is also in agreement to the similar sensitivity of both cell lines to this drug (Fig. 41, Fig. 43, Table 8). This showed that results can be compared between the different cell-lines. In fact T98G cells attached stronger to cell culture plate surfaces and were better suited for metabolomics measurements. For the opposite reason HEK293 cells were found to be better suited for FACS analysis.

The presence of sorbose marked the biggest difference between the isomers; it was further increased with longer incubation time and therefore seemed implausible to be a contamination in the GA preparation. Externally applied D-or L-sorbose had no effect on growth or viability with concentrations up to 10 mM (Fig. 54). If this compound is taken up by the cells it could be phosphorylated by hexokinase, resulting in sorbose-6-phosphate or by fructokinase, resulting in the inhibitory sorbose-1-phosphate. Whereas L-sorbose is no substrate of brain hexokinase (Sols and Crane, 1954) it is an accepted substrate for liver fructokinase (Raushel and Cleland, 1977). T98G cells consumed fructose in the media completely (Fig. 66), indicating that they offer a high activity of fructose-breakdown with all the available enzymes, but interestingly this does not affect their sensitivity to sorbose or glyceraldehyde.

Cells were further tested for the inhibitory effect of both isomers of glyceraldehyde, by measuring the incorporation of u-^{13}C-labeled glucose in presence of this inhibitor compared to an untreated control (Fig. 36). Here the inhibitory effect of L-GA was evidently higher, than that of the D-isomer (Fig. 45+Fig. 46) which is in full agreement with the literature (Lardy et al., 1950).

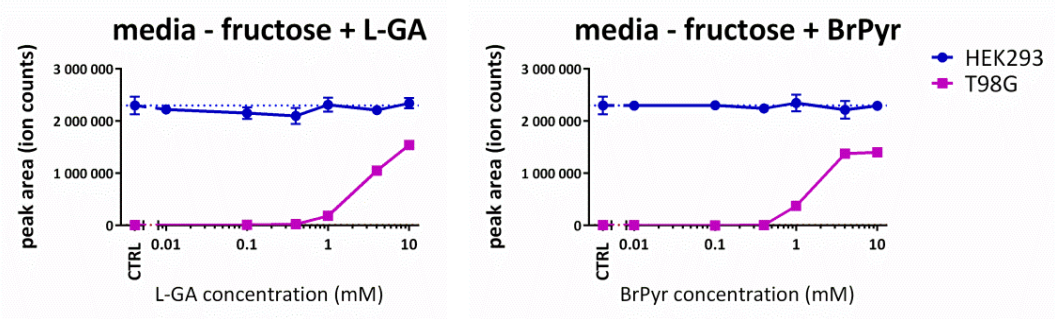

Fig. 66 – The consumption of media fructose in T98G cells is inhibited under influence of glycolytic inhibitors. T98G cells or HEK293 cells were treated 24 hours after seeding with different concentrations of either L-GA or BrPyr and the remaining amount of fructose in media was measured after 24 hours of incubation. HEK-cells (blue) do not consume fructose, but T98G cells consumed fructose completely. The fructose-consumption in T98G cells was inhibited with increasing concentrations of both inhibitors, similar to glucose-consumption (Fig. 43).

A small decrease in the level of glucose-phosphate was detected, but this did not negatively affect label in G6P or downstream intermediates of glycolysis under D-GA treatment. In stark contrast L-GA decreased the label incorporation behind F6P formation. When considering the decrease in label incorporation as the more descriptive difference than metabolite concentration (see above) then the main inhibition is not on the hexokinase reaction, as proposed (Lardy et al., 1950). The inhibition appeared to be located between F6P and 3PGA, a consistent finding between different tested cell lines (Fig. 47). These data showed the importance of performing experiments in full cellular context, as early experiments to discover GA function were made with isolated enzymes or cell extracts.

With the current data the inhibition cannot be localized on a single enzyme but to a small number of enzymatic reactions. Also an inhibition of triosephosphate-dehydrogenase (nowadays: GAPDH) was reported (Needham et al., 1951). The activity of phosphofructokinase is further sensitive to a decrease in the pH-level; the production of glycerate from glyceraldehyde acidifies cells (MacDonald et al., 2006) and this could also decrease the activity of this enzyme. The production of glycerate was similar for both isomers but inhibition of glycolysis was stronger for L-GA, so this might probably not explain the inhibition. Another possibility is competitive inhibition of aldolase. Without further supply of DHAP, GA cannot be fused to fructose-1-P or sorbose-1-P and might rest in the binding pocket, inhibiting an entry of F16BP.

5.8. BrPyr is very effective inhibitor of glycolysis in the tested concentration

In agreement with previous studies (Birsoy et al., 2013; Pereira da Silva et al., 2009) we observed an increased concentration of hexose phosphates after BrPyr treatment, indicating that hexokinase is not the major target of this inhibitor. The decrease in label incorporation is partially balanced by an increase in pool size. Further, a strong decline of carbon flow downstream of GAPDH, represented in the disappearance of 3PGA and virtually no ^{13}C ending in pyruvate, lactate and citrate, clearly identifies this enzyme as the true target of BrPyr (Barnard et al., 1993; Ganapathy-Kanniappan et al., 2009).

The strong inhibition of this compound might be partially explained by the concentration used, that was chosen to enable a direct comparison in the inhibitory strengths of the tested compounds, but was found to be above the EC_{50} (section 4.3.2). Further experiments with lower concentrations might reveal if a remarkably inhibition of glycolysis is also detectable in concentration range capable of inhibiting growth, viability or glucose consumption.

5.9. The failure of 2DG to inhibit glycolysis

In contrast to L-GA and BrPyr that showed remarkable inhibitory effect on glycolysis, 2-deoxyglucose evidently failed to exhibit a selective effect to glycolysis. 2 mM of 2DG reduced the ^{13}C-labeled fraction of hexose phosphates by only 20 %, and did not affect the labeled intensity of pyruvate or lactate. In contrast a time- and concentration-dependent increase of 2-deoxyglucose-phosphate, resulting from phosphorylation by hexokinase, was clearly detectable (Fig. 49).

Strikingly, cells adapted to 2DG treatment by increasing carbon flow into citrate (Fig. 50) a finding also reported earlier (Letnansky and Seelich, 1960; Sauermann, 1967). From these results, we summarized an accumulation of 2-deoxyglucose-phosphate that cannot be further utilized and depletes the cellular phosphate pool by consuming ATP and scavenging phosphate. Depending on the strength of depletion, the ADP re-phosphorylation and ATP dependent processes might stop High concentrations of 2DG (10 mM) further reduced the intensity of glycolytic intermediates however isotope incorporation rates in G6P remained unaltered.

Moreover, in the last years criticism raised for 2DG as glycolytic inhibitor. It has been shown that 2DG treatment interferes with glycosylation of proteins, inducing stress in the endoplasmic reticulum, an effect that is reversible by addition of mannose, which is not sufficient to supplement inhibited glycolysis (Kang and Hwang, 2006; Kurtoglu et al., 2007). These side effects

may be more important in sense of growth inhibition than the proposed but not substantiated effect as glycolytic inhibitor.

5.10. Comparison of the tested compounds and characterization as possible therapeutics

All three analyzed compounds are very special compounds in view as possible therapeutic drugs: They are small, polar, very reactive and effective only in high doses. More importantly, their reactivity is part of the action of these compounds, to trap them inside cells and transform the compounds into the reactive form (GA, 2DG) or to chemically bind the compound to an enzyme and inhibit its activity (BrPyr). Unfortunately unwanted side reactions of these compounds can't be excluded.

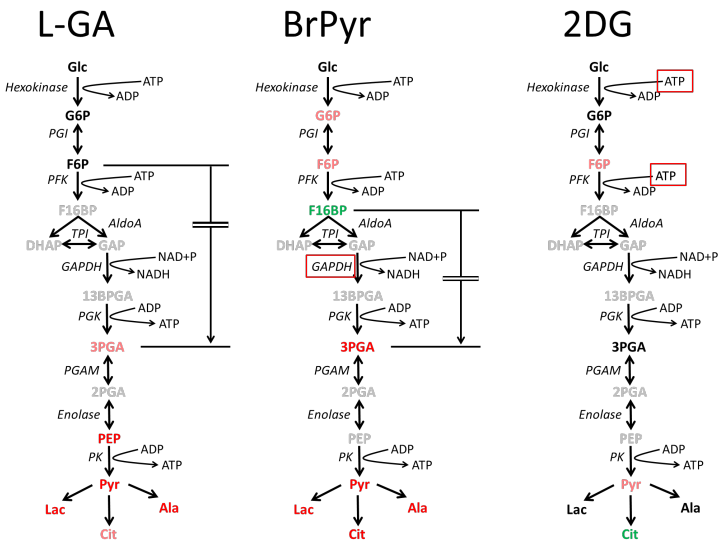

Fig. 67 – Comparison of the inhibitory effects of the three tested compounds. The color of the compounds indicates the change in the flux into these compounds: black= unchanged, grey= not detected, pink= slight decrease, red= strong decrease, green= increase.

During drug discovery processes an identified precursor is typically modified to a more stable or/and more effective compound (Bleicher et al., 2003; Korfmacher, 2003). However due to their small size and the inherent need for chemical reactivity this appears to be less possible, as even small modifications in their structure might affect their reactivity. Nevertheless creating labile derivatives which are split into reactive compounds appears to be possible. For glyceraldehyde thiazolidines were tested, but failed, probably because of a decreased breakdown under anaerobic conditions (Margraf-Modersohn et al., 1970). For 3-bromopyruvate a modification (3-bromo-2-oxopropionate-1-propyl ester) was recently introduced, which is cleaved inside the cells

by esterases. The compound delivered similar effects as 3-bromopyruvate but had a higher stability (Levy et al., 2012; Xu et al., 2005a).

It was not a primary aim of this study to judge the usefulness of these compounds as potential therapeutic target, but to learn more about their possible action, in particular on short time scales after drug application to identify their first direct targets. Even when a compound was identified to be active in cell culture a similar action *in vivo* needs to be thoroughly validated before application. As an example, 2DG gave promising results *in vitro*, but showed only poor success when applied alone *in vivo* (Tannock et al., 1983) but increased sensitivity to radiation (Dwarakanath et al., 2009). Even if none of these compounds will be used as a single therapeutic agent, it might increase the effect when used in combination with other compounds (Cheong et al., 2011).

A deeper understanding of how these compounds work will help to find potential useful combinations, this includes a deeper knowledge how the compounds affect the metabolism and are metabolized. Eventually proteomic data reveal the enzymatic setup of a cell or tissue and help to predict if a tumor is sensitive to treatment with one of these drugs, by absence or lowered activity of enzymes able to degrade the inhibitor or its toxic products. Ultimately different inhibitors might be combined, even with non-toxic compounds to decrease or overcome degradation of inhibitors or reduce side effect to healthy cells. One interesting idea is to fuel organisms, treated with glycolytic inhibitors with lactate, as this is supposed to be only used by healthy cells but not cancers (Nijsten and van Dam, 2009).

5.11. GA and further effects to glucose sensing

Glyceraldehyde was reported to stimulate insulin secretion in pancreatic beta-cells even more than similar glucose concentration (Jain et al., 1975) and was therefore used for decades as tool to study insulin secretion (MacDonald et al., 2006). Remarkably the insulin-stimulatory effect of D-GA was reported to be higher than that of L-GA and is at least partially based on metabolism of this compound (Alcazar et al., 1995; MacDonald, 1989). It was further reported that prolonged incubation or too high concentrations led to the swimming phenotype and dead cells (MacDonald et al., 2006).

These data suggests a possible function of this compound in glucose sensing mechanisms, acting at intracellular sensors or by imbalancing metabolite or energy levels. I hypothesized that glycolytic inhibition by glyceraldehyde hindered the usage of glucose to produce ATP and drives cells into a growth crises when glucose is detected by the cells and cells started to divide (Fig. 68).

It was found that the presence of glucose and glutamine is necessary to stimulate G1 to S-phase progression (Colombo et al., 2011).

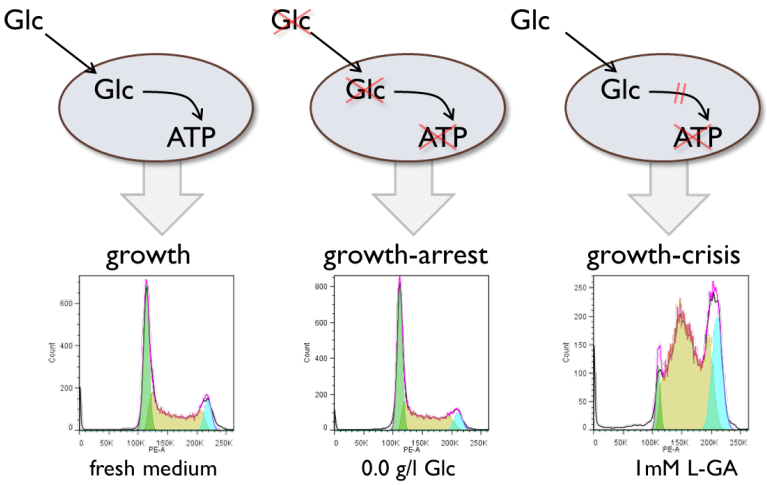

Fig. 68 - Hypothesis of induced growth crises by depleting ATP level in presence of depleting glucose. The absence of glucose is sensed by intracellular glucose-sensing mechanisms and the depletion of ATP. If glucose cannot be converted metabolically to ATP the contrasting signals drive cells into S-phase that cannot finished due to limited energy.

It was further tested if glyceraldehyde affected the ATP level inside cells (Fig. 69 - left). In fact, both isomers decrease ATP level already after 15 minutes to a level similar to the one obtained after 8 hours of glucose starvation, and with similar results obtained after longer incubation (not shown). The similarity of both isomers in decreasing ATP level in contrast to different effects to glycolysis (Fig. 45- Fig. 47) indicates that the conversion of glyceraldehyde rather than the inhibition of glycolysis affected the ATP levels. The transformation of both isomers, at least on the short time scale, appeared to be similar for both compounds and might include at least one ATP consuming step. The conversion of glyceraldehyde to glyceric acid produces NADH and to glycerol consumes NADPH (Van Heyningen, 1969). High rates of transformation of glyceraldehyde might therefore additionally influence NADH and NADPH values, which was indeed shown in pancreatic beta cells (MacDonald et al., 2006).

Additionally the phosphorylation status of AMPK, an important intracellular sensor of energy level (Hardie et al., 2012) was determined under the influence of low glucose levels, or presence of BrPyr and GA, by western blot analysis of phospho-AMPK performed by Raphaela Fritsche in our lab (Fig. 69 - right). She found that glucose deprivation lead to a phosphorylation of AMPK, which was found much stronger under influence of BrPyr. In contrast glyceraldehyde had no effect. The difference between both isomers in sense of growth effect, stress phenotype, metabolic inhibition

and influence to intracellular energy sensing remain interesting and could be further investigated in future.

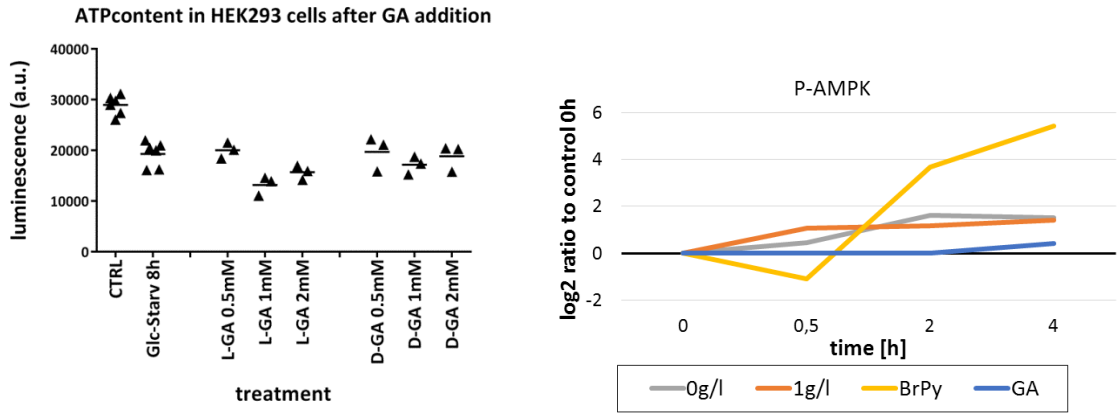

Fig. 69 – Drug effects to energy signaling inside of cells. Left: ATP content in HEK293 cells after 15 minutes of incubation with different amounts of glyceraldehyde compared to untreated cells or cells starved for glucose for eight hours and detected with luminescence ATP detection kit. Right: Amount of phospho-AMPK in HEK293 cells at different time points after treatment with reduced amounts of glucose, 1 mM Bromopyruvate (BrPy) or 1 mM L-GA (GA).

5.12. *In vivo* application of isotopic labeled compounds in mice

Achieving a complete label in *in vivo* studies in animals is nearly impossible and even reaching stationary (unchanged) label incorporation requires a long continuous feeding with labeled substrates, by food or infusion. This requires high amount of the substrate, making the experiment very expensive. Additionally the heavy carbons distribute through multiple tissues and compounds making it complicate to interpret the results. Therefore an incomplete and instationary labeling may to be applied *in vivo*. The strategies to measure, calculate and interpret labeling experiments established in in-vitro studies were transferred to animal models. Here two pilot studies to discover the time frame and potential substrate usages were performed.

The first experiment, with injection of ^{13}C-pyruvate revealed that a single injection of a labeled compound resulted in a sharp pulse labeling, peaking at seven minutes and decreasing until 14 minutes, proposing time scales for future experiments between five and ten minutes.

In the second experiment the different substrate usage for glucose and glutamine was tested with an interesting mouse model. In this mouse the males spontaneously develop liver cancer (Dubois et al., 1991) which serves as model for hepatocellular cancer (HCC) in human, one of the main types of liver cancer (Perz et al., 2006). Therefore these mice were used to understand

development and progression of cancer and to test cancer therapies targeting these differences. I found remarkable differences in the substrate usage between both sexes. The labeling in lactate was much higher in males, indicating a higher carbon flow from ^{13}C-glucose to lactate, compared to the situation in female, healthy mice. In contrast to that dramatically higher label incorporation into metabolites of the TCA-cycle was found, pointing towards a higher activity of TCA-cycle in healthy, female mice (Fig. 59 - Fig. 61).

Taken together these results clearly indicate a switch in the metabolic state, from a state well balanced between glycolysis and TCA-cycle in female (healthy) mice to an increase in glycolysis and lactate production and a lower TCA-cycle activity in cancerous male mice. These results were not unexpected, and perfectly fit to the current understanding of cancer metabolism. Nevertheless it is important to show that this model-organism indeed exhibits the cancer-phenotype and that the established method is able to monitor the effect. With this as starting point further experiments addressing the development and a potential tumor therapy within these mice will be performed.

Notably in both sexes we found evidence for a reverse TCA-cycle, by the finding of substantial label incorporation in the m+5 position of citrate, under ^{13}C-glutamine labeling (Fig. 62). Activity of a reverse TCA cycle in perfused rat livers was already shown in 1994 (Des Rosiers et al., 1994), but nowadays reversed TCA cycle activity is most often discussed in terms of cancer metabolism and under hypoxic conditions (Fendt et al., 2013; Filipp et al., 2012b). The intensity of the incorporated label was higher in the female mice, indicating an increased activity of the TCA cycle, but the pattern was similar between both sexes (Fig. 62). Together with an elevated TCA-cycle activity in female mice a remarkable amount of label (5%) was found in lactate after glutamine labeling (Fig. 59), pointing towards a possible routing from glutamine to lactate, in sense of gluconeogenesis. It should be pointed out, that only a low number of animals were used for this pilot study (n=1-4 per condition), so these preliminary data need to be substantiated with further experimental data. A repeated experiment with more replicates was performed already and awaits analysis.

3-bromopyruvate and glyceraldehyde were already successfully used in *in vivo* studies and showed a decreased tumor growth when being injected in close proximity to the tumor or shortly after its transplantation. (Apple et al., 1970; Bennett and Connon, 1966; Geschwind et al., 2002; Kim et al., 2007; Vali et al., 2008; Warburg et al., 1963)

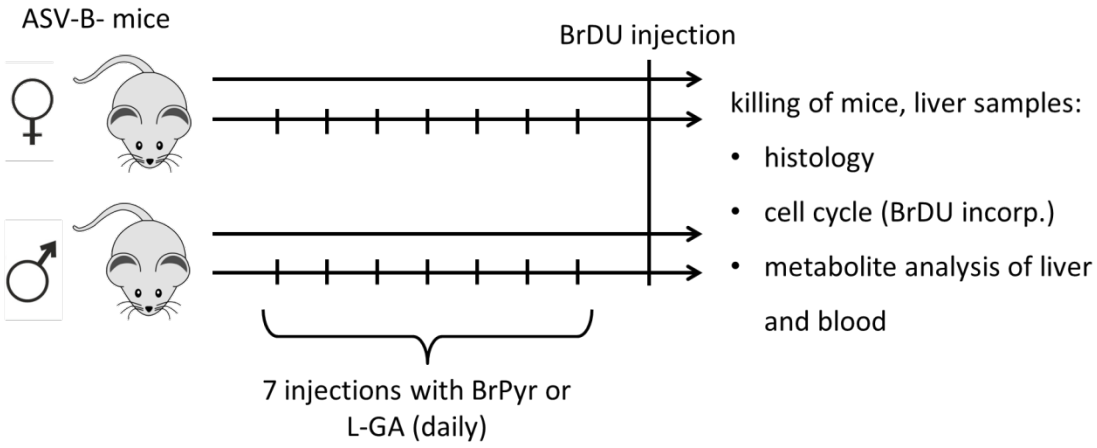

Fig. 70 – Future plan to monitor effects of glycolytic inhibitors to HCC model mice during tumor development. Female and male ASV-B mice, 14 weeks old will receive daily injections of either Bromoyruvate (BrPyr), L-glyceraldehyde or PBS as control, with daily vitality checks. After 1 week they receive BrDU to measure activity of S-phase of the cell-cycle. 2 hours later mice will be killed, one part of the liver will be frozen for metabolite measurements and the remainder will be used for histology and BrDU incorporation assay.

5.13. Conclusion and outlook

Leaving the field of plant metabolomics were I started during my diploma-thesis (Kempa et al., 2009; Wienkoop et al., 2010) and entering the area of mammalian metabolomics together with dynamic ^{13}C labeling studies and toxicology involved some difficult lessons to be learned. Starting from off the beaten tracks, some basic questions were addressed, having been either overlooked or considered as answered a long time ago.

First, the subtracting of natural label by use of measured reference samples instead of calculating it from sum formulas is a simple but effective approach and was reported by Biemann such a long time ago that it is buried deep in the libraries (Biemann, 1962). This and similar methods as the one by Jennings (Jennings and Matthews, 2005) were regularly cited but not shown that this could in fact have an advantage over mathematical calculations.

Secondly, I wanted to know if it is possible to use and understand the outcome of labeling data without putting it into a mathematical model. It was shown that with a complex model and enough computation it was possible to derive and describe intracellular fluxes by measuring only isotopomer pattern in lactate under different glucose sources (Henry et al., 2011). However, with more assumptions that have to be made, the impact of wrong assumption or unknown interaction increases (van Winden et al., 2001). Instead, we aimed at a comprehensive measurement of as many entities as possible to deliver high quality data. In fact, the coverage as

well as the reproducibility is very good, which together with absolute quantification of metabolite abundances opens the possibility of including the data into models that will surely be developed in the future.

Indeed I could show that differences between several conditions could be detected and described quantitatively even when applying only a single labeling substrate (u-^{13}C-glucose) for a single time point. Certainly, the insight will increase with more time points, treatments, concentrations and putting data into models, but experiment and measurement time will also grow. Currently some compounds were measured around their detection limits, so they are not detected in all conditions, but usually the coverage of metabolites is very high. Further attempts to increase the coverage of measured compounds, e.g. by applying additional techniques as LC-MS or CE-MS or by modifying extraction strategies to selectively increase efficacy towards the most important compounds (e.g. phosphorylated intermediates of glycolysis) can further strengthens this approach.

The established pSIRM-approach is flexible enough to monitor changes in metabolism within minutes after perturbing the system. This was shown by testing the impact of different reported inhibitors of glycolysis, with results fitting to expectations for Bromopyruvate, delivering unexpected results for glyceraldehyde and showing unspecifity in the action of 2DG. With this approach the effect of these and other compounds to the metabolism can be tested, after a short incubation time, to monitor direct effect to certain enzymes, or after a longer inhibition to detect chronic rearrangement of metabolism. With this, potential drugs can be better characterized before testing these compounds *in vivo*.

Effectively the same strategy can be applied *in vivo.* With this the differences between healthy and cancerous tissues and animals can be detected, indicating targets for a metabolic therapy and to monitor the outcome of the therapy. These efforts will be further expanded, this work is one important first step.

6. BIBLIOGRAPHY

Alcazar, O., E. Gine, Z. Qiu-Yue, and J. Tamarit-Rodriguez. 1995. The stimulation of insulin secretion by D-glyceraldehyde correlates with its rate of oxidation in islet cells. *The Biochemical journal*. 310:215-220.

Antoniewicz, M.R., J.K. Kelleher, and G. Stephanopoulos. 2007. Accurate assessment of amino acid mass isotopomer distributions for metabolic flux analysis. *Analytical chemistry*. 79:7554-7559.

Antony, G., L.W. White, and B.R. Landau. 1969. Metabolism of D- and L-glyceraldehyde in adipose tissue: a stereochemical probe for glycerokinase activity. *Journal of lipid research*. 10:521-527.

Apple, M.A., F.C. Ludwig, and D.M. Greenberg. 1970. Selective cancer growth inhibition in mice by dihydroxypropanal without concomitant inhibition of bone marrow or other normal tissue. *Oncology*. 24:210-222.

Bachelard, H.S. 1971. Specificity and kinetic properties of monosaccharide uptake into guinea pig cerebral cortex in vitro. *Journal of neurochemistry*. 18:213-222.

Bachelard, H.S., A.G. Clark, and M.F. Thompson. 1971. Cerebral-cortex hexokinase. Elucidation of reaction mechanisms by substrate and dead-end inhibitor kinetic analysis. *The Biochemical journal*. 123:707-715.

Baer, E., and H.O.L. Fischer. 1938. Prepararion of L-glyceric aldehyde. *Science*. 88:108.

Bak, L.K., A. Schousboe, U. Sonnewald, and H.S. Waagepetersen. 2006. Glucose is necessary to maintain neurotransmitter homeostasis during synaptic activity in cultured glutamatergic neurons. *Journal of cerebral blood flow and metabolism : official journal of the International Society of Cerebral Blood Flow and Metabolism*. 26:1285-1297.

Barnard, J.P., B. Reynafarje, and P.L. Pedersen. 1993. Glucose catabolism in African trypanosomes. Evidence that the terminal step is catalyzed by a pyruvate transporter capable of facilitating uptake of toxic analogs. *The Journal of biological chemistry*. 268:3654-3661.

Bennett, L.R., and F.E. Connon. 1966. Comparative effects of DL-glyceraldehyde, 6-mercaptopurine, methotrexate and 5-fluorouracil on the Ehrlich ascites carcinoma in vivo. *International journal of cancer. Journal international du cancer*. 1:291-295.

Berglund, M., and M.E. Wieser. 2011. Isotopic compositions of the elements 2009 (IUPAC Technical Report). *Pure Appl. Chem.* 83:397–410.

Biemann, K. 1962. Mass spectrometry : organic chemical applications. McGraw-Hill, New York [u.a.]. XII, 370 S. pp.

Birsoy, K., T. Wang, R. Possemato, O.H. Yilmaz, C.E. Koch, W.W. Chen, A.W. Hutchins, Y. Gultekin, T.R. Peterson, J.E. Carette, T.R. Brummelkamp, C.B. Clish, and D.M. Sabatini. 2013. MCT1-mediated transport of a toxic molecule is an effective strategy for targeting glycolytic tumors. *Nature genetics*. 45:104-108.

Bleicher, K.H., H.J. Bohm, K. Muller, and A.I. Alanine. 2003. Hit and lead generation: beyond high-throughput screening. *Nature reviews. Drug discovery*. 2:369-378.

Brand, K. 1985. Glutamine and glucose metabolism during thymocyte proliferation. Pathways of glutamine and glutamate metabolism. *The Biochemical journal*. 228:353-361.

Brock, N., and T. Niekamp. 1965. Zur Frage der cytostatischen Wirksamkeit von D-Glycerinaldehyd. *Z Krebs-forsch*. 67:93-104.

Calvin, M., and A.A. Benson. 1949. The Path of Carbon in Photosynthesis IV: The Identity and Sequence of the Intermediates in Sucrose Synthesis. *Science*. 109:140-142.

Chassagnole, C., N. Noisommit-Rizzi, J.W. Schmid, K. Mauch, and M. Reuss. 2002. Dynamic modeling of the central carbon metabolism of Escherichia coli. *Biotechnol Bioeng*. 79:53-73.

Chen, Z., W. Lu, C. Garcia-Prieto, and P. Huang. 2007. The Warburg effect and its cancer therapeutic implications. *Journal of Bioenergetics and Biomembranes*. 39:267-274.

Cheong, J.H., E.S. Park, J. Liang, J.B. Dennison, D. Tsavachidou, C. Nguyen-Charles, K. Wa Cheng, H. Hall, D. Zhang, Y. Lu, M. Ravoori, V. Kundra, J. Ajani, J.S. Lee, W. Ki Hong, and G.B. Mills. 2011. Dual inhibition of tumor energy pathway by 2-deoxyglucose and metformin is effective against a broad spectrum of preclinical cancer models. *Molecular cancer therapeutics*. 10:2350-2362.

Colombo, S.L., M. Palacios-Callender, N. Frakich, S. Carcamo, I. Kovacs, S. Tudzarova, and S. Moncada. 2011. Molecular basis for the differential use of glucose and glutamine in cell proliferation as revealed by synchronized HeLa cells. *Proc Natl Acad Sci U S A*. 108:21069-21074.

Cox, J., and M. Mann. 2008. MaxQuant enables high peptide identification rates, individualized p.p.b.-range mass accuracies and proteome-wide protein quantification. *Nat Biotechnol*. 26:1367-1372.

Darzynkiewicz, Z., H. Crissman, and J.W. Jacobberger. 2004. Cytometry of the cell cycle: cycling through history. *Cytometry A*. 58:21-32.

DeBerardinis, R.J., A. Mancuso, E. Daikhin, I. Nissim, M. Yudkoff, S. Wehrli, and C.B. Thompson. 2007. Beyond aerobic glycolysis: transformed cells can engage in glutamine metabolism that exceeds the requirement for protein and nucleotide synthesis. *Proceedings of the National Academy of Sciences of the United States of America*. 104:19345-19350.

Des Rosiers, C., C.A. Fernandez, F. David, and H. Brunengraber. 1994. Reversibility of the mitochondrial isocitrate dehydrogenase reaction in the perfused rat liver. Evidence from isotopomer analysis of citric acid cycle intermediates. *The Journal of biological chemistry*. 269:27179-27182.

Dolbeare, F., H. Gratzner, M.G. Pallavicini, and J.W. Gray. 1983. Flow cytometric measurement of total DNA content and incorporated bromodeoxyuridine. *Proc Natl Acad Sci U S A*. 80:5573-5577.

Dubois, N., M. Bennoun, I. Allemand, T. Molina, G. Grimber, M. Daudet-Monsac, R. Abelanet, and P. Briand. 1991. Time-course development of differentiated hepatocarcinoma and lung metastasis in transgenic mice. *Journal of hepatology*. 13:227-239.

Dunn, W.B. 2008. Current trends and future requirements for the mass spectrometric investigation of microbial, mammalian and plant metabolomes. *Physical biology*. 5.

Dunn, W.B., D.I. Broadhurst, H.J. Atherton, R. Goodacre, and J.L. Griffin. 2011. Systems level studies of mammalian metabolomes: the roles of mass spectrometry and nuclear magnetic resonance spectroscopy. *Chemical Society reviews*. 40:387-426.

Dwarakanath, B.S., D. Singh, A.K. Banerji, R. Sarin, N.K. Venkataramana, R. Jalali, P.N. Vishwanath, B.K. Mohanti, R.P. Tripathi, V.K. Kalia, and V. Jain. 2009. Clinical studies for improving radiotherapy with 2-deoxy-D-glucose: present status and future prospects. *Journal of cancer research and therapeutics*. 5 Suppl 1:S21-26.

Eden, E., N. Geva-Zatorsky, I. Issaeva, A. Cohen, E. Dekel, T. Danon, L. Cohen, A. Mayo, and U. Alon. 2011. Proteome half-life dynamics in living human cells. *Science*. 331:764-768.

Estevez-Garcia, I.O., V. Cordoba-Gonzalez, E. Lara-Padilla, A. Fuentes-Toledo, R. Falfan-Valencia, R. Campos-Rodriguez, and E. Abarca-Rojano. 2014. Glucose and glutamine metabolism control by APC and SCF during the G1-to-S phase transition of the cell cycle. *Journal of physiology and biochemistry*.

Ewald, B., D. Sampath, and W. Plunkett. 2008. Nucleoside analogs: molecular mechanisms signaling cell death. *Oncogene*. 27:6522-6537.

Fan, T.W., A.N. Lane, R.M. Higashi, M.A. Farag, H. Gao, M. Bousamra, and D.M. Miller. 2009. Altered regulation of metabolic pathways in human lung cancer discerned by (13)C stable isotope-resolved metabolomics (SIRM). *Molecular cancer*. 8:41.

Fan, T.W., P.K. Lorkiewicz, K. Sellers, H.N. Moseley, R.M. Higashi, and A.N. Lane. 2012. Stable isotope-resolved metabolomics and applications for drug development. *Pharmacol Ther*. 133:366-391.

Farkash-Amar, S., E. Eden, A. Cohen, N. Geva-Zatorsky, L. Cohen, R. Milo, A. Sigal, T. Danon, and U. Alon. 2012. Dynamic Proteomics of Human Protein Level and Localization across the Cell Cycle. *PloS one*. 7:e48722.

Fendt, S.M., E.L. Bell, M.A. Keibler, B.A. Olenchock, J.R. Mayers, T.M. Wasylenko, N.I. Vokes, L. Guarente, M.G. Vander Heiden, and G. Stephanopoulos. 2013. Reductive glutamine metabolism is a function of the alpha-ketoglutarate to citrate ratio in cells. *Nature communications*. 4:2236.

Fiehn, O. 2002. Metabolomics--the link between genotypes and phenotypes. *Plant molecular biology*. 48:155-171.

Filipp, F.V., B. Ratnikov, J. De Ingeniis, J.W. Smith, A.L. Osterman, and D.A. Scott. 2012a. Glutamine-fueled mitochondrial metabolism is decoupled from glycolysis in melanoma. *Pigment cell & melanoma research*. 25:732-739.

Filipp, F.V., D.A. Scott, Z.A. Ronai, A.L. Osterman, and J.W. Smith. 2012b. Reverse TCA cycle flux through isocitrate dehydrogenases 1 and 2 is required for lipogenesis in hypoxic melanoma cells. *Pigment cell & melanoma research*. 25:375-383.

Gambhir, S.S. 2002. Molecular imaging of cancer with positron emission tomography. *Nat Rev Cancer*. 2:683-693.

Ganapathy-Kanniappan, S., J.F. Geschwind, R. Kunjithapatham, M. Buijs, J.A. Vossen, I. Tchernyshyov, R.N. Cole, L.H. Syed, P.P. Rao, S. Ota, and M. Vali. 2009. Glyceraldehyde-3-phosphate dehydrogenase (GAPDH) is pyruvylated during 3-bromopyruvate mediated cancer cell death. *Anticancer research*. 29:4909-4918.

Garber, K. 2004. Energy Boost: The Warburg Effect Returns in a New Theory of Cancer. *Journal of the National Cancer Institute*. 96:1805-1806.

Geschwind, J.F., Y.H. Ko, M.S. Torbenson, C. Magee, and P.L. Pedersen. 2002. Novel therapy for liver cancer: direct intraarterial injection of a potent inhibitor of ATP production. *Cancer research*. 62:3909-3913.

Giammarioli, A.M., L. Gambardella, C. Barbati, D. Pietraforte, A. Tinari, M. Alberton, L. Gnessi, R.J. Griffin, M. Minetti, and W. Malorni. 2012. Differential effects of the glycolysis inhibitor 2-deoxy-D-glucose on the activity of pro-apoptotic agents in metastatic melanoma cells, and induction of a cytoprotective autophagic response. *International journal of cancer. Journal international du cancer*. 131:E337-347.

Goldberg, L., R. Israeli, and Y. Kloog. 2012. FTS and 2-DG induce pancreatic cancer cell death and tumor shrinkage in mice. *Cell death & disease*. 3:e284.

Gong, J., F. Traganos, and Z. Darzynkiewicz. 1995. Threshold expression of cyclin E but not D type cyclins characterizes normal and tumour cells entering S phase. *Cell proliferation*. 28:337-346.

Granchi, C., and F. Minutolo. 2012. Anticancer agents that counteract tumor glycolysis. *ChemMedChem*. 7:1318-1350.

Groheux, D., M. Espie, S. Giacchetti, and E. Hindie. 2013. Performance of FDG PET/CT in the clinical management of breast cancer. *Radiology*. 266:388-405.

Gullberg, J., P. Jonsson, A. Nordstrom, M. Sjostrom, and T. Moritz. 2004. Design of experiments: an efficient strategy to identify factors influencing extraction and derivatization of Arabidopsis thaliana samples in metabolomic studies with gas chromatography/mass spectrometry. *Analytical biochemistry*. 331:283-295.

Guppy, M., P. Leedman, X. Zu, and V. Russell. 2002. Contribution by different fuels and metabolic pathways to the total ATP turnover of proliferating MCF-7 breast cancer cells. *The Biochemical journal*. 364:309-315.

Hagopian, K., J.J. Ramsey, and R. Weindruch. 2008. Enzymes of glycerol and glyceraldehyde metabolism in mouse liver: effects of caloric restriction and age on activities. *Bioscience reports*. 28:107-115.

Halket, J.M., D. Waterman, A.M. Przyborowska, R.K. Patel, P.D. Fraser, and P.M. Bramley. 2005. Chemical derivatization and mass spectral libraries in metabolic profiling by GC/MS and LC/MS/MS. *Journal of experimental botany*. 56:219-243.

Han, X., and R.W. Gross. 2005. Shotgun lipidomics: electrospray ionization mass spectrometric analysis and quantitation of cellular lipidomes directly from crude extracts of biological samples. *Mass spectrometry reviews*. 24:367-412.

Hanahan, D., and R.A. Weinberg. 2011. Hallmarks of cancer: the next generation. *Cell*. 144:646-674.

Hardie, D.G., F.A. Ross, and S.A. Hawley. 2012. AMPK: a nutrient and energy sensor that maintains energy homeostasis. *Nature reviews. Molecular cell biology*. 13:251-262.

Hellerstein, M.K., and R.A. Neese. 1999. Mass isotopomer distribution analysis at eight years: theoretical, analytic, and experimental considerations. *The American journal of physiology*. 276:E1146-1170.

Hellman, B., L.A. Idahl, A. Lernmark, J. Sehlin, and I.B. Taljedal. 1974. The pancreatic beta-cell recognition of insulin secretagogues. Comparisons of glucose with glyceraldehyde isomers and dihydroxyacetone. *Archives of biochemistry and biophysics*. 162:448-457.

Henry, O., M. Jolicoeur, and A. Kamen. 2011. Unraveling the metabolism of HEK-293 cells using lactate isotopomer analysis. *Bioprocess and biosystems engineering*. 34:263-273.

Hiller, K., C.M. Metallo, J.K. Kelleher, and G. Stephanopoulos. 2010. Nontargeted elucidation of metabolic pathways using stable-isotope tracers and mass spectrometry. *Analytical chemistry*. 82:6621-6628.

Hiller, K., A. Wegner, D. Weindl, T. Cordes, C.M. Metallo, J.K. Kelleher, and G. Stephanopoulos. 2013. NTFD--a stand-alone application for the non-targeted detection of stable isotope-labeled compounds in GC/MS data. *Bioinformatics*. 29:1226-1228.

Hofmann, U., K. Maier, A. Niebel, G. Vacun, M. Reuss, and K. Mauch. 2008. Identification of metabolic fluxes in hepatic cells from transient 13C-labeling experiments: Part I. Experimental observations. *Biotechnol Bioeng*. 100:344-354.

Hsu, P.P., and D.M. Sabatini. 2008. Cancer cell metabolism: Warburg and beyond. *Cell*. 134:703-707.

Huege, J., J. Goetze, F. Dethloff, B. Junker, and J. Kopka. 2014. Quantification of stable isotope label in metabolites via mass spectrometry. *Methods Mol Biol*. 1056:213-223.

Ihrlund, L.S., E. Hernlund, O. Khan, and M.C. Shoshan. 2008. 3-Bromopyruvate as inhibitor of tumour cell energy metabolism and chemopotentiator of platinum drugs. *Molecular oncology*. 2:94-101.

Ishihama, Y., J. Rappsilber, and M. Mann. 2006. Modular stop and go extraction tips with stacked disks for parallel and multidimensional Peptide fractionation in proteomics. *Journal of proteome research*. 5:988-994.

Jackman, J., and P.M. O'Connor. 2001. Methods for synchronizing cells at specific stages of the cell cycle. *Curr Protoc Cell Biol*. Chapter 8:Unit 8 3.

Jain, K., J. Logothetopoulos, and P. Zucker. 1975. The effects of D- and L-glyceraldehyde on glucose oxidation, insulin secretion and insulin biosynthesis by pancreatic islets of the rat. *Biochimica et biophysica acta*. 399:384-394.

Jennings, M.E., 2nd, and D.E. Matthews. 2005. Determination of complex isotopomer patterns in isotopically labeled compounds by mass spectrometry. *Analytical chemistry*. 77:6435-6444.

Juan, G., J. Gong, F. Traganos, and Z. Darzynkiewicz. 1996. Unscheduled expression of cyclins D1 and D3 in human tumour cell lines. *Cell proliferation*. 29:259-266.

Junker, B.H., C. Klukas, and F. Schreiber. 2006. VANTED: a system for advanced data analysis and visualization in the context of biological networks. *BMC bioinformatics*. 7:109.

Kang, H.T., and E.S. Hwang. 2006. 2-Deoxyglucose: an anticancer and antiviral therapeutic, but not any more a low glucose mimetic. *Life sciences*. 78:1392-1399.

Kell, D.B. 2004. Metabolomics and systems biology: making sense of the soup. *Current opinion in microbiology*. 7:296-307.

Kempa, S., J. Hummel, T. Schwemmer, M. Pietzke, N. Strehmel, S. Wienkoop, J. Kopka, and W. Weckwerth. 2009. An automated GCxGC-TOF-MS protocol for batch-wise extraction and alignment of mass isotopomer matrixes from differential 13C-labelling experiments: a

case study for photoautotrophic-mixotrophic grown Chlamydomonas reinhardtii cells. *Journal of basic microbiology*. 49:82-91.

Kim, W., J.H. Yoon, J.M. Jeong, G.J. Cheon, T.S. Lee, J.I. Yang, S.C. Park, and H.S. Lee. 2007. Apoptosis-inducing antitumor efficacy of hexokinase II inhibitor in hepatocellular carcinoma. *Mol Cancer Ther*. 6:2554-2562.

Ko, Y.H., and B.A. McFadden. 1990. Alkylation of isocitrate lyase from Escherichia coli by 3-bromopyruvate. *Archives of biochemistry and biophysics*. 278:373-380.

Ko, Y.H., P.L. Pedersen, and J.F. Geschwind. 2001. Glucose catabolism in the rabbit VX2 tumor model for liver cancer: characterization and targeting hexokinase. *Cancer letters*. 173:83-91.

Ko, Y.H., H.A. Verhoeven, M.J. Lee, D.J. Corbin, T.J. Vogl, and P.L. Pedersen. 2012. A translational study "case report" on the small molecule "energy blocker" 3-bromopyruvate (3BP) as a potent anticancer agent: from bench side to bedside. *J Bioenerg Biomembr*. 44:163-170.

Koek, M.M., B. Muilwijk, M.J. van der Werf, and T. Hankemeier. 2006. Microbial metabolomics with gas chromatography/mass spectrometry. *Analytical chemistry*. 78:1272-1281.

Kopka, J., N. Schauer, S. Krueger, C. Birkemeyer, B. Usadel, E. Bergmuller, P. Dormann, W. Weckwerth, Y. Gibon, M. Stitt, L. Willmitzer, A.R. Fernie, and D. Steinhauser. 2005. GMD@CSB.DB: the Golm Metabolome Database. *Bioinformatics*. 21:1635-1638.

Korfmacher, W.A. 2003. Lead optimization strategies as part of a drug metabolism environment. *Current opinion in drug discovery & development*. 6:481-485.

Krebs, H.A., and W.A. Johnson. 1937. The Role of Citric Acid in Intermediate Metabolism in Animal Tissues. *Enzymologia*. 4:148-156.

Krude, T. 1999. Mimosine arrests proliferating human cells before onset of DNA replication in a dose-dependent manner. *Exp Cell Res*. 247:148-159.

Kuich, P.H.J. 2014. Towards understanding organ-derived metabolic signatures in blood. *In* Biology, Chemistry and Pharmacy. Vol. PhD. Freie Universität Berlin.

Kurtoglu, M., N. Gao, J. Shang, J.C. Maher, M.A. Lehrman, M. Wangpaichitr, N. Savaraj, A.N. Lane, and T.J. Lampidis. 2007. Under normoxia, 2-deoxy-D-glucose elicits cell death in select tumor types not by inhibition of glycolysis but by interfering with N-linked glycosylation. *Mol Cancer Ther*. 6:3049-3058.

Lalande, M. 1990. A reversible arrest point in the late G1 phase of the mammalian cell cycle. *Exp Cell Res*. 186:332-339.

Landau, B.R., and W. Merlevede. 1963. Initial reactions in the metabolism of D- and L-glyceraldehyde by rat liver. *The Journal of biological chemistry*. 238:861-867.

Lane, A.N., T.W. Fan, R.M. Higashi, J. Tan, M. Bousamra, and D.M. Miller. 2009. Prospects for clinical cancer metabolomics using stable isotope tracers. *Experimental and molecular pathology*. 86:165-173.

Lardy, H.A., V.D. Wiebelhaus, and K.M. Mann. 1950. The mechanism by which glyceraldehyde inhibits glycolysis. *The Journal of biological chemistry*. 187:325-337.

Lee, W.N., L.O. Byerley, E.A. Bergner, and J. Edmond. 1991. Mass isotopomer analysis: theoretical and practical considerations. *Biological mass spectrometry*. 20:451-458.

Lei, Z., D.V. Huhman, and L.W. Sumner. 2011. Mass spectrometry strategies in metabolomics. *The Journal of biological chemistry*. 286:25435-25442.

Letnansky, K., and F. Seelich. 1960. Über die Beeinflussung von Reaktionen des Citronensäure-Cyclus durch 2-Deoxy-D-Glucose. *Z Krebsforsch*. 64:1-6.

Levy, A.G., P.E. Zage, L.J. Akers, M.L. Ghisoli, Z. Chen, W. Fang, S. Kannan, T. Graham, L. Zeng, A.R. Franklin, P. Huang, and P.A. Zweidler-McKay. 2012. The combination of the novel glycolysis inhibitor 3-BrOP and rapamycin is effective against neuroblastoma. *Investigational new drugs*. 30:191-199.

Li, C., Z. Xiao, Z. Chen, X. Zhang, J. Li, X. Wu, X. Li, H. Yi, M. Li, G. Zhu, and S. Liang. 2006. Proteome analysis of human lung squamous carcinoma. *Proteomics*. 6:547-558.

Linehan, W.M., and T.A. Rouault. 2013. Molecular pathways: Fumarate hydratase-deficient kidney cancer--targeting the Warburg effect in cancer. *Clinical cancer research : an official journal of the American Association for Cancer Research*. 19:3345-3352.

Locasale, J.W., A.R. Grassian, T. Melman, C.A. Lyssiotis, K.R. Mattaini, A.J. Bass, G. Heffron, C.M. Metallo, T. Muranen, H. Sharfi, A.T. Sasaki, D. Anastasiou, E. Mullarky, N.I. Vokes, M. Sasaki, R. Beroukhim, G. Stephanopoulos, A.H. Ligon, M. Meyerson, A.L. Richardson, L. Chin, G. Wagner, J.M. Asara, J.S. Brugge, L.C. Cantley, and M.G. Vander Heiden. 2011. Phosphoglycerate dehydrogenase diverts glycolytic flux and contributes to oncogenesis. *Nature genetics*. 43:869-874.

MacDonald, M.J. 1989. Does glyceraldehyde enter pancreatic islet metabolism via both the triokinase and the glyceraldehyde phosphate dehydrogenase reactions? A study of these enzymes in islets. *Archives of biochemistry and biophysics*. 270:15-22.

MacDonald, M.J., F.W. Chaplen, C.K. Triplett, Q. Gong, and H. Drought. 2006. Stimulation of insulin release by glyceraldehyde may not be similar to glucose. *Archives of biochemistry and biophysics*. 447:118-126.

MacDonald, M.J., R.J. Mertz, and R.S. Rana. 1989. Glyceraldehyde phosphate: an insulin secretagogue with possible effects on inositol phosphate formation in pancreatic islets. *Archives of biochemistry and biophysics*. 269:194-200.

MacNaught, A.D., and A. Wilkinson. 1997. IUPAC. Compendium of Chemical Terminology, 2nd ed. (the "Gold Book"). Blackwell Scientific Publications, Oxford.

Maier, K., U. Hofmann, M. Reuss, and K. Mauch. 2010. Dynamics and control of the central carbon metabolism in hepatoma cells. *BMC systems biology*. 4:54.

Malaisse, W.J., A. Herchuelz, J. Levy, A. Sener, D.G. Pipeleers, G. Devis, G. Somers, and E.V. Obberghen. 1975. The stimulus-secretion coupling of glucose-induced insulin release XIX. The insulinotropic effect of glyceraldehyde. *Molecular and cellular endocrinology*. 4:1-12.

Margraf-Modersohn, D., P. Siegmund, and F. Korber. 1970. Hemmung der aeroben Glykolyse von Ascites-Tumor-Zellen durch Thiazolidine des L-glycerinaldehyds. *Naunyn-Schmiedebergs Archiv fur Pharmakologie*. 267:241-248.

Mashego, M.R., L. Wu, J.C. Van Dam, C. Ras, J.L. Vinke, W.A. Van Winden, W.M. Van Gulik, and J.J. Heijnen. 2004. MIRACLE: mass isotopomer ratio analysis of U-13C-labeled extracts. A new method for accurate quantification of changes in concentrations of intracellular metabolites. *Biotechnol Bioeng*. 85:620-628.

Mastrobuoni, G., S. Irgang, M. Pietzke, H.E. Assmus, M. Wenzel, W.X. Schulze, and S. Kempa. 2012. Proteome dynamics and early salt stress response of the photosynthetic organism Chlamydomonas reinhardtii. *BMC genomics*. 13:215.

Mendel, B. 1929. Krebszelle und Glycerinaldehyd. *Klin Wochenschr*. 8:169-170.

Mendel, B., F. Strelitz, and D. Mundell. 1938. L-Glyceric aldehyde and tumor metabolism. *Science*. 88:149-150.

Metallo, C.M., P.A. Gameiro, E.L. Bell, K.R. Mattaini, J. Yang, K. Hiller, C.M. Jewell, Z.R. Johnson, D.J. Irvine, L. Guarente, J.K. Kelleher, M.G. Vander Heiden, O. Iliopoulos, and G. Stephanopoulos. 2012. Reductive glutamine metabolism by IDH1 mediates lipogenesis under hypoxia. *Nature*. 481:380-384.

Meyerhof, O., K. Lohmann, and P. Schuster. 1936. Über die Aldolase, ein Kohlenstoff-verknüpfendes Ferment. II. Mitteilung: Aldolkondensation von Dioxyacetonphosphorsäure mit Glycerinaldehyd. *Biochem Z.* 286:319-335.

Millard, P., F. Letisse, S. Sokol, and J.C. Portais. 2012. IsoCor: correcting MS data in isotope labeling experiments. *Bioinformatics*. 28:1294-1296.

Moncada, S., E.A. Higgs, and S.L. Colombo. 2012. Fulfilling the metabolic requirements for cell proliferation. *The Biochemical journal*. 446:1-7.

Moseley, H.N. 2010. Correcting for the effects of natural abundance in stable isotope resolved metabolomics experiments involving ultra-high resolution mass spectrometry. *BMC bioinformatics*. 11:139.

Munger, J., B.D. Bennett, A. Parikh, X.J. Feng, J. McArdle, H.A. Rabitz, T. Shenk, and J.D. Rabinowitz. 2008. Systems-level metabolic flux profiling identifies fatty acid synthesis as a target for antiviral therapy. *Nat Biotechnol*. 26:1179-1186.

Murphy, T.A., C.V. Dang, and J.D. Young. 2013. Isotopically nonstationary 13C flux analysis of Myc-induced metabolic reprogramming in B-cells. *Metabolic engineering*. 15:206-217.

Nanchen, A., T. Fuhrer, and U. Sauer. 2007. Determination of metabolic flux ratios from 13C-experiments and gas chromatography-mass spectrometry data: protocol and principles. *Methods Mol Biol*. 358:177-197.

Needham, D.M., L. Siminovitch, and S.M. Rapkine. 1951. On the mechanism of the inhibition of glycolysis by glyceraldehyde. *Biochemical Journal*. 49:113-124.

Needham, J., and H. Lehmann. 1937. Intermediary carbohydrate metabolism in embryonic life: Glyceraldehyde and glucolysis. *The Biochemical journal*. 31:1913-1925.

Neubig, R.R., M. Spedding, T. Kenakin, and A. Christopoulos. 2003. International Union of Pharmacology Committee on Receptor Nomenclature and Drug Classification. XXXVIII. Update on terms and symbols in quantitative pharmacology. *Pharmacological reviews*. 55:597-606.

Nijsten, M.W., and G.M. van Dam. 2009. Hypothesis: using the Warburg effect against cancer by reducing glucose and providing lactate. *Medical hypotheses*. 73:48-51.

Noh, K., K. Gronke, B. Luo, R. Takors, M. Oldiges, and W. Wiechert. 2007. Metabolic flux analysis at ultra short time scale: isotopically non-stationary 13C labeling experiments. *J Biotechnol*. 129:249-267.

Noh, K., and W. Wiechert. 2011. The benefits of being transient: isotope-based metabolic flux analysis at the short time scale. *Applied microbiology and biotechnology*. 91:1247-1265.

Olsen, J.V., M. Vermeulen, A. Santamaria, C. Kumar, M.L. Miller, L.J. Jensen, F. Gnad, J. Cox, T.S. Jensen, E.A. Nigg, S. Brunak, and M. Mann. 2010. Quantitative phosphoproteomics reveals widespread full phosphorylation site occupancy during mitosis. *Science signaling*. 3:ra3.

Ong, S.E., B. Blagoev, I. Kratchmarova, D.B. Kristensen, H. Steen, A. Pandey, and M. Mann. 2002. Stable isotope labeling by amino acids in cell culture, SILAC, as a simple and accurate approach to expression proteomics. *Molecular & cellular proteomics : MCP*. 1:376-386.

Patterson, B.W., and R.R. Wolfe. 1993. Concentration dependence of methyl palmitate isotope ratios by electron impact ionization gas chromatography/mass spectrometry. *Biological mass spectrometry*. 22:481-486.

Pedersen, P.L. 2007. Warburg, me and Hexokinase 2: Multiple discoveries of key molecular events underlying one of cancers' most common phenotypes, the "Warburg Effect", i.e., elevated glycolysis in the presence of oxygen. *J Bioenerg Biomembr*. 39:211-222.

Pelicano, H., D.S. Martin, R.H. Xu, and P. Huang. 2006. Glycolysis inhibition for anticancer treatment. *Oncogene*. 25:4633-4646.

Pereira da Silva, A.P., T. El-Bacha, N. Kyaw, R.S. dos Santos, W.S. da-Silva, F.C. Almeida, A.T. Da Poian, and A. Galina. 2009. Inhibition of energy-producing pathways of HepG2 cells by 3-bromopyruvate. *The Biochemical journal*. 417:717-726.

Perz, J.F., G.L. Armstrong, L.A. Farrington, Y.J. Hutin, and B.P. Bell. 2006. The contributions of hepatitis B virus and hepatitis C virus infections to cirrhosis and primary liver cancer worldwide. *Journal of hepatology*. 45:529-538.

Raushel, F.M., and W.W. Cleland. 1977. Bovine liver fructokinase: purification and kinetic properties. *Biochemistry*. 16:2169-2175.

Roessner-Tunali, U., B. Hegemann, A. Lytovchenko, F. Carrari, C. Bruedigam, D. Granot, and A.R. Fernie. 2003. Metabolic profiling of transgenic tomato plants overexpressing hexokinase reveals that the influence of hexose phosphorylation diminishes during fruit development. *Plant Physiol*. 133:84-99.

Saeed, A.I., V. Sharov, J. White, J. Li, W. Liang, N. Bhagabati, J. Braisted, M. Klapa, T. Currier, M. Thiagarajan, A. Sturn, M. Snuffin, A. Rezantsev, D. Popov, A. Ryltsov, E. Kostukovich, I. Borisovsky, Z. Liu, A. Vinsavich, V. Trush, and J. Quackenbush. 2003. TM4: a free, open-source system for microarray data management and analysis. *Biotechniques*. 34:374-378.

Sauermann, G. 1967. Der Einfluss von 2-Deoxy-D-Glucose auf die Glucoseoxydation in Ascites-Tumor-Zellen. *Z Krebsforsch*. 69:44-50.

Schauder, P., B. Schindler, U. Panten, J.C. Brown, H. Frerichs, and W. Creutzfeldt. 1977. Insulin release from isolated rat pancreatic islets induced by alpha-ketoisocapronic acid, L-leucine, D-glucose or D-glyceraldehyde: effect of gastric inhibitory polypeptide or glucagon. *Molecular and cellular endocrinology*. 7:115-123.

Schramm, T. 1965. Modellversuche zu Fragen einer Tumortherapie durch Glyzerinaldehyd. *Acta biologica et medica Germanica*. 15:343-347.

Schwanhausser, B., D. Busse, N. Li, G. Dittmar, J. Schuchhardt, J. Wolf, W. Chen, and M. Selbach. 2011. Global quantification of mammalian gene expression control. *Nature*. 473:337-342.

Schwanhausser, B., M. Gossen, G. Dittmar, and M. Selbach. 2009. Global analysis of cellular protein translation by pulsed SILAC. *Proteomics*. 9:205-209.

Sillero, M.A., A. Sillero, and A. Sols. 1969. Enzymes involved in fructose metabolism in liver and the glyceraldehyde metabolic crossroads. *European journal of biochemistry / FEBS*. 10:345-350.

Sols, A., and R.K. Crane. 1954. Substrate specificity of brain hexokinase. *The Journal of biological chemistry*. 210:581-595.

Stickland, L.H. 1941. The inhibition of glucolysis by glyceraldehyde. *The Biochemical journal*. 35:859-871.

Szecowka, M., R. Heise, T. Tohge, A. Nunes-Nesi, D. Vosloh, J. Huege, R. Feil, J. Lunn, Z. Nikoloski, M. Stitt, A.R. Fernie, and S. Arrivault. 2013. Metabolic fluxes in an illuminated Arabidopsis rosette. *The Plant cell*. 25:694-714.

Tannock, I.F., P. Guttman, and A.M. Rauth. 1983. Failure of 2-deoxy-D-glucose and 5-thio-D-glucose to kill hypoxic cells of two murine tumors. *Cancer research*. 43:980-983.

Tennant, D.A., R.V. Duran, and E. Gottlieb. 2010. Targeting metabolic transformation for cancer therapy. *Nat Rev Cancer*. 10:267-277.

Thiele, I., N. Swainston, R.M. Fleming, A. Hoppe, S. Sahoo, M.K. Aurich, H. Haraldsdottir, M.L. Mo, O. Rolfsson, M.D. Stobbe, S.G. Thorleifsson, R. Agren, C. Bolling, S. Bordel, A.K. Chavali, P. Dobson, W.B. Dunn, L. Endler, D. Hala, M. Hucka, D. Hull, D. Jameson, N. Jamshidi, J.J. Jonsson, N. Juty, S. Keating, I. Nookaew, N. Le Novere, N. Malys, A. Mazein, J.A. Papin, N.D. Price, E. Selkov, Sr., M.I. Sigurdsson, E. Simeonidis, N. Sonnenschein, K. Smallbone, A. Sorokin, J.H. van Beek, D. Weichart, I. Goryanin, J. Nielsen, H.V. Westerhoff, D.B. Kell, P. Mendes, and B.O. Palsson. 2013. A community-driven global reconstruction of human metabolism. *Nat Biotechnol*. 31:419-425.

Vali, M., J.A. Vossen, M. Buijs, J.M. Engles, E. Liapi, V.P. Ventura, A. Khwaja, O. Acha-Ngwodo, G. Shanmugasundaram, L. Syed, R.L. Wahl, and J.F. Geschwind. 2008. Targeting of VX2 rabbit liver tumor by selective delivery of 3-bromopyruvate: a biodistribution and survival study. *The Journal of pharmacology and experimental therapeutics*. 327:32-37.

van der Werf, M.J., K.M. Overkamp, B. Muilwijk, L. Coulier, and T. Hankemeier. 2007. Microbial metabolomics: toward a platform with full metabolome coverage. *Analytical biochemistry*. 370:17-25.

Van Heyningen, R. 1969. The metabolism of D-glyceraldehyde by the lens. *The Biochemical journal*. 112:211-220.

van Winden, W., P. Verheijen, and S. Heijnen. 2001. Possible pitfalls of flux calculations based on (13)C-labeling. *Metabolic engineering*. 3:151-162.

van Winden, W.A., C. Wittmann, E. Heinzle, and J.J. Heijnen. 2002. Correcting mass isotopomer distributions for naturally occurring isotopes. *Biotechnol Bioeng*. 80:477-479.

Vermeulen, K., D.R. Van Bockstaele, and Z.N. Berneman. 2003. The cell cycle: a review of regulation, deregulation and therapeutic targets in cancer. *Cell proliferation*. 36:131-149.

Wang, J., D. Duncan, Z. Shi, and B. Zhang. 2013. WEB-based GEne SeT AnaLysis Toolkit (WebGestalt): update 2013. *Nucleic Acids Res*. 41:W77-83.

Warburg, O. 1956. On the origin of cancer cells. *Science*. 123:309-314.

Warburg, O., K. Gawehn, W. Geissler A, and S. Lorenz. 1963. Über Heilung von Mäuse-Ascites-Krebs durch D- und L-Glycerinaldehyd. *In* Clinical Chemistry and Laboratory Medicine. Vol. 1. 175.

Watson, P.A., H.H. Hanauske-Abel, A. Flint, and M. Lalande. 1991. Mimosine reversibly arrests cell cycle progression at the G1-S phase border. *Cytometry*. 12:242-246.

Weckwerth, W. 2003. Metabolomics in systems biology. *Annual review of plant biology*. 54:669-689.

Wick, A.N., D.R. Drury, and T.N. Morita. 1955. 2-Deoxyglucose; a metabolic block for glucose. *Proc Soc Exp Biol Med*. 89:579-582.

Wick, A.N., D.R. Drury, H.I. Nakada, and J.B. Wolfe. 1957. Localization of the primary metabolic block produced by 2-deoxyglucose. *The Journal of biological chemistry*. 224:963-969.

Wiechert, W. 2001. 13C metabolic flux analysis. *Metabolic engineering*. 3:195-206.

Wiechert, W., and K. Noh. 2013. Isotopically non-stationary metabolic flux analysis: complex yet highly informative. *Curr Opin Biotechnol*. 24:979-986.

Wienkoop, S., J. Weiss, P. May, S. Kempa, S. Irgang, L. Recuenco-Munoz, M. Pietzke, T. Schwemmer, J. Rupprecht, V. Egelhofer, and W. Weckwerth. 2010. Targeted proteomics for Chlamydomonas reinhardtii combined with rapid subcellular protein fractionation, metabolomics and metabolic flux analyses. *Molecular bioSystems*. 6:1018-1031.

Wise, D.R., P.S. Ward, J.E. Shay, J.R. Cross, J.J. Gruber, U.M. Sachdeva, J.M. Platt, R.G. DeMatteo, M.C. Simon, and C.B. Thompson. 2011. Hypoxia promotes isocitrate dehydrogenase-dependent carboxylation of alpha-ketoglutarate to citrate to support cell growth and viability. *Proc Natl Acad Sci U S A*. 108:19611-19616.

Wishart, D.S., C. Knox, A.C. Guo, R. Eisner, N. Young, B. Gautam, D.D. Hau, N. Psychogios, E. Dong, S. Bouatra, R. Mandal, I. Sinelnikov, J. Xia, L. Jia, J.A. Cruz, E. Lim, C.A. Sobsey, S. Shrivastava, P. Huang, P. Liu, L. Fang, J. Peng, R. Fradette, D. Cheng, D. Tzur, M. Clements, A. Lewis, A. De Souza, A. Zuniga, M. Dawe, Y. Xiong, D. Clive, R. Greiner, A. Nazyrova, R. Shaykhutdinov, L. Li, H.J. Vogel, and I. Forsythe. 2009. HMDB: a knowledgebase for the human metabolome. *Nucleic Acids Res*. 37:D603-610.

Wittmann, C., and E. Heinzle. 1999. Mass spectrometry for metabolic flux analysis. *Biotechnol Bioeng*. 62:739-750.

Woodward, G.E., and M.T. Hudson. 1955. Phosphorylation of 2-deoxy-D-glucose by yeast hexokinase: Competition between 2-deoxy-d-glucose and glucose. *Journal of the Franklin Institute*. 259:543-547.

Xi, H., M. Kurtoglu, H. Liu, M. Wangpaichitr, M. You, X. Liu, N. Savaraj, and T.J. Lampidis. 2011. 2-Deoxy-D-glucose activates autophagy via endoplasmic reticulum stress rather than ATP depletion. *Cancer chemotherapy and pharmacology*. 67:899-910.

Xu, R.H., H. Pelicano, H. Zhang, F.J. Giles, M.J. Keating, and P. Huang. 2005a. Synergistic effect of targeting mTOR by rapamycin and depleting ATP by inhibition of glycolysis in lymphoma and leukemia cells. *Leukemia*. 19:2153-2158.

Xu, R.H., H. Pelicano, Y. Zhou, J.S. Carew, L. Feng, K.N. Bhalla, M.J. Keating, and P. Huang. 2005b. Inhibition of glycolysis in cancer cells: a novel strategy to overcome drug resistance associated with mitochondrial respiratory defect and hypoxia. *Cancer research*. 65:613-621.

Zamboni, N. 2011. 13C metabolic flux analysis in complex systems. *Curr Opin Biotechnol*. 22:103-108.

Zamboni, N., S.M. Fendt, M. Ruhl, and U. Sauer. 2009. (13)C-based metabolic flux analysis. *Nat Protoc*. 4:878-892.

Zamboni, N., E. Fischer, and U. Sauer. 2005. FiatFlux--a software for metabolic flux analysis from 13C-glucose experiments. *BMC bioinformatics*. 6:209.

Zecchin, K.G., F.A. Rossato, H.F. Raposo, D.R. Melo, L.C. Alberici, H.C. Oliveira, R.F. Castilho, R.D. Coletta, A.E. Vercesi, and E. Graner. 2011. Inhibition of fatty acid synthase in melanoma cells activates the intrinsic pathway of apoptosis. *Laboratory investigation; a journal of technical methods and pathology*. 91:232-240.

Zhang, B., S. Kirov, and J. Snoddy. 2005. WebGestalt: an integrated system for exploring gene sets in various biological contexts. *Nucleic Acids Res*. 33:W741-748.

Zhang, X.D., E. Deslandes, M. Villedieu, L. Poulain, M. Duval, P. Gauduchon, L. Schwartz, and P. Icard. 2006. Effect of 2-deoxy-D-glucose on various malignant cell lines in vitro. *Anticancer research*. 26:3561-3566.

Zwingmann, C., C. Richter-Landsberg, and D. Leibfritz. 2001. 13C isotopomer analysis of glucose and alanine metabolism reveals cytosolic pyruvate compartmentation as part of energy metabolism in astrocytes. *Glia*. 34:200-212.

7. PUBLICATIONS

Proteome dynamics and early salt stress response of the photosynthetic organism Chlamydomonas reinhardtii. Mastrobuoni G*, Irgang S*, Pietzke M*, Assmus HE, Wenzel M, Schulze WX, Kempa S. (*contributed equally)

BMC Genomics. 2012 May 31;13:215.

- In this article the first basic correction strategy for label incorporation was applied. With this we could show that arginine given to an auxotrophic *Chlamydomonas* mutant was intensively transformed to proline and putrescine under salt stress conditions.

Pulsed stable isotope resolved metabolomic studies of cancer cells

Matthias Pietzke & Stefan Kempa

Methods in Enzymology. - ***Oncometabolism,*** edited by **Lorenzo Galluzzi and Guido Kramer**

- In this review-like article the concept and possible applications of stable isotope resolved metabolomics are presented; parts of this were used in the introduction.

Decoding the dynamics of cellular metabolism and the action of 3-bromopyruvate and 2 -deoxyglucose using pSIRM Pietzke M*, Zasada C*, Mudrich S, Kempa S (*contributed equally)

Cancer & Metabolism – resubmitted after revision

- Here the majority of the validation experiments, from section 1 and the application of the pSIRM approach towards the understanding of inhibitory action of 2DG and BrPyr is reported.

8. APPENDIX

Suppl. table 1 - putative metabolites identified in the first round of characterization of HEK293-cell extract sample with their GMD-ID and retention index. Additional abbreviations used: NA=unknowns listed in GMD, MP=main peak, BP=bypeak

No.	compound	RI	No.	compound	RI
1	Pyruvic acid (1MEOX) (1TMS)	1041	61	Dihydroxyacetone phosphate (1MEOX) (3TMS) MP	1741
2	Lactic acid, DL- (2TMS)	1049	62	Ornithine (3TMS)	1750
3	Valine (1TMS)	1082	63	Dihydroxyacetone phosphate (1MEOX) (3TMS) BP	1751
4	Alanine (2TMS)	1093	64	Glycerol-3-phosphate (4TMS)	1756
5	Hydroxylamine (3TMS)	1103	65	Glucopyranose [-H20] (4TMS)	1762
6	Glycine (2TMS)	1113	66	Ethanolaminephosphate (4TMS)	1776
7	Leucine (1TMS)	1151	67	Glutamic acid, N-acetyl- (2TMS)	1781
8	Hexanoic acid, 2-ethyl- (1TMS)	1158	68	Glyceric acid-3-phosphate (4TMS)	1797
9	Butanoic acid, 2-amino- (2TMS)	1165	69	Citric acid (4TMS)	1809
10	Proline (1TMS)	1173	70	Lysine (3TMS)	1847
11	Isoleucine (1TMS)	1174	71	Fructose MP	1859
12	Valine (2TMS)	1212	72	Fructose BP	1869
13	NA_1235.67_PRED	1247	73	Lysine (4TMS)	1913
14	Benzoic acid, (1TMS)	1254	74	13-C-Sorbitol (InternalStandard)	1922
15	Serine (2TMS)	1263	75	NA_1946.58_PRED	1949
16	Alanine, N-acetyl-, DL- (1TMS)	1268	76	Gulonic acid (6TMS)	1951
17	Ethanolamine (3TMS)_1261.63	1270	77	Glucopyranose, D- (5TMS)	1970
18	Leucine (2TMS)	1277	78	NA_1963.46_PRED	1972
19	Glycerol (3TMS)	1277	79	Pantothenic acid, D- (3TMS)	1987
20	Isoleucine (2TMS)	1299	80	NA_2011.36_PRED (phosphate)	2015
21	Threonine, DL- (2TMS)	1302	81	NA_2013.82	2021
22	Proline (2TMS)	1304	82	Hexadecanoic acid (1TMS)	2047
23	Glycine (3TMS)	1313	83	Inositol, myo- (6TMS)	2081
24	Succinic acid (2TMS)	1324	84	NA_2097.8_PRED	2097
25	Uracil (2TMS)	1353	85	Ribose-5-phosphate (1 MEOX) (5TMS) MP	2098
26	Fumaric acid (2TMS)	1361	86	Ribose-5-phosphate (1 MEOX) (5TMS) BP	2102
27	Alanine (3TMS)	1366	87	Ribulose-5-phosphate (1MEOX) (5TMS) MP	2109
28	Serine (3TMS)	1368	88	Cystathionine (2TMS)	2116
29	Threonine (3TMS)	1392	89	Glycerophosphoglycerol (5TMS)	2179
30	Alanine [+CO2] (2TMS)	1409	90	Tryptophan (3TMS)	2203
31	Aspartic acid (2TMS)	1431	91	?unknown phosphate	2235
32	Alanine, beta- (3TMS)	1432	92	Octadecanoic acid (1TMS)	2245
33	Malic acid (3TMS)	1485	93	Fructose-1-phosphate (1MEOX) (6TMS) MP	2284
34	Nicotinamide (1TMS)	1486	94	Fructose-6-phosphate (1MEOX) (6TMS) MP	2298
35	Threitol (4TMS)	1493	95	Glucose-6-phosphate (1MEOX) (6TMS) MP	2311
36	Erythritol (4TMS)	1493	96	Glucose-6-phosphate (1MEOX) (6TMS) BP	2332
37	Serine, N-acetyl- (2TMS)	1503	97	NA_2361.81_PRED	2354
38	Pyroglutamic acid (1TMS)	1504	98	?unknown phosphate?	2378
39	Methionine (2TMS)	1516	99	?unknown (fatty acid?)	2406
40	Aspartic acid (3TMS)	1516	100	myo-Inositol-1-phosphate (7TMS)	2411
41	Pyroglutamic acid (2TMS)	1521	101	Eicosanoic acid (1TMS)	2453
42	Proline, 4-hydroxy-, trans- (3TMS)	1522	102	Uridine (3TMS)	2461
43	Butanoic acid, 4-amino- (3TMS)	1527	103	Kont: Phthalate	2556
44	Glutamic acid (2TMS)	1533	104	NA_2581.15_PRED	2594
45	Glutamine [-H2O] (2TMS) MP	1536	105	Adenosine (3TMS)	2603
46	Threonic acid (4TMS)	1538	106	? Unknown disaccarid	2624
47	Creatinine (3TMS)	1552	107	Sucrose (8TMS)	2627
48	Phenylalanine (1TMS)	1552	108	Lactose, alpha- (1MEOX) (8TMS) MP	2675
49	Cysteine (3TMS)	1554	109	Fructose-1,6-diphosphate (1MEOX) (7TMS) MP	2698
50	Glutaric acid, 2-hydroxy- (3TMS)	1575	110	Fructose-1,6-diphosphate (1MEOX) (7TMS) BP	2704
51	Glutaric acid, 2-oxo- (1MEOX) (2TMS) MP	1578	111	Maltose (1MEOX) (8TMS) MP	2721

52	Proline [+CO2] (2TMS)	1585	112	Maltose (1MEOX) (8TMS) BP	2746
53	Hypotaurine (3TMS)	1600	113	Isomaltose (1MEOX) (8TMS) MP	2850
54	Asparagine (2TMS)	1602	114	Uridine 5'-monophosphate (5TMS)	2879
55	Glutamic acid (3TMS)	1622	115	Guanosine-5-monophosphate (6TMS)	3060
56	Phenylalanine (2TMS)	1629	116	Cholesterol (1TMS)	3160
57	Asparagine (3TMS)	1671			
58	Ribitol (5TMS)	1714			
59	NA_1733.35_PRED (phosphate?)	1731			
60	Putrescine (4TMS)	1734			

Suppl. table 2 - Composition of the latest version of the Quant-Mix. The amount of each compound is given in pmol for the lowest calibration point (1:200 dilution) and the highest calibration point (1:1).

	amount in quant-mix (pmol)	
compound	**lowest**	**highest**
Lactic Acid	2231	446190
Glucose	1943	388544
Pyruvate	1454	290803
L-Threonine	839	167898
L-Glutamine	684	136855
L-Glutamic acid	680	135934
L-Alanine	673	134695
L-Serine	571	114188
L-Pyroglutamic acid	465	92937
L-Leucine	457	91484
D-Ribose 5-Phosphate	456	91208
Dihydroxyacetonephosphate	441	88183
Fructose	416	83259
meso-Erythritol	409	81887
Uridine 5′-monophosphate	407	81489
Glycine	333	66605
Glycerol	326	65154
Glyceraldehyde-3-P	323	64668
L-Proline	304	60801
Glutaric acid-2-hydroxy	286	57268
myo-Inositol	278	55506
Fructose-1,6-bisphosphate	271	54288
Citric acid	260	52051
L-Phenylalanine	242	48429
Malic acid	224	44746
Creatinine	221	44201
3-Phosphoglyceric acid	217	43478
L-Valine	213	42680
Succinic acid	212	42341
L-Isoleucine	191	38116
Fumaric acid	172	34462
α-Ketoglutaric acid	171	34223
D-Glucose 6-phosphate disodium salt hydrate	164	32884
Glutaric acid	151	30278
3-Hydroxybutyric acid	144	28818
Glycerol-3-P	135	26996
Uracil	134	26764
L-Asparagine	114	22707
L-Lysine	103	20531
GMP	101	20113
Ribose	100	19983
Adenosine	94	18709
Hypotaurine	92	18323
D-Pantothenic acid	84	16788
D-Glyceric acid	80	15987
Phosphoenolpyruvic acid	75	15036
L-Aspartic acid	75	15025
6-P-Gluconate	73	14616
Fructose-6-P	66	13154
a-D-Glucose 1-phosphate	59	11894
L-Arginine	57	11481
β-Alanine	56	11225
Inosine	56	11184
L-Tyrosine	55	11038
L-Tryptophan	49	9793
γ-Aminobutyric acid	48	9697

Cytosine	45	9001
L-Cysteine	41	8254
2-deoxy-D-ribose	37	7455
Adenine	37	7400
L-Methionine	34	6702
Putrescine	31	6208
Glucosamine	23	4638

Suppl. table 3 - Composition of the latest version of the Ident-Mix. Every compound is present in exactly two different ident-mixtures, a "X" denotes if the compound is present in the given one. Similar compounds with similar retention behavior are present in different composition pattern.

	present in ident-mix:			
compound	A	B	C	D
2-Aminobutyric acid			X	X
2-Deoxy-D-ribose	X			X
2-Deoxy-Glucose			X	X
2-Hydroxyglutaric acid	X			X
3-Hydroxybutyric acid	X	X		
3-Phosphoglyceric acid		X		X
6-Phosphogluconic acid	X			X
Adenine			X	X
Adenosine	X	X		
a-D-Glucose 1-phosphate			X	X
Arabitol			X	X
beta-Hydroxypyruvic acid		X		X
cis-Aconitic acid	X			X
Citric acid		X		X
Creatinine		X	X	
Cytosine	X	X		
D-Erythrose 4-phosphate	X			X
D-Fructose 1,6-bisphosphate		X	X	
D-Fructose 6-phosphate	X		X	
D-Galacturonic acid		X		X
D-Gluconic acid		X	X	
D-Glucose 6-phosphate	X	X		
D-Glucuronic acid	X		X	
D-Glyceric acid	X	X		
Dihydroxacetone phosphate	X	X		
DL-3-Aminoisobutyric acid		X	X	
D-Lactose		X		X
DL-Glyceraldehyde 3-phosphate			X	X
DL-Homocysteine	X		X	
D-Pantothenic acid	X			X
D-Ribose 5-Phosphate			X	X
D-Ribulose 5-phosphate	X	X		
Fructose		X	X	
Fructose 1-phosphate		X		X
Fumaric acid	X		X	
Galactitol		X	X	
Galactosamine			X	X
Galactose	X		X	
Glucosamine	X	X		
Glucose		X		X
Glutaric acid	X	X		
Glycerol			X	X
Glycerol-3-P		X	X	
Glycine	X		X	
Hypotaurine	X		X	
Hypoxanthine		X		X
Inosine			X	X
Isocitric acid	X		X	
Lactic Acid		X	X	
L-Alanine		X	X	
L-Arginine	X		X	
L-Asparagine		X		X
L-Aspartic acid	X		X	
L-Cystathionine	X			X
L-Cysteine		X		X
L-Glutamic acid	X	X		
L-Glutamine			X	X

L-Isoleucine	X			X
L-Leucine		X	X	
L-Lysine	X		X	
L-Methionine			X	X
L-Phenylalanine		X	X	
L-Proline	X	X		
L-Pyroglutamic acid	X			X
L-Serine			X	X
L-Threonine			X	X
L-Tryptophan		X	X	
L-Tyrosine		X		X
L-Valine		X		X
Maleic acid		X	X	
Malic acid		X		X
Maltose			X	X
Mannose	X			X
meso-Erythritol	X	X		
myo-Inositol			X	X
N-Acetyl-Galactcosamine		X		X
N-Acetyl-Glucosamine	X		X	
N-Acetyl-L-glutamic acid		X	X	
Ornithine		X		X
Phosphoenolpyruvic acid	X			X
Putrescine	X			X
Pyruvic acid	X			X
Ribitol	X	X		
Ribose		X		X
Sorbitol	X			X
Spermidine	X		X	
Spermine		X		X
Succinic acid	X			X
Sucrose	X		X	
Taurine		X		X
Thymine		X		X
Trehalose, a-a	X	X		
Uracil	X		X	
Urea	X		X	
Uric acid	X	X		
Uridine	X			X
Uridine 5′-monophosphate		X	X	
Xylose	X		X	
α-Ketoglutaric acid		X	X	
β-Alanine	X			X
γ-Aminobutyric acid	X		X	

Suppl. table 4 - Concentrations of metabolites in T98G cells, grown at 2.5 g/l glucose. Averages and standard deviations were calculated for six technical replicates.

	Quantity in (pmol / 10^6 cells)		
Compound	Average ± STDEV		
Adenine	77	±	15
Alanine	841	±	89
Alanine, beta-	623	±	122
Asparagine	202	±	15
Aspartic acid	251	±	22
Butanoic acid, 2-amino	3,965	±	702
Butanoic acid, 3-hydroxy	51	±	7
Citric acid	327	±	17
Fructose	1,068	±	32
Fructose-1,6,diphosphate	773	±	45
Fructose-6-phosphate	48	±	5
Fumaric acid	135	±	6
Glucose-6-phosphate	532	±	27
Glutaric acid, 2-hydroxy	98	±	5
Glutaric acid, 2-oxo	235	±	6
Glyceric acid	30	±	2
Glyceric-acid-3-phosphate	133	±	7
Glycerol-3-phosphate	90	±	5
Glycine	2,332	±	135
Inositol, myo	1,203	±	20
Isoleucine	1,960	±	170
Lactic acid	9,873	±	1,269
Leucine	2,409	±	134
Lysine	1,512	±	238
Malic acid	547	±	22
Methionine	1,009	±	74
Pantothenic acid	142	±	3
Proline	892	±	56
Putrescine	36	±	1
Pyruvic acid	195	±	31
Ribose-5-phosphate	185	±	11
Serine	2,546	±	154
Succinic acid	30	±	8
Threonine	4,971	±	339
Tyrosine	1,101	±	173
Uracil	111	±	21
Uridine-5-monophosphate	8,410	±	615
Valine	333	±	17

Suppl. table 5 – Recovery of metabolites in Quant mix after addition of a complex biological samples.

Compound	Recovery (%)
Uracil	69.1
Fructose-6-phosphate	75.3
Glycine	84.8
Phenylalanine	86.7
Alanine, beta-	91.3
Alanine	92.1
Fumaric acid	102.2
Glucose-1/6-phosphate	102.7
Glyceric acid-3-phosphate	104.2
Lactic acid	104.2
Putrescine	104.5
Cinnamic acid, trans-	104.7
Leucine	106.6
Valine	106.8
Glutaric acid, 2-oxo-	107.0
Fructose	108.1
Butanoic acid, 3-hydroxy-	109.8
Fructose	110.6
Proline	110.8
Glycerol	111.9
Adenine	112.9
Hypotaurine	113.4
Inositol, myo-	115.9
Citric acid	116.4
Pyroglutamic acid	119.5
Glutaric acid	119.6
Serine	119.6
Erythritol	122.2
Glycerol-3-phosphate	122.5
Glutaric acid, 2-hydroxy-	124.1
Succinic acid	124.6
Glyceric acid	125.0
Ribose	125.6
Malic acid	126.9
Threonine	128.2
Cytosine	132.3
Pantothenic acid	135.1
Pyruvic acid	148.3
Average	111.2

Suppl. table 6 - Biological and technical variation of ^{13}C-glucose incorporation: T98G cells were incubated with u-^{13}C glucose for 3 minutes and harvest as well as label incorporation was calculated as described. T98G cells cultivated with ^{12}C-glucose were treated similar for the determination of natural ^{13}C-abundance (control). Italic values indicate theoretically impossible negative values caused by the calculation strategy and technical variances.

		Average (^{13}C-Glc incorporation in %) ± STDEV					
Compound	Mass	Control		Technical repl.		Biological repl.	
3PGA	357	-1.1	± 8.0	77.7	± 4.0	83.2	± 2.1
Ala	188	0.3	± 0.7	4.7	± 1.3	5.5	± 0.6
Cit	273	0.0	± 0.8	4.2	± 2.0	7.1	± 1.2
F16BP	217	0.0	± 1.9	78.8	± 1.0	79.7	± 0.7
Fru	217	0.0	± 0.5	10.7	± 0.7	7.7	± 0.7
F6P	217	0.3	± 3.3	84.0	± 4.8	83.2	± 4.0
Fum	245	0.0	± 0.8	0.9	± 0.7	0.6	± 0.2
G6P	217	0.0	± 1.0	74.6	± 0.5	74.3	± 0.4
Glut-OH	198	-1.5	± 3.0	3.2	± 2.4	1.5	± 1.6
Glycerol	205	0.0	± 3.8	-2.9	± 1.4	-1.9	± 1.2
Glyc3P	357	0.0	± 2.6	6.7	± 2.7	8.9	± 1.3
Gly	276	0.0	± 0.6	0.2	± 0.6	-0.1	± 0.3
Lac	219	0.0	± 3.2	17.9	± 0.4	18.4	± 2.7
Mal	245	0.0	± 0.8	0.7	± 0.7	0.2	± 1.1
Pyr	174	0.0	± 2.5	18.9	± 3.0	17.3	± 1.3
Suc	247	0.2	± 2.5	-1.5	± 2.3	1.0	± 1.2

Suppl. table 7 - Subtracting of multiple NOIs when label is present at multiple positions in a compound.

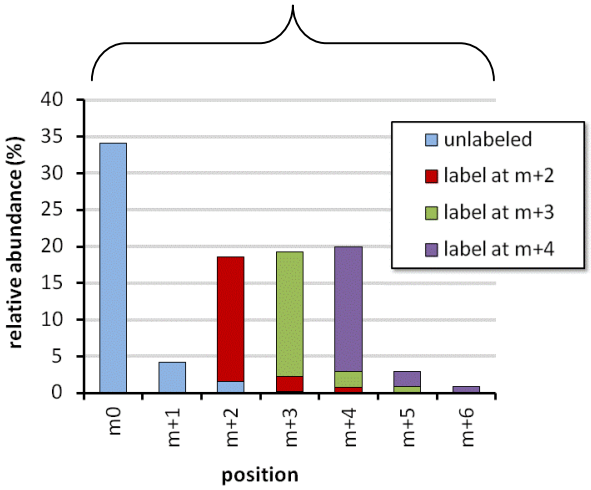

step	position		m0	m+1	m+2	m+3	m+4	m+5	m+6	sum of isotopologues with its NOIs
A	measured intensity		34,14	4,19	18,63	19,29	19,96	2,94	0,85	
B	unlabeled		**34,14**							40,03
C	calc. NOI from unlabeled			4,19	1,56	0,13	0,01	0	0	
D	label on m+1			**0**						0,0
	calc. NOI from m+1				0	0	0	0	0	
E	label on m+2				**17,07**					20,02
F	calc. NOI from m+2					2,10	0,78	0,06	0,01	
G	label on m+3					**17,07**				20,01
H	calc. NOI from m+3						2,10	0,78	0,06	
I	label on m+4						**17,07**			19,95
J	calc. NOI from m+4							2,10	0,78	
K	Residues		0,00	0,00	0,00	0,00	0,00	0,00	0,00	
	mass isotopomer distribution		34,14	0	17,07	17,07	17,07	0,00	0,00	
L	sum of isotopomers	85,35								100,0
M	total label (%)		40,0	0,0	20,0	20,0	20,0	0,0	0,0	

The measured intensity at all positions (A) is defined by the sum of "real" heavy isotopologues and natural occurring isotopes (NOIs). The m0 position represents the unlabeled state (B). With the use of an unlabeled reference the NOIs originating from the m0 mass were calculated (C) and subtracted from the measured intensity at the m+1 position, the remainder is the measured intensity of the m+1 isotopologue, which is in this case not present (D), therefore also the NOIs from m+1 are absent. The subtraction of C from A delivers the intensity of the m+2 isotopologue (E), which serves as starting point to calculate its NOIs (F). The same is repeated with m+3 and m+4 (G-J) until no residues are left (K). The isotopologues at every position sum up to 85.35% (L), dividing each intensity by this number gives the right amount of total incorporated label (M). The same result will be obtained by summing up the isotopologues with its NOIs (last column).

Suppl. table 8 – Selected enzymes of central carbon metabolism, and their H/L ratios after release from mimosine treatment.

protein	gene name	H/L ratio measured after release from block and growth in SILAC media												
		0h	2h	4h	6h	8h	10h	12h	14h	16h	18h	20h	22h	24h
Fatty acid desaturase 2	FADS2	0,32	0,36	1,11	2,17	3,09	4,43	4,56	4,35	3,04	4,16	4,52	5,56	3,54
Long-chain-fatty-acid--CoA ligase 4	ACSL4	0,15	0,15	0,22	0,27	0,47	0,64	0,92	1,00	1,08	1,35	1,70	1,50	1,78
Succinate dehydrogenase [ubiquinone] flavoprotein subunit, mitochondrial	SDHA	0,16	0,44	0,72	0,28	0,37	0,48	0,57	1,03	0,95	0,58	1,07	1,63	1,22
Isocitrate dehydrogenase [NAD] subunit beta, mitochondrial	IDH3B	0,19	0,12	0,16	0,30	0,36	0,52	0,67	0,70	0,76	0,97	1,20	1,35	1,46
Long-chain-fatty-acid--CoA ligase 1	ACSL1	0,28	0,57	0,17	0,32	0,30	0,28	0,44	0,59	0,58	NaN	0,96	2,31	1,12
Glutaminase kidney isoform, mitochondrial	GLS	0,16	0,15	0,19	0,22	0,35	0,48	0,57	0,58	0,73	0,87	1,03	1,10	1,01
Isopentenyl-diphosphate Delta-isomerase 1	IDI1	0,16	0,15	0,25	0,34	0,41	0,56	0,51	0,49	0,61	0,71	0,75	0,84	1,08
Mannose-1-phosphate guanyltransferase alpha	GMPPA	0,50	0,36	0,33	0,22	0,31	0,40	0,51	0,50	0,53	0,56	0,70	0,73	0,77
2-oxoglutarate and iron-dependent oxygenase domain-containing protein 1	OGFOD1	0,09	0,11	0,11	0,16	0,23	0,31	0,41	0,52	0,58	0,72	1,04	1,00	1,10
Mannose-6-phosphate isomerase	MPI	0,28	0,32	0,49	0,33	0,46	0,33	0,47	0,74	0,88	0,54	0,48	0,46	0,50
PDZ and LIM domain protein 2	PDLIM2	0,22	0,23	0,22	0,26	0,32	0,38	0,54	0,63	0,55	0,62	0,96	0,76	NaN
Aconitate hydratase, mitochondrial	ACO2	0,11	0,12	0,10	0,18	0,26	0,34	0,44	0,46	0,50	0,59	0,75	0,82	0,90
Acetoacetyl-CoA synthetase	AACS	0,23	0,22	0,18	0,27	0,29	0,30	0,40	0,43	0,47	0,41	0,76	0,65	0,82
Pyruvate dehydrogenase phosphatase regulatory subunit, mitochondrial	PDPR	0,23	0,14	0,24	0,32	0,43	0,52	0,47	0,48	0,41	0,61	0,49	0,64	NaN
Alanine aminotransferase 2	GPT2	0,16	0,14	0,24	0,25	0,44	0,44	0,51	0,53	0,42	NaN	0,55	0,60	0,68
2-oxoisovalerate dehydrogenase subunit alpha, mitochondrial	BCKDHA	0,21	0,22	0,28	0,29	0,30	0,49	0,38	0,59	0,41	NaN	0,54	NaN	0,77
2-oxoglutarate dehydrogenase, mitochondrial	OGDH	0,10	0,11	0,17	0,22	0,25	0,30	0,37	0,38	0,43	0,50	0,66	0,68	0,81
Long-chain-fatty-acid--CoA ligase 3	ACSL3	0,19	0,13	0,17	0,20	0,29	0,37	0,41	0,39	0,39	0,48	0,60	0,66	0,69
Cytoplasmic aconitate hydratase	ACO1	0,16	0,23	0,14	0,21	0,26	0,31	0,36	0,40	0,39	0,48	0,67	0,64	0,72
L-xylulose reductase	DCXR	0,14	NaN	0,20	0,16	0,33	0,18	NaN	NaN	0,42	0,42	0,29	0,34	0,27
Alpha-ketoglutarate-dependent dioxygenase FTO	FTO	0,18	0,17	0,12	0,19	0,25	0,29	0,31	0,39	0,36	0,54	0,57	0,62	0,70
Acetolactate synthase-like protein	ILVBL	0,18	0,23	0,19	0,27	0,26	0,27	0,37	0,44	0,38	NaN	0,48	0,50	0,61
Aldehyde dehydrogenase X, mitochondrial	ALDH1B1	0,24	0,20	0,21	0,21	0,22	0,27	0,30	0,32	0,38	0,41	0,60	0,49	0,64
6-phosphofructo-2-kinase/fructose-2,6-bisphosphatase 4	PFKFB4	0,21	0,21	0,30	0,32	0,36	0,49	NaN	0,36	NaN	0,40	0,43	NaN	NaN
Branched-chain-amino-acid aminotransferase, mitochondrial	BCAT2	0,10	0,13	0,17	0,26	0,24	0,31	0,40	0,37	0,39	0,31	0,46	0,51	0,63
Mannose-1-phosphate guanyltransferase beta	GMPPB	0,19	0,29	0,22	0,17	0,19	0,26	0,32	0,32	0,34	0,32	0,50	0,51	0,57
2-oxoisovalerate dehydrogenase subunit beta, mitochondrial	BCKDHB	0,15	0,17	0,12	0,27	0,25	0,29	0,33	0,33	0,35	0,45	0,43	0,43	0,61
Phosphoenolpyruvate carboxykinase [GTP], mitochondrial	PCK2	0,10	0,37	0,34	0,15	0,18	0,21	0,26	0,35	0,54	0,40	0,46	0,31	0,43
Phosphoglycerate kinase 1	PGK1	0,03	0,05	0,11	0,18	0,24	0,30	0,41	0,41	0,33	0,37	0,49	0,55	0,61
Glutamine--fructose-6-phosphate aminotransferase [isomerizing] 1	GFPT1	0,12	0,15	0,13	0,16	0,18	0,23	0,37	0,38	0,35	0,38	0,53	0,49	0,58

Suppl. table 8 - continued

protein	gene name	H/L ratio measured after release from block and growth in SILAC media												
		0h	2h	4h	6h	8h	10h	12h	14h	16h	18h	20h	22h	24h
Fructose-bisphosphate aldolase C	ALDOC	0,08	0,07	0,11	0,17	0,24	0,30	0,37	0,38	0,33	0,39	0,47	0,53	0,61
Phosphoglucomutase-2	PGM2	0,14	0,20	0,15	0,22	0,26	0,27	0,30	0,33	0,33	0,39	0,41	0,51	0,51
Hexokinase-2	HK2	0,11	0,16	0,19	0,23	0,25	0,25	0,32	0,33	0,35	0,35	0,49	0,55	0,46
Fructose-2,6-bisphosphatase TIGAR	TIGAR	0,13	0,07	0,12	0,14	0,17	0,21	0,26	0,32	0,38	0,46	0,55	0,57	0,61
NAD-dependent malic enzyme, mitochondrial	ME2	0,32	0,29	0,25	0,17	0,24	0,29	0,24	0,28	0,21	0,32	0,42	0,47	0,47
ATP-citrate synthase	ACLY	0,10	0,10	0,12	0,14	0,21	0,27	0,31	0,32	0,33	0,40	0,49	0,51	0,62
6-phosphofructokinase, muscle type	PFKM	0,13	NaN	0,29	0,34	0,20	0,26	0,25	0,27	0,31	0,29	0,33	0,36	0,49
Aldehyde dehydrogenase, mitochondrial	ALDH2	0,13	0,08	0,11	0,16	0,18	0,24	0,30	0,31	0,31	0,40	0,46	0,50	0,62
Fructose-bisphosphate aldolase A	ALDOA	0,05	0,03	0,10	0,15	0,21	0,28	0,35	0,37	0,31	0,36	0,44	0,51	0,60
Isocitrate dehydrogenase [NADP], mitochondrial	IDH2	0,08	0,05	0,08	0,14	0,20	0,27	0,32	0,33	0,32	0,40	0,43	0,50	0,59
Phosphomannomutase 2	PMM2	0,11	0,09	0,12	0,15	0,18	0,20	0,32	0,35	0,31	0,33	0,48	0,53	0,55
Pyruvate dehydrogenase E1 component subunit alpha, somatic form, mitochondrial	PDHA1	0,13	0,09	0,15	0,15	0,20	0,25	0,26	0,27	0,33	0,39	0,42	0,46	0,59
6-phosphofructokinase, liver type	PFKL	0,10	0,12	0,13	0,19	0,20	0,25	0,30	0,31	0,28	0,36	0,42	0,48	0,53
Aspartate aminotransferase, cytoplasmic	GOT1	0,09	0,09	0,11	0,14	0,17	0,20	0,28	0,29	0,27	0,35	0,48	0,58	0,59
Pyruvate carboxylase, mitochondrial	PC	0,11	0,14	0,15	0,21	0,22	0,28	0,27	0,31	0,31	0,42	0,36	0,41	0,45
Isocitrate dehydrogenase [NAD] subunit alpha, mitochondrial	IDH3A	0,19	0,20	0,16	0,18	0,14	0,19	0,23	0,25	0,27	0,36	0,44	0,47	0,51
L-lactate dehydrogenase A chain	LDHA	0,07	0,07	0,14	0,18	0,22	0,28	0,34	0,33	0,28	0,32	0,36	0,44	0,52
Aldose reductase	AKR1B1	0,06	0,07	0,04	0,07	0,09	0,15	0,23	0,31	0,26	0,35	0,67	0,54	0,60
Glyceraldehyde-3-phosphate dehydrogenase	GAPDH	0,04	0,04	0,09	0,13	0,18	0,24	0,31	0,33	0,30	0,35	0,43	0,44	0,54
Enolase-phosphatase E1	ENOPH1	0,19	0,16	0,16	0,18	0,18	0,26	0,26	0,23	0,24	NaN	0,37	0,43	0,45
Gamma-enolase	ENO2	0,11	0,10	0,17	0,23	0,25	0,26	0,30	0,30	0,25	0,28	0,35	0,34	0,39
Branched-chain-amino-acid aminotransferase, cytosolic	BCAT1	0,06	0,20	0,09	0,17	0,66	0,20	0,21	0,21	0,25	0,30	0,26	0,33	0,37
Phosphoglucomutase-1	PGM1	0,07	0,08	0,10	0,16	0,20	0,25	0,31	0,28	0,27	0,32	0,36	0,42	0,50
Hexokinase-1	HK1	0,11	0,09	0,10	0,14	0,18	0,22	0,27	0,27	0,29	0,34	0,39	0,42	0,51
Glucosidase 2 subunit beta	PRKCSH	0,05	0,09	0,09	0,11	0,16	0,20	0,27	0,28	0,28	0,33	0,43	0,46	0,54
Pyruvate kinase isozymes M1/M2	PKM	0,05	0,05	0,08	0,13	0,17	0,24	0,28	0,29	0,26	0,33	0,37	0,44	0,51
Triosephosphate isomerase	TPI1	0,02	0,03	0,08	0,13	0,18	0,22	0,30	0,29	0,26	0,33	0,37	0,45	0,54
Alpha-enolase	ENO1	0,13	0,11	0,12	0,17	0,19	0,22	0,27	0,27	0,25	0,29	0,36	0,37	0,43
Asparagine synthetase [glutamine-hydrolyzing]	ASNS	0,17	0,17	0,09	0,15	0,11	0,11	0,26	0,27	0,27	0,27	0,43	0,35	0,47
Ribose-phosphate pyrophosphokinase 1	PRPS1	0,15	0,09	0,08	0,13	0,15	0,18	0,24	0,24	0,27	0,32	0,41	0,37	0,47

Suppl. table 8 - continued

protein	gene name	H/L ratio measured after release from block and growth in SILAC media														
		0h	2h	4h	6h	8h	10h	12h	14h	16h	18h	20h	22h	24h		
Fatty acid synthase;[Acyl-carrier-protein] S-acetyltransferase	FASN	0,12	0,10	0,10	0,12	0,17	0,24	0,21	0,21	0,24	0,34	0,37	0,40	0,45		
Glucose-6-phosphate isomerase	GPI	0,03	0,03	0,08	0,12	0,17	0,22	0,31	0,31	0,23	0,27	0,39	0,40	0,47		
3-hydroxyisobutyrate dehydrogenase, mitochondrial	HIBADH	0,11	0,14	0,13	0,19	0,13	0,18	0,22	0,21	0,26	0,36	0,31	0,35	0,44		
Aspartyl/asparaginyl beta-hydroxylase	ASPH	0,09	0,07	0,09	0,12	0,15	0,18	0,25	0,25	0,24	0,33	0,39	0,40	0,45		
Malate dehydrogenase, cytoplasmic	MDH1	0,03	0,06	0,07	0,12	0,15	0,19	0,25	0,26	0,22	0,30	0,37	0,46	0,50		
Alcohol dehydrogenase [NADP(+)]	AKR1A1	0,08	0,12	0,09	0,14	0,14	0,17	0,23	0,24	0,22	0,33	0,38	0,35	0,43		
Pyruvate dehydrogenase E1 component subunit beta, mitochondrial	PDHB	0,10	0,10	0,11	0,13	0,13	0,18	0,21	0,23	0,26	0,31	0,35	0,37	0,44		
Glutamate dehydrogenase 1, mitochondrial;Glutamate dehydrogenase 2, mitochondrial	GLUD1; GLUD2	0,07	0,07	0,10	0,11	0,15	0,17	0,21	0,22	0,28	0,32	0,38	0,34	0,45		
Phosphoglycerate mutase 1	PGAM1	0,04	0,04	0,08	0,13	0,17	0,21	0,27	0,27	0,23	0,27	0,31	0,39	0,46		
Glycerol-3-phosphate dehydrogenase, mitochondrial	GPD2	0,14	0,12	0,15	0,17	0,17	0,19	0,22	0,21	0,22	0,27	0,28	0,34	0,37		
Alcohol dehydrogenase class-3	ADH5	0,13	0,07	0,12	0,13	0,14	0,16	0,23	0,23	0,19	0,27	0,33	0,38	0,44		
6-phosphofructokinase type C	PFKP	0,10	0,09	0,09	0,13	0,16	0,20	0,24	0,22	0,24	0,26	0,32	0,34	0,40		
Citrate synthase, mitochondrial	CS	0,11	0,09	0,10	0,11	0,14	0,17	0,20	0,23	0,23	0,29	0,31	0,34	0,45		
Malate dehydrogenase, mitochondrial	MDH2	0,04	0,04	0,04	0,08	0,11	0,15	0,22	0,23	0,24	0,30	0,38	0,38	0,47		
6-phosphogluconolactonase	PGLS	0,07	0,10	0,08	0,12	0,14	0,17	0,26	0,23	0,19	0,26	0,31	0,33	0,41		
Isocitrate dehydrogenase [NADP] cytoplasmic	IDH1	0,12	0,14	0,08	0,18	0,14	0,16	0,19	0,20	0,17	0,26	0,27	0,36	0,38		
Glyoxylate reductase/hydroxypyruvate reductase	GRHPR	0,15	0,10	0,09	0,15	0,16	0,14	0,18	0,20	0,19	0,27	0,28	0,35	0,32		
Aspartate aminotransferase, mitochondrial	GOT2	0,09	0,07	0,07	0,08	0,11	0,13	0,20	0,21	0,22	0,29	0,34	0,35	0,42		
Sorbitol dehydrogenase	SORD	0,16	0,12	0,10	0,13	0,12	0,14	0,15	0,14	0,23	0,22	0,24	0,27	0,30		
D-3-phosphoglycerate dehydrogenase	PHGDH	0,06	0,05	0,05	0,08	0,11	0,14	0,22	0,21	0,18	0,23	0,26	0,33	0,40		
L-lactate dehydrogenase B chain	LDHB	0,05	0,02	0,04	0,07	0,09	0,11	0,14	0,14	0,14	0,19	0,23	0,27	0,33		
6-phosphogluconate dehydrogenase, decarboxylating	PGD	0,06	0,06	0,06	0,06	0,08	0,10	0,14	0,14	0,14	0,19	0,25	0,26	0,29		
Transaldolase	TALDO1	0,02	0,02	0,03	0,05	0,07	0,09	0,14	0,14	0,14	0,21	0,26	0,28	0,32		
Aldo-keto reductase family 1 member C3	AKR1C3	0,07	0,06	0,06	0,09	0,08	0,09	0,13	0,17	0,11	0,17	0,15	0,24	0,25		
Glucose-6-phosphate 1-dehydrogenase	G6PD	0,05	0,04	0,03	0,04	0,06	0,08	0,12	0,12	0,11	0,17	0,20	0,22	0,25		
Aldo-keto reductase family 1 member C1	AKR1C1	0,03	0,05	0,03	0,04	0,05	0,07	0,11	0,11	0,11	0,18	0,17	0,23	0,25		
Transketolase	TKT	0,02	0,03	0,03	0,04	0,06	0,08	0,11	0,11	0,09	0,13	0,15	0,20	0,22		
Aldo-keto reductase family 1 member C2	AKR1C2	0,01	0,02	0,01	0,01	0,03	0,05	0,09	0,08	0,10	0,15	0,12	0,20	0,21		
Aldehyde dehydrogenase, dimeric NADP-preferring	ALDH3A1	0,06	0,04	0,06	0,06	0,05	0,07	0,07	0,08	0,07	0,13	0,09	0,12	0,14		
Aldo-keto reductase family 1 member B10	AKR1B10	0,05	0,06	0,05	0,05	0,06	0,03	0,05	0,05	0,06	0,09	0,10	0,11	0,12		

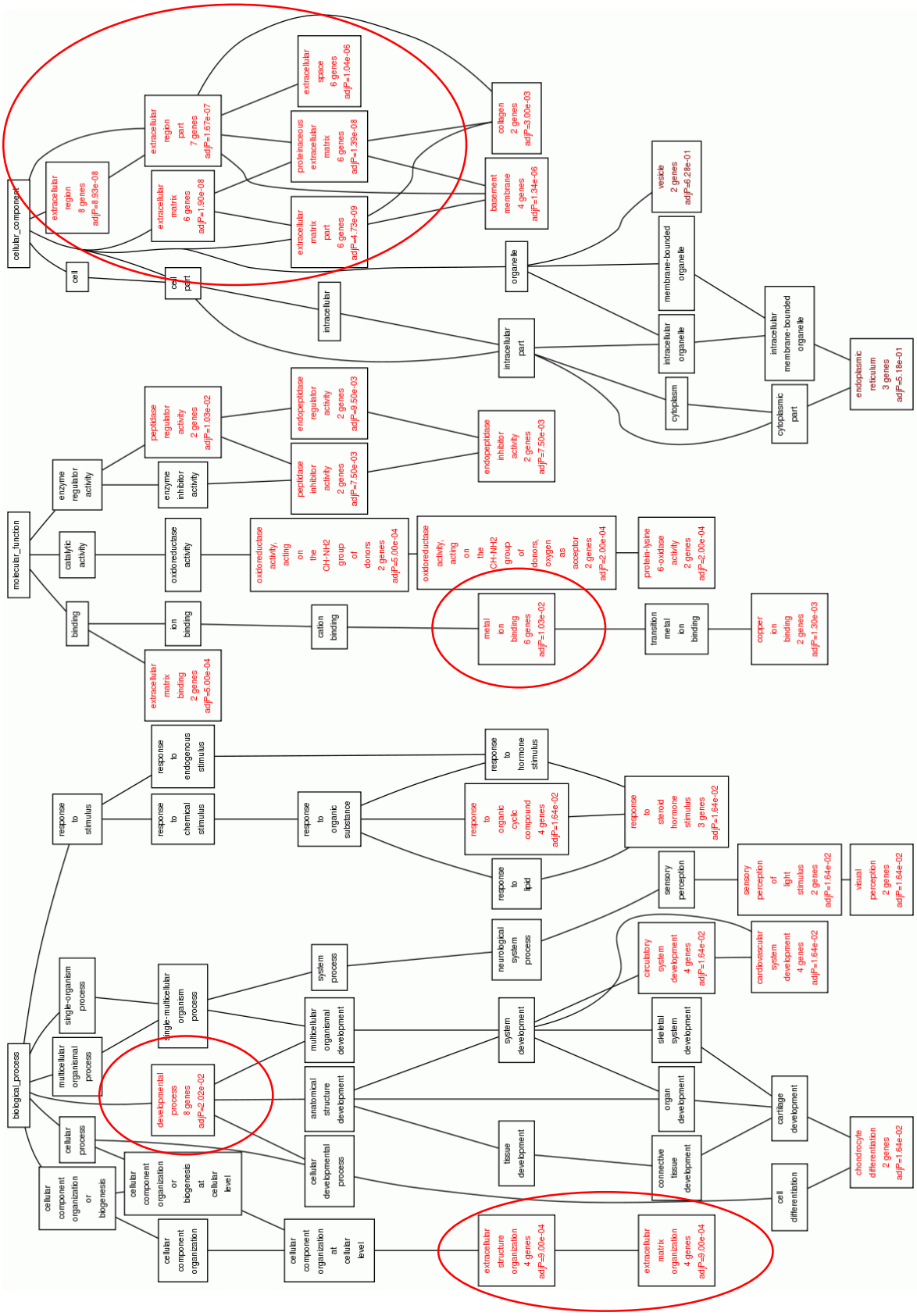

Suppl. Fig. 1 – GO enrichment of proteins found in Cluster 1 after clustering of mimosine-treated protein-samples and analysis with WebGestalt. Red entries indicate significant enrichment with an $p<0.05$.

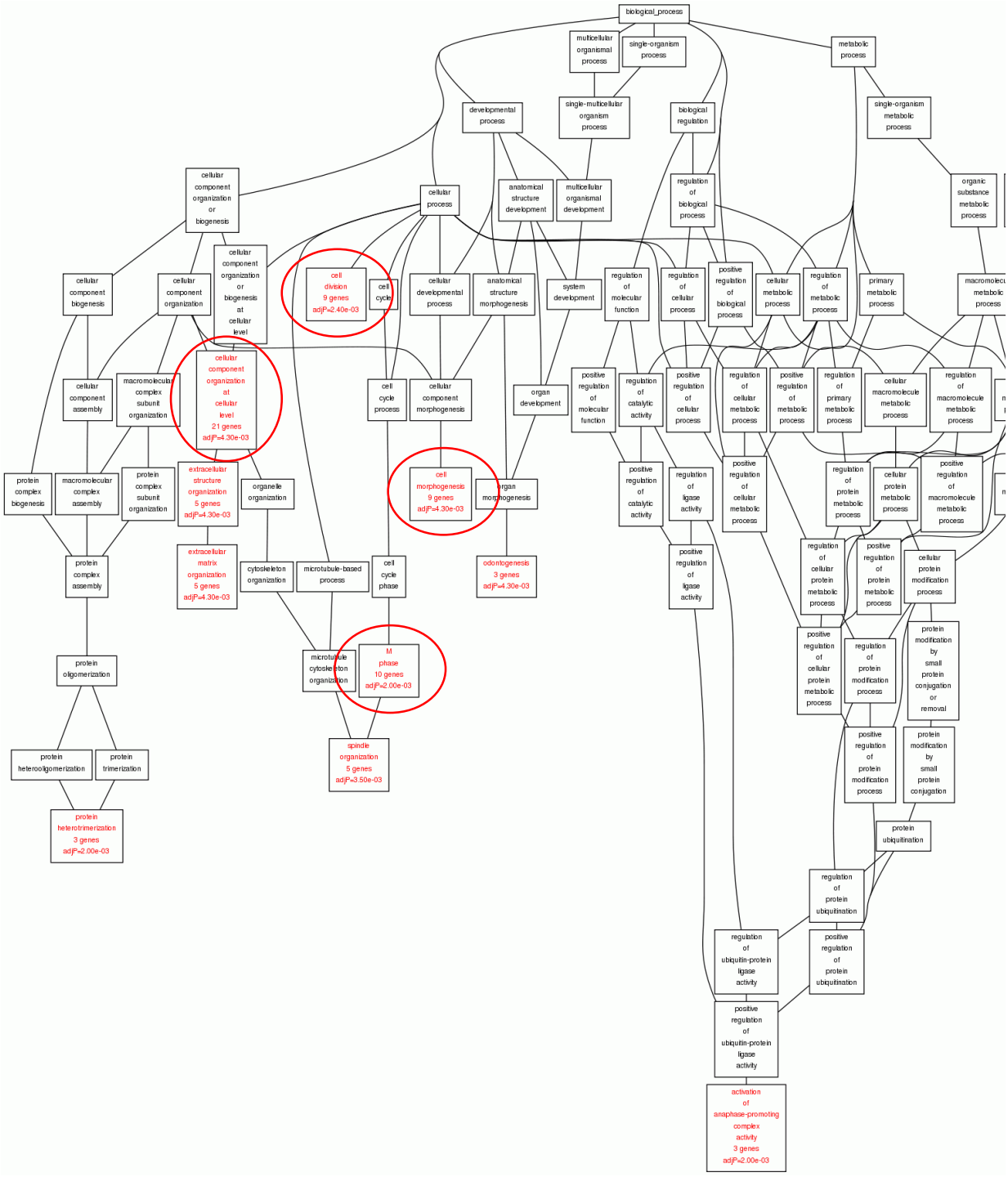

Suppl. Fig. 2A - GO enrichment of proteins found in Cluster 2 after clustering of mimosine-treated protein-samples and analysis with WebGestalt – Part 1. GO categories in the top 10 that also have a p value < 0.05 are colored red. GO categories in the top 10 that have a p value > 0.05 are colored brown, and the black ones are the parents of the top 10 categories.

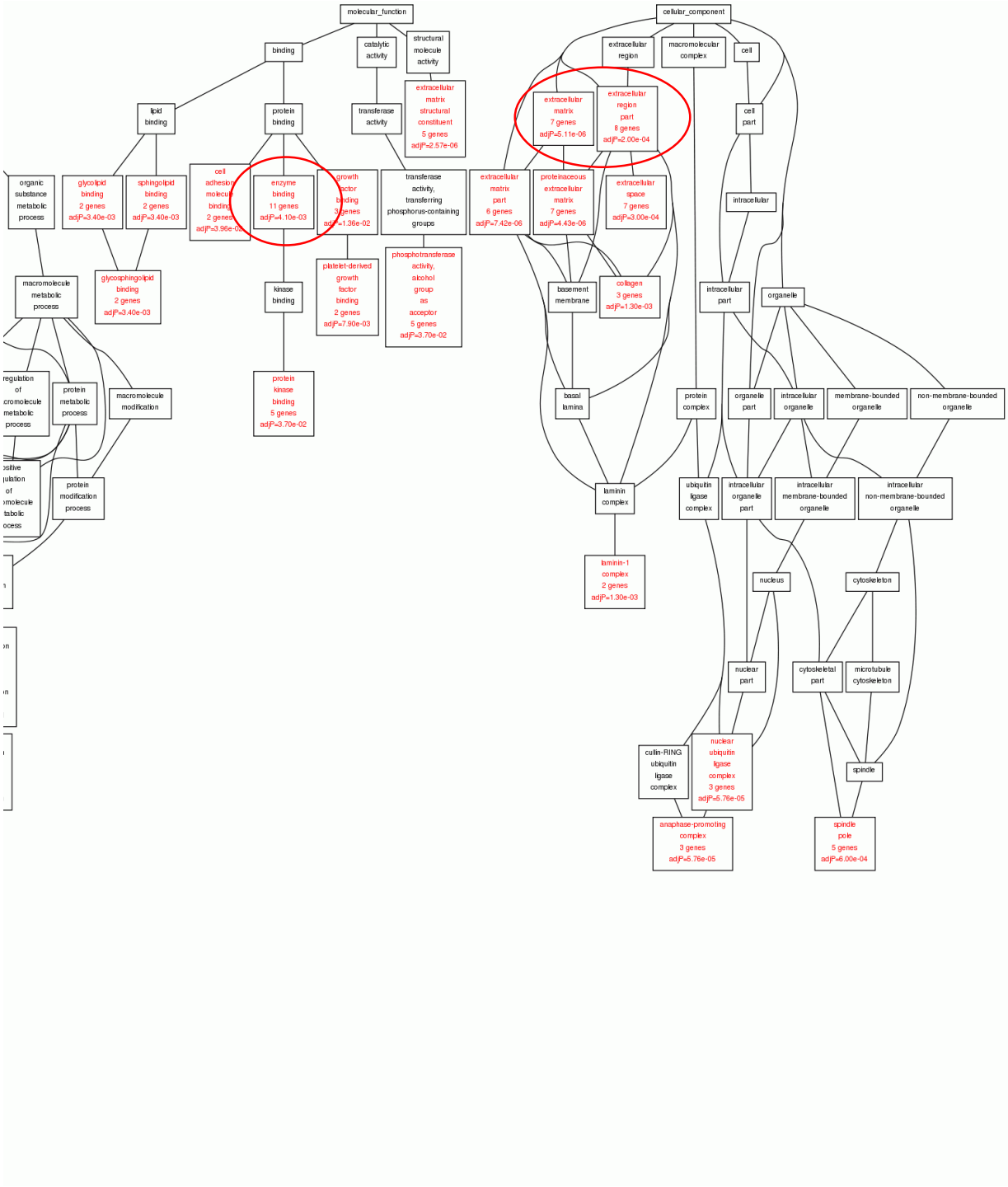

Suppl. Fig. 3 - GO enrichment of proteins found in Cluster 2 after clustering of mimosine-treated protein-samples and analysis with WebGestalt – Part 2. GO categories in the top 10 that also have a p value < 0.05 are colored red. GO categories in the top 10 that have a p value > 0.05 are colored brown, and the black ones are the parents of the top 10 categories.

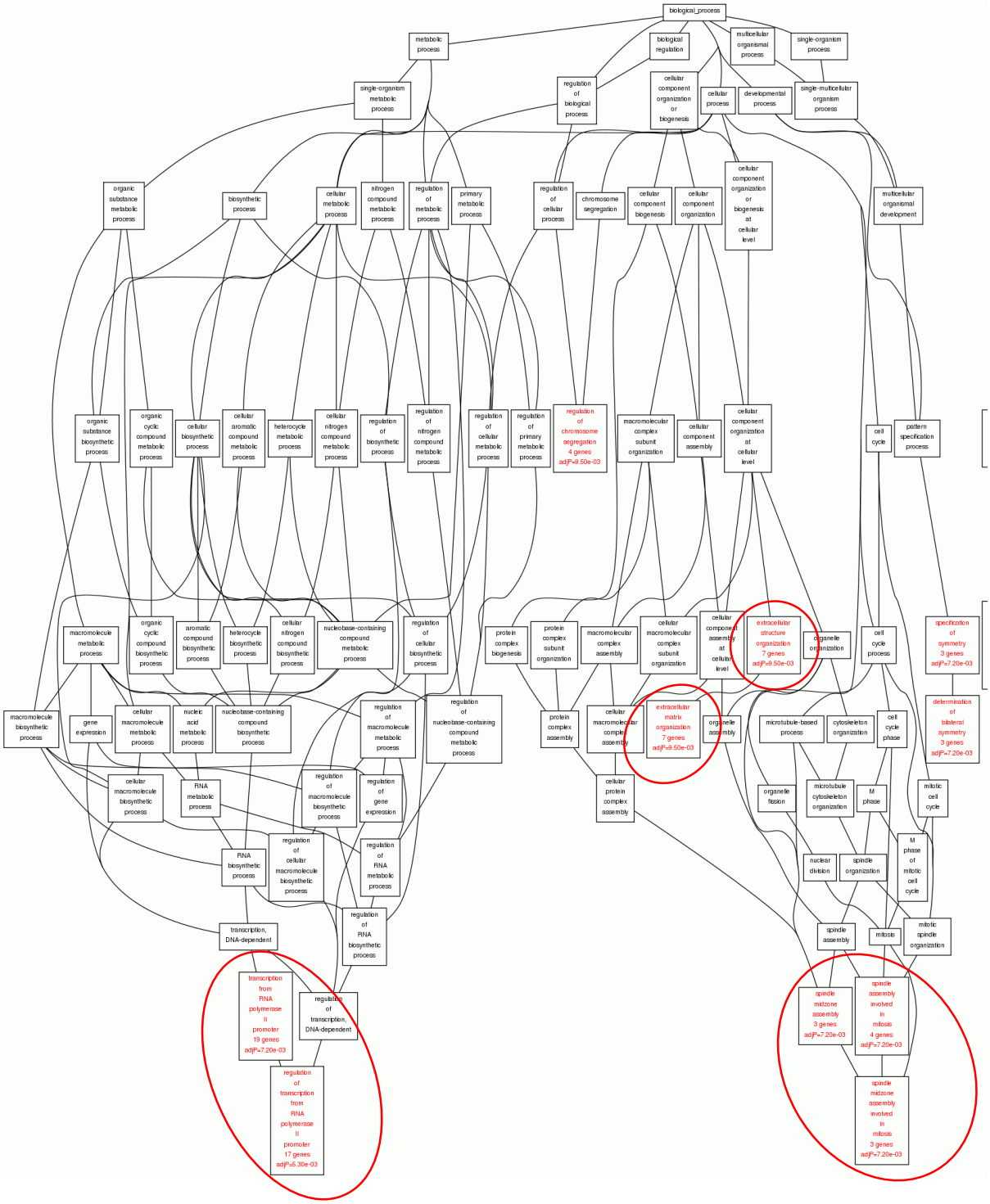

Suppl. Fig. 4 -GO enrichment of proteins found in Cluster 3 after clustering of mimosine-treated protein-samples and analysis with WebGestalt – Part 1. GO categories in the top 10 that also have a p value < 0.05 are colored red. GO categories in the top 10 that have a p value > 0.05 are colored brown, and the black ones are the parents of the top 10 categories.

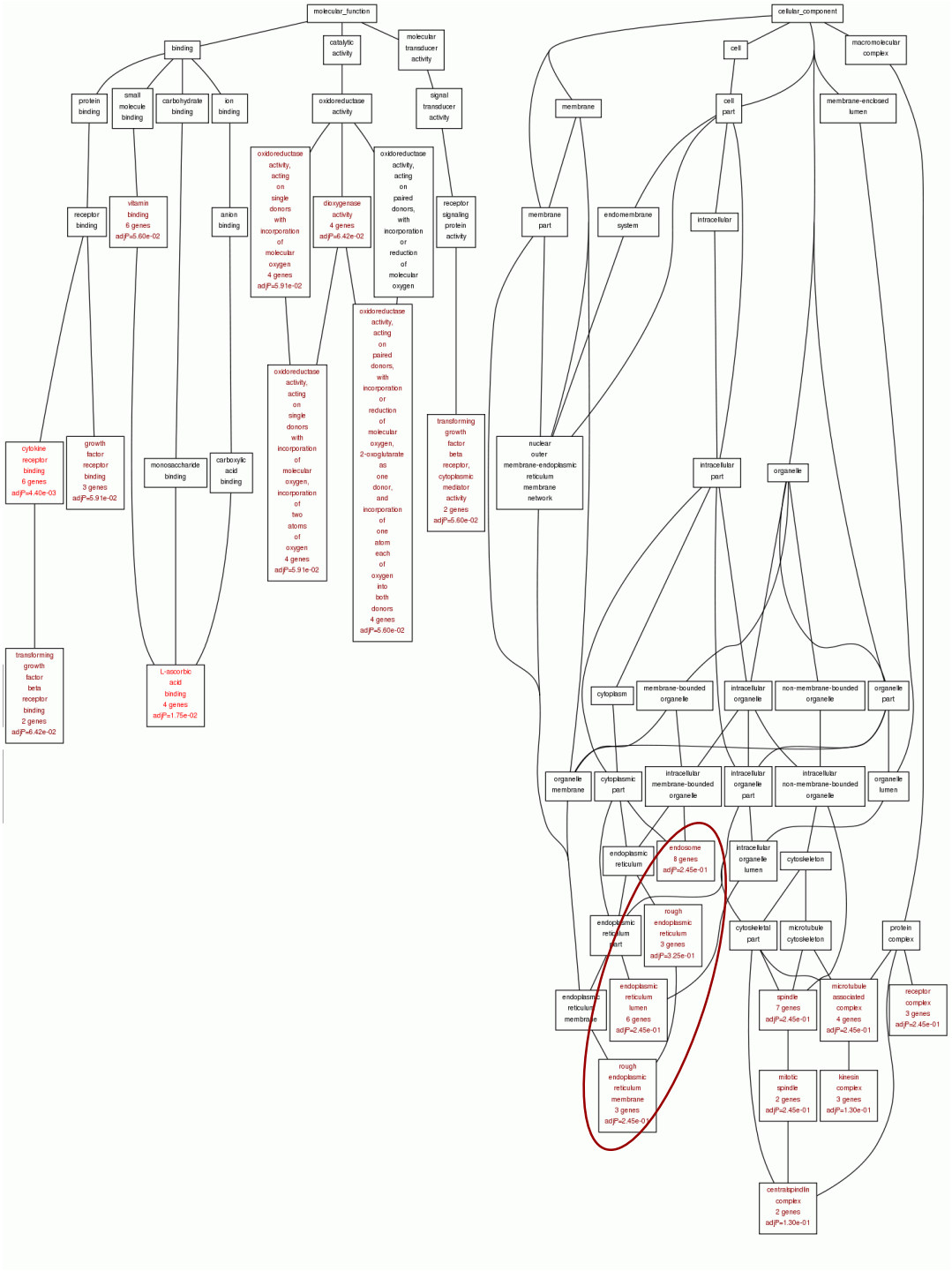

Suppl. Fig. 5 -GO enrichment of proteins found in Cluster 3 after clustering of mimosine-treated protein-samples and analysis with WebGestalt – Part 2. GO categories in the top 10 that also have a p value < 0.05 are colored red. GO categories in the top 10 that have a p value > 0.05 are colored brown, and the black ones are the parents of the top 10 categories.

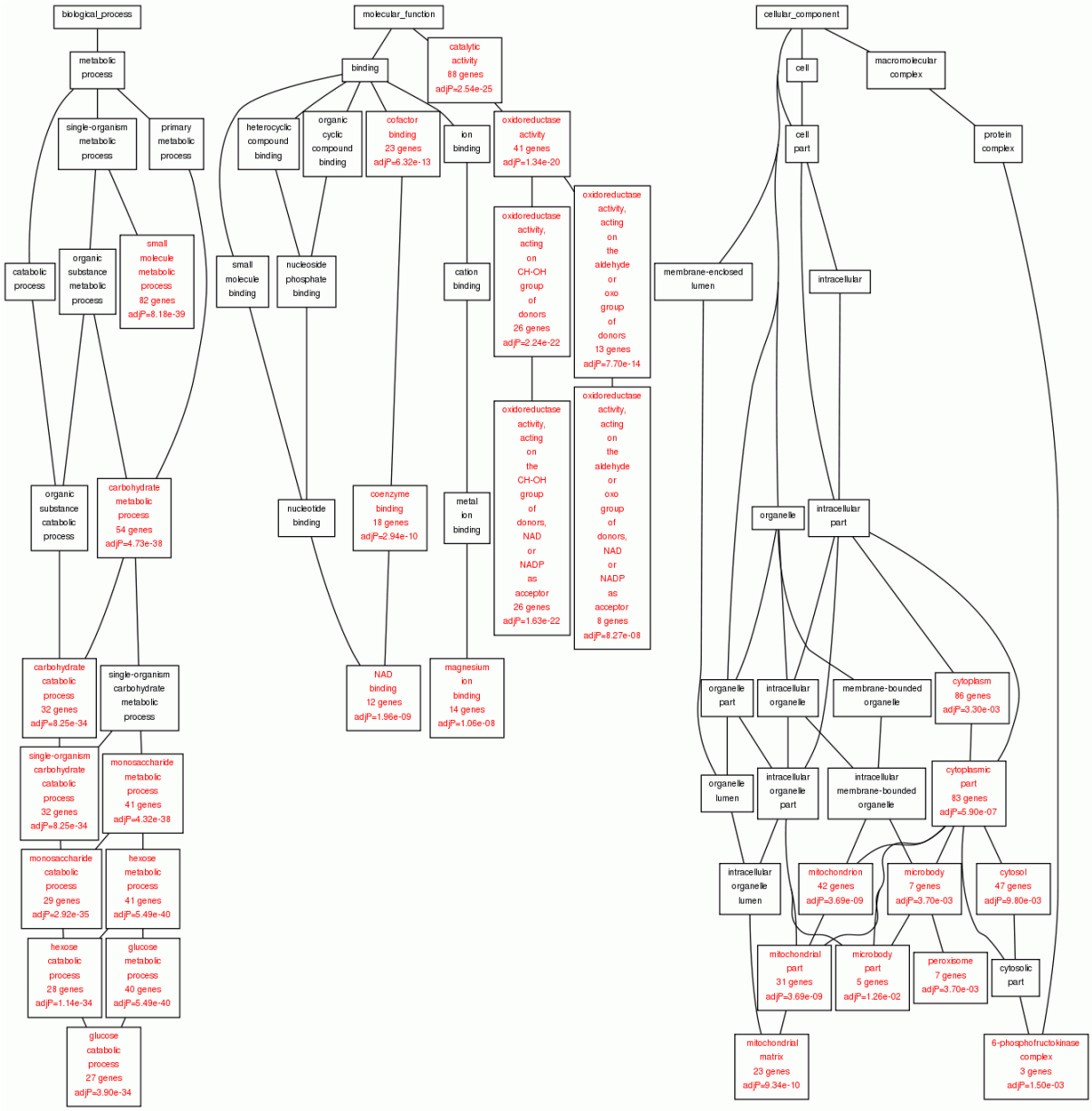

Suppl. Fig. 6 -GO enrichment of proteins found in Cluster of selected metabolic enzymes after clustering of mimosine-treated protein-samples and analysis with WebGestalt. GO categories in the top 10 that also have a p value < 0.05 are colored red. GO categories in the top 10 that have a p value > 0.05 are colored brown, and the black ones are the parents of the top 10 categories.